JOHANNES GUTENBERG UNIVERSITÄT MAINZ

JG|U

Challenges in the Calculation of Molecular Energies and Properties in a Magnetic Field using Unitary Coupled-Cluster Theory

Dissertation
zur Erlangung des Grades
"Doktorin der Naturwissenschaften"
im Promotionsfach Chemie

am Fachbereich Chemie, Pharmazie,
Geographie und Geowissenschaften
der Johannes Gutenberg-Universität Mainz

Laura Grazioli
geb. in Sondrio, Italien

Mainz, 2024

1. Gutachter: Prof. Dr. Jürgen Gauß
2. Gutachter: Prof. Dr. Stella Stopkowicz

Tag der mündlichen Prüfung: 22.07.2024

Der Dichter, der aus eig'nem Fleisse
zu Wort' und Reimen, die er erfand,
aus Tönen auch fügt eine neue Weise,
der wird als *Meistersinger* erkannt.

Richard Wagner, *Die Meistersinger von Nürnberg*

Acknowledgements

Looking back at my four years in Mainz, I realise there is so much to be thankful for and so many people I am grateful to. I want to thank my supervisor, Prof. Stella Stopkowicz, who offered me to work on a topic I really enjoyed and gave me strength in moments in which I needed it. I am thankful for the opportunities she offered me, travelling to conferences and summer schools, from which I had so much to learn. I am also grateful for her support as a female scientist, giving me the opportunity to participate in the Ada Lovelace program.
I am truly indebted to my second supervisor, Prof. Jürgen Gauß, who has played an important role in my academic and personal development during my time in Mainz. I enjoyed our long conversations in the office on opera, German language, history, Italian culture and so much more, which have been of great inspiration for me. I really enjoyed our frequent trips to the Oper Frankfurt and the discussions about the music and stagings. I will keep precious memory of this aspect of my life in Mainz. I will miss this part of the office everyday life and am looking forward to more musical experiences together. I am really thankful for his help in the understanding of the various aspects of response theory which were not decipherable by myself, for his efforts in teaching me the skills needed for an academic career, first of all the trust in what I have achieved and the skill of writing in a convincing way.
I am also grateful to Prof. Filippo Lipparini, without whom my period in Mainz would not have been possible. I am thankful for his constant advice during at least five years, becoming a source of inspiration and of trust for my academic choices.
I am also indebted to Prof. Benedetta Mennucci, who became my mentor in the Ada-Lovelace program. I would like to thank her for the support and understanding of my career choices, for many conversations from which I received a more optimistic view on my future and a clearer perspective on the many possibilities in academia.

I would like to thank my group, the Theoretical Chemistry AK at JGU. After the difficulties of a PhD start during the pandemic, I enjoyed the atmosphere in the group, which by now feels quite familiar. For the work in the present thesis, I have to thank Maximilian Braun and Simon Blaschke for helping me understand the ambiguous aspects on MCD theory, and Laurenz Monzel for the long discussions on QED theory.
It is not obvious to find some friends among the colleagues, but I have been lucky to build some deeper bonds with some of them. In particular, I owe so much to Marios-Petros Kitsaras, who has been a fantastic friend over the past four years. I am thankful for so many interesting discussions, journeys (both for conferences and for private explorations, even on the traces of the ancient Greeks and Romans), and everyday life spent together. I enjoyed sharing the passion for music with him and visiting so many operas and concerts together. I am really grateful for his support in hard times and his advice whenever I needed.
A special acknowledgement goes to my colleague and dear friend Sophia Burger, who endured my company (and my cooking skills) for the past few years. I am grateful for the support she gave me throughout my time here and her deep understanding of my feelings,

for the interest in my language and culture, even visiting me in Italy, and also for the fun in office life. Everyday life would have been less colorful without her company and jokes. I am thankful for the many evenings we spent together, having a Meisterdinner and enjoying the company of each other.
I would also like to thank my colleague Jonas Greiner, with whom I had long scientific conversations on a daily basis, even when each of us was just meant to listen to the other's problems. In the past few years, I knew there would be at least one break in the working afternoon, when I heard Jonas' steps coming towards my office.
I want to thank my friend Tommaso Nottoli, for the time we spent together in Mainz. He made me feel much more comfortable in the group during the first period, as I could just walk by his office to have a conversation in Italian whenever I needed. I thank him for sharing so many experiences, evenings at the opera, walks through the city or cooking (and an Easter of isolation during the pandemic).

My life in Mainz would not have been the same without my dear friend Giuseppe Santangelo, with whom I share not only culture and language, but also ideals and interests. I want to thank him for many evenings spent together cooking, learning modern Greek, or simply discussing on politics, philosophy, archaeology, or just our lives.

I would also like to thank my friend Francesca Bonaiti, whom I met during the Ada Lovelace program at the JGU. We found out to share so much, not only our roots in northern Italy, but also the very similar research we are doing and common thoughts and interests. I thank her for many cooking evenings at her place and all the support we gave each other over the past years

Real friendship does not depend on geographical distances. I owe so much to my best friend Rosario Riso, with whom I have shared joys and also sorrows over the past nine years. At university, people used to call us team mates, and I feel to have found the best team mate I could. I have to thank Rosario for his daily support, even though being so far away, for his optimistic attitude, for his bright ideas and for simply being my best friend. I really wish him all the best, for his personal and academic life.

I really enjoyed becoming part of the Frankfurt Scottish Country Dance Club FSCDC, where I spent most of my Tuesday evenings. Dancing has been an important part of my life in Germany, travelling for workshops and balls, and I am thankful to all the people who shared these moments with me. In particular, I thank Anselm and Marie for their weekly support and so many interesting conversations on the way back to Mainz.

Since my time in Pisa, I have always had a person to look up to, la mamma pisana, Cristina Vannini. I would like to thank her for always being there for me, for giving advice both on the career and personal choices, helping me to develop my personality.

I would not be the same person without my wonderful family. I have had the luck of having as family members the people I respect and love most. They are my anchor and the source of my strength, the only people I can fully rely on, whenever I need help, support, discussion. I am so grateful for continuing to share with them my everyday life (the 7:40-breakfast tradition has been a certainty for the past years now), for the fun we have when we are together, for the deep understanding of each other. It feels too little to just say thank you.
I am deeply convinced that my life would not have been the same without my twin-sister Simona. She is much more to me than I can express. She is the most intelligent person I know, with a very special sense of humor and a enormous culture. I am so happy to share my biggest passions for science, dancing, music, arts, literature and so much more with her.

For the past few years we have lived in different countries, but this has not altered the very unique bond we share. I am sure this will never change.
My mother Gaby and my father Fabio have been my pillars my whole life long. I feel so grateful for everything they gave to me, for the special relationship we have, for the reciprocal trust and support at every time of day and night. I thank my mother for having always encouraged me to explore new things, in particular when staying away from home. My life in Mainz would have been much more difficult without her determination of teaching me German since I was a child, always giving new stimuli for my personal development. I am thankful for her visits here, for the experiences we shared, for her parcels delivered by the German post in hard times, for her advice on everything.
My father has always been a great inspiration to me, in his view on life. I am grateful for our long discussions on politics, on economics, on everyday life, and to his realistic interpretation of situations. He taught me not to take things too seriously, and to enjoy my life. I thank my father for the shared experiences, for his advice whenever I needed him, for his sense of humor and the ability to say always the right thing.
I owe special gratitude to my grandmother Oma Linda, who made my life in Germany less lonely. Having a piece of my family at just a few hours by train made me feel more at home here. I thank her for the fantastic weekends I spent in Köln, for her parcels, for her understanding of my personality and her wisdom when I did not know how to structure my life. I admire her so much, for her strength and kindness, for her determination and wisdom, and owe so much to her.
I also thank uncle Dirk and my cousin Lena for their support whenever I was in Köln, for the numerous times they waited for me at airports or train stations, for having trust in me. I think I could not have had a better family and want to dedicate this thesis to them.

Contents

Chapter 1

Introduction

Ever since the antiquity, the mathematical description of the surrounding world is a priority of mankind, common to all civilisations. The fascination for the rational understanding of the laws of nature can be seen as a constant throughout history. The 20th century has experienced a revolution in the thinking about natural phenomena, through the development of quantum mechanics. In fact, a completely new mind set and language had to be developed, often going against the principles of our intuition. Famous is, for example, the quote by Richard Feynman *I think I can safely say that nobody understands quantum mechanics*, giving an idea of the entity of the revolutionary scope of this theory. Having its roots in the works of Heisenberg[1] and Schrödinger,[2] quantum mechanics marks a revolution in the understanding of phenomena which could not be explained through classical mechanics: famous examples are the black-body radiation[3] and the photoelectric effect.[4] The birth of quantum chemistry may be identified with the quantum-mechanical description of the chemical bond by London and Heitler.[5] From that moment, quantum chemistry has developed into a sophisticated and predictive theory for the understanding of chemical phenomena. The mathematical object describing the interactions a system experiences is called *Hamiltonian*. Its form depends on the physical forces which are taken into consideration. The particles forming the system under study are quantum-mechanically described through a *wave function*. The full analytical description of chemical systems is feasible only for the hydrogen atom. For larger systems, the challenge consists in finding approximations to the parameterisation of the wave function which are still accurate.

Among all approximations discussed in the literature, the exponential parameterisation of Coupled-Cluster (CC) theory plays a leading role due to the accuracy of its results.[6–8] Throughout the years, a plethora of different CC flavours has been explored and developed.[9–24] Restrictions of the excitation space lead to the methods of Coupled Cluster with Singles and Doubles (CCSD),[25] Coupled Cluster with Singles, Doubles and Triples (CCSDT),[26,27] Coupled Cluster with Singles, Doubles, Triples and Quadruples (CCSDTQ)[28] and so on. Enlarging the excitation space certainly leads to better accuracy, but also to an increase of the computational cost of the method. Approximations based on perturbation theory have been formulated to find a compromise between accuracy and cost: some examples are the Second-Order approximate Coupled Cluster with Singles and Doubles (CC2),[29] Third-Order approximate Coupled Cluster with Singles, Doubles and Triples (CC3)[30] or non-iterative approximations as the so-called *gold-standard* Coupled Cluster with Singles and Doubles and perturbative Triples (CCSD(T) approach).[31] The characterisation of excited states can be achieved using Equation-Of-Motion (EOM) CC theory.[32,33]

For many chemical applications, these methods are highly successful. However, they also

possess some limitations. First, the description of excited states near conical intersections by means of EOM-CC theory leads to a wrong characterisation of the intersection itself. Ref. 34 showed examples for which complex energy values are found near such intersections and their occurrence has been analysed.[35] Apart from conical intersections, also the presence of a magnetic field leads to complex energy values. This is an unwanted result, as the energy is a physical observable, meaning that it can be measured and is thus required to be real. In the cases of conical intersections and in finite magnetic fields, complex energy values do not have any physical meaning (they will be referred to as *unphysical*) and their appearance is to be considered a shortcoming of CC theory. The possibility to obtain complex energy values originates from the non-Hermitian form of the energy expression defined in the CC framework. Furthermore, CC theory may also lead to negative transition probabilities, resulting in negative and hence unphysical oscillator strengths.[36,37]
Another limitation of CC theory is found in the field of quantum computing, a field in continuous expansion in recent years.[38–42] Already Feynman[43] and later Abrams and Lloyd[44] suggested the use of quantum computers for quantum chemistry and many algorithms were developed in this context (a short overview is provided in refs. 45 and 46). In quantum computing, states need to be prepared through quantum operations, which are usually unitary. The accuracy in the description of electron correlation makes CC theory a good candidate for the parameterisation of the wave function. However, the CC ansatz cannot be easily implemented through the quantum operations available on a quantum computer.[45]

In summary, limitations in the applicability of CC theory are encountered in three main areas: near conical intersections, in magnetic fields and in quantum computing. Complex energies are found to arise due to the non-Hermiticity of the CC expression for the energy (i.e., the energy expression no longer corresponds to an expectation value of a Hermitian operator). This motivates an alternative to standard CC theory via a unitary parameterisation of the wave function, which maintains the advantages given by the exponential parameterisation of CC theory. In particular, the exponential parameterisation allows the fulfillment of size-consistency,[47] i.e., the additivity of the energies of non-interacting systems. The so-called *unitary coupled-cluster* theory combines the advantages of the exponential parameterisation with a Hermitian expression for the energy calculation, therefore ensuring real energies. The first attempt to formulate such a theory dates back to the late 1970s.[48] The UCC ansatz, however, involves some complications in the development of the working equations which do not find correspondence in CC theory, as they originate from the unitary ansatz. Through the decades, a variety of different unitary coupled-cluster schemes has been suggested.[49–51] The UCC parameterisation of the wave function is able to solve the issues observed in the CC case. In fact, the energy values near conical intersections and in finite magnetic fields are real by construction. Furthermore, a unitary parameterisation of the wave function leads to a straightforward application in the field of quantum computing.[45,46,52,53]

UCC theory can hence be seen an alternative to standard CC theory. The UCC method can be applied not only to the three aforementioned fields, but can also be exploited in all areas of quantum chemistry. UCC theory also needs to account for the description of the excited states, in order to be able to describe conical intersections between such states. Beyond the calculation of energies of ground and excited states, the characterisation of molecular systems is often achieved by spectroscopic means, for which the evaluation of molecular properties is needed.[30,54–58] One major aim of this thesis consists in the formulation of a theory for the calculation of molecular properties in the UCC framework. In the literature, properties of non-variational, approximate wave functions are often calculated through the evaluation of expectation values.[59–63] However, in the case of Coupled-Cluster theory, the expectation-value formulation can lead to non size-extensive properties.[64] It is therefore im-

portant to consider the theoretical framework of response theory for CC, in order to lead to the response-theory formalism[37] for UCC.

In the present work, the unitary coupled cluster ansatz is exploited for the case of an external magnetic field.[65–69] In particular the focus is on strong magnetic fields as those observed in the astrophysical context; the description of astrophysical conditions still represents a challenge for modern quantum chemistry. Molecular systems in this context often experience conditions which are far from those obtainable on Earth, for example magnetic fields of a strength which cannot be reproduced on our planet,[70] urging for a rethinking of chemical concepts. Strong magnetic fields exist on magnetic white dwarf stars.[71–75] Most stars reaching the end of their lifetime (approximately 97%) are below the critical mass to become neutron stars or black holes, and evolve into white dwarf stars.[76] These are dense stellar objects surrounded by an atmosphere which can contain H, He, and other heavier elements, some of which originate from accretion from planetary debris.[77–95] Being at the end of their life cycle, white dwarfs eventually reach temperatures low enough to permit the formation of molecules (among the detected ones, H_2, CH, and C_2).[84,85,95] Interestingly, more than 25% of all white dwarf stars are characterised by a strong magnetic field, with field strengths up to 100000 T.[96,97] Under these circumstances, the magnetic forces cannot be treated as a perturbation to the Coulomb forces, and the theoretical description of the physics of the system needs to treat Coulomb and Lorenz forces at the same level. This regime is usually referred to as *mixing regime*, where the magnetic fields are typically of the order of the atomic unit B_0, which corresponds to about 235000 T. The interpretation of spectra from the atmospheres of magnetic white dwarfs[98] has pushed the theoretical research towards the formulation of finite-field approaches (i.e., approaches with explicit consideration of an external magnetic field) in recent years.[65–67,78,87,99–116] Molecules in strong magnetic fields have been first investigated in the 1980s,[78,87,99–102] exploring the field strengths of the mixing regime. In the literature, analyses consider non-linear molecules, as well as non-parallel orientations with respect to the magnetic field.[65,67,103–113]
The inclusion of magnetic-field dependent terms in the Hamiltonian opens new challenges, as the wave function is no longer real. The complex form of the wave function implies that complex algebra is needed for the computation, requiring a significantly higher memory and computational effort.

The finite-field methodology is of interest not only for the exotic settings of magnetic white dwarf stars, but can also be exploited for the calculation of magnetic circular dichroism (MCD) spectra, which use the magnetic field for the investigation of the structure of molecules.[117–120] Magnetic-field effects allow to analyse transitions that are not detected by other spectroscopies, therefore providing a powerful tool for the characterisation of molecular systems. The theoretical prediction of MCD spectra has been extensively studied in the literature.[107,121–129] The usually exploited approach is based on field-free calculations accounting for the effect of the magnetic field through a perturbative expansion. A in principle simpler procedure for the calculation of MCD spectra is introduced here in the context of UCC theory, which includes the finite-field effects to infinite order.[107] The computation of these spectra is based on the evaluation of transition dipole moments in the presence of the magnetic field.

The analysis of molecules interacting with electromagnetic fields can be completed by discussing the case in which strong coupling of matter and light is induced via confinement of fields inside an electromagnetic cavity. The chemistry inside such cavities has gained interest in the community in recent years, as it has an experimentally measurable effect on chemical properties.[130131–142] From an experimental point of view, it has been demonstrated that the coupling of light and matter influences reaction rates, slowing down or catalysing a

given reaction, and may induce selectivity in the formation of the products.[143–151] In order to understand and predict the effects of this strong-coupling regime, a set of new quantum-chemical methods has been proposed in the theoretical community. The description of light and matter coupling needs to treat fermions (electrons) and bosons (photons) at the same time. Thus, a formalism adopting the framework of quantum electrodynamics (QED) has been developed. The methods describing chemistry in an electromagnetic cavity have been conceived on the basis of the molecular quantum theories in use: quantum electrodynamics density functional theory (QEDFT),[140,141,152] quantum electrodynamics Hartree-Fock (QED-HF),[136,137] quantum electrodynamics coupled cluster (QED-CC),[136,153–155] quantum electrodynamics FCI (QED-FCI)[137] and others.[156–159] Among these, QED-CC can be used as starting point for the development of a UCC approach in a cavity, the quantum electrodynamics unitary coupled cluster approach (QED-UCC).

In chapter 2 a compact summary of the foundations of electrodynamics and quantum chemistry is provided, discussing in particular CC theory. The framework of response theory is provided and applied to CC theory.

In chapter 3, the fundamental equations for UCC energies are developed and compared to the corresponding versions in the CC framework. Special attention is given to the analysis of the analogies and differences originating from the different parameterisations of the two methods. Two perturbative truncation schemes of the unitarily transformed Hamiltonian are analysed, defined by the approximation at second (UCC2) and third order (UCC3) of the equations solving for the wave function parameters (amplitudes).[160] UCC response theory is then developed for the description of molecular properties.

In chapter 4, the focus is placed on the implementation of the working equations. For each method the explicit formulation for the programmable expressions is discussed. The implementation of these equations presupposes the ability to handle complex algebra. Most quantum chemistry codes do not possess this capability. The implementation of the discussed theories was possible in the QCUMBRE program package[161] which is specialised on finite-field calculations and possesses the infrastructure working with a complex wave function. The presentation of the challenges faced in the implementation is accompanied by an insight into the most efficient and low-scaling formulation of the expressions. A discussion on the actual steps performed by the program when calculating UCC properties is presented.

Once the theory for the computation of energies and properties has been developed, it is applied to molecular systems in order to test whether the discussed UCC is accurate enough to be used in place of CC theory. The discussion of the results on the chosen systems is the topic of chapter 5. First, the accuracy of the UCC method is assessed and compared to CC results for systems which are well-described by CC theory. The issue of complex energies is discussed through the examples of the water molecule, in a strong magnetic field, and the excited states of boric acid, as the latter prove to be problematic already in the field free case. The issue of negative transition probabilities is discussed next, introducing as examples the silicon dication and the CH^+ cation.

Chapter 6 aims at the characterisation of MCD spectra through a finite-field approach. The spectra obtained for CC and UCC are compared for urea and cyclopropane. Lastly, a comparison of the spectra obtained with the developed finite-field approach with experimental spectra of pyrazine and pyrimidine is discussed.

Chapter 7 provides a discussion on QED theory, going from its general formulation to its application to quantum chemistry, leading to the first development of QED-UCC2. This method has been developed to describe a molecular system in a cavity, to which an additional external magnetic field is applied. A pilot application is given by the investigation of the phenomenon of perpendicular paramagnetic bonding[66,162] in an electromagnetic cav-

ity, calculated for the He_2 molecule. Here, the predictivity of QED-UCC2 is discussed in comparison to the more expensive QED-CCSD approach.

In chapter 8, the theoretical advances given by this thesis are summarised, discussing the general results which have been found applying the UCC formalism to the investigated molecular systems. Furthermore, an outlook on the most intriguing perspectives of the present work are given.

Chapter 2

Theory

As this thesis aims at the description of molecular systems interacting with a magnetic field, this chapter provides some preliminary tools on wave-function methods and electromagnetic fields.

2.1 Molecular Hamiltonian

The Schrödinger equation is the fundamental equation for a quantum mechanical description of particles

$$(\hat{H} - i\frac{\partial}{\partial t})\,|\Psi\rangle = 0. \tag{2.1.1}$$

For a conservative system, also a time-independent version of the Schrödinger equation can be formulated as $\hat{H}\,|\Psi\rangle = E\,|\Psi\rangle$. In the field-free setting, the molecular Hamiltonian is

$$\hat{H} = \hat{T}_\mathrm{e} + \hat{T}_\mathrm{N} + \hat{V}_\mathrm{ee} + \hat{V}_\mathrm{NN} + \hat{V}_\mathrm{eN}, \tag{2.1.2}$$

where $\hat{T}_\mathrm{e}$ represents the kinetic energy of the electrons, $\hat{T}_\mathrm{N}$ the kinetic energy of the nuclei, $\hat{V}_\mathrm{ee}$ the Coulomb interactions between two electrons, $\hat{V}_{eN}$ the Coulomb interactions of electrons and nuclei, and $\hat{V}_\mathrm{NN}$ the Coulomb interactions between two nuclei.

In atomic units, where the mass and the elementary charge, as well as $\hbar$ are fixed to one, the molecular Hamiltonian reads

$$\hat{H} = -\sum_i \frac{\nabla^2_{\mathbf{r}_i}}{2} - \sum_I \frac{\nabla^2_{\mathbf{R}_I}}{2M_I} + \sum_{i>j} \frac{1}{|\mathbf{r}_i - \mathbf{r}_j|} + \sum_{I>J} \frac{Z_I Z_J}{|\mathbf{R}_I - \mathbf{R}_J|} - \sum_{iI} \frac{1}{|\mathbf{r}_i - \mathbf{R}_I|}, \tag{2.1.3}$$

where the sum over i, j runs over the electrons, while the capital letters I, J are used to label the nuclei. Electronic coordinates are marked with $\mathbf{r}_i$, nuclear ones with $\mathbf{R}_I$. Z_I corresponds to the atomic number, M_I to the nuclear mass. As the nuclear masses are much larger than the mass of the electron, it is common to consider the nuclei as fixed and the electrons as instantaneously adapting to a change in the nuclear positions (*Born-Oppenheimer* (BO) approximation). This nearly complete though approximate separation in the degrees of freedom allows to assume an adiabatic formulation of the wave function as the product of a nuclear and an electronic part

$$|\Psi_\mathrm{exact}(\mathbf{r};\mathbf{R})\rangle = |\Psi_\mathrm{nuc}(\mathbf{R})\rangle\,|\Psi_\mathrm{el}(\mathbf{r};\mathbf{R})\rangle\,. \tag{2.1.4}$$

The electronic wave function depends on the electronic coordinates as variables and the nuclear coordinates as parameters, while the nuclear part depends only on the nuclear positions. The electronic eigenstates Ψ^n_el and energies E^n_el are found by solving the electronic

Schrödinger equation

$$\hat{H}_{\mathrm{el}}\,|\Psi^n_{\mathrm{el}}\rangle = E^n_{\mathrm{el}}(\mathbf{R})\,|\Psi^n_{\mathrm{el}}\rangle\,, \qquad \hat{H}_{\mathrm{el}} = \hat{T}_{\mathrm{e}} + \hat{V}_{\mathrm{ee}} + \hat{V}_{\mathrm{eN}}. \tag{2.1.5}$$

After having solved the electronic part of the Schrödinger equation, the nuclear part is

$$(\hat{T}_{\mathrm{N}} + \hat{V}_{\mathrm{NN}} + E^n_{\mathrm{el}}(\mathbf{R}))\,|\Psi^n_{\mathrm{el}}(\mathbf{r};\mathbf{R})\rangle\,|\Psi^n_{\mathrm{nuc}}(\mathbf{R})\rangle = E^n_{\mathrm{tot}}\,|\Psi^n_{\mathrm{el}}(\mathbf{r};\mathbf{R})\rangle\,|\Psi^n_{\mathrm{nuc}}(\mathbf{R})\rangle\,. \tag{2.1.6}$$

Projection on an electronic eigenstate $\langle\Psi^m_{\mathrm{el}}|$ over the electronic coordinates yields

$$\langle\Psi^m_{\mathrm{el}}(\mathbf{r};\mathbf{R})|\,(\hat{T}_{\mathrm{N}} + \hat{V}_{\mathrm{NN}} + E^n_{\mathrm{el}}(\mathbf{R}))\,|\Psi^n_{\mathrm{el}}(\mathbf{r};\mathbf{R})\rangle\,|\Psi^n_{\mathrm{nuc}}(\mathbf{R})\rangle = E^n_{\mathrm{tot}}\,\langle\Psi^m_{\mathrm{el}}(\mathbf{r};\mathbf{R})|\Psi^n_{\mathrm{el}}(\mathbf{r};\mathbf{R})\rangle\,|\Psi^n_{\mathrm{nuc}}(\mathbf{R})\rangle\,. \tag{2.1.7}$$

Different eigenstates satisfy the orthonormality condition $\langle\Psi^m_{\mathrm{el}}|\Psi^n_{\mathrm{el}}\rangle = \delta_{mn}$. The nuclear potential $\hat{V}_{\mathrm{NN}}$ depends only on the nuclear coordinates. An effective potential V^m_{eff} is defined as

$$\langle\Psi^m_{\mathrm{el}}|\,(\hat{V}_{\mathrm{NN}} + E^n_{\mathrm{el}}(\mathbf{R}))\,|\Psi^n_{\mathrm{nuc}}\rangle\,|\Psi^n_{\mathrm{el}}\rangle = V^m_{\mathrm{eff}}\delta_{mn}\,|\Psi^n_{\mathrm{nuc}}\rangle \tag{2.1.8}$$

The BO approximation neglects any contribution given by applying the nuclear kinetic operator on the electronic wave function, thereby assuming this term to be small

$$\hat{T}_{\mathrm{N}}\,|\Psi^n_{\mathrm{el}}(\mathbf{r};\mathbf{R})\rangle\,|\Psi^n_{\mathrm{nuc}}(\mathbf{R})\rangle \sim |\Psi^n_{\mathrm{el}}(\mathbf{r};\mathbf{R})\rangle\,\hat{T}_{\mathrm{N}}\,|\Psi^n_{\mathrm{nuc}}(\mathbf{R})\rangle\,. \tag{2.1.9}$$

The total energy of the system in the BO approximation is given by the following equation

$$(\hat{T}_{\mathrm{N}} + \hat{V}^m_{\mathrm{eff}})\,|\Psi^m_{\mathrm{nuc}}(\mathbf{R})\rangle = E^{m,\mathrm{BO}}_{\mathrm{tot}}\,|\Psi^m_{\mathrm{nuc}}(\mathbf{R})\rangle\,. \tag{2.1.10}$$

The BO approximation is usually exploited in quantum chemistry. However, there are some physical settings, for example near conical intersections, in which a slight perturbation in the nuclear coordinates leads to a large change in the electronic wave function. In these cases, the BO approximation is not a good approximation.[163–166]

2.2 Electromagnetic fields

The Hamiltonian in eq. 2.1.3 describes a molecule in free space. However, molecular systems can also interact with electromagnetic fields. A description of the fundamental laws of electrodynamics is at the basis of the correct formulation of the Hamilton operator describing these systems.

A particle of charge q moving with velocity $\mathbf{v}$ in an electromagnetic field experiences the *Lorentz force*

$$\mathbf{F} = q(\mathbf{E} + \mathbf{v}\times\mathbf{B}). \tag{2.2.1}$$

The electric field $\mathbf{E}$ and the magnetic field $\mathbf{B}$ are coupled by the fundamental equations of electrodynamics, the Maxwell equations.

$$\nabla\cdot\mathbf{E} = \frac{\rho}{\varepsilon_0} \qquad \text{(Gauss' law)}, \tag{2.2.2}$$

$$\nabla\times\mathbf{B} = \mu_0\left(\mathbf{J} + \varepsilon_0\frac{\partial\mathbf{E}}{\partial t}\right) \qquad \text{(Ampère's law)}, \tag{2.2.3}$$

$$\nabla\cdot\mathbf{B} = 0, \tag{2.2.4}$$

$$\nabla\times\mathbf{E} = -\frac{\partial\mathbf{B}}{\partial t} \qquad \text{(Maxwell-Faraday's equation)}. \tag{2.2.5}$$

The first two equations are referred to as *inhomogeneous* Maxwell equations, because of the presence of the sources on the right hand-side: ρ is the charge density, $\mathbf{J}$ the current density;

in vacuum, these equations become homogeneous. ε_0 and μ_0 are the electric permittivity and the magnetic permeability, respectively. The Maxwell equations need to be satisfied simultaneously; the electric and magnetic fields are thus coupled.

Exploiting the vector identity $\nabla \cdot \nabla \times \mathbf{v} = 0$, the third Maxwell equation is automatically satisfied by expressing the magnetic field as the curl of a vector potential

$$\mathbf{B} = \nabla \times \mathbf{A}. \tag{2.2.6}$$

Inserting this expression for the magnetic field in Faraday's law (eq. 2.2.5) yields

$$\nabla \times (\mathbf{E} + \frac{\partial \mathbf{A}}{\partial t}) = 0. \tag{2.2.7}$$

As a general continuously twice-differentiable function f satisfies the vector identity $\nabla \times \nabla f = 0$, the following relation can be written

$$\mathbf{E} + \frac{\partial \mathbf{A}}{\partial t} = -\nabla \varphi. \tag{2.2.8}$$

The electric and magnetic fields can therefore be expressed through a scalar and a vector potential; their components are found by solving the inhomogeneous Maxwell equations, as these contain the sources of the system.

The introduction of the scalar potential φ and the vector potential $\mathbf{A}$ has the advantage of reducing the number of functions from six (the three components of the electric-field vector $\mathbf{E}$ and the three components of the magnetic-field vector $\mathbf{B}$) to four (the scalar potential φ and the three components of the vector potential $\mathbf{A}$). However, this reduction is associated with some freedom in the choice of the potentials (*gauge freedom*). A transformation of the form

$$\begin{aligned} \varphi' &= \varphi - \frac{\partial f}{\partial t} \\ \mathbf{A}' &= \mathbf{A} + \nabla f \end{aligned} \tag{2.2.9}$$

leads to the same fields $(\mathbf{E}, \mathbf{B})$

$$\begin{aligned} \mathbf{E}' &= -\frac{\partial \mathbf{A}'}{\partial t} - \nabla \varphi' = -\frac{\partial \mathbf{A}}{\partial t} - \frac{\partial \nabla f}{\partial t} - \nabla \varphi + \nabla \frac{\partial f}{\partial t} = \mathbf{E}, \\ \mathbf{B}' &= \nabla \times \mathbf{A}' = \nabla \times \mathbf{A} + \nabla \times \nabla f = \mathbf{B}. \end{aligned} \tag{2.2.10}$$

Thus f may be chosen to obtain $\mathbf{A}$ and φ which satisfy some additional conditions. In this thesis, the *Coulomb gauge* will be exploited, characterised by a divergenceless vector potential

$$\nabla \cdot \mathbf{A} = 0. \tag{2.2.11}$$

However, it has to be noted that the adoption of the Coulomb gauge, though restricting the degrees of freedom, does not uniquely determine the potentials. The Coulomb gauge is usually adopted in non-relativistic theory, in which instantaneous interactions between charges are assumed. Note that it is not the only possible choice and other gauges are advantageous for other applications.*

In the Coulomb gauge, eq. 2.2.2 and 2.2.3 are given by

$$\nabla^2 \varphi = -\frac{\rho}{\varepsilon_0}, \tag{2.2.12}$$

$$\nabla^2 \mathbf{A} - \frac{1}{c^2} \frac{\partial^2 \mathbf{A}}{\partial t^2} = -\frac{\mathbf{J}}{\varepsilon_0 c^2} + \frac{1}{c^2} \frac{\partial \nabla \varphi}{\partial t}. \tag{2.2.13}$$

*For example, in the relativistic setting, the Lorenz gauge is often adopted, where the condition is $\nabla \cdot \mathbf{A} + \frac{1}{c} \frac{\mathrm{d}\varphi}{\mathrm{d}t} = 0$.

It has been proven in the literature[167,168] that any sufficiently smooth, rapidly decaying vector field can be decomposed into the sum of a curl-free part and a divergence-free part. Exploiting this theorem for eq. 2.2.13, the curl-free vector field is

$$\nabla^2\mathbf{A} - \frac{1}{c^2}\frac{\partial^2\mathbf{A}}{\partial t^2} = -\frac{\mathbf{J}^{\perp}}{\varepsilon_0 c^2}, \tag{2.2.14}$$

while the divergence-free part is

$$0 = \frac{\mathbf{J}^{\parallel}}{\varepsilon_0} - \frac{\partial\nabla\varphi}{\partial t}. \tag{2.2.15}$$

The continuity equation itself is found to be a reformulation of eq. 2.2.12, taking the divergence of eq. 2.2.15 and using the definition of $\nabla^2\varphi$ from eq. 2.2.12

$$\nabla\cdot\mathbf{J} + \frac{\partial\rho}{\partial t} = 0. \tag{2.2.16}$$

2.3 Hamiltonian in a magnetic field

In the previous section, the fundamental laws of electrodynamics have been discussed. The description of the interaction of a particle with the electromagnetic field can be performed both via the Newtonian formalism and the Hamiltonian formalism. The latter is exploited here, as it is more suitable for the transition to quantum mechanics. For a particle in an electromagnetic field, the Hamiltonian function is

$$H = \frac{\boldsymbol{\pi}^2}{2m} + q\varphi, \tag{2.3.1}$$

where $\boldsymbol{\pi}$ is the kinetic momentum of the system, given by $\boldsymbol{\pi} = \mathbf{p} - q\mathbf{A}$ and m the electronic mass. The transition from classical to quantum mechanics is given by substituting

$$\mathbf{p} \to \hat{\mathbf{p}} = -i\hbar\nabla \qquad \mathbf{r} \to \hat{\mathbf{r}} \qquad H \to \hat{H} = i\hbar\frac{\partial}{\partial t}. \tag{2.3.2}$$

From the definitions of the Hamiltonian in eq. 2.3.1 and eq. 2.3.2 and by acting on a wave function $\Psi(r,t)$, the following equation is obtained

$$i\hbar\frac{\partial}{\partial t}\Psi(r,t) = [\frac{1}{2m}(-i\hbar\nabla - q\mathbf{A})\cdot(-i\hbar\nabla - q\mathbf{A}) + q\varphi]\Psi(r,t). \tag{2.3.3}$$

However, eq. 2.3.1 describes a system in the non-relativistic frame. Pauli noticed that this formulation does not correctly represent all physical properties of a system, as it neglects the intrinsic angular momentum (spin) of the electrons.[169] To account for the spin in the Hamiltonian, he introduced the formulation

$$\hat{H} = \frac{(\hat{\boldsymbol{\sigma}}\cdot\hat{\boldsymbol{\pi}})^2}{2m} + q\varphi, \tag{2.3.4}$$

where $\hat{\boldsymbol{\sigma}}$ contains three operators, which in their matrix representation are the Pauli spin matrices. It is related to the spin operator by the condition $\hat{\mathbf{s}} = \hbar\frac{\hat{\boldsymbol{\sigma}}}{2}$. With some manipulation and exploiting the Dirac identity $(\hat{\boldsymbol{\sigma}}\cdot\mathbf{A})(\hat{\boldsymbol{\sigma}}\cdot\mathbf{B}) = \mathbf{A}\cdot\mathbf{B} + i\hat{\boldsymbol{\sigma}}\cdot(\mathbf{A}\times\mathbf{B})$, the Hamilton function in classical mechanics becomes

$$\hat{H} = \frac{\hat{\boldsymbol{\pi}}^2}{2m} - \frac{q\hbar}{2m}\mathbf{B}\cdot\hat{\boldsymbol{\sigma}} + q\varphi. \tag{2.3.5}$$

From eq. 2.3.5 and eq. 2.3.2, the following equation is obtained

$$i\hbar\frac{\partial}{\partial t}\Psi(r,t) = [\frac{1}{2m}(-i\hbar\nabla - q\mathbf{A})\cdot(-i\hbar\nabla - q\mathbf{A}) - \frac{q\hbar}{2m}\mathbf{B}\cdot\hat{\boldsymbol{\sigma}} + q\varphi]\Psi(r,t), \tag{2.3.6}$$

which corresponds to the time-dependent *Schrödinger equation* in an electromagnetic field. The action of the kinetic momentum operator squared can be simplified as follows

$$\begin{aligned}\hat{\pi}^2\Psi &= (\hat{\mathbf{p}} - q\mathbf{A})\cdot(\hat{\mathbf{p}} - q\mathbf{A})\Psi = \hat{\mathbf{p}}^2\Psi - q\hat{\mathbf{p}}\cdot\mathbf{A}\Psi - q\mathbf{A}\cdot\hat{\mathbf{p}}\Psi + q^2A^2\Psi \\ &= \hat{\mathbf{p}}^2\Psi - q\underbrace{(\hat{\mathbf{p}}\cdot\mathbf{A})}_{-i\hbar\nabla\cdot\mathbf{A}=0}\Psi - 2q\mathbf{A}\cdot\hat{\mathbf{p}}\Psi + q^2\mathbf{A}^2\Psi.\end{aligned} \tag{2.3.7}$$

The Schrödinger equation therefore reads

$$\hat{H} = \frac{\hat{\mathbf{p}}^2}{2m} - \frac{q}{m}\mathbf{A}\cdot\hat{\mathbf{p}} - \frac{q}{m}\mathbf{B}\cdot\hat{\mathbf{s}} + \frac{q^2}{2m}\mathbf{A}^2 + q\varphi. \tag{2.3.8}$$

In the case of a uniform constant magnetic field, the vector potential is given by

$$\mathbf{A}_\mathrm{O}(\mathbf{r}) = \frac{1}{2}\mathbf{B}\times(\mathbf{r} - \mathbf{R}_\mathrm{O}), \tag{2.3.9}$$

where $\mathbf{R}_\mathrm{O}$ is an arbitrary point in space, chosen as origin coordinate on which the vector potential is defined. The second term in eq. 2.3.8 can be simplified

$$\mathbf{A}\cdot\hat{\mathbf{p}} = \frac{1}{2}\mathbf{B}\times(\mathbf{r} - \mathbf{R}_\mathrm{O})\cdot\hat{\mathbf{p}} = \frac{1}{2}\mathbf{B}\cdot(\mathbf{r} - \mathbf{R}_\mathrm{O})\times\hat{\mathbf{p}} = \frac{1}{2}\mathbf{B}\cdot\hat{\mathbf{L}}_\mathrm{O}, \tag{2.3.10}$$

where the angular momentum operator $\hat{\mathbf{L}}_\mathrm{O} = (\mathbf{r} - \mathbf{R}_\mathrm{O})\times\hat{\mathbf{p}}$ has been introduced.* The diamagnetic term gives‡

$$\mathbf{A}^2 = \frac{1}{4}(\mathbf{B}\times(\mathbf{r} - \mathbf{R}_\mathrm{O}))\cdot(\mathbf{B}\times(\mathbf{r} - \mathbf{R}_\mathrm{O})) = \frac{1}{4}(B^2(\mathbf{r} - \mathbf{R}_\mathrm{O})^2 - (\mathbf{B}\cdot(\mathbf{r} - \mathbf{R}_\mathrm{O}))^2). \tag{2.3.11}$$

From now on, the equations will be applied to electrons. Atomic units are used, with the following conventions: $m = 1, q = -1, \hbar = 1$. With these conventions, the Hamiltonian in its final form is

$$\hat{H} = \frac{\hat{\mathbf{p}}^2}{2} + \frac{1}{2}\mathbf{B}\cdot\hat{\mathbf{L}}_\mathrm{O} + \mathbf{B}\cdot\hat{\mathbf{s}} + \frac{1}{8}(B^2(\mathbf{r} - \mathbf{R}_\mathrm{O})^2 - (\mathbf{B}\cdot(\mathbf{r} - \mathbf{R}_\mathrm{O}))^2) - \varphi. \tag{2.3.12}$$

The Hamiltonian depends on the magnetic field through both linear and quadratic terms in $\mathbf{B}$. The linear terms are called *paramagnetic* and couple the magnetic field to the angular momentum and the spin of the system. The first is usually referred to as *orbital-Zeeman* term and splits degenerate orbitals according to their angular momentum; it favours high negative angular momenta. The second is labelled *spin-Zeeman* term and splits degenerate states with different spins; it favours high-spin open shell systems with a large negative spin component aligned along the magnetic field. The term quadratic in $\mathbf{B}$ is called *diamagnetic* and results in a positive contribution to the energy of the system. It can be seen as a confining term in the plane perpendicular to the direction of the magnetic field.

In the presence of an external magnetic field, the full Hamiltonian for a molecular system is

$$\begin{aligned}\hat{H} = \hat{H}_0 &+ \frac{1}{2}\sum_i \mathbf{B}\cdot\hat{\mathbf{L}}_{iO} + \sum_i \mathbf{B}\cdot\hat{\mathbf{s}}_i + \frac{1}{8}\sum_i (B^2 r_{iO}^2 - (\mathbf{B}\cdot\mathbf{r}_{iO})^2) \\ &+ \frac{1}{2}\sum_I \mathbf{B}\cdot\hat{\mathbf{L}}_{IO} + \sum_I \mathbf{B}\cdot\hat{\mathbf{s}}_I + \frac{1}{8}\sum_I (B^2 r_{IO}^2 - (\mathbf{B}\cdot\mathbf{r}_{IO})^2),\end{aligned} \tag{2.3.13}$$

where $\hat{H}_0$ is the field-free Hamiltonian of eq. 2.1.3.

*The vector identity $(\mathbf{a}\times\mathbf{b})\cdot\mathbf{c} = (\mathbf{b}\times\mathbf{c})\cdot\mathbf{a} = (\mathbf{c}\times\mathbf{a})\cdot\mathbf{b}$ has been exploited.

‡The vector identity $(\mathbf{a}\times\mathbf{b})\cdot(\mathbf{a}\times\mathbf{b}) = (\mathbf{a}\cdot\mathbf{a})(\mathbf{b}\cdot\mathbf{b}) - (\mathbf{a}\cdot\mathbf{b})^\mathbf{2}$ has been exploited.

2.4 Hartree-Fock Theory

The simplest ansatz for an electronic wave function, satisfying the requirements of antisymmetry, is given by the Slater determinant (SD)

$$\Psi_{\mathrm{SD}} = \frac{1}{\sqrt{N!}} \begin{vmatrix} \varphi_1(1) & \varphi_2(1) & \dots & \varphi_N(1) \\ \varphi_1(2) & \varphi_2(2) & & \\ \vdots & & \ddots & \\ \varphi_1(N) & & & \varphi_N(N) \end{vmatrix} = |\varphi_1\varphi_2\dots\varphi_N\rangle\,.$$

Here φ_i labels the different spin orbitals, while the number in brackets (for example (j)) represents all spatial and spin variables of the j-th electron. The SD is a normalised wave function, provided that the orbitals are orthonormal, giving

$$\langle\Psi_{\mathrm{SD}}|\Psi_{\mathrm{SD}}\rangle = \langle\varphi_1\varphi_2\dots\varphi_N|\varphi_1\varphi_2\dots\varphi_N\rangle = 1. \tag{2.4.1}$$

This ansatz for the wave function is adopted by the *Hartree-Fock* method.[170–173]

The Hartree-Fock wave function and energy are found by minimising the expectation value of the Hamilton operator

$$E_{\mathrm{HF}} = \langle\Psi_{\mathrm{SD}}|\,\hat{H}\,|\Psi_{\mathrm{SD}}\rangle = \sum_i \langle\varphi_i|\,\hat{h}\,|\varphi_i\rangle + \frac{1}{2}\sum_{ij}\langle\varphi_i\varphi_j||\varphi_i\varphi_j\rangle\,, \tag{2.4.2}$$

with respect to the choice of the spin orbitals, where $\hat{h}$ is the one-electron operator in the Hamiltonian, while $\langle\varphi_i\varphi_j||\varphi_i\varphi_j\rangle$ is the antisymmetrised two-electron integral

$$\langle\varphi_i\varphi_j||\varphi_i\varphi_j\rangle = \langle\varphi_i(1)\varphi_j(2)|\,\frac{1}{r_{12}}\,|\varphi_i(1)\varphi_j(2)\rangle - \langle\varphi_i(1)\varphi_j(2)|\,\frac{1}{r_{12}}\,|\varphi_j(1)\varphi_i(2)\rangle\,. \tag{2.4.3}$$

The first integral in eq. 2.4.3 describes the Coulomb interaction between the electronic densities of electron 1 in orbital φ_i with electron 2 in orbital φ_j. The action of the *Coulomb operator* on the φ_i orbital is given as

$$\hat{J}_j\,|\varphi_i(1)\rangle = \int \varphi_j(2)^*\frac{1}{r_{12}}\varphi_i(1)\varphi_j(2)\mathrm{d}\mathbf{r}_2\mathrm{d}\sigma_2, \tag{2.4.4}$$

where the integration is performed with respect to the spatial and spin coordinates ($\mathbf{r}_2$ and σ_2, respectively) of the second electron. The Coulomb integral $\langle\varphi_i(1)\varphi_j(2)|\,\frac{1}{r_{12}}\,|\varphi_i(1)\varphi_j(2)\rangle$ is usually written as $\langle\varphi_i\varphi_j|\varphi_i\varphi_j\rangle$ and denoted J_{ij}.
The exchange integral $\langle\varphi_i(1)\varphi_j(2)|\,\frac{1}{r_{12}}\,|\varphi_j(1)\varphi_i(2)\rangle$ is usually written as $\langle\varphi_i\varphi_j|\varphi_j\varphi_i\rangle$ and denoted K_{ij}. The second integral in eq. 2.4.3 is the exchange integral and is a purely quantum-mechanical effect, arising from the antisymmetry of the wave function. The exchange operator is defined through its action on the orbital φ_i

$$\hat{K}_j\,|\varphi_i(1)\rangle = \int \varphi_j(2)^*\frac{1}{r_{12}}\varphi_i(2)\varphi_j(1)\mathrm{d}\mathbf{r}_2\mathrm{d}\sigma_2. \tag{2.4.5}$$

The HF energy is expressed as

$$E_{\mathrm{HF}} = h_{ii} + \frac{1}{2}\sum_{ij}(J_{ij} - K_{ij}). \tag{2.4.6}$$

The optimal energy is obtained through a minimisation procedure with respect to the orbitals. This procedure is based on the variational principle: the HF energy calculated with

a Slater determinant constructed with some chosen orbitals is always larger than or equal to the exact energy of the system,

$$E_{\mathrm{HF}} \geq E_{\mathrm{exact}}. \tag{2.4.7}$$

Therefore, the minimum of the energy functional in eq. 2.4.6 with respect to the orbitals gives the best approximation to the exact energy in the HF framework. The wave function with the lowest energy is found by searching for stationary points in the energy functional, through the minimisation of a Lagrange functional, which imposes the orthonormality of the spin orbitals as constraint. This leads to the *Hartree-Fock* equations

$$\hat{F}\left|\varphi_i\right\rangle = \sum_j \varepsilon_{ij}\left|\varphi_j\right\rangle, \qquad \hat{F} = \hat{h} + \sum_j (\hat{J}_j - \hat{K}_j). \tag{2.4.8}$$

$\hat{F}$ is referred to as the *Fock operator*; the elements ε_{ij} are Lagrange multipliers used in the minimisation. The solution of the HF equations is not unique and the Lagrange multipliers do not have any physical meaning. Applying a unitary transformation $\mathbf{U}$ to the spin orbitals and to the Fock operator, an equivalent formulation of the HF equations is obtained

$$\hat{F}\left|\varphi_i\right\rangle = \sum_j \varepsilon_{ij}\left|\varphi_j\right\rangle \underset{\mathbf{U}}{\rightarrow} \hat{F}\left|\varphi'_i\right\rangle = \sum_j \varepsilon'_{ij}\left|\varphi'_j\right\rangle, \tag{2.4.9}$$

where it has been used that the Fock operator is invariant under unitary transformation, giving $\hat{F}' = \hat{F}$. Without loss of generality, the unitary transformation $\mathbf{U}$ diagonalising $\boldsymbol{\varepsilon}'$ can be chosen, and the so-called *canonical* HF equations are obtained

$$\hat{F}\left|\varphi_i\right\rangle = \varepsilon_i\left|\varphi_i\right\rangle. \tag{2.4.10}$$

ε_i are the elements of the diagonalised matrix, $\varepsilon'_{ij} = \varepsilon_i\delta_{ij}$. These matrix elements can be interpreted as the orbital energies of the orbitals ϕ_i in eq. 2.4.10. A common choice for the spin orbitals is to express them via the product of a spatial orbital and a spin function (either α or β)

$$\varphi_i^{\alpha}(\mathbf{r},\boldsymbol{\sigma}) = \phi_i^{\alpha}(\mathbf{r})\alpha(\boldsymbol{\sigma}) \qquad \varphi_i^{\beta}(\mathbf{r},\boldsymbol{\sigma}) = \phi_i^{\beta}(\mathbf{r})\beta(\boldsymbol{\sigma}). \tag{2.4.11}$$

Integration over the spin coordinate leads to the HF equations depending only on the spatial orbitals. In the case of a closed-shell system, all spatial orbitals are doubly occupied, giving pairs of spin orbitals with the same spatial part, $\phi_i^{\alpha} = \phi_i^{\beta} = \phi_i$. This variant is referred to as *restricted Hartree-Fock (RHF)* method.[174] In the most general case of an open-shell system, the choice of having $\phi_i^{\alpha} = \phi_i^{\beta} = \phi_i^{\mathrm{ROHF}}$ for the doubly-occupied orbitals (*restricted open-shell Hartree-Fock (ROHF)*)[175] maintains solutions for the HF wave function that are eigenfunctions of the spin operators $\hat{S}^2$. However, this might not be the only way to describe an open-shell system, where the most general ansatz of different spatial orbitals for the α and β spin orbitals is often applied, giving $\phi_i^{\alpha} \neq \phi_i^{\beta}$ (*unrestricted Hartree-Fock (UHF)*).[176]

For the solution of the HF equations, the spatial orbitals are usually expressed as a linear combination of atomic orbitals $\{\chi_\mu\}$ (LCAO ansatz)

$$\phi_i^{\sigma} = \sum_\mu c_{\mu i}\chi_\mu, \tag{2.4.12}$$

where $c_{\mu i}$ are the molecular orbital (MO) coefficients.

Substituting the LCAO ansatz in eq. 2.4.10, the *Roothaan-Hall* equations are obtained

$$\mathbf{FC} = \mathbf{SC}\boldsymbol{\varepsilon}, \tag{2.4.13}$$

where $\mathbf{F}$ is the Fock matrix ($F_{\mu\nu} = \langle\chi_\mu|\,\hat{F}\,|\chi_\nu\rangle$), $\mathbf{S}$ the overlap matrix of the basis set ($S_{\mu\nu} = \langle\chi_\mu|\chi_\nu\rangle$). $\mathbf{C}$ are the molecular orbital (MO) coefficients and $\boldsymbol{\varepsilon}$ is the diagonal matrix of the SCF orbital energies.

The MO coefficients are found through diagonalisation of the Fock matrix (after orthogonalisation of the basis set); however, the Fock matrix $\mathbf{F}(\mathbf{C})$ itself depends on the MO coefficients through the Coulomb and the exchange terms $(\mathbf{J}(\mathbf{C}), \mathbf{K}(\mathbf{C}))$. The Roothaan-Hall equations 2.4.13 are pseudo eigenvalue equations and need to be solved iteratively, through the so-called *self-consistent field (SCF)* method. Starting from a guess $\mathbf{C}_0$ matrix, the Fock matrix is diagonalised and new MO coefficients are found, which are used to form the Fock matrix of the next step. This procedure is repeated until self-consistency is reached.

The Hartree-Fock method is the simplest theory describing an atomic or molecular system of N electrons. The HF energy can be seen as the sum of one-electron energies and the interactions of each electron with the mean field generated by all the others. The HF method gives a good approximation of the electronic energy; however, it does not account for the dependence of the motion of the electrons on the position of all other electrons. The only correlation of the electrons accounted for in HF theory comes from the antisymmetric form of the wave function and is achieved through the exchange operator. If a single SD is still sufficient to give a qualitatively correct description of the wave function, the system is said to be *dynamically correlated*.[177,178] However, there are cases in which a single Slater determinant is not able to describe a molecular system in a qualitative correct way (multi-reference character). In these cases, the so-called *static correlation* is needed for a correct description of the electronic structure.[179–181]

A more accurate treatment of electronic correlation is the aim of the *post-HF* methods, i.e., methods trying to describe electron correlation on top of Hartree-Fock theory.

2.4.1 London orbitals

The previous section has discussed the HF theory for the field-free case. In the case of a magnetic field, HF theory can be applied using the magnetic-field Hamiltonian in eq. 2.3.12 instead of the Hamiltonian of the field-free case. A major difference to the field-free Hamiltonian is apparent. Both the orbital-Zeeman and the diamagnetic terms depend on the chosen gauge origin. Shifting the gauge origin results in a different vector potential

$$\mathbf{A}_{\mathrm{G}}(\mathbf{r}) = \frac{1}{2}\mathbf{B} \times (\mathbf{r} - \mathbf{R}_{\mathrm{G}}) = \mathbf{A}_{\mathrm{O}}(\mathbf{r}) - \mathbf{A}_{\mathrm{O}}(\mathbf{R}_{\mathrm{G}}). \tag{2.4.14}$$

A shift in the gauge origin corresponds to a *gauge-origin transformation*, i.e. a transformation changing the gauge-origin without affecting the physical fields:

$$\mathbf{A}_{\mathrm{G}}(\mathbf{r}) = \mathbf{A}_{\mathrm{O}}(\mathbf{r}) + \nabla f \qquad f = \mathbf{A}_{\mathrm{O}}(\mathbf{G}) \cdot \mathbf{r}. \tag{2.4.15}$$

Every gauge-origin transformation can be seen as a unitary transformation of the Hamiltonian

$$(\hat{H}' - i\frac{\partial}{\partial t}) = e^{-if}(\hat{H} - i\frac{\partial}{\partial t})e^{if}. \tag{2.4.16}$$

Requiring that the Schrödinger equation is satisfied in the new gauge,

$$(\hat{H}' - i\frac{\partial}{\partial t})\Psi' = (\hat{H} - i\frac{\partial}{\partial t})\Psi, \tag{2.4.17}$$

the wave function needs to transform accordingly as $\Psi' = e^{-if}\Psi$. A gauge transformation changes the form of the Hamiltonian and of the exact wave function but maintains the values of the observable quantities.

In the specific case of the transformation due to the shift of the gauge origin, the wave function transforms as

$$\Psi_G = e^{i\mathbf{A}_\mathrm{O}(\mathbf{G})\cdot\mathbf{r}}\Psi_O = e^{-\frac{i}{2}\mathbf{B}\times(\mathbf{O}-\mathbf{G})\cdot\mathbf{r}}\Psi_O. \tag{2.4.18}$$

To ease the notation, here $\mathbf{O}$ and $\mathbf{G}$ have been used to indicate $\mathbf{R}_\mathrm{O}$ and $\mathbf{R}_\mathrm{G}$, respectively. This phase factor induces rapid oscillations in the wave functions, which are not correctly described by the standard atomic orbital (AO) basis.[182] In order to solve the problematic dependence on the gauge origin, the phase factor can directly be included in the basis functions

$$|\omega_\mu(\boldsymbol{r},\boldsymbol{B})\rangle = \mathrm{e}^{-\frac{i}{2}\boldsymbol{B}\times(\boldsymbol{K}_\mu-\boldsymbol{O})\cdot\boldsymbol{r}}\,|\chi_\mu(\boldsymbol{r})\rangle\,, \tag{2.4.19}$$

where χ_μ is the standard AO centered at $\mathbf{K}_\mu$. These basis functions are known as *gauge-including atomic orbitals (GIAOs)* or *London orbitals*.[183,184] Calculations with these orbitals are rigorously gauge-origin independent and have been shown to achieve fast basis set convergence.[185]

2.5 Second quantisation

For the description of electronic correlation the wave function needs to be represented by more than one Slater determinant. As the theory complicates, a more intuitive and flexible formalism has to be introduced. In *second quantisation*, SDs are represented as vectors in a vector space:

$$|n\rangle = |n_1, n_2, n_3, \ldots, n_N\rangle \qquad n_i = \begin{cases} 1 & \text{if } \varphi_i \text{ occupied} \\ 0 & \text{if } \varphi_i \text{ unoccupied} \end{cases} \tag{2.5.1}$$

The vector $|n\rangle$ contains the occupation numbers of the ordered spin orbitals and is therefore referred to as *occupation number* (ON) vector. An orthonormal basis of spin orbitals is assumed; the scalar product of two Slater determinants therefore is $\langle n|m\rangle = \delta_{n,m} = \prod_i^N n_i m_i$. In second quantisation, not only observables are represented through operators, but also wave functions can be constructed from *creation* and *annihilation* operators, acting on a given ON vector. The vacuum state, where all spin orbitals are unoccupied, is written as $|\mathrm{vac}\rangle = |0,0,0,\ldots,0\rangle$.

The creation operator is defined through its action of creating an electron in an unoccupied orbital

$$\hat{a}_p^\dagger\,|n\rangle = \Gamma_p \delta_{n_p,0}\,|n_1, n_2, \ldots, 1_p, \ldots, n_N\rangle\,. \tag{2.5.2}$$

Analogously, the annihilation operator annihilates an electron in an occupied orbital

$$\hat{a}_p\,|n\rangle = \Gamma_p \delta_{n_p,1}\,|n_1, n_2, \ldots, 0_p, \ldots, n_N\rangle\,, \tag{2.5.3}$$

where $\Gamma_p = \prod_{i=1}^{p-1}(-1)^{n_i}$.

A specific SD can be expressed as a string of creation operators acting on the vacuum

$$|\Psi\rangle = \hat{a}_i^\dagger \hat{a}_j^\dagger \hat{a}_k^\dagger \ldots |\mathrm{vac}\rangle = |\varphi_i\varphi_j\varphi_k\ldots\rangle\,. \tag{2.5.4}$$

The fermionic properties satisfied by the SD are here automatically fulfilled by their algebra, defined by the anticommutator relations

$$[\hat{a}_p^\dagger, \hat{a}_q^\dagger]_+ = 0, \qquad [\hat{a}_p, \hat{a}_q]_+ = 0, \qquad [\hat{a}_p^\dagger, \hat{a}_q]_+ = \delta_{pq}. \tag{2.5.5}$$

Antisymmetry is guaranteed by $\hat{a}_p^\dagger \hat{a}_q^\dagger = -\hat{a}_q^\dagger \hat{a}_p^\dagger$, while the Pauli principle is given by $\hat{a}_p^\dagger \hat{a}_p^\dagger = 0$.

In second quantisation, one and two-electron operators are

$$\hat{O} = \sum_{pq} o_{pq} \hat{a}_p^\dagger \hat{a}_q \qquad \hat{G} = \frac{1}{4} \sum_{pqrs} g_{pqrs} \hat{a}_p^\dagger \hat{a}_q^\dagger \hat{a}_s \hat{a}_r, \tag{2.5.6}$$

where $o_{pq} = \int \varphi_p^*(\mathbf{r}) \hat{O} \varphi_q(\mathbf{r}) \mathrm{d}\mathbf{r}$ and $g_{pqrs} = \langle \varphi_p \varphi_q || \varphi_r \varphi_s \rangle$.

In second quantisation, expectation values of a given operator can be seen as the expectation value of a string of annihilation and creation operators on a reference state.

A string of operators is called *normal ordered* if all annihilation operators are positioned to the right end of the operator string and the creation operators on the left. This concept is relevant as for a normal-ordered string of operators the expectation value of the vacuum state vanishes,

$$\langle \mathrm{vac} | \, \hat{a}_p^\dagger \hat{a}_q^\dagger \dots \hat{a}_r \hat{a}_s \, | \mathrm{vac} \rangle = 0, \tag{2.5.7}$$

under the condition that the product does not consist of a constant term. For a given string $\hat{X}$ of creation and annihilation operators, its normal order $N(\hat{X})$ is defined as

$$N(\hat{X}) = (-1)^n \hat{a}_p^\dagger \hat{a}_q^\dagger \dots \hat{a}_r \hat{a}_s, \tag{2.5.8}$$

where $(-1)^n$ is the factor accounting for the number n of pairwise swaps needed to obtain a normal ordered string from $\hat{X}$. Note that in general $\hat{X} \neq N(\hat{X})$. Before introducing a central theorem in second quantisation, the *contraction* between two operators is defined. The contraction between the operators $\hat{b}$ and $\hat{c}$, written as $\hat{b}\hat{c}$, needs to be defined as the difference between the product of the two operators and the normal-ordered product of the two operators,

$$\hat{b}\hat{c} = \hat{b}\hat{c} - N(\hat{b}\hat{c}). \tag{2.5.9}$$

For creation and annihilation operators, the following relations apply

$$\hat{a}_p^\dagger \hat{a}_q^\dagger = 0, \qquad \hat{a}_p \hat{a}_q = 0, \qquad \hat{a}_p \hat{a}_q^\dagger = \delta_{pq}, \qquad \hat{a}_p^\dagger \hat{a}_q = 0. \tag{2.5.10}$$

With this mathematical tool, the following theorem (*Wick's theorem*) can be formulated.[186] A string of creation and annihilation operators $\hat{X}$ can be written in normal-ordered form as

$$\hat{X} = N(\hat{X}) + \sum_{\text{contractions}} N(\overbrace{X}) \tag{2.5.11}$$

where $\sum_{\text{contractions}} N(\overbrace{X})$ is the sum of all normal products in which there are one, two, three, *etc.* contractions between the creation or annihilation operators. This formulation is of interest when evaluating the expectation value of $\hat{X}$ on the vacuum state. Only the fully contracted terms, i.e., the terms in which all operators are contracted with another operator in the string, can give a contribution.

In quantum chemistry, a much more adopted reference state is the HF determinant. It is therefore of interest to find a picture in which the HF state can be considered a vacuum state, on which to define creation and annihilation operators. This picture is called *Fermi picture* and considers the formalism of *quasi-particles*. The creation of an electron in the virtual orbitals is seen as the creation of a particle, the annihilation of an electron in the occupied orbitals is seen as the creation of a hole. The holes and particles are therefore the quasi-particles which can be added to the HF-reference state, which is here called *Fermi vacuum*. The corresponding quasi-particle creation and annihilation operators can be formulated

$$\begin{aligned} \hat{b}_a^\dagger &= \hat{a}_a^\dagger \qquad \hat{b}_a = \hat{a}_a \\ \hat{b}_i^\dagger &= \hat{a}_i \qquad \hat{b}_i = \hat{a}_i^\dagger. \end{aligned} \tag{2.5.12}$$

For the quasi-particle operators $\hat{b}_p, \hat{b}_p^\dagger$ the same commutator relations as in eq. 2.5.5 hold. A string of operators can be defined as *normal-ordered* with respect to the Fermi vacuum if all quasi-particle annihilation operators are positioned to the right end of the operator string and the quasi-particle creation operators on the left. In this case, the normal ordering of the operator $\hat{X}$ is written as $\{\hat{X}\}$.
Wick's theorem can be exploited to understand the importance of commutators in quantum chemistry. Here this result is discussed in order to be used in the future discussion. The commutator $[\hat{A}, \hat{B}]$ can be written as

$$[\hat{A}, \hat{B}] = \{\hat{A}\hat{B}\} + \sum_{\text{contractions}} \{\hat{\overbracket{A}\hat{B}}\} - \{\hat{B}\hat{A}\} - \sum_{\text{contractions}} \{\hat{\overbracket{B}\hat{A}}\}. \tag{2.5.13}$$

If both operators have an even number of operators, the relation $\{\hat{A}\hat{B}\} = \{\hat{B}\hat{A}\}$ holds, leaving

$$[\hat{A}, \hat{B}] = \sum_{\text{contractions}} \{\hat{\overbracket{A}\hat{B}}\} - \sum_{\text{contractions}} \{\hat{\overbracket{B}\hat{A}}\}, \tag{2.5.14}$$

showing that only the connected terms (those with at least one contraction) contribute to the commutator.

The Hamilton operator $\hat{H}$ can be related to its normal-ordered form $\hat{H}_N$ via the following relation

$$\hat{H} = E_{\text{HF}} + \sum_{pq} f_{pq} \{\hat{a}_p^\dagger \hat{a}_q\} + \frac{1}{4} \sum_{pqrs} \langle pq||rs\rangle \{\hat{a}_p^\dagger \hat{a}_q^\dagger \hat{a}_s \hat{a}_r\} = E_{\text{HF}} + \hat{H}_N. \tag{2.5.15}$$

2.6 Parameterisation of the correlated wave function

In Hartree-Fock theory, the ground-state wave function is described through a single SD. However, it has been noted that this ansatz does not account for static and dynamic correlation. The *configuration-interaction (CI)* method[187–190] describes the wave function through a linear combination of SD, where the coefficients c_i are determined variationally

$$|\Psi_{\text{CI}}\rangle = \sum_i c_i |\Phi_i\rangle . \tag{2.6.1}$$

Φ_i are Slater determinants and c_i the corresponding expansion coefficients. The CI energy optimisation procedure determines the coefficients

$$\frac{\partial}{\partial c_i} \frac{\langle \Psi_{\text{CI}}| \hat{H} |\Psi_{\text{CI}}\rangle}{\langle \Psi_{\text{CI}}|\Psi_{\text{CI}}\rangle} = 0. \tag{2.6.2}$$

This corresponds to solving the eigenvalue problem $\mathbf{HC} = E\mathbf{C}$, where $\mathbf{C}$ is the vector containing the expansion coefficients. In principle, an exact description of the wave function (within the given AO basis) is obtained by distributing all electrons among all orbitals; this method is called *full configuration interaction (FCI)*.[189,190] However, it is obvious that the number of determinants to be considered scales very rapidly with the number of electrons and orbitals, making FCI not suitable for the treatment of large molecular systems.

The FCI parameterisation can be referred to a particular reference state, for example the HF determinant. In the formalism of second quantisation, the FCI wave function is written as

$$|\Psi_{\text{FCI}}\rangle = \sum_{n=0}^{N} \hat{C}_n |0\rangle \qquad \hat{C}_n = \frac{1}{(n!)^2} \sum_{ijk\ldots}^{abc\ldots} c_{ijk\ldots}^{abc\ldots} \{\hat{a}^\dagger \hat{b}^\dagger \hat{c}^\dagger \ldots \hat{k}\hat{j}\hat{i}\}, \tag{2.6.3}$$

where the excitation operators are grouped in single, double, triple *etc.* excitations with respect to the reference. The creation and annihilation operators are here written in the simplified notation of just writing the indices ($\hat{a}_p$ is indicated by $\hat{p}$ and $\hat{a}_p^\dagger$ by $\hat{p}^\dagger$). The full expansion may be truncated at a chosen excitation level, in order to be feasible for larger systems. Common truncations are CI with double excitations $\hat{C} = \hat{C}_0 + \hat{C}_2$ (CID) and CI with singles and doubles $\hat{C} = \hat{C}_0 + \hat{C}_1 + \hat{C}_2$ (CISD).

The CI methods provide an improvement in the characterisation of molecular energies with respect to HF. However, it shows major problems in the case of the truncated CI expansion. It can be shown that the present ansatz does not satisfy the requirement of *size-extensivity* for the energy, i.e., correct scaling with system size. A given method is said to be size-consitent if, for two non-interacting systems A and B, the following relation is satisfied

$$E_{\mathrm{A+B}} = E_{\mathrm{A}} + E_{\mathrm{B}}. \tag{2.6.4}$$

Here $E_{\mathrm{A+B}}$ labels the energy computed considering A and B as one system, while E_{A} and E_{B} represent the energies of the individual subsystems. The energy does not correctly scale with system size and therefore is not additive. The lack of size-extensivity makes the CI approach not suitable for the description of large molecules.[47]

2.7 Coupled-Cluster Theory

One of the most used developments in electronic structure theory is given by the so-called Coupled Cluster theory. This approach was first introduced in nuclear physics,[191] and then transferred to quantum chemistry by Čížek.[6,192–194] This formalism solves the issue of size-extensivity present in truncated CI methods.
The Coupled-Cluster wave function is parameterised as

$$|\Psi\rangle = e^{\hat{T}} |0\rangle, \tag{2.7.1}$$

where $|0\rangle$ is a reference wave function; for all derivations in this thesis, the HF SD is chosen as reference. The exponential operator consists of the sum of single, double, triple, *etc.* excitations

$$\hat{T} = \hat{T}_1 + \hat{T}_2 + \hat{T}_3 + \ldots, \qquad \hat{T}_n = \frac{1}{(n!)^2} \sum t_{ijk\ldots}^{abc\ldots} \{a^\dagger i b^\dagger j c^\dagger k \ldots\} = t_\mu \hat{\tau}_\mu. \tag{2.7.2}$$

The exponential operator is defined through its Taylor series

$$e^{\hat{T}} = 1 + \hat{T} + \frac{1}{2}\hat{T}^2 + \frac{1}{3!}\hat{T}^3 + \cdots = \sum_n \frac{1}{n!}\hat{T}^n. \tag{2.7.3}$$

In this formulation, each excitation level is not given only by the corresponding *connected excitation* $\hat{T}_n$ operator (for example $\hat{T}_2$ for a double excitation), but also by the so-called *disconnected excitations*, i.e., the product of operators with matching excitation level (for example $\frac{1}{2}\hat{T}_1\hat{T}_1$). A correspondence between the $\hat{T}$ operator of CC and the $\hat{C}$ operator of FCI (eq. 2.6.3) can be established. For the first four orders in excitation

$$\begin{aligned}
\hat{C}_0 &= 1, \\
\hat{C}_1 &= \hat{T}_1, \\
\hat{C}_2 &= \hat{T}_2 + \frac{1}{2}\hat{T}_1^2, \\
\hat{C}_3 &= \hat{T}_3 + \hat{T}_1\hat{T}_2 + \frac{1}{3!}\hat{T}_1^3, \\
\hat{C}_4 &= \hat{T}_4 + \hat{T}_1\hat{T}_3 + \frac{1}{2}\hat{T}_2\hat{T}_1^2 + \frac{1}{2}\hat{T}_2^2 + \frac{1}{4!}\hat{T}_1^4.
\end{aligned} \tag{2.7.4}$$

Furthermore, it can be shown that the full CC expansion is equivalent to FCI.[47,195]

The time independent Schrödinger equation for the CC ansatz becomes

$$\hat{H}e^{\hat{T}}\left|0\right\rangle = E_{\mathrm{CC}}e^{\hat{T}}\left|0\right\rangle. \tag{2.7.5}$$

The CC ground-state energy is found via projection on $\langle 0|\, e^{-\hat{T}}$

$$E_{\mathrm{CC}} = \langle 0|\, e^{-\hat{T}}\hat{H}e^{\hat{T}}\left|0\right\rangle = \langle 0|\,\bar{H}\left|0\right\rangle, \tag{2.7.6}$$

where the notation $\bar{H} = e^{-\hat{T}}\hat{H}e^{\hat{T}}$ for the similarity-transformed Hamiltonian has been adopted. Subtracting the HF energy on both sides, the following expression is obtained

$$\underbrace{(\hat{H} - E_{\mathrm{HF}})}_{\hat{H}_{\mathrm{N}}}e^{\hat{T}}\left|0\right\rangle = \underbrace{(E_{\mathrm{CC}} - E_{\mathrm{HF}})}_{\Delta E_{\mathrm{CC}}}e^{\hat{T}}\left|0\right\rangle. \tag{2.7.7}$$

The projection of this equation on the reference determinant allows to find the CC correlation energy $\Delta E_{\mathrm{CC}} = \langle 0|\,\bar{H}_{\mathrm{N}}\left|0\right\rangle$. The amplitudes t_μ in eq. 2.7.2 are found by projecting eq. 2.7.7 on the set of excited determinants $\{\Phi_\mu\}$ (these equations will be referred to as *amplitude equations*)

$$\langle\Phi_\mu|\, e^{-\hat{T}}\hat{H}_{\mathrm{N}}e^{\hat{T}}\left|0\right\rangle = 0. \tag{2.7.8}$$

Note that $e^{-\hat{T}} \neq e^{\hat{T}^\dagger}$, leading to a non-Hermitian similarity-transformed Hamiltonian. The operator $e^{-\hat{T}}$ is still an excitation operator, while $e^{\hat{T}^\dagger}$ is a de-excitation one. Therefore, the energy expression in the CC framework is not Hermitian.*

It may be shown that the major problem of truncated CI is here solved by the exponential ansatz of CC theory: the energy formulation in eq. 2.7.6 is size-consistent even when the excitation operator is truncated. For two non-interacting systems A and B the wave function is multiplicative,

$$\left|\Psi_{\mathrm{A+B}}\right\rangle = e^{\hat{T}_{\mathrm{A}}+\hat{T}_{\mathrm{B}}}\left|0\right\rangle = e^{\hat{T}_{\mathrm{A}}}e^{\hat{T}_{\mathrm{B}}}\left|0\right\rangle = \mathscr{A}\left|\Psi_{\mathrm{A}}\right\rangle\left|\Psi_{\mathrm{B}}\right\rangle, \tag{2.7.9}$$

where $\mathscr{A}$ is an antisymmetrisation operator. The Hamiltonian of the system $A+B$ can be written as the sum $\hat{H}_{\mathrm{A+B}} = \hat{H}_{\mathrm{A}} + \hat{H}_{\mathrm{B}}$, due to the fact that the two systems A and B are not interacting. The expectation value in eq. 2.7.6 gives

$$\begin{aligned}\langle\Psi_{\mathrm{A+B}}|\,\hat{H}_{\mathrm{A+B}}\left|\Psi_{\mathrm{A+B}}\right\rangle &= \langle 0|\, e^{-\hat{T}_{\mathrm{A}}}e^{-\hat{T}_{\mathrm{B}}}(\hat{H}_{\mathrm{A}} + \hat{H}_{\mathrm{B}})e^{\hat{T}_{\mathrm{A}}}e^{\hat{T}_{\mathrm{B}}}\left|0\right\rangle = \\ &= \langle 0|\, e^{-\hat{T}_{\mathrm{A}}}\hat{H}_{\mathrm{A}}e^{\hat{T}_{\mathrm{A}}}\left|0\right\rangle + \langle 0|\, e^{-\hat{T}_{\mathrm{B}}}\hat{H}_{\mathrm{B}}e^{\hat{T}_{\mathrm{B}}}\left|0\right\rangle = E_{\mathrm{A}} + E_{\mathrm{B}}.\end{aligned} \tag{2.7.10}$$

The cross terms $\langle 0|\, e^{-\hat{T}_{\mathrm{A}}}\hat{H}_{\mathrm{B}}e^{\hat{T}_{\mathrm{A}}}\left|0\right\rangle$ and $\langle 0|\, e^{-\hat{T}_{\mathrm{B}}}\hat{H}_{\mathrm{A}}e^{\hat{T}_{\mathrm{B}}}\left|0\right\rangle$ vanish, as the Hamilton operator of one system does not act on the wave function of the other system. This proof shows that the CC energy is size-consistent.[47]

In order to derive CC working equations, the similarity-transformed Hamiltonian needs to be expanded. For two generic operators $\hat{A}, \hat{B}$, the *Baker-Campbell-Hausdorff* (BCH) equation[50] holds

$$\begin{aligned}e^{-\hat{B}}\hat{A}e^{\hat{B}} &= \hat{A} + [\hat{A},\hat{B}] + \frac{1}{2}[[\hat{A},\hat{B}],\hat{B}] + \frac{1}{3!}[[[\hat{A},\hat{B}],\hat{B}],\hat{B}] + \frac{1}{4!}[[[[\hat{A},\hat{B}],\hat{B}],\hat{B}],\hat{B}] + \cdots = \\ &= \sum_n \frac{1}{n!}\underbrace{[[[[\hat{A},\hat{B}],\hat{B}],\ldots],\hat{B}]}_{n\text{ commutators}}.\end{aligned} \tag{2.7.11}$$

*With slightly improper wording, in this thesis the expression *non-Hermitian energy* refers to the fact that the CC energy is defined through the expectation value of a non-Hermitian operator.

The similarity-transformed Hamiltonian becomes

$$e^{-\hat{T}}\hat{H}_{\mathrm{N}}e^{\hat{T}} = \hat{H}_{\mathrm{N}} + [\hat{H}_{\mathrm{N}},\hat{T}] + \frac{1}{2}[[\hat{H}_{\mathrm{N}},\hat{T}],\hat{T}] + \frac{1}{3!}[[[\hat{H}_{\mathrm{N}},\hat{T}],\hat{T}],\hat{T}] + \frac{1}{4!}[[[[\hat{H}_{\mathrm{N}},\hat{T}],\hat{T}],\hat{T}],\hat{T}] + \dots \tag{2.7.12}$$

This expansion can be evaluated by means of Wick's theorem (eq. 2.5.14). Both $\hat{H}_{\mathrm{N}}$ and $\hat{T}$ satisfy the conditions of being normal ordered and with an even number on creation or annihilation operators; in addition, noone of these operators possesses a constant part. Therefore, in eq. 2.7.12 only connected terms are obtained. It is apparent that the Hamiltonian can be connected at most with four $\hat{T}$ operators, as it is a two-electron operator made of four creation or annihilation operators. The BCH expansion truncates after the fourth commutator and the following expansion is exact

$$e^{-\hat{T}}\hat{H}_{\mathrm{N}}e^{\hat{T}} = \hat{H}_{\mathrm{N}} + [\hat{H}_{\mathrm{N}},\hat{T}] + \frac{1}{2}[[\hat{H}_{\mathrm{N}},\hat{T}],\hat{T}] + \frac{1}{3!}[[[\hat{H}_{\mathrm{N}},\hat{T}],\hat{T}],\hat{T}] + \frac{1}{4!}[[[[\hat{H}_{\mathrm{N}},\hat{T}],\hat{T}],\hat{T}],\hat{T}]. \tag{2.7.13}$$

2.7.1 Equation-Of-Motion Coupled-Cluster (EOM-CC) Theory

A treatment of excited states is obtained by means of the so-called *Equation-Of-Motion* CC theory.[16,22–24,32,33,196] The excited states are parameterised via an excitation operator acting on the CC ground state

$$|\Psi_{\mathrm{exc}}\rangle = \hat{R}e^{\hat{T}}|0\rangle, \tag{2.7.14}$$

where $\hat{R}$ is a linear excitation operator of the form

$$\hat{R} = r_0 + \hat{R}_1 + \hat{R}_2 + \hat{R}_3 + \dots \qquad \hat{R}_n = \frac{1}{(n!)^2}\sum r^{abc\dots}_{ijk\dots}\{a^\dagger i b^\dagger j c^\dagger k \dots\} = r_\mu \hat{\tau}_\mu. \tag{2.7.15}$$

The Schrödinger equation for an excited state is

$$\hat{H}\hat{R}e^{\hat{T}}|0\rangle = E_{\mathrm{exc}}\hat{R}e^{\hat{T}}|0\rangle. \tag{2.7.16}$$

The excitation energy $\Delta E_{\mathrm{exc}} = E_{\mathrm{exc}} - E_{\mathrm{CC}}$ can be isolated and the following equation is obtained

$$\begin{aligned} \underbrace{(\hat{H} - E_{\mathrm{CC}})}_{(\hat{H}_{\mathrm{N}} + E_{\mathrm{HF}} - E_{\mathrm{CC}})}\ \hat{R}e^{\hat{T}}|0\rangle &= \underbrace{(E_{\mathrm{exc}} - E_{\mathrm{CC}})}_{\Delta E_{\mathrm{exc}}}\hat{R}e^{\hat{T}}|0\rangle \\ \hat{H}_{\mathrm{N}}\hat{R}e^{\hat{T}}|0\rangle - \underbrace{(E_{\mathrm{CC}} - E_{\mathrm{HF}})\hat{R}e^{\hat{T}}}_{\hat{R}\hat{H}_{\mathrm{N}}e^{T}}|0\rangle &= \Delta E_{\mathrm{exc}}\hat{R}e^{\hat{T}}|0\rangle. \end{aligned} \tag{2.7.17}$$

By multiplying with $e^{-\hat{T}}$ from the left and by noting that $[\hat{R},\hat{T}] = 0$, as both $\hat{R}$ and $\hat{T}$ are excitation operators, the following equation is obtained

$$e^{-\hat{T}}\hat{H}_{\mathrm{N}}e^{\hat{T}}\hat{R}|0\rangle - \hat{R}e^{-\hat{T}}\hat{H}_{\mathrm{N}}e^{\hat{T}}|0\rangle = \Delta E_{\mathrm{exc}}\hat{R}|0\rangle \implies [\bar{H}_{\mathrm{N}},\hat{R}]|0\rangle = \Delta E_{\mathrm{exc}}\hat{R}|0\rangle. \tag{2.7.18}$$

The r_μ amplitudes in eq. 2.7.15 are determined through projection on the excited determinants

$$\langle\Phi_\mu|[\bar{H}_{\mathrm{N}},\hat{R}]|0\rangle = \Delta E_{\mathrm{exc}}\underbrace{\langle\Phi_\mu|\hat{R}|0\rangle}_{r_\mu} \implies \sum_{\mu\nu}(\bar{H}_{\mathrm{N}})_{C,\mu\nu}r_\nu = \Delta E_{\mathrm{exc}}r_\mu, \tag{2.7.19}$$

or, in matrix form

$$\bar{\mathbf{H}}_{\mathrm{N}}\mathbf{R} = \Delta E_{\mathrm{exc}}\mathbf{R}. \tag{2.7.20}$$

Usually this form is preferred to the one in eq. 2.7.16, as the ground-state solution has already been found with the CC ansatz. Note that eq. 2.7.20 is a CI-like problem.

The matrix $\mathbf{A}$ with real eigenvalue λ may be considered.* The left eigenvector $\mathbf{v}$ of a non-Hermitian square matrix $\mathbf{A}$ does not correspond to the right eigenvector $\mathbf{u}$ with same real eigenvalue λ:

$$\mathbf{v}^\dagger\mathbf{A} = \lambda\mathbf{v}^\dagger, \qquad \mathbf{A}\mathbf{u} = \lambda\mathbf{u} \text{ where } \mathbf{v} \neq \mathbf{u}. \tag{2.7.21}$$

The similarity-transformed Hamiltonian matrix is non-Hermitian and therefore has a set of right-hand side eigenvectors and a different set of left-hand side eigenvectors, which are not simply obtainable by conjugation of the right eigenstates.

In the framework of EOM-CC theory, these are parameterised through a de-excitation operator $\hat{L}$

$$\langle\Psi_{\mathrm{exc}}| = \langle 0|\,\hat{L}e^{-\hat{T}}, \tag{2.7.22}$$

with the definition

$$\hat{L} = l_0 + \sum_{ia} l_a^i\{\hat{i}^\dagger\hat{a}\} + \frac{1}{4}\sum_{ijab} l_{ab}^{ij}\{\hat{i}^\dagger\hat{j}^\dagger\hat{b}\hat{a}\} + \cdots = \sum_\mu l_\mu\tau_\mu^\dagger. \tag{2.7.23}$$

This parameterisation does not allow $\hat{L}$ and $e^{-\hat{T}}$ to swap places, as the two operators do not commute: $[\hat{L}, e^{-\hat{T}}] \neq 0$.

The Schrödinger equation for the left eigenstate reads

$$\langle 0|\,\hat{L}e^{-\hat{T}}\hat{H} = E_{\mathrm{CC}}\,\langle 0|\,\hat{L}e^{-\hat{T}}. \tag{2.7.24}$$

Multiplying with $e^{\hat{T}}$ from the right, and projecting on the excited determinants, the matrix equation is

$$\mathbf{L}\bar{\mathbf{H}}_{\mathrm{N}} = \mathbf{L}\Delta E_{\mathrm{exc}}. \tag{2.7.25}$$

The operators $\hat{L}$ and $\hat{R}$ satisfy the so-called *biorthonormality condition*

$$\langle\Psi_m|\Psi_n\rangle = \delta_{mn} \implies \langle 0|\,\hat{L}_m e^{-\hat{T}}e^{\hat{T}}\hat{R}_n\,|0\rangle = \langle 0|\,\hat{L}_m\hat{R}_n\,|0\rangle = \delta_{mn}. \tag{2.7.26}$$

Note that the CC ground state can be expressed by means of the EOM-CC parameterisation taking $\hat{R} = \hat{1}$. Furthermore, the presence of a non-zero r_0 term in eq. 2.7.15 for the parameterisation of the excited states implies that a contribution from the ground state can be present in the excited states. For the left-side ground state $\langle\Psi_{\mathrm{GS}}| = \langle 0|\,\hat{L}_0e^{-\hat{T}}$, the amplitude equation gives

$$\langle 0|\,\hat{L}_0\bar{H}\,|\Phi_\mu\rangle = 0 \implies \langle 0|\,\hat{L}_0\bar{H}\hat{\tau}_\mu\,|0\rangle = 0. \tag{2.7.27}$$

This expression will be again encountered in the calculation of CC ground-state properties in sec. 2.8. The parameterisation of $\hat{L}_0$ is analogous to the response operator $\hat{\Lambda}$, which is found there

$$\langle\Psi_{\mathrm{GS}}| = \langle 0|\,(1+\hat{\Lambda})e^{-\hat{T}} \qquad \hat{\Lambda} = \sum_{ia}\lambda_a^i\{\hat{i}^\dagger\hat{a}\} + \frac{1}{4}\sum_{ijab}\lambda_{ab}^{ij}\{\hat{i}^\dagger\hat{j}^\dagger\hat{b}\hat{a}\} + \cdots = \sum_\mu\lambda_\mu\tau_\mu^\dagger. \tag{2.7.28}$$

*Note that for a square matrix with real eigenvalues, the left and right eigenvalues are the same. This can be easily seen, noting that the eigenvalues of $\mathbf{A}$ and of $\mathbf{A}^\dagger$ are the same. In fact, take the left eigenvector $\mathbf{v}$, which satisfies the eigenvalue equation $\mathbf{v}^\dagger\mathbf{A} = \lambda\mathbf{v}^\dagger$. Performing the transposition of this relation, $\mathbf{A}^\dagger\mathbf{v} = \lambda\mathbf{v}$ is obtained, for real values of λ. Therefore, λ is also an eigenvalue of $\mathbf{A}^\dagger$. As stated above, eigenvalues of a square matrix and its transpose are the same. Therefore, the left and right eigenvalues of a square matrix are the same.

For all other states, l_0 needs to be zero, in order to satisfy the biorthonormality condition $\langle 0|\hat{L}_k\hat{R}_0|0\rangle = 0$, for every excited state k.

At this point it has to be noted that the left eigenstates are not needed for the calculation of excited states energies. For that, diagonalisation of eq. 2.7.20 leads to the right eigenstates and excited-state energies. Only when computing molecular properties, the left eigenstates are also needed.

2.7.2 Unphysical results in CC theory

CC theory offers an accurate treatment of the correlation energy, getting more and more accurate when going to higher truncations of the excitation space. In almost all cases, the calculated energies are real. However, it has been documented in literature that complex energy values can occur.[9,34,197,198] These cases are discussed hereafter.

- Hättig[197] first noted that complex excited-state energies appear in vicinity of conical intersections,[199–202] where the potential energy surfaces of two states coincide.[34] In the case of a conical intersection, the Hamiltonian matrix is real, and in the FCI framework the energy values are real. In ref. 35 it has been shown that a real Hamiltonian matrix can have complex eigenvalues in the case of a defective matrix.[198] A matrix is called defective when it presents an eigenvalue of multiplicity $m > 1$, but only fewer than m eigenvectors. A defective matrix therefore is not diagonalisable. In ref. 35 it has been discussed that varying the entries of a given matrix in a continuous manner, the eigenvalues also vary continuously and may do the transition from real to complex passing via a multiple eigenvalue, i.e., a point of degeneracy. This general mathematical observation can be exploited for the investigation of the eigenvalues of the Hamiltonian matrix in proximity of a conical intersection. A continuous variation of the matrix elements of the FCI Hamiltonian can be constructed to connect the FCI matrix to the EOM-CC Hamiltonian matrix. The FCI eigenvalues are known to be real; on the connection to the EOM-CC matrix, they are also varying in a continuous manner. If two eigenvalues are very close in the FCI case, they may coincide for some point on the connection going to EOM-CCSD, becoming degenerate, i.e. an intersection of the potential energy surfaces occurs. As stated before for a generic matrix, it was shown that complex energy values can occur after the degeneracy. A continuous connection can be constructed between the FCI and EOM-CC energy values. When two FCI eigenvalues are very close to each other, it may happen that they coincide on the connection between FCI and EOM-CC, leading to a defective Hamiltonian matrix: complex energies are demonstrated to occur in pairs of conjugated eigenvalues. In ref. 35 it was also shown that a qualitatively wrong description of the intersection is obtained.

- In the case of a complex-valued Hamiltonian matrix, as for example the finite-field one,[65,108,114] the eigenvalues of the FCI Hamiltonian matrix are still real. Exploiting the same idea of a continuous connection from the FCI to the CC Hamiltonian, it is shown in ref. 35 that every deviation from the FCI matrix which breaks the Hermiticity can lead to the occurrence of complex eigenvalues. Unlike what was demonstrated for a real-valued Hamiltonian matrix, eigenvalues do not have to appear in pairs. In ref. 35, complex eigenvalues have been observed for various systems. For the examples reported, the imaginary part of the EOM-CCSD energies is always of the same order of magnitude as the difference between the real part of the exact FCI results and the EOM-CCSD ones.

- It can be mentioned at this point that a complex-valued Hamiltonian matrix can also be obtained in relativistic calculations including spin-orbit coupling.[203–206] The same kind of reasoning which applies to the CC description of systems in a magnetic field can thus be continued here. However, the spin-orbit coupling is usually a small contribution and, unlike the magnetic field, its value is fixed.

- Another limit of CC theory is found in the description of systems characterised by a complex Abelian point group. These point groups possess pairs of complex irreducible representations. The excited states belonging to the complex irreducible representations have a complex wave function and are degenerate in exact theory.[207] The exact degeneracy allows to form real linear combinations of the wave functions which are real. Therefore, despite the single wave functions being complex, the computation can be performed with real numbers only. In the framework of EOM-CC theory, the non-Hermiticity of the similarity-transformed Hamiltonian matrix leads to a lift in the degeneracy, giving pairs of complex-conjugate energy values. In the EOM-CC framework it is therefore not possible to form real linear combinations from the complex wave functions of the pairs of states. This computation is therefore simply not possible with the EOM-CC method via a real code; with a complex code, an imaginary part is found.

The imaginary part in the CC energies may be considered as a deficiency of the CC theory. Ignoring the problem and taking only the real part of the results is not mathematically rigorous and can possibly lead to an incorrect description of the system. In this thesis, the idea of a Hermitian Coupled Cluster formalism is pursued, in order to avoid the occurrence of unphysical results by construction.

Note that the discussion in this chapter focuses on the cases in which complex energies are a consequence of the non-Hermiticity of the CC and EOM-CC energy expression. This is different in the field of electronic resonances, where non-Hermitian quantum mechanics is developed to study decay processes. In the field of resonances, the theory is constructed in a way that a physical interpretation of the imaginary part of the energy can be given, as it is related to the lifetime of metastable states.[208–211]

2.8 Molecular properties

The calculation of energies is often not sufficient to characterise the complexity of a molecular system. A more complete description can be achieved, for example, considering molecular properties, which play an important role in many experimental applications, for example in the world of spectroscopy. The development of a formalism for the calculation of molecular properties has been and is therefore of major importance to predict the behaviour of molecular systems. In this section, the case of an exact parameterisation of the wave function is analysed; then the case of an approximate parameterisation is considered, with a focus on CC and UCC. The theory developed in this thesis will be discussed in future publications.[212,213]

2.8.1 Single-state properties

The aim of this section is to formulate a theory for the calculation of UCC properties. Starting from the expression known from quantum mechanics, a convenient reformulation of this expression is discussed, in order to obtain a formalism suitable for truncated and non-variational wave functions, as in the case of UCC theory.

The most intuitive approach to the calculation of properties is provided by quantum mechanics, where a property X is usually computed taking the expectation value of the corresponding operator $\hat{X}$

$$X = \langle \Psi | \hat{X} | \Psi \rangle . \tag{2.8.1}$$

One may apply this intuitive formulation to approximate theories, as for example CC theory. However, it is discussed later in this chapter that the formalism of expectation values in the EOM-CC framework is not *size-extensive*.[214] It is preferable to find a formalism which can be exploited both by CC and UCC theory.

The discussion starts by analysing the problems arising from the application of eq. 2.8.1 in CC theory. First, a mathematical framework for the understanding of size-extensivity is constructed and applied to CC theory.

Locality and additivity of operators

The concept of the size-extensivity of a method is usually formulated analysing the energy, but it can be generalised to properties. A method is said to be size-extensive if for two non-interacting systems A and B the energy of the joint system $A+B$ corresponds to the sum of the energy of subsystem A and the energy of subsystem B.

$$E_{\mathrm{A+B}} = E_{\mathrm{A}} + E_{\mathrm{B}} \tag{2.8.2}$$

Here $E_{\mathrm{A+B}}$ labels the energy of the system given by both subsystems A and B, while E_{A} and E_{B} represent the energies of the individual systems calculated in absence of the other system. From a physical point of view, size-extensivity is required also for molecular dipoles. An insightful analysis of the behaviour of the operators involved in the calculation of properties is needed for the development of a theory satisfying the physical requirement of size-extensivity. For a rigorous discussion, the concepts of *local*, *additive*, and *semi-additive* operators are useful to be introduced.

Assume a set of MOs localised either on subsystem A or on subsystem B. The operators discussed in this section are assumed not to have a constant term. An operator is *local* if it consists only of sums of strings of creation/annihilation operators localised on the same fragment,

$$\hat{O}_{\mathrm{A+B}} = \hat{O}_{\mathrm{A}} + \hat{O}_{\mathrm{B}}. \tag{2.8.3}$$

Most physical operators are local, for example the dipole operator, the Hamilton operator, *etc.* It is therefore important to understand their features before applying the discussion to quantum chemistry.
An operator is *non-local* when an extra term contributes to the operator of the joint system, localised neither completely on A nor on B,

$$\hat{O}_{\mathrm{A+B}} = \hat{O}_{\mathrm{A}} + \hat{O}_{\mathrm{B}} + \hat{O}_{\mathrm{AB}}. \tag{2.8.4}$$

An example of a non-local operator is the spin operators, as the spin of a joint system cannot be determined from spin operators based on each fragment.
The behaviour of the CI-expansion operator $\hat{C}$ (sec. 2.6) can be analysed as an example. From the discussion of the CI wave function, it is here recalled that the wave functions for the single systems A and B are, respectively, $|\Psi_{\mathrm{CI}}\rangle_{\mathrm{A}} = \sum_n \hat{C}_n^{\mathrm{A}} |0\rangle$, and $|\Psi_{\mathrm{CI}}\rangle_{\mathrm{B}} = \sum_n \hat{C}_n^{\mathrm{B}} |0\rangle$. Let's assume the $\hat{C}$ operator is local. Then the operator of the system $A+B$ is $\hat{C}^{\mathrm{A+B}} = \hat{C}^{\mathrm{A}} + \hat{C}^{\mathrm{B}}$, giving the wave function $|\Psi_{\mathrm{A+B}}\rangle = \sum_n (\hat{C}_n^{\mathrm{A}} + \hat{C}_n^{\mathrm{B}}) |0\rangle$. The wave function for the system $A+B$ is therefore a linear combination of determinants describing either excitations of system A or of system B, but is not able to describe the case in which both systems are simultaneously

excited. In order to describe such a state, an operator $\hat{C}_{\mathrm{AB}}$ needs to be introduced, giving $\hat{C}_{\mathrm{A+B}} = \hat{C}_{\mathrm{A}} + \hat{C}_{\mathrm{B}} + \hat{C}_{\mathrm{AB}}$. The CI-operator $\hat{C}$ is therefore a non-local operator.

A local operator is called *additive* when the operators $\hat{O}_{\mathrm{A}}$ and $\hat{O}_{\mathrm{B}}$ in eq. 2.8.3 correspond to the operators defined when considering only system A or only system B, respectively.
A non-local operator is called *semi-additive* if the operators $\hat{O}_{\mathrm{A}}$ and $\hat{O}_{\mathrm{B}}$ in eq. 2.8.4 are the same operators as those for the isolated system A or for the isolated system B, respectively.

The calculation of properties involves expectation values of the form $\langle\Psi|\,\hat{X}\,|\Psi\rangle$. For the properties of interest in this thesis. The operator $\hat{X}$ is additive, giving $\hat{X}_{\mathrm{A+B}} = \hat{X}_{\mathrm{A}} + \hat{X}_{\mathrm{B}}$. However, this is not sufficient to obtain a size-extensive formulation of the properties, as the operators parameterising the wave function need to be considered as well. In order to understand under which circumstances the expression $\langle\Psi|\,\hat{X}\,|\Psi\rangle$ is size-extensive, the products of operators are analysed. The product of two local additive normal-ordered operators $\hat{O}_{\mathrm{A+B}}$ and $\hat{Q}_{\mathrm{A+B}}$ is not local, as cross terms arise which are not localised on just one fragment

$$\hat{O}_{\mathrm{A+B}}\hat{Q}_{\mathrm{A+B}} = \hat{O}_{\mathrm{A}}\hat{Q}_{\mathrm{A}} + \hat{O}_{\mathrm{B}}\hat{Q}_{\mathrm{B}} + \hat{O}_{\mathrm{A}}\hat{Q}_{\mathrm{B}} + \hat{O}_{\mathrm{B}}\hat{Q}_{\mathrm{A}}. \tag{2.8.5}$$

However, assuming that the operators do not have any constant terms, the expectation value with respect to the Fermi vacuum is additive, as the cross terms vanish,

$$\langle 0|\,\hat{O}_{\mathrm{A+B}}\hat{Q}_{\mathrm{A+B}}\,|0\rangle = \langle 0|\,\hat{O}_{\mathrm{A}}\hat{Q}_{\mathrm{A}}\,|0\rangle + \langle 0|\,\hat{O}_{\mathrm{B}}\hat{Q}_{\mathrm{B}}\,|0\rangle + \langle 0|\,\hat{O}_{\mathrm{A}}\hat{Q}_{\mathrm{B}}\,|0\rangle + \langle 0|\,\hat{O}_{\mathrm{B}}\hat{Q}_{\mathrm{A}}\,|0\rangle\,. \tag{2.8.6}$$

The product of two local operators $\hat{O}$ and $\hat{Q}$ in normal order can be analysed through Wick's theorem (eq. 2.5.14):

$$\langle 0|\,\hat{O}\hat{Q}\,|0\rangle = \underbrace{\langle 0|\,\{\hat{O}\hat{Q}\}\,|0\rangle}_{=0} + \sum_{\text{contractions}} \langle 0|\,\overbrace{\hat{O}\hat{Q}}\,|0\rangle \tag{2.8.7}$$

The only non-vanishing contributions come from the fully contracted terms. For the products in eq. 2.8.6, contractions are only possible between either $\hat{O}_{\mathrm{A}}$ and $\hat{Q}_{\mathrm{A}}$ or $\hat{O}_{\mathrm{B}}$ and $\hat{Q}_{\mathrm{B}}$, while the cross terms are disconnected (they cannot be contracted as they cannot have any orbital indices in common, due to the fact that the orbitals are localised on different fragments). Their expectation values therefore vanish, leading to an additive expression for the expectation value of the product of two additive operators,

$$\langle 0|\,\hat{O}_{\mathrm{A+B}}\hat{Q}_{\mathrm{A+B}}\,|0\rangle = \langle 0|\,\hat{O}_{\mathrm{A}}\hat{Q}_{\mathrm{A}}\,|0\rangle + \langle 0|\,\hat{O}_{\mathrm{B}}\hat{Q}_{\mathrm{B}}\,|0\rangle\,. \tag{2.8.8}$$

Furthermore, it holds that the commutator of two additive operators is additive, as the commutator of two operators localised on two different non-interacting fragments vanishes,

$$[\hat{O}_{\mathrm{A+B}}, \hat{Q}_{\mathrm{A+B}}] = [\hat{O}_{\mathrm{A}}, \hat{Q}_{\mathrm{A}}] + [\hat{O}_{\mathrm{B}}, \hat{Q}_{\mathrm{B}}] + [\hat{O}_{\mathrm{A}}, \hat{Q}_{\mathrm{B}}] + [\hat{O}_{\mathrm{B}}, \hat{Q}_{\mathrm{A}}] = [\hat{O}_{\mathrm{A}}, \hat{Q}_{\mathrm{A}}] + [\hat{O}_{\mathrm{B}}, \hat{Q}_{\mathrm{B}}]. \tag{2.8.9}$$

In the case of the product of an additive operator $\hat{O}_{\mathrm{A+B}} = \hat{O}_{\mathrm{A}} + \hat{O}_{\mathrm{B}}$ and a semi-additive operator $\hat{Q}_{\mathrm{A+B}} = \hat{Q}_{\mathrm{A}} + \hat{Q}_{\mathrm{B}} + \hat{Q}_{\mathrm{AB}}$, the cross terms need to be analysed,

$$\begin{aligned}\langle 0|\,\hat{O}_{\mathrm{A+B}}\hat{Q}_{\mathrm{A+B}}\,|0\rangle = {} & \langle 0|\,\hat{O}_{\mathrm{A}}\hat{Q}_{\mathrm{A}}\,|0\rangle + \langle 0|\,\hat{O}_{\mathrm{B}}\hat{Q}_{\mathrm{B}}\,|0\rangle + \langle 0|\,\hat{O}_{\mathrm{B}}\hat{Q}_{\mathrm{AB}}\,|0\rangle + \langle 0|\,\hat{O}_{\mathrm{A}}\hat{Q}_{\mathrm{AB}}\,|0\rangle + \\ & \langle 0|\,\hat{O}_{\mathrm{B}}\hat{Q}_{\mathrm{A}}\,|0\rangle + \langle 0|\,\hat{O}_{\mathrm{A}}\hat{Q}_{\mathrm{B}}\,|0\rangle\,.\end{aligned} \tag{2.8.10}$$

As before, the terms $\langle 0|\,\hat{O}_{\mathrm{B}}\hat{Q}_{\mathrm{A}}\,|0\rangle$ and $\langle 0|\,\hat{O}_{\mathrm{A}}\hat{Q}_{\mathrm{B}}\,|0\rangle$ vanish, as they cannot be fully contracted in the formalism of Wick's theorem. The terms arising from the lack of additivity, $\langle 0|\,\hat{O}_{\mathrm{B}}\hat{Q}_{\mathrm{AB}}\,|0\rangle$ and $\langle 0|\,\hat{O}_{\mathrm{A}}\hat{Q}_{\mathrm{AB}}\,|0\rangle$, also vanish, because of the same reason. In fact, the orbitals localised on fragment B, contributing to $\hat{Q}_{\mathrm{AB}}$, cannot be contracted with orbitals of $\hat{O}_{\mathrm{A}}$, as this operator is local; therefore $\langle 0|\,\hat{O}_{\mathrm{A}}\hat{Q}_{\mathrm{AB}}\,|0\rangle$ vanishes. The same reasoning is valid

for $\langle 0|\hat{O}_{\mathrm{B}}\hat{Q}_{\mathrm{AB}}|0\rangle$. From this result, it appears that the expectation value of the product of an additive and a semi-additive operator is additive, giving:

$$\langle 0|(\hat{O}_{\mathrm{A}}+\hat{O}_{\mathrm{B}})(\hat{Q}_{\mathrm{A}}+\hat{Q}_{\mathrm{B}}+\hat{Q}_{\mathrm{AB}})|0\rangle = \langle 0|\hat{O}_{\mathrm{A}}\hat{Q}_{\mathrm{A}}|0\rangle + \langle 0|\hat{O}_{\mathrm{B}}\hat{Q}_{\mathrm{B}}|0\rangle . \tag{2.8.11}$$

Additivity also needs to be discussed for products of two semi-additive operators,

$$\begin{aligned}&\langle 0|(\hat{O}_{\mathrm{A}}+\hat{O}_{\mathrm{B}}+\hat{O}_{\mathrm{AB}})(\hat{Q}_{\mathrm{A}}+\hat{Q}_{\mathrm{B}}+\hat{Q}_{\mathrm{AB}})|0\rangle = \langle 0|\hat{O}_{\mathrm{A}}\hat{Q}_{\mathrm{A}}|0\rangle + \langle 0|\hat{O}_{\mathrm{B}}\hat{Q}_{\mathrm{B}}|0\rangle + \\ &\langle 0|\hat{O}_{\mathrm{B}}\hat{Q}_{\mathrm{AB}}|0\rangle + \langle 0|\hat{O}_{\mathrm{A}}\hat{Q}_{\mathrm{AB}}|0\rangle + \langle 0|\hat{O}_{\mathrm{AB}}\hat{Q}_{\mathrm{A}}|0\rangle + \langle 0|\hat{O}_{\mathrm{AB}}\hat{Q}_{\mathrm{B}}|0\rangle + \\ &\langle 0|\hat{O}_{\mathrm{B}}\hat{Q}_{\mathrm{A}}|0\rangle + \langle 0|\hat{O}_{\mathrm{A}}\hat{Q}_{\mathrm{B}}|0\rangle + \langle 0|\hat{O}_{\mathrm{AB}}\hat{Q}_{\mathrm{AB}}|0\rangle .\end{aligned} \tag{2.8.12}$$

Following the considerations of the two preceding cases, the non-vanishing terms are

$$\langle 0|(\hat{O}_{\mathrm{A}}+\hat{O}_{\mathrm{B}}+\hat{O}_{\mathrm{AB}})(\hat{Q}_{\mathrm{A}}+\hat{Q}_{\mathrm{B}}+\hat{Q}_{\mathrm{AB}})|0\rangle = \langle 0|\hat{O}_{\mathrm{A}}\hat{Q}_{\mathrm{A}}|0\rangle + \langle 0|\hat{O}_{\mathrm{B}}\hat{Q}_{\mathrm{B}}|0\rangle + \langle 0|\hat{O}_{\mathrm{AB}}\hat{Q}_{\mathrm{AB}}|0\rangle , \tag{2.8.13}$$

where the last term introduces a non-additive contribution in the expectation value.

In quantum chemistry, expectation values involving more than two operators are evaluated for the calculation of molecular energies and properties. Assuming the operators $\hat{Q}_{\mathrm{A+B}}$ and $\hat{S}_{\mathrm{A+B}}$ to be additive and the operator $\hat{O}_{\mathrm{A+B}}$ to be semi-additive, the expectation value of the product $\hat{O}_{\mathrm{A+B}}\hat{S}_{\mathrm{A+B}}\hat{Q}_{\mathrm{A+B}}$ is discussed,

$$\begin{aligned}&\langle 0|\hat{O}_{\mathrm{A+B}}\hat{S}_{\mathrm{A+B}}\hat{Q}_{\mathrm{A+B}}|0\rangle = \langle 0|(\hat{O}_{\mathrm{A}}+\hat{O}_{\mathrm{B}}+\hat{O}_{\mathrm{AB}})(\hat{S}_{\mathrm{A}}+\hat{S}_{\mathrm{B}})(\hat{Q}_{\mathrm{A}}+\hat{Q}_{\mathrm{B}})|0\rangle = \\ &= \langle 0|\hat{O}_{\mathrm{A}}\hat{S}_{\mathrm{A}}\hat{Q}_{\mathrm{A}}|0\rangle + \langle 0|\hat{O}_{\mathrm{B}}\hat{S}_{\mathrm{B}}\hat{Q}_{\mathrm{B}}|0\rangle + \langle 0|\hat{O}_{\mathrm{AB}}\hat{S}_{\mathrm{A}}\hat{Q}_{\mathrm{B}}|0\rangle + \langle 0|\hat{O}_{\mathrm{AB}}\hat{S}_{\mathrm{B}}\hat{Q}_{\mathrm{A}}|0\rangle + \\ &\underbrace{\langle 0|\hat{O}_{\mathrm{A}}\hat{S}_{\mathrm{B}}\hat{Q}_{\mathrm{B}}|0\rangle}_{=0} + \underbrace{\langle 0|\hat{O}_{\mathrm{B}}\hat{S}_{\mathrm{A}}\hat{Q}_{\mathrm{A}}|0\rangle}_{=0} + \underbrace{\langle 0|\hat{O}_{\mathrm{AB}}\hat{S}_{\mathrm{A}}\hat{Q}_{\mathrm{A}}|0\rangle}_{=0} + \underbrace{\langle 0|\hat{O}_{\mathrm{AB}}\hat{S}_{\mathrm{B}}\hat{Q}_{\mathrm{B}}|0\rangle}_{=0} = \\ &= \langle 0|\hat{O}_{\mathrm{A}}\hat{S}_{\mathrm{A}}\hat{Q}_{\mathrm{A}}|0\rangle + \langle 0|\hat{O}_{\mathrm{B}}\hat{S}_{\mathrm{B}}\hat{Q}_{\mathrm{B}}|0\rangle + \langle 0|\hat{O}_{\mathrm{AB}}\hat{S}_{\mathrm{A}}\hat{Q}_{\mathrm{B}}|0\rangle + \langle 0|\hat{O}_{\mathrm{AB}}\hat{S}_{\mathrm{B}}\hat{Q}_{\mathrm{A}}|0\rangle .\end{aligned} \tag{2.8.14}$$

The terms can be analysed with Wick's theorem: $\langle 0|\hat{O}_{\mathrm{AB}}\hat{S}_{\mathrm{A}}\hat{Q}_{\mathrm{A}}|0\rangle$ vanishes as the indices in $\hat{O}_{\mathrm{AB}}$ referring to orbitals located on B cannot be contracted with any of the indices on $\hat{S}_{\mathrm{A}}$ or $\hat{Q}_{\mathrm{A}}$; an analogous reasoning is applied to $\langle 0|\hat{O}_{\mathrm{AB}}\hat{S}_{\mathrm{A}}\hat{Q}_{\mathrm{A}}|0\rangle$. In a similar manner, $\langle 0|\hat{O}_{\mathrm{A}}\hat{S}_{\mathrm{B}}\hat{Q}_{\mathrm{B}}|0\rangle$ vanishes, as the indices in $\hat{O}_{\mathrm{A}}$ referring to orbitals located on A cannot be contracted any of the indices on $\hat{S}_{\mathrm{B}}$ or $\hat{Q}_{\mathrm{B}}$. The same reasoning can be applied to the analogous term $\langle 0|\hat{O}_{\mathrm{B}}\hat{S}_{\mathrm{A}}\hat{Q}_{\mathrm{A}}|0\rangle$. However, the terms $\langle 0|\hat{O}_{\mathrm{AB}}\hat{S}_{\mathrm{A}}\hat{Q}_{\mathrm{B}}|0\rangle$ and $\langle 0|\hat{O}_{\mathrm{AB}}\hat{S}_{\mathrm{B}}\hat{Q}_{\mathrm{A}}|0\rangle$ do not necessarily vanish, as the indices of the operator $\hat{O}_{\mathrm{AB}}$ can be contracted with either $\hat{S}_{\mathrm{A}}$ and $\hat{Q}_{\mathrm{B}}$ or $\hat{S}_{\mathrm{B}}$ and $\hat{Q}_{\mathrm{A}}$. The product of three operators, one of which being semi-additive and two of which being additive, does not give an additive expectation value. In order to obtain an additive expectation value, the expression $\hat{O}_{\mathrm{A+B}}[\hat{S}_{\mathrm{A+B}},\hat{Q}_{\mathrm{A+B}}]$ can be exploited. This product corresponds to the product between the semi-additive operator $\hat{O}_{\mathrm{A+B}}$ and the operator $[\hat{S}_{\mathrm{A+B}},\hat{Q}_{\mathrm{A+B}}]$, which was shown in eq. 2.8.9 to be additive. The additivity of the expectation value can be proven here

$$\begin{aligned}&\langle 0|\hat{O}_{\mathrm{A+B}}[\hat{S}_{\mathrm{A+B}},\hat{Q}_{\mathrm{A+B}}]|0\rangle = \langle 0|(\hat{O}_{\mathrm{A}}+\hat{O}_{\mathrm{B}}+\hat{O}_{\mathrm{AB}})[\hat{S}_{\mathrm{A}}+\hat{S}_{\mathrm{B}},\hat{Q}_{\mathrm{A}}+\hat{Q}_{\mathrm{B}}]|0\rangle = \\ &= \langle 0|\hat{O}_{\mathrm{A}}[\hat{S}_{\mathrm{A}},\hat{Q}_{\mathrm{A}}]|0\rangle + \langle 0|\hat{O}_{\mathrm{B}}[\hat{S}_{\mathrm{B}},\hat{Q}_{\mathrm{B}}]|0\rangle + \underbrace{\langle 0|\hat{O}_{\mathrm{AB}}[\hat{S}_{\mathrm{A}},\hat{Q}_{\mathrm{A}}]|0\rangle}_{=0} + \underbrace{\langle 0|\hat{O}_{\mathrm{AB}}[\hat{S}_{\mathrm{B}},\hat{Q}_{\mathrm{B}}]|0\rangle}_{=0} + \\ &\underbrace{\langle 0|\hat{O}_{\mathrm{A}}[\hat{S}_{\mathrm{B}},\hat{Q}_{\mathrm{B}}]|0\rangle}_{=0} + \underbrace{\langle 0|\hat{O}_{\mathrm{B}}[\hat{S}_{\mathrm{A}},\hat{Q}_{\mathrm{A}}]|0\rangle}_{=0} = \\ &= \langle 0|\hat{O}_{\mathrm{A}}[\hat{S}_{\mathrm{A}},\hat{Q}_{\mathrm{A}}]|0\rangle + \langle 0|\hat{O}_{\mathrm{B}}[\hat{S}_{\mathrm{B}},\hat{Q}_{\mathrm{B}}]|0\rangle .\end{aligned} \tag{2.8.15}$$

The term $\langle 0|\,\hat{O}_{\mathrm{AB}}[\hat{S}_{\mathrm{A}},\hat{Q}_{\mathrm{A}}]\,|0\rangle$ vanishes as the orbital indices in $\hat{O}_{\mathrm{AB}}$ referring to orbitals located on B cannot be contracted with any of the indices on $\hat{S}_{\mathrm{A}}$ or $\hat{Q}_{\mathrm{A}}$. The same motivation explains the vanishing of $\langle 0|\,\hat{O}_{\mathrm{AB}}[\hat{S}_{\mathrm{A}},\hat{Q}_{\mathrm{A}}]\,|0\rangle$. In a similar manner, $\langle 0|\,\hat{O}_{\mathrm{A}}[\hat{S}_{\mathrm{B}},\hat{Q}_{\mathrm{B}}]\,|0\rangle$ vanishes, as the indices in $\hat{O}_{\mathrm{A}}$ referring to orbitals located on A cannot be contracted with any of the indices on $\hat{S}_{\mathrm{B}}$ or $\hat{Q}_{\mathrm{B}}$. The same reasoning can be applied to the term $\langle 0|\,\hat{O}_{\mathrm{B}}[\hat{S}_{\mathrm{A}},\hat{Q}_{\mathrm{A}}]\,|0\rangle$.
Note that the formulation in eq. 2.8.15 is additive, as all non-local contributions vanish, though not being connected. The insertion of a second commutator, i.e., $[\hat{O}_{\mathrm{A+B}},[\hat{S}_{\mathrm{A+B}},\hat{Q}_{\mathrm{A+B}}]]$, would lead to full connectedness. However, the second commutator is not necessary to achieve additivity for the corresponding expectation value. The expression $\langle 0|\,\hat{O}[\hat{S},\hat{Q}]\,|0\rangle$ is said to be *linked*.

Size-extensivity in the CC energy

The categories defined in the previous section may be applied to the CC operators, in order to show the size-extensivity of CC ground-state theory:

- by construction, the Hamiltonian of two non-interacting systems is local and additive, $\hat{H}_{\mathrm{A+B}} = \hat{H}_{\mathrm{A}} + \hat{H}_{\mathrm{B}}$.
- the excitation operator can be shown to be local and additive, as the excitations are either localised on A or on B: $\hat{T}_{\mathrm{A+B}} = \hat{T}_{\mathrm{A}} + \hat{T}_{\mathrm{B}}$. This result can be demonstrated through the amplitude equations

$$\begin{aligned}
0 &= \langle\phi_p|\,e^{-\hat{T}}\hat{H}e^{\hat{T}}\,|0\rangle = \\
&= \langle\phi_p|\,\hat{H} + [\hat{H},\hat{T}] + \frac{1}{2}[[\hat{H},\hat{T}],\hat{T}] + \ldots\,|0\rangle = \\
&= \langle\phi_p|\,\hat{H}_{\mathrm{A}} + [\hat{H}_{\mathrm{A}},\hat{T}_{\mathrm{A}}] + \frac{1}{2}[[\hat{H}_{\mathrm{A}},\hat{T}_{\mathrm{A}}],\hat{T}_{\mathrm{A}}] + \ldots\,|0\rangle + \\
&\quad \langle\phi_p|\,\hat{H}_{\mathrm{B}} + [\hat{H}_{\mathrm{B}},\hat{T}_{\mathrm{B}}] + \frac{1}{2}[[\hat{H}_{\mathrm{B}},\hat{T}_{\mathrm{B}}],\hat{T}_{\mathrm{B}}] + \ldots\,|0\rangle + \\
&\quad \langle\phi_p|\,[\hat{H}_{\mathrm{A}},\hat{T}_{\mathrm{B}}] + [\hat{H}_{\mathrm{B}},\hat{T}_{\mathrm{A}}] + \frac{1}{2}([[\hat{H}_{\mathrm{A}},\hat{T}_{\mathrm{B}}],\hat{T}_{\mathrm{A}}] + [[\hat{H}_{\mathrm{B}},\hat{T}_{\mathrm{B}}],\hat{T}_{\mathrm{A}}] + [[\hat{H}_{\mathrm{B}},\hat{T}_{\mathrm{A}}],\hat{T}_{\mathrm{A}}]) + \ldots\,|0\rangle = \\
&= \langle\phi_p|\,e^{-\hat{T}_{\mathrm{A}}}\hat{H}_{\mathrm{A}}e^{\hat{T}_{\mathrm{A}}}\,|0\rangle + \langle\phi_p|\,e^{-\hat{T}_{\mathrm{B}}}\hat{H}_{\mathrm{B}}e^{\hat{T}_{\mathrm{B}}}\,|0\rangle\,.
\end{aligned} \tag{2.8.16}$$

  The amplitude equations for the entire systems consist of the sum of the amplitude equations for system A, and the amplitude equations for system B, as the commutators between operators localised on different fragments vanish $[\hat{H}_{\mathrm{A}},\hat{T}_{\mathrm{B}}] = [\hat{H}_{\mathrm{B}},\hat{T}_{\mathrm{A}}] = 0$.
- as all excitation operators commute, the exponential ansatz can be factorised: $e^{\hat{T}_{\mathrm{A+B}}} = e^{\hat{T}_{\mathrm{A}}+\hat{T}_{\mathrm{B}}} = e^{\hat{T}_{\mathrm{A}}}e^{\hat{T}_{\mathrm{B}}}$.

In the framework of Equation-Of-Motion (EOM) CC theory, $\hat{R}$ is shown to be local.[215] Considering system A in an excited state and system B in the ground state gives $\hat{R}_{\mathrm{A+B}} = \hat{R}_{\mathrm{A}} \otimes \hat{1}_{\mathrm{B}}$. The additivity of this operator is shown analysing the amplitude equation for the two non-interacting systems:

$$\begin{aligned}
&\langle\phi_p|\,(\bar{H}_{\mathrm{A}} + \bar{H}_{\mathrm{B}} - E_{\mathrm{A,exc}} - E_{\mathrm{B,ground}})\hat{R}_{\mathrm{A}}\,|0\rangle = 0 \\
&\langle\phi_p|\,\underbrace{(\bar{H}_{\mathrm{A}} - E_{\mathrm{A,exc}})\hat{R}_{\mathrm{A}}\,|0\rangle}_{=0} + \langle\phi_p|\,\hat{R}_{\mathrm{A}}\,|0\rangle\,\underbrace{\langle 0|\,\bar{H}_{\mathrm{B}} - E_{\mathrm{B,ground}}\,|0\rangle}_{=0} = 0.
\end{aligned} \tag{2.8.17}$$

The first term vanishes because of the Schrödinger equation for the excited state A, while the second term vanishes because of the Schrödinger equation of the ground state of system

B. Therefore $\hat{R}$ is additive, as the excitation of subsystem A when considering the whole system $A+B$ corresponds to the excitation of subsystem A when considering only A.

The left eigenstates are only semiadditive: it is shown in ref. 215 that the $\hat{L}$ operator of eq. 2.7.22 can be written as $\hat{L}_{\mathrm{A+B}} = \hat{L}_{\mathrm{A}} + \hat{L}_{\mathrm{AB}}$ for the case in which system A is excited, while system B is in its ground state. From the amplitude equation for the left hand-side, $\langle 0|\,\hat{L}(\bar{H}-E)\,|\phi_p\rangle = 0$, the semi-additivity can be shown:

$$\begin{aligned}
0 &= \langle 0|\,(\hat{L}_{\mathrm{A}}+\hat{L}_{\mathrm{AB}})(\bar{H}_{\mathrm{A}}+\bar{H}_{\mathrm{B}}-E_{\mathrm{A,exc}}-E_{\mathrm{B,ground}})\,|\phi_p\rangle = \\
&= \langle 0|\,\hat{L}_{\mathrm{A}}(\bar{H}_{\mathrm{A}}+\bar{H}_{\mathrm{B}}-E_{\mathrm{A,exc}}-E_{\mathrm{B,ground}})\,|\phi_p\rangle + \langle 0|\,\hat{L}_{\mathrm{AB}}(\bar{H}_{\mathrm{A}}+\bar{H}_{\mathrm{B}}-E_{\mathrm{A,exc}}-E_{\mathrm{B,ground}})\,|\phi_p\rangle = \\
&= \underbrace{\langle 0|\,\hat{L}_{\mathrm{A}}(\bar{H}_{\mathrm{A}}-E_{\mathrm{A,exc}})}_{=0}\,|\phi_p\rangle + \underbrace{\langle 0|\,(\bar{H}_{\mathrm{B}}-E_{\mathrm{B,ground}})\,|0\rangle\,\langle 0|\,\hat{L}_{\mathrm{A}}\,|\phi_p\rangle}_{=0} + \\
&\quad + \langle 0|\,\hat{L}_{\mathrm{AB}}(\bar{H}_{\mathrm{A}}+\bar{H}_{\mathrm{B}}-E_{\mathrm{A,exc}}-E_{\mathrm{B,ground}})\,|\phi_p\rangle\,.
\end{aligned} \tag{2.8.18}$$

The first term corresponds to the amplitude equation for $\hat{L}_{\mathrm{A}}$, while the second term is the Schrödinger equation for the ground state on system B and vanishes. The third term provides an equation determining $\hat{L}_{\mathrm{AB}}$, which is not localised on any of the fragments. The presence of $\hat{L}_{\mathrm{AB}}$ therefore gives origin to the semi-additivity of the $\hat{L}$ operator.

It is important to analyse under which conditions the semi-additivity of the $\hat{L}$ operator does not affect the additivity of the energies. An accurate analysis of the ground-state energy shows that the additive Hamilton operator leads to additive ground-state energies

$$E_{\mathrm{A+B,GS}} = \langle 0|\,\bar{H}\,|0\rangle = \langle 0|\,\bar{H}_{\mathrm{A}}\,|0\rangle + \langle 0|\,\bar{H}_{\mathrm{B}}\,|0\rangle = E_{\mathrm{A}} + E_{\mathrm{B}}. \tag{2.8.19}$$

For the energy of excited states, the EOM expression is analysed.

$$\begin{aligned}
&\langle 0|\,\hat{L}\bar{H}\hat{R}\,|0\rangle = \langle 0|\,(\hat{L}_{\mathrm{A}}+\hat{L}_{\mathrm{AB}})\bar{H}\hat{R}_{\mathrm{A}}\,|0\rangle = \\
&\underbrace{\langle 0|\,\hat{L}_{\mathrm{A}}\bar{H}_{\mathrm{A}}\hat{R}_{\mathrm{A}}\,|0\rangle}_{=E_{\mathrm{A,exc}}} + \underbrace{\langle 0|\,\hat{L}_{\mathrm{A}}\bar{H}_{\mathrm{B}}\hat{R}_{\mathrm{A}}\,|0\rangle}_{=E_{\mathrm{B,ground}}} + \underbrace{\langle 0|\,\hat{L}_{\mathrm{AB}}\bar{H}_{\mathrm{A}}\hat{R}_{\mathrm{A}}\,|0\rangle}_{=0} + \underbrace{\langle 0|\,\hat{L}_{\mathrm{AB}}\bar{H}_{\mathrm{B}}\hat{R}_{\mathrm{A}}\,|0\rangle}_{=0} \\
&= E_{\mathrm{A,exc}} + E_{\mathrm{B,ground}}
\end{aligned} \tag{2.8.20}$$

The last two terms vanish due to the amplitude equations.
Therefore, additivity is guaranteed both for ground- and excited-states energies.

Size-extensivity in EOM-CC properties

A similar investigation may be carried out for the calculation of properties. The definition of properties in eq. 2.8.1 via the expectation value can be applied to the EOM-CC framework, where the left state is parameterised as $\langle\Psi| = \langle 0|\,\hat{L}e^{-\hat{T}}$ and the right one as $|\Psi\rangle = \hat{R}e^{\hat{T}}\,|0\rangle$. Eq. 2.8.1 can be written as follows

$$X = \langle 0|\,\hat{L}\bar{X}\hat{R}\,|0\rangle\,. \tag{2.8.21}$$

Following the discussion in sec. 2.8.1, two non-interacting systems A and B are considered, with A in an excited state and B in its ground state. In the aforementioned section, the operator $\hat{L}_{\mathrm{A+B}}$ was shown to be semi-additive, giving $\hat{L}_{\mathrm{A+B}} = \hat{L}_{\mathrm{A}} + \hat{L}_{\mathrm{AB}}$, while the operator $\hat{R}_{\mathrm{A+B}}$ was proven to be additive, equal to $\hat{R}_{\mathrm{A}}$. As most physical operators, the operator $\hat{X}_{\mathrm{A+B}}$ is assumed to be local and additive, such that the equality $\hat{X}_{\mathrm{A+B}} = \hat{X}_{\mathrm{A}} + \hat{X}_{\mathrm{B}}$ holds.

The expression in eq. 2.8.21 may be discussed applying these definitions:

$$\langle 0|\,\hat{L}\bar{X}\hat{R}\,|0\rangle = \langle 0|\,(\hat{L}_{\mathrm{A}}+\hat{L}_{\mathrm{AB}})\bar{X}\hat{R}_{\mathrm{A}}\,|0\rangle = \underbrace{\langle 0|\,\hat{L}_{\mathrm{A}}\bar{X}_{\mathrm{A}}\hat{R}_{\mathrm{A}}\,|0\rangle}_{=\bar{X}_{\mathrm{A,exc}}} + \underbrace{\langle 0|\,\hat{L}_{\mathrm{A}}\bar{X}_{\mathrm{B}}\hat{R}_{\mathrm{A}}\,|0\rangle}_{=\bar{X}_{\mathrm{B,ground}}} + \underbrace{\langle 0|\,\hat{L}_{\mathrm{AB}}\bar{X}_{\mathrm{A}}\hat{R}_{\mathrm{A}}\,|0\rangle}_{=0} + \langle 0|\,\hat{L}_{\mathrm{AB}}\bar{X}_{\mathrm{B}}\hat{R}_{\mathrm{A}}\,|0\rangle\,. \tag{2.8.22}$$

While the third term always vanishes, the presence of the fourth term leads to a lack of additivity for property X. The formulation in eq. 2.8.1 can prove problematic for EOM-CC theory, as the lack of additivity for example in the calculation of dipole moments is not physical. Therefore, a reformulation of eq. 2.8.1 is needed, which can be applied to the calculation of properties for approximate wave functions.

The approach of *response theory*[216,217] is hereafter explained for the exact case. The expression in eq. 2.8.76 has to be reformulated to be used for approximate methods, yielding size-extensivity.

Exact theory

A molecular system may be subjected to an external perturbation ε, inducing an external potential $\hat{V}$. The Hamiltonian is constructed from the unperturbed Hamiltonian $\hat{H}_0$ and an additional potential $\hat{V}$, giving $\hat{H} = \hat{H}_0 + \hat{V}$. In the following discussion, the potential $\hat{V}$ is considered linear in the perturbation, yielding a general form $\hat{V} = \hat{X}\cdot\varepsilon$. For example, when focusing on dipole moments, the perturbation is induced by the electric field ϵ, and the potential is expressed as $\hat{V} = -\hat{\mu}\cdot\epsilon$.

The exact wave function is a solution of the time-independent Schrödinger equation

$$\hat{H}\,|\Psi\rangle = E\,|\Psi\rangle\,. \tag{2.8.23}$$

Differentiation of the energy with respect to the perturbation gives

$$X = \frac{\mathrm{d}E}{\mathrm{d}\varepsilon} = \underbrace{\left\langle \frac{\mathrm{d}\Psi}{\mathrm{d}\varepsilon}\middle|\,\hat{H}\,\middle|\Psi\right\rangle}_{E\left\langle\frac{\mathrm{d}\Psi}{\mathrm{d}\varepsilon}|\Psi\right\rangle} + \underbrace{\left\langle \Psi\middle|\,\hat{H}\,\middle|\frac{\mathrm{d}\Psi}{\mathrm{d}\varepsilon}\right\rangle}_{E\left\langle\Psi|\frac{\mathrm{d}\Psi}{\mathrm{d}\varepsilon}\right\rangle} + \left\langle \Psi\middle|\,\frac{\mathrm{d}\hat{H}}{\mathrm{d}\varepsilon}\,\middle|\Psi\right\rangle = E\frac{\mathrm{d}}{\mathrm{d}\varepsilon}\langle\Psi|\Psi\rangle + \left\langle \Psi\middle|\,\frac{\mathrm{d}\hat{H}}{\mathrm{d}\varepsilon}\,\middle|\Psi\right\rangle, \tag{2.8.24}$$

where the Schrödinger equation for the right eigenstate, $\hat{H}\,|\Psi\rangle = E\,|\Psi\rangle$, and for the left eigenstate, $\langle\Psi|\,\hat{H} = E\,\langle\Psi|$, were substituted into eq. 2.8.24 to simplify the first two terms. Further simplification is achieved considering that the wave function is normalised, yielding $\frac{\mathrm{d}}{\mathrm{d}\varepsilon}\langle\Psi|\Psi\rangle = 0$. Eq. 2.8.24 reduces to

$$X = \frac{\mathrm{d}E}{\mathrm{d}\varepsilon} = \left\langle \Psi\middle|\,\frac{\mathrm{d}\hat{H}}{\mathrm{d}\varepsilon}\,\middle|\Psi\right\rangle = \langle\Psi|\,\hat{X}\,|\Psi\rangle\,. \tag{2.8.25}$$

In this case, differentiation of the energy with respect to the perturbation is equivalent to eq. 2.8.1, building the bridge to the expectation value form known from quantum mechanics. This result is known as the *Hellmann-Feynman* theorem.[218]
Under the assumption that the differentiation does not affect the basis functions used in the computation, this theorem holds also in the case of an approximated variational wave function. For a variationally optimised wave function, any first-order variation of the energy functional with respect to the wave function vanishes, giving

$$0 = \delta E = \delta\,\langle\Psi|\,\hat{H}\,|\Psi\rangle = \langle\delta\Psi|\,\hat{H}\,|\Psi\rangle + \langle\Psi|\,\hat{H}\,|\delta\Psi\rangle\,. \tag{2.8.26}$$

Differentiation of the energy with respect to the perturbation leads to three terms

$$X = \frac{\mathrm{d}E}{\mathrm{d}\varepsilon} = \underbrace{\left\langle \frac{\mathrm{d}\Psi}{\mathrm{d}\varepsilon}\middle|\hat{H}\middle|\Psi\right\rangle + \left\langle \Psi\middle|\hat{H}\middle|\frac{\mathrm{d}\Psi}{\mathrm{d}\varepsilon}\right\rangle}_{=0 \text{ var. princ.}} + \left\langle \Psi\middle|\frac{\mathrm{d}\hat{H}}{\mathrm{d}\varepsilon}\middle|\Psi\right\rangle = \langle\Psi|\,\hat{X}\,|\Psi\rangle\,. \tag{2.8.27}$$

Though not satisfying the Schrödinger equation, for a variational wave function the first two terms still vanish, due to the variational principle in eq. 2.8.26. The expectation-value approach is therefore equivalent to the differentiation of the energy also in this case. From this starting point, the theory is expanded to non-variational wave functions.

EOM-CC single-state properties

EOM-CC theory is an example of a method dealing with a non-variational wave function. Thus, the sum of all terms containing the differentiated wave function $\frac{\mathrm{d}\tilde{\Psi}}{\mathrm{d}\varepsilon}$ in eq. 2.8.24 does not vanish and the Hellmann-Feynman theorem does not hold. A different approach to EOM-CC properties is found through the calculation of derivatives.[30,64,115,219–223] A discussion of the theoretical treatment of EOM-CC properties is provided here, as it represents the starting point for the development of EOM-UCC properties.

In EOM-CC, the energy is obtained from the expectation value of a non-Hermitian operator, giving

$$E_{\mathrm{CC}} = \langle 0|\,\hat{L}e^{-\hat{T}}\hat{H}e^{\hat{T}}\hat{R}\,|0\rangle = \langle 0|\,\hat{L}\bar{H}\hat{R}\,|0\rangle\,. \tag{2.8.28}$$

The property X is obtained by means of differentiation with respect to the perturbation ε,

$$\frac{\mathrm{d}E_{\mathrm{CC}}}{\mathrm{d}\varepsilon} = \langle 0|\,\frac{\mathrm{d}\hat{L}}{\mathrm{d}\varepsilon}\underbrace{\bar{H}\hat{R}\,|0\rangle}_{=E_{\mathrm{exc}}} + \langle 0|\,\hat{L}\frac{\mathrm{d}\bar{H}}{\mathrm{d}\varepsilon}\hat{R}\,|0\rangle + \underbrace{\langle 0|\,\hat{L}\bar{H}}_{=E_{\mathrm{exc}}}\frac{\mathrm{d}\hat{R}}{\mathrm{d}\varepsilon}\,|0\rangle\,. \tag{2.8.29}$$

It is shown hereafter that eq. 2.8.28 is stationary with respect to $\hat{L}$ and $\hat{R}$,

$$\langle 0|\,\delta\hat{L}\bar{H}\hat{R}\,|0\rangle + \langle 0|\,\hat{L}\bar{H}\delta\hat{R}\,|0\rangle = E_{\mathrm{exc}}(\langle 0|\,\delta\hat{L}\hat{R}\,|0\rangle + \langle 0|\,\hat{L}\delta\hat{R}\,|0\rangle) = E_{\mathrm{exc}}\delta\,\langle 0|\,\hat{L}\hat{R}\,|0\rangle = 0. \tag{2.8.30}$$

Therefore, the sum of the first and third terms in eq. 2.8.29 vanish. Only the second term in eq. 2.8.29 contributes to the calculation of properties, which are found by differentiating the similarity-transformed Hamiltonian

$$\frac{\mathrm{d}E_{\mathrm{CC}}}{\mathrm{d}\varepsilon} = \langle 0|\,\hat{L}\frac{\mathrm{d}\bar{H}}{\mathrm{d}\varepsilon}\hat{R}\,|0\rangle = \langle 0|\,\hat{L}\frac{\mathrm{d}(e^{-\hat{T}}\hat{H}e^{\hat{T}})}{\mathrm{d}\varepsilon}\hat{R}\,|0\rangle\,. \tag{2.8.31}$$

The response of the wave function to the perturbation is enclosed in the differentiation of the exponential operator $e^{\hat{T}}$. The differentiation of the exponential form is rather straightforward when considering the definition of an exponential operator

$$\frac{\mathrm{d}e^{\hat{T}}}{\mathrm{d}\varepsilon} = \frac{\mathrm{d}}{\mathrm{d}\varepsilon}\sum_{n=0}^{\infty}\frac{1}{n!}\hat{T}^n = \sum_{n=1}^{\infty}\frac{1}{n!}n\frac{\mathrm{d}\hat{T}}{\mathrm{d}\varepsilon}\hat{T}^{(n-1)} = \frac{\mathrm{d}\hat{T}}{\mathrm{d}\varepsilon}e^{\hat{T}}. \tag{2.8.32}$$

The factorisation of the differentiated sum to give the exponential operator is allowed by the fact that all $\hat{T}$ operators are excitations and therefore commute with each other. Using eq. 2.8.32 for the differentiation of the EOM-CC energy in eq. 2.8.31, the following expression

is obtained

$$\begin{aligned}\frac{\mathrm{d}E_{\mathrm{CC}}}{\mathrm{d}\varepsilon} &= \langle 0|\,\hat{L}e^{-\hat{T}}\frac{\mathrm{d}\hat{H}}{\mathrm{d}\varepsilon}e^{\hat{T}}\hat{R}\,|0\rangle + \langle 0|\,\hat{L}\frac{\mathrm{d}e^{-\hat{T}}}{\mathrm{d}\varepsilon}\hat{H}e^{\hat{T}}\hat{R}\,|0\rangle + \langle 0|\,\hat{L}e^{-\hat{T}}\hat{H}\frac{\mathrm{d}e^{\hat{T}}}{\mathrm{d}\varepsilon}\hat{R}\,|0\rangle = \\ &= \langle 0|\,\hat{L}e^{-\hat{T}}\hat{X}e^{\hat{T}}\hat{R}\,|0\rangle + \langle 0|\,\hat{L}[e^{-\hat{T}}\hat{H}e^{\hat{T}},\frac{\mathrm{d}\hat{T}}{\mathrm{d}\varepsilon}]\hat{R}\,|0\rangle = \\ &= \langle 0|\,\hat{L}\bar{X}\hat{R}\,|0\rangle + \langle 0|\,\hat{L}[\bar{H},\frac{\mathrm{d}\hat{T}}{\mathrm{d}\varepsilon}]\hat{R}\,|0\rangle\,.\end{aligned} \tag{2.8.33}$$

Comparing this result to the expectation-value approach, there is the additional presence of the second term, which describes how the CC amplitudes respond to the presence of the perturbation. Note that, according to eq. 2.8.33, the perturbed amplitudes $\frac{\mathrm{d}t_\mu}{\mathrm{d}\varepsilon}$ are needed for the calculation of the property X. In the limit in which the EOM-CC wave function is not truncated and goes to the FCI limit, the second term vanishes,[224] showing that this term is due to the truncation of the EOM-CC parameterisation.

Before discussing the issue of the perturbed amplitudes further, some considerations have to be made. As was discussed in sec. 2.8.22, the first term in eq. 2.8.33 does not ensure size-extensivity. A linked formulation of the energy automatically solves this issue, as its differentiation is still linked. The example of eq. 2.8.15 can here be exploited, as the properties are determined over expectation values of three operators, two of which are additive ($\hat{X}$ and $\hat{R}$) and one semi-additive ($\hat{L}$). The energy can be rewritten with the goal of introducing the commutator $[\hat{H},\hat{R}]$ in eq. 2.8.28

$$E_{\mathrm{CC}} = \langle 0|\,\hat{L}[\bar{H},\hat{R}]\,|0\rangle + \langle 0|\,\hat{L}\hat{R}\bar{H}\,|0\rangle\,, \tag{2.8.34}$$

where the commutator is obtained by adding and subtracting the term $\langle 0|\,\hat{L}\hat{R}\bar{H}\,|0\rangle$, which corresponds to the ground-state energy, as

$$\langle 0|\,\hat{L}\hat{R}\bar{H}\,|0\rangle = \langle 0|\,\hat{L}\hat{R}\underbrace{(|0\rangle\langle 0| + \sum_n |n\rangle\langle n|)}_{\text{resolution of identity}}\bar{H}\,|0\rangle = \underbrace{\langle 0|\,\hat{L}\hat{R}\,|0\rangle}_{=1}\underbrace{\langle 0|\,\bar{H}\,|0\rangle}_{E_{\mathrm{GS}}} + \sum_n \langle 0|\,\hat{L}\hat{R}\,|n\rangle\underbrace{\langle n|\,\bar{H}\,|0\rangle}_{=0}. \tag{2.8.35}$$

The last term vanishes because of the amplitude equations. This reformulation of the energy expression gives

$$E_{\mathrm{CC}} = \langle 0|\,\hat{L}[\bar{H},\hat{R}]\,|0\rangle + E_{\mathrm{GS}}. \tag{2.8.36}$$

Its differentiation now yields an additive formulation of properties,

$$\frac{\mathrm{d}E_{\mathrm{CC}}}{\mathrm{d}\varepsilon} = \langle 0|\,\hat{L}[\bar{X},\hat{R}]\,|0\rangle + \langle 0|\,\hat{L}[[\bar{H},\frac{\mathrm{d}\hat{T}}{\mathrm{d}\varepsilon}],\hat{R}]\,|0\rangle + \langle 0|\,\bar{X}\,|0\rangle\,. \tag{2.8.37}$$

Unlike the expectation value approach (eq. 2.8.22), the differentiation of the energy leads to a size-extensive formulation for one-electron properties.

As observed before, the perturbed excitation operator $\frac{\mathrm{d}\hat{T}}{\mathrm{d}\varepsilon}$ needs to be computed to evaluate the property X. For different kinds of perturbation, as for example for the electric field, the magnetic field, a shift of nuclear coordinates, *etc.*, a new set of perturbed amplitudes is evaluated and new equations need to be solved. Therefore, a different approach is here used, the *Lagrange functional approach*, presented in the next section.

Lagrange functional approach

A well-established approach to avoid the evaluation of the perturbed amplitudes is given by the Lagrange functional approach method,[225–227] used in the field of constrained optimisa-

tion.* A Lagrange functional is built from the function $f(\alpha,\varepsilon)$ to be differentiated and a set of constraints $g_i(\alpha,\varepsilon)=0$, multiplied by the Lagrange multipliers λ_i

$$\mathscr{L} = f(\alpha,\varepsilon)+\sum_i \lambda_i g_i(\alpha,\varepsilon). \tag{2.8.38}$$

Having added functions $g_i(\alpha,\varepsilon)=0$ equal to zero for all values of ε, the total differentiation of the functional $\mathscr{L}$ corresponds to the differentiation of the function f: $\frac{\mathrm{d}f}{\mathrm{d}\varepsilon}=\frac{\mathrm{d}\mathscr{L}}{\mathrm{d}\varepsilon}$ (the differentiation of the constraint is vanishing, $\frac{\mathrm{d}g(\alpha,\varepsilon)}{\mathrm{d}\varepsilon}=0$). The Lagrange multipliers are found by imposing stationarity of the Lagrange functional with respect to all parameters $\frac{\partial\mathscr{L}}{\partial\alpha}=0$. Stationarity with respect to the Lagrange multipliers is already satisfied by the form of the constraints: $\frac{\partial\mathscr{L}}{\partial\lambda_i}=g_i(\alpha)=0$.

Once the set of Lagrange multipliers satisfying the stationarity conditions has been found, the wanted derivative can be computed as

$$\frac{\mathrm{d}\mathscr{L}}{\mathrm{d}\varepsilon}=\frac{\partial\mathscr{L}}{\partial\varepsilon}+\underbrace{\frac{\partial\mathscr{L}}{\partial\alpha}}_{=0}\frac{\partial\alpha}{\partial\varepsilon}+\sum_i\underbrace{\frac{\partial\mathscr{L}}{\partial\lambda_i}}_{=0}\frac{\partial\lambda_i}{\partial\varepsilon}=\frac{\partial\mathscr{L}}{\partial\varepsilon}. \tag{2.8.39}$$

The last two terms vanish due to the imposed stationarity conditions, and the total differentiation reduces to a partial differentiation of the Lagrange functional.

Lagrange functional for EOM-CC properties

The Lagrangian approach can be applied to the computation of molecular properties. In EOM-CC theory, the function $f(\alpha)$ is the energy, while the amplitude equations are imposed as constraints. The ground-state properties are found through the following Lagrange functional

$$\mathscr{L}_{\mathrm{CC}} = E_{\mathrm{CC}}+\sum_\mu \lambda_\mu \langle\phi_\mu|\,\bar{H}\,|0\rangle = \langle 0|\,(1+\Lambda)\bar{H}\,|0\rangle + E_{\mathrm{CC}}. \tag{2.8.40}$$

This equation can be recognised as the ground-state energy expression in the EOM-CC framework, therefore identifying the Lagrange multipliers with the $\hat{\lambda}$ operator of eq. 2.7.28. The stationarity condition with respect to each CC amplitude t_μ leads to exactly the equations for the EOM-CC left ground state,

$$\frac{\partial\mathscr{L}_{\mathrm{CC}}}{\partial t_\mu}=\langle 0|\,(1+\hat{\Lambda})[\bar{H},\hat{\tau}_\mu]\,|0\rangle=0. \tag{2.8.41}$$

For excited-state properties, the Lagrange functional may be written in the following form

$$\mathscr{L}_{\mathrm{CC}} = \langle 0|\,\hat{L}[\bar{H},\hat{R}]\,|0\rangle+\langle 0|\,\bar{H}\,|0\rangle+\langle 0|\,\hat{Z}\bar{H}\,|0\rangle-\eta\,\langle 0|\,\hat{L}\hat{R}-1\,|0\rangle\,, \tag{2.8.42}$$

where $\hat{Z}=\sum_{ia}\zeta_i^a\{\hat{i}^\dagger\hat{a}\}+\sum_{ijab}\zeta_{ij}^{ab}\{\hat{i}^\dagger\hat{j}^\dagger\hat{b}\hat{a}\}+\ldots$ is a de-excitation operator having as amplitudes ζ_μ the Lagrange multipliers imposing the amplitude equations. η is the multiplier of the normalisation condition of the wave function. The stationarity condition with respect to the amplitudes in this case yields the so-called *Zeta-equations*,[227]

$$\frac{\partial\mathscr{L}_{\mathrm{CC}}}{\partial t_\mu}=\langle 0|\,\hat{L}[[\bar{H},\hat{\tau}_\mu],\hat{R}]\,|0\rangle+\langle 0|\,[\bar{H},\hat{\tau}_\mu]\,|0\rangle+\langle 0|\,\hat{Z}[\bar{H},\hat{\tau}_\mu]\,|0\rangle=0. \tag{2.8.43}$$

*The term *Lagrangian method* is quite improper here, as the imposed constraints are already fulfilled. Therefore, it cannot be classified as a proper constrained optimisation problem. A more suitable denomination would be *Envelope-theorem method*.[228] However, the improper terminology of Lagrangian method is the one used in the literature and is therefore used in this thesis.

Note that the commutator $[\bar{H}, \hat{\tau}_\mu]$ comes from the differentiation of the similarity transformed Hamiltonian,

$$\frac{\mathrm{d}(e^{-\hat{T}}\bar{H}e^{\hat{T}})}{\mathrm{d}t_\mu} = \frac{\mathrm{d}e^{-\hat{T}}}{\mathrm{d}t_\mu}\bar{H}e^{\hat{T}} + e^{-\hat{T}}\bar{H}\frac{\mathrm{d}e^{\hat{T}}}{\mathrm{d}t_\mu} = -\hat{\tau}_\mu e^{-\hat{T}}\bar{H}e^{\hat{T}} + e^{-\hat{T}}\bar{H}e^{\hat{T}}\hat{\tau}_\mu = [\bar{H}, \hat{\tau}_\mu]. \tag{2.8.44}$$

The fact that all excitation operators commute has been exploited in order to obtain $[\bar{H}, \hat{\tau}_\mu]$. The Zeta-equations 2.8.43 allow to find the ζ multipliers. Differentiation with respect to $\hat{L}$ leads to the equation $[\bar{H}, \hat{R}]\,|0\rangle - \eta\hat{R}\,|0\rangle = 0$. From EOM-CC theory, the Lagrange multiplier η therefore corresponds to the excitation energy, giving $\eta = \Delta E_{\mathrm{exc}}$. Once the Lagrange multipliers have been determined, the property X is computed through partial differentiation of $\mathscr{L}_{\mathrm{CC}}$.

$$X = \frac{\mathrm{d}\mathscr{L}_{\mathrm{CC}}}{\mathrm{d}\varepsilon} = \frac{\partial\mathscr{L}_{\mathrm{CC}}}{\partial\varepsilon} = \langle 0|\,\hat{L}[\bar{X}, \hat{R}]\,|0\rangle + \langle 0|\,\bar{X}\,|0\rangle + \langle 0|\,\hat{Z}\bar{X}\,|0\rangle \tag{2.8.45}$$

From this expression, it is possible to define the one-electron density matrix $\mathbf{D}$ of the system,

$$D_{pq} = \langle 0|\,\hat{L}[\hat{a}_p^\dagger\hat{a}_q, \hat{R}]\,|0\rangle + \langle 0|\,\hat{a}_p^\dagger\hat{a}_q\,|0\rangle + \langle 0|\,\hat{Z}\hat{a}_p^\dagger\hat{a}_q\,|0\rangle\,. \tag{2.8.46}$$

The calculated property X can be written in terms of the density matrix $\mathbf{D}$, giving $X = \sum_{pq} D_{pq}x_{pq}$. The coefficients x_{pq} are obtained from the expression of the operator $\hat{X}$ in second quantisation, where x_{pq} are the integrals $x_{pq} = \int \phi_p^*(\mathbf{r})X(\mathbf{r})\phi_q(\mathbf{r})\mathrm{d}\mathbf{r}$ over the orbital basis set $\{\phi_p\}$. For different molecular properties, the same density matrix can be used and multiplied with the corresponding x_{pq} integrals, while the computation of the perturbed amplitudes requires a specific set of solving equations for each kind of perturbation.

As a final remark, it should be noted that the effect given by the relaxation of the HF orbitals due to the presence of the perturbation is neglected in the computation of the properties.

2.8.2 Transition dipole moments

The goal of this section is to develop a framework for the computation of transition dipole moments, in order to apply it to UCC theory.

In quantum mechanics, the transition dipole moment between an initial state and a final state is defined as

$$T_{fi} = \langle\Psi_f|\,\hat{\mu}\,|\Psi_i\rangle\,, \tag{2.8.47}$$

where $\hat{\mu}$ is the dipole operator and Ψ_i, Ψ_f are the time-independent wave functions of the initial and final states, respectively. From a physical point of view, it is apparent that the transition $\Psi_f \to \Psi_i$ is linked to the transition $\Psi_i \to \Psi_f$, as their transition dipole moments are conjugate of each other

$$T_{if} = \langle\Psi_i|\,\hat{\mu}\,|\Psi_f\rangle = T_{fi}^*. \tag{2.8.48}$$

This symmetry should not be broken by approximate parameterisations of the wave functions, in order to be physically consistent.

However, the formulation in eq. 2.8.47 poses some problems when applied to approximate methods. One example is given by EOM-CC theory, for which eq. 2.8.47 yields $T_{fi} = \langle 0|\,\hat{L}_f e^{-\hat{T}}\hat{X}e^{\hat{T}}\hat{R}_i\,|0\rangle$. As seen for single-state properties, this formulation does not give additive properties, due to the semi-additivity of the operator $\hat{L}$. The method for the calculation of the transition dipole moments can be made size-extensive by means of a reformulation of T_{fi}. Eq. 2.8.15 may be exploited once more, in order to separate the linked and the non-linked parts of the EOM-CC transition dipole moments

$$T_{fi} = \langle 0|\,\hat{L}_f[\bar{X}, \hat{R}_i]\,|0\rangle + \langle 0|\,\hat{L}_f\hat{R}_i\bar{X}\,|0\rangle\,. \tag{2.8.49}$$

The first term has the form discussed in eq. 2.8.15 and is linked, while the second one is non-linked. The equation can be manipulated in order to find a linked form. For an arbitrary excitation operator $\hat{A}$, the following relation holds

$$\langle 0|\,\hat{L}_f[\bar{H},\hat{A}]\hat{R}_i\,|0\rangle - \langle 0|\,\hat{L}_f(E_f-E_i)\hat{A}\hat{R}_i\,|0\rangle = 0. \tag{2.8.50}$$

Adding eqs. 2.8.49 and 2.8.50, the EOM-CC transition dipole moments are expressed by

$$\begin{aligned} T_{fi} = {} & \langle 0|\,\hat{L}_f[\bar{X},\hat{R}_i]\,|0\rangle + \langle 0|\,\hat{L}_f[[\bar{H},\hat{A}],\hat{R}_i]\,|0\rangle \\ & + \langle 0|\,\hat{L}_f\hat{R}_i\bar{X}\,|0\rangle + \langle 0|\,\hat{L}_f\hat{R}_i[\bar{H},\hat{A}]\,|0\rangle - \langle 0|\,\hat{L}_f(E_f-E_i)\hat{A}\hat{R}_i\,|0\rangle\,. \end{aligned} \tag{2.8.51}$$

The terms in the first line are linked, while the second line groups the non-linked part of the equation. In order to have a size-extensive theory, the second line needs to vanish. This result can be achieved by recognising that the differentiation of the time-dependent amplitude equation leads to an equation similar in form to eq. 2.8.51

$$\begin{aligned} 0 = {} & \frac{\mathrm{d}}{\mathrm{d}\varepsilon}\langle 0|\,e^{-\hat{T}}(\hat{H}-i\frac{\partial}{\partial t})e^{\hat{T}}\,|0\rangle = \\ = {} & \langle\mu|\,\bar{X}\,|0\rangle - \langle\mu|\,\frac{\mathrm{d}\hat{T}}{\mathrm{d}\varepsilon}e^{-\hat{T}}\hat{H}e^{\hat{T}}\,|0\rangle + \langle\mu|\,e^{-\hat{T}}\hat{H}\frac{\mathrm{d}\hat{T}}{\mathrm{d}\varepsilon}e^{\hat{T}}\,|0\rangle - \omega\,\langle\mu|\,\frac{\mathrm{d}\hat{T}}{\mathrm{d}\varepsilon}\,|0\rangle = \\ = {} & \langle\mu|\,\bar{X}\,|0\rangle + \langle\mu|\,[\bar{H},\frac{\mathrm{d}\hat{T}}{\mathrm{d}\varepsilon}]\,|0\rangle - \omega\,\langle\mu|\,\frac{\mathrm{d}\hat{T}}{\mathrm{d}\varepsilon}\,|0\rangle\,. \end{aligned} \tag{2.8.52}$$

The last term in eq. 2.8.52 comes from the time-dependent part of the Schrödinger equation, as

$$\frac{\mathrm{d}}{\mathrm{d}\varepsilon}\langle 0|\,e^{-\hat{T}}(-i\frac{\partial}{\partial t})e^{\hat{T}}\,|0\rangle = \frac{\mathrm{d}}{\mathrm{d}\varepsilon}\langle 0|\,e^{-\hat{T}}(-i\frac{\partial\hat{T}}{\partial t})e^{\hat{T}}\,|0\rangle = \frac{\mathrm{d}}{\mathrm{d}\varepsilon}\langle 0|-i\frac{\partial\hat{T}}{\partial t}\,|0\rangle\,. \tag{2.8.53}$$

The time dependence in the CC amplitudes can be written as $\hat{T}(t)=\hat{T}e^{i\omega t}$. Substituting the time-dependent expression of the amplitudes in eq. 2.8.53 leads to the last term in eq. 2.8.52. Eq. 2.8.51 therefore vanishes for the choice $\hat{A}=\frac{\mathrm{d}\hat{T}}{\mathrm{d}\varepsilon}$ and $\omega=\omega_{fi}=E_f-E_i$.

A size-extensive theory of the EOM-CC transition dipole moment involves the calculation of perturbed amplitudes,

$$T_{fi} = \langle 0|\,\hat{L}_f[\bar{X},\hat{R}_i]\,|0\rangle + \langle 0|\,\hat{L}_f[[\bar{H},\frac{\mathrm{d}\hat{T}}{\mathrm{d}\varepsilon}],\hat{R}_i]\,|0\rangle\,. \tag{2.8.54}$$

From this discussion, it is clear that the form in eq. 2.8.47 can be exploited in the case of an exact parameterisation of the wave function, but leads to a non-size extensive theory in the case of the EOM-CC framework.[214] Therefore, this theory needs to be reformulated, in order to be applicable both to FCI and to the approximations EOM-CC and EOM-UCC. The powerful tool of *response theory*[219] is here discussed for transition dipole moments.

Exact theory

In the most general setting, the molecular system described by the time-independent Hamiltonian $\hat{H}_0$ can experience a time-dependent perturbation, resulting in a time-dependent potential $\hat{V}(t)$. The corresponding time-dependent Hamiltonian is $\hat{H}=\hat{H}_0+\hat{V}(t)$. A transition between an initial state Ψ_i and a final state Ψ_f can be induced by a time-dependent periodic perturbation of the form

$$\hat{V}(t) = \sum_k e^{i\omega_k t}\hat{X}\cdot\varepsilon(\omega_k). \tag{2.8.55}$$

For example, for a perturbation induced by an electric field ε, $V(t)$ is expressed through the coupling of the field to the dipole operator $\hat{\mu}$: $\hat{V} = -\sum_k e^{i\omega_k t}\hat{\mu}\cdot\boldsymbol{\varepsilon}_k$. The transition occurs if the frequency of the oscillating field corresponds to the energy difference between the two states, i.e., if $\omega = \omega_{fi} = E_f - E_i$.
The concepts outlined in sec. 2.8.1 are here generalised to the time-dependent frame, in order to be applied to the calculation of transition dipole moments. The exact wave function satisfies the time-dependent Schrödinger equation

$$(\hat{H} - i\frac{\partial}{\partial t})\Psi(t) = 0. \tag{2.8.56}$$

The wave function $\Psi(t)$, being a solution of the Schrödinger equation, satisfies the following stationarity condition[57]

$$\left\langle \delta\Psi \middle| (\hat{H} - i\frac{\partial}{\partial t})\Psi \right\rangle + \left\langle (\hat{H} - i\frac{\partial}{\partial t})\Psi \middle| \delta\Psi \right\rangle = 0. \tag{2.8.57}$$

The equations may be simplified by writing the time-dependent wave function subjected to a periodic perturbation as the product of a function $e^{-i\phi(t)}$, dependent on a phase $\phi_i(t)$ due to the time evolution, and a *phase-isolated* part $\tilde{\Psi}(t)$, *

$$\Psi(t) = e^{-i\phi(t)}\tilde{\Psi}(t). \tag{2.8.58}$$

Note that, while $\Psi(t)$ fulfills the original Schrödinger equation, $\tilde{\Psi}(t)$ does not

$$(\hat{H} - i\frac{\partial}{\partial t})\Psi(t) = (\hat{H} - i\frac{\partial}{\partial t})e^{-i\phi(t)}\tilde{\Psi}(t) = 0 \implies (\hat{H} - i\frac{\partial}{\partial t})\tilde{\Psi}(t) = Q(t)\tilde{\Psi}(t). \tag{2.8.59}$$

$Q(t)$ is called *quasi-energy*[230,231] (as it has an analogous role to the energy in the time-independent framework, where the time evolution is simply $\Psi(t) = e^{-iEt}\Psi(0)$) and is defined as the time differentiated phase function $Q(t) = \dot{\phi}(t)$. For the phase-isolated wave function, the stationarity condition becomes[232]

$$\left\langle \delta\tilde{\Psi} \middle| (\hat{H} - i\frac{\partial}{\partial t} - Q(t)) \middle| \tilde{\Psi} \right\rangle + \left\langle (\hat{H} - i\frac{\partial}{\partial t} - Q(t))\tilde{\Psi} \middle| \delta\tilde{\Psi} \right\rangle = 0. \tag{2.8.60}$$

Note that the terms depending on the quasi-energy vanish, as $Q(t)(\left\langle \delta\tilde{\Psi} \middle| \tilde{\Psi} \right\rangle + \left\langle \tilde{\Psi} \middle| \delta\tilde{\Psi} \right\rangle) = Q(t)\delta\left\langle \tilde{\Psi} \middle| \tilde{\Psi} \right\rangle = 0$. The stationarity condition yields

$$\delta\left\langle \tilde{\Psi} \middle| (\hat{H} - i\frac{\partial}{\partial t}) \middle| \tilde{\Psi} \right\rangle + i\frac{\partial}{\partial t}\left\langle \tilde{\Psi} \middle| \delta\tilde{\Psi} \right\rangle = 0. \tag{2.8.61}$$

In the time-independent limit, the relation $\delta\left\langle \tilde{\Psi} \middle| \hat{H} \middle| \tilde{\Psi} \right\rangle$ is found, corresponding to the variational criterion of sec. 2.8.1. However, eq. 2.8.61 does not state that the quasi-energy is variational, as $\delta Q \neq 0$, as can be seen by writing eq. 2.8.61 as

$$\delta Q(t) + i\frac{\partial}{\partial t}\left\langle \tilde{\Psi} \middle| \delta\tilde{\Psi} \right\rangle = 0. \tag{2.8.62}$$

*This partition can be performed following the so-called *Floquet theory*.[229] This theory analyses solutions of the time-dependent Schrödinger equation with a time-periodic Hamiltonian. Here only its most important result is exploited, i.e., the possibility to partition the wave function into a phase-dependent and a phase-isolated part.

It has been discussed that properties are calculated through differentiation with respect to the perturbation. Differentiation of the time-averaged quasi-energy $\{Q\}_T$ gives

$$\frac{\mathrm{d}\{Q\}_T}{\mathrm{d}\varepsilon} \qquad Q = \left\langle \tilde{\Psi}(t) \right| (\hat{H} - i\frac{\partial}{\partial t}) \left| \tilde{\Psi}(t) \right\rangle . \tag{2.8.63}$$

$\{Q\}_T$ is the time average of Q over the period T, necessary in order to obtain a property not dependent on the time t. For a periodic function $f(t)$, its time average is defined as $\{f\}_T = \frac{1}{T}\int_0^T f(t)dt$. In the case of periodic functions, time averaging allows only terms not to vanish if the overall phase of a term, given by the sum of all phases of the operators and wave functions in a product, adds to zero: $\sum_k \omega_k = 0$. Time averaging may be seen as the connection between time-dependent and time-independent theory, as the time-dependence of the periodic perturbation is averaged to a time-independent quantity. Differentiation of the quasi-energy with respect to the perturbation of particular frequency ω_k yields

$$\frac{\mathrm{d}Q}{\mathrm{d}\varepsilon(\omega_k)} = \left\langle \frac{\mathrm{d}\tilde{\Psi}}{\mathrm{d}\varepsilon} \right| (\hat{H} - i\frac{\partial}{\partial t}) \left| \tilde{\Psi} \right\rangle + \left\langle \tilde{\Psi} \right| (\hat{H} - i\frac{\partial}{\partial t}) \left| \frac{\mathrm{d}\tilde{\Psi}}{\mathrm{d}\varepsilon} \right\rangle + \left\langle \tilde{\Psi} \right| \hat{X} e^{-i\omega_k t} \left| \tilde{\Psi} \right\rangle . \tag{2.8.64}$$

This expression can be simplified through the stationarity condition in eq. 2.8.61

$$\frac{\mathrm{d}Q}{\mathrm{d}\varepsilon(\omega_k)} = -i\frac{\partial}{\partial t}\left\langle \tilde{\Psi} \middle| \frac{\mathrm{d}\tilde{\Psi}}{\mathrm{d}\varepsilon} \right\rangle + \left\langle \tilde{\Psi} \right| \hat{X} e^{-i\omega_k t} \left| \tilde{\Psi} \right\rangle \implies \frac{\mathrm{d}Q}{\mathrm{d}\varepsilon(\omega_k)} + i\frac{\partial}{\partial t}\left\langle \tilde{\Psi} \middle| \frac{\mathrm{d}\tilde{\Psi}}{\mathrm{d}\varepsilon} \right\rangle = \left\langle \tilde{\Psi} \right| \hat{X} e^{-i\omega_k t} \left| \tilde{\Psi} \right\rangle . \tag{2.8.65}$$

From this expression, the connection between time-independent and time-dependent theory is apparent: in the time-independent limit the quasi-energy Q corresponds to the energy E. The second term in eq. 2.8.65, involving the time derivative, contains the response of the wave function. Langhoff *et al.* have shown that this term vanishes for a variational wave function when performing time averaging,[232] establishing the connection to the time-independent theory

$$\frac{\mathrm{d}\{Q\}_T}{\mathrm{d}\varepsilon(\omega_k)} = \left\langle \tilde{\Psi} \right| \hat{X} \left| \tilde{\Psi} \right\rangle = X. \tag{2.8.66}$$

From the time averaging, only the component with $\omega = 0$ does not vanish, i.e., the constant part of the potential $\hat{V}$. Therefore, in the exact case eqs. 2.8.1 and 2.8.66 have the same form. In exact theory, the differentiation of the time-averaged quasi-energy leads to the calculation of the property X. At this point of the discussion, it is clear that the quasi-energy formalism is a generalisation of the time-independent energy formalism. For a time-independent perturbation, the equations discussed here are reduced to the form of sec. 2.8.1 and the time-independent form can be exploited.

The time-dependent formalism of the quasi-energy here introduced is motivated by the need to formulate a theory for the transition dipole moments which can be applied to approximate wave-function parameterisations. In particular, it has been discussed that the correct behaviour of transition dipole moments in the EOM-CC framework is obtained only when considering a time-dependent formulation of the amplitude equations. Therefore, the shift to the time-dependent framework had to be defined. The quasi-energy formulation can be generalised to the treatment of transition dipole moments. Looking at the transition $\Psi_i \to \Psi_f$, the transition matrix element Q_{fi} is defined as

$$Q_{fi} = \langle \Psi_f(t) | (\hat{H} - i\frac{\partial}{\partial t}) | \Psi_i(t) \rangle . \tag{2.8.67}$$

Note that in the exact case Q_{fi} is equal to zero. As the single wave functions are stationary states of the Hamilton operator, the stationarity condition with respect to the variation of

the wave functions gives

$$\langle\delta\Psi_f|\,(\hat{H}-i\frac{\partial}{\partial t})\,|\Psi_i\rangle+\langle\Psi_f|\,(\hat{H}-i\frac{\partial}{\partial t})\,|\delta\Psi_i\rangle+i\frac{\partial}{\partial t}\,\langle\Psi_f|\delta\Psi_i\rangle=0. \tag{2.8.68}$$

The initial and the final states can both be written separating the phase-isolated part and the one describing the time-evolution (which reduces to e^{-iEt} in the time-independent frame), yielding

$$|\Psi_i\rangle=e^{-i\phi_i(t)}\left|\tilde{\Psi}_i\right\rangle,\qquad |\Psi_f\rangle=e^{-i\phi_f(t)}\left|\tilde{\Psi}_f\right\rangle. \tag{2.8.69}$$

Note that the phase $\phi(t)$ is in general different for the two states. The stationarity condition in eq. 2.8.68 can be expressed through the phase-isolated wave functions, where the phase factors add but are not vanishing

$$\begin{aligned}&\left\langle\delta\tilde{\Psi}_f\right|e^{i(\phi_f(t)-\phi_i(t))}(\hat{H}-i\frac{\partial}{\partial t}-\dot{\phi}_i(t))\left|\tilde{\Psi}_i\right\rangle+\left\langle\tilde{\Psi}_f\right|e^{i(\phi_f(t)-\phi_i(t))}(\hat{H}-i\frac{\partial}{\partial t}-\dot{\phi}_i(t))\left|\delta\tilde{\Psi}_i\right\rangle\\&+i\frac{\partial}{\partial t}e^{i(\phi_f(t)-\phi_i(t))}\left\langle\tilde{\Psi}_f\right|\left.\delta\tilde{\Psi}_i\right\rangle=0.\end{aligned} \tag{2.8.70}$$

The phase-isolated wave functions can also be applied to the formulation of Q_{fi}. The dependence on the difference in phase can be factorised in front of the Hamilton operator

$$\begin{aligned}Q_{fi}=\langle\Psi_f(t)|\,(\hat{H}-i\frac{\partial}{\partial t})\,|\Psi_i(t)\rangle&=\left\langle\tilde{\Psi}_f(t)\right|e^{i(\phi_f(t)-\phi_i(t))}(\hat{H}-i\frac{\partial}{\partial t}-\dot{\phi}_i(t))\left|\tilde{\Psi}_i(t)\right\rangle=\\&=\left\langle\tilde{\Psi}_f(t)\right|e^{i(\phi_f(t)-\phi_i(t))}(\hat{H}-i\frac{\partial}{\partial t}-Q_i(t))\left|\tilde{\Psi}_i(t)\right\rangle,\end{aligned} \tag{2.8.71}$$

where in the last line the definition $\dot{\phi}_i(t)=Q_i(t)$ has been used.* Differentiation with respect to the perturbation of frequency ω_{fi} and time averaging to impose the resonance condition gives

$$\begin{aligned}\frac{\mathrm{d}\{Q_{fi}\}_T}{\mathrm{d}\varepsilon(\omega_{fi})}=&\{\left\langle\frac{\mathrm{d}}{\mathrm{d}\varepsilon(\omega_{fi})}\tilde{\Psi}_f(t)\right|e^{i(\phi_f(t)-\phi_i(t))}(\hat{H}-i\frac{\partial}{\partial t}-Q_i(t))\left|\tilde{\Psi}_i(t)\right\rangle\}_T\\&+\{\left\langle\tilde{\Psi}_f(t)\right|e^{i(\phi_f(t)-\phi_i(t))}(\hat{H}-i\frac{\partial}{\partial t}-Q_i(t))\left|\frac{\mathrm{d}}{\mathrm{d}\varepsilon(\omega_{fi})}\tilde{\Psi}_i(t)\right\rangle\}_T\\&+\{\left\langle\tilde{\Psi}_f(t)\right|e^{i(\phi_f(t)-\phi_i(t))}\frac{\mathrm{d}}{\mathrm{d}\varepsilon(\omega_{fi})}(\hat{H}-i\frac{\partial}{\partial t}-Q_i(t))\left|\tilde{\Psi}_i(t)\right\rangle\}_T.\end{aligned} \tag{2.8.72}$$

The stationarity condition in eq. 2.8.70 can be used to simplify the first two terms in eq. 2.8.72, yielding

$$\frac{\mathrm{d}\{Q_{fi}\}_T}{\mathrm{d}\varepsilon(\omega_{fi})}=-i\{\frac{\partial}{\partial t}e^{i\omega_{fi}t}\left\langle\tilde{\Psi}_f\right|\left.\frac{\mathrm{d}\tilde{\Psi}_i}{\mathrm{d}\varepsilon(\omega_{fi})}\right\rangle\}_T+\{\left\langle\tilde{\Psi}_f\right|e^{i\omega_{fi}t}\frac{\mathrm{d}\hat{H}}{\mathrm{d}\varepsilon(\omega_{fi})}\left|\tilde{\Psi}_i\right\rangle\}_T=0. \tag{2.8.73}$$

This differentiation is equal to zero, as Q_{fi} is equal to zero. The first term can be interpreted by means of time-dependent perturbation theory, as $\frac{\mathrm{d}\tilde{\Psi}}{\mathrm{d}\varepsilon}$ can be seen as the first-order

*The choice of including the phase factor in the ket state would result in having Q_f multiplying the orthonormality condition. $\left\langle\tilde{\Psi}_f(t)\right|e^{i(\phi_f(t)-\phi_i(t))}(\hat{H}-i\frac{\partial}{\partial t}-Q_i(t))\left|\tilde{\Psi}_i(t)\right\rangle$ is equivalent to $\left\langle\tilde{\Psi}_f(t)\right|(\hat{H}-i\frac{\partial}{\partial t}-Q_f(t))e^{i(\phi_f(t)-\phi_i(t))}\left|\tilde{\Psi}_i(t)\right\rangle$.

contribution of a perturbed wave function.[‡] The term $i\{\frac{\partial}{\partial t}e^{i\omega_{fi}t}\left\langle\tilde{\Psi}_f\right|\frac{\mathrm{d}\tilde{\Psi}_i}{\mathrm{d}\varepsilon(\omega_{fi})}\right\rangle\}_T$ corresponds to the transition dipole moment T_{fi}. The definition of the transition dipole moments can be derived from eq. 2.8.73, giving

$$T_{fi} = \{\left\langle\tilde{\Psi}_f\right| e^{i\omega_{fi}t}\frac{\mathrm{d}\hat{H}}{\mathrm{d}\varepsilon(\omega_{fi})}\left|\tilde{\Psi}_i\right\rangle\}_T. \tag{2.8.75}$$

Performing a time averaging of eq. 2.8.73 ensures the fulfillment of the resonance condition which is only necessary in order to have a transition between two states, as the second term does not vanish when the frequency ω_{fi} matches the oscillation frequency of the operator $\mu \sim e^{-i\omega_{fi}t}$. In the exact case, the original form is regained

$$T_{fi} = \{\left\langle\tilde{\Psi}_f\right| e^{i\omega_{fi}t}\frac{\mathrm{d}\hat{H}}{\mathrm{d}\varepsilon(\omega_{fi})}\left|\tilde{\Psi}_i\right\rangle\}_T = \left\langle\tilde{\Psi}_f\right|\hat{\mu}\left|\tilde{\Psi}_i\right\rangle. \tag{2.8.76}$$

Note that due to the time average, the only component of the perturbation which gives a non-vanishing contribution to the transition dipole moment is the one oscillating with a phase factor $e^{-i\omega_{fi}t}$. This result is obtained only when the stationarity condition in eq. 2.8.70 holds.

EOM-CC transition dipole moments

For EOM-CC, Q_{fi} from eq. 2.8.71 is expressed as

$$Q_{fi} = \langle 0|\hat{L}_f e^{-\hat{T}}(\hat{H} - i\frac{\partial}{\partial t} - Q_f)e^{\hat{T}}\hat{R}_i e^{i\omega_{fi}t}|0\rangle \tag{2.8.77}$$

As seen for the single-state properties, this expression does not lead to size-intensive transition dipole moments. In order to have size-extensive properties, Q_{fi} may be recast in a connected form, by adding and subtracting $\langle 0|\hat{L}_f\hat{R}_i e^{-\hat{T}}(\hat{H} - i\frac{\partial}{\partial t})e^{\hat{T}}e^{i\omega_{fi}t}|0\rangle$.

$$Q_{fi} = \langle 0|\hat{L}_f[e^{-\hat{T}}(\hat{H} - i\frac{\partial}{\partial t} - Q_f)e^{\hat{T}}, \hat{R}_i]e^{i\omega_{fi}t}|0\rangle + \langle 0|\hat{L}_f\hat{R}_i e^{-\hat{T}}(\hat{H} - i\frac{\partial}{\partial t} - Q_f)e^{\hat{T}}e^{i\omega_{fi}t}|0\rangle \tag{2.8.78}$$

From the discussion in sec. 2.8.1, the operator $\hat{L}_f$ is known to be semi-additive, while $\hat{X}$ and and $\hat{R}_i$ are additive. Following eq. 2.8.15, the introduction of a commutator between two of the three operators guarantees that the whole formulation is size-extensive. The second

[‡]In time-dependent perturbation theory, the eigenstates of the unperturbed Hamiltonian $\hat{H}_0$ can be written as $|\Psi_i(t)\rangle = a_i(t)e^{-iE_i t}|i\rangle + \sum_{s\neq i} a_s(t)e^{-iE_s t}|s\rangle$. For the expansion coefficients, the expression at first order are found to be

$$a_i^{(1)} = 1 - i\int_o^t e^{i\omega_{ii}\tau}\langle\Psi_i|\frac{\mathrm{d}\hat{V}}{\mathrm{d}\varepsilon}|\Psi_i\rangle\, d\tau, \qquad a_f^{(1)} = -i\int_o^t e^{i\omega_{fi}\tau}\langle\Psi_i|\frac{\mathrm{d}\hat{V}}{\mathrm{d}\varepsilon}\left|\Psi_f\right\rangle d\tau. \tag{2.8.74}$$

The first term on the right hand-side of eq. 2.8.73 can be rewritten as $i\frac{\partial}{\partial t}e^{i\omega_{fi}t}\left\langle\frac{\mathrm{d}\tilde{\Psi}_f}{\mathrm{d}\varepsilon(\omega_{fi})}\right|\left.\tilde{\Psi}_i\right\rangle$, which corresponds to the overlap between the zeroth-order wave function Ψ_i and the first-order wave function $\Psi_f^{(1)}$. From the discussed form of $a_f(t)$ is appears that $\left\langle\frac{\mathrm{d}\tilde{\Psi}_f}{\mathrm{d}\varepsilon(\omega_{fi})}\right|\left.\tilde{\Psi}_i\right\rangle = a_f^{(1)*}$ and the whole first term on the right hand-side of eq. 2.8.73 simplifies to $i\frac{\partial}{\partial t}e^{i\omega_{fi}t}(i\int_o^t e^{-i\omega_{fi}\tau}\left\langle\Psi_f\right|\hat{\mu}|\Psi_i\rangle\, d\tau) = \left\langle\Psi_f\right|\hat{\mu}|\Psi_i\rangle$. In quantum mechanics this quantity is the transition moment $\left\langle\Psi_f\right|\hat{\mu}|\Psi_i\rangle = T_{fi}$.

term can be shown to vanish by inserting the resolution of identity

$$\begin{aligned}&\langle 0|\,\hat{L}_f\hat{R}_i(|0\rangle\langle 0| + \sum_\mu |\mu\rangle\langle\mu|)e^{-\hat{T}}(\hat{H} - i\frac{\partial}{\partial t})e^{\hat{T}}e^{i\omega_{fi}t}\,|0\rangle = \\ &\underbrace{\langle 0|\,\hat{L}_f\hat{R}_i\,|0\rangle}_{=\delta_{if}=0}\langle 0|\,e^{-\hat{T}}(\hat{H} - i\frac{\partial}{\partial t})e^{\hat{T}}e^{i\omega_{fi}t}\,|0\rangle + \sum_\mu \langle 0|\,\hat{L}_f\hat{R}_i\,|\mu\rangle\underbrace{\langle\mu|\,e^{-\hat{T}}(\hat{H} - i\frac{\partial}{\partial t})e^{\hat{T}}e^{i\omega_{fi}t}\,|0\rangle}_{=0} = 0.\end{aligned} \tag{2.8.79}$$

The biorthonormality constraint for the first term and the amplitude equation for the second cause the whole expression to vanish.

The form in eq. 2.8.77 is stationary with respect to the $\hat{L}$, $\hat{R}$ operators, but not with respect to $\hat{T}$, giving the stationarity condition

$$\begin{aligned}&\langle 0|\,\delta\hat{L}_f e^{-\hat{T}}(\hat{H} - i\frac{\partial}{\partial t} - Q_f)e^{\hat{T}}\hat{R}_i e^{i\omega_{fi}t}\,|0\rangle \\ &+ \langle 0|\,\hat{L}_f e^{-\hat{T}}(\hat{H} - i\frac{\partial}{\partial t} - Q_f)e^{\hat{T}}\delta\hat{R}_i e^{i\omega_{fi}t}\,|0\rangle + i\frac{\partial}{\partial t}e^{i\omega_{fi}t}\langle 0|\,\hat{L}_f\delta\hat{R}_i\,|0\rangle = 0.\end{aligned} \tag{2.8.80}$$

Differentiation of the quasi-energy with respect to the perturbation and time averaging yields

$$\begin{aligned}\frac{\mathrm{d}\{Q_{fi}\}_T}{\mathrm{d}\varepsilon} = &\{\langle 0|\,\frac{\mathrm{d}\hat{L}_f}{\mathrm{d}\varepsilon}e^{-\hat{T}}(\hat{H} - i\frac{\partial}{\partial t} - Q_f)e^{\hat{T}}\hat{R}_i e^{i\omega_{fi}t}\,|0\rangle\}_T \\ &+ \{\langle 0|\,\hat{L}_f e^{-\hat{T}}(\hat{H} - i\frac{\partial}{\partial t} - Q_f)e^{\hat{T}}\frac{\mathrm{d}\hat{R}_i}{\mathrm{d}\varepsilon}e^{i\omega_{fi}t}\,|0\rangle\}_T \\ &+ \{\langle 0|\,\hat{L}_f\left(\frac{\mathrm{d}}{\mathrm{d}\varepsilon}e^{-\hat{T}}\right)(-i\frac{\partial}{\partial t})e^{\hat{T}}\hat{R}_i e^{i\omega_{fi}t}\,|0\rangle\}_T \\ &+ \{\langle 0|\,\hat{L}_f\left(\frac{\mathrm{d}}{\mathrm{d}\varepsilon}e^{-\hat{T}}\right)(\hat{H} - Q_f)e^{\hat{T}}\hat{R}_i e^{i\omega_{fi}t}\,|0\rangle\}_T.\end{aligned} \tag{2.8.81}$$

Substituting the stationarity condition in eq. 2.8.73 and recognising the definition of the transition dipole moment as expressed in sec. 2.8.2, the transition dipole moment is given

$$\begin{aligned}T_{fi} = \{\langle 0|\,\hat{L}_f[\frac{\mathrm{d}e^{-\hat{T}}\hat{H}e^{\hat{T}}}{\mathrm{d}\varepsilon}, \hat{R}_i]e^{i\omega_{fi}t}\,|0\rangle\}_T = &\langle 0|\,\hat{L}_f[e^{-\hat{T}}\hat{\mu}e^{\hat{T}}, \hat{R}_i]\,|0\rangle \\ &+ \langle 0|\,\hat{L}_f[[e^{-\hat{T}}\hat{H}e^{\hat{T}}, \frac{\partial\hat{T}(\omega_{fi})}{\partial\varepsilon}], \hat{R}_i]\,|0\rangle\,.\end{aligned} \tag{2.8.82}$$

Note that differentiation of the similarity-transformed Hamiltonian is here mandatory, therefore requiring the computation of the perturbed amplitudes. As seen for single-state properties, perturbed amplitudes need to be computed separately for every perturbation; the Lagrange formulation, leading to transition densities, is therefore preferred.[115] The Lagrange functional $\mathscr{L}_{fi}$ here is

$$\begin{aligned}\mathscr{L}_{fi} = &\langle 0|\,\hat{L}_f[e^{-\hat{T}}\hat{H}e^{\hat{T}}, \hat{R}_i]e^{i\omega_{fi}t}\,|0\rangle - Q_f\langle 0|\,\hat{L}_f e^{i\omega_{fi}t}\hat{R}_i\,|0\rangle \\ &- \langle 0|\,\hat{Z}(\omega)e^{-\hat{T}}(\hat{H} - i\frac{\partial}{\partial t})e^{\hat{T}}\,|0\rangle - \eta\langle 0|\,\hat{L}_f\hat{R}_i - \delta_{fi}\,|0\rangle\,,\end{aligned} \tag{2.8.83}$$

where the constraints are given by the amplitude equation in time-dependent CC theory and the biorthonormality condition in EOM-CC. Note that the Lagrangian gains the form

in eq. 2.8.42 in the case of $i = f$.
The transition dipole moment is found through partial differentiation of the Lagrangian

$$T_{fi} = \frac{\partial\{\mathscr{L}_{fi}\}_T}{\partial\varepsilon(\omega_{fi})} = \{\langle 0|\,\hat{L}_f[e^{-\hat{T}}\frac{\partial\hat{H}}{\partial\varepsilon(\omega_{fi})}e^{\hat{T}},\hat{R}_i]e^{i\omega_{fi}t}\,|0\rangle\}_T - \{\langle 0|\,\hat{Z}(\omega_{fi})e^{-\hat{T}}\frac{\partial\hat{H}}{\partial\varepsilon(\omega_{fi})}e^{\hat{T}}\,|0\rangle\}_T. \tag{2.8.84}$$

The differentiation $\frac{\partial\hat{H}}{\partial\varepsilon(\omega_{fi})}$ gives the part of the perturbation oscillating with a phase factor $e^{-i\omega_{fi}t}$, i.e., $\frac{\partial\hat{H}}{\partial\varepsilon(\omega_{fi})} = \hat{\mu}e^{-i\omega_{fi}t}$. Looking at the second term in the equation, the time averaging imposes that $\hat{Z}(\omega)$ has a phase factor $e^{i\omega_{fi}t}$.
The Lagrange multipliers $\hat{Z}$ are found by imposing the stationarity conditions with respect to the amplitudes

$$\begin{aligned}\frac{\partial\{\mathscr{L}_{fi}\}_T}{\partial t_\nu(\omega_{fi})} &= \{\langle 0|\,\hat{L}_f[[\bar{H},\frac{\partial\hat{T}}{\partial t_\nu(\omega_{fi})}],\hat{R}_i]e^{i\omega_{fi}t}\,|0\rangle\}_T \\ &\quad - \{\langle 0|\,\hat{Z}(\omega_{fi})\Big([\bar{H},\frac{\partial\hat{T}}{\partial t_\nu(\omega_{fi})}] - i\frac{\partial}{\partial t_\nu(\omega_{fi})}\frac{\partial\hat{T}}{\partial t}\Big)\,|0\rangle\}_T.\end{aligned} \tag{2.8.85}$$

Due to the time averaging of the first term, the part of $\frac{\partial\hat{T}}{\partial t_\nu(\omega_{fi})}$ which leads to a non-vanishing contribution needs to oscillate with a phase factor $e^{-i\omega_{fi}t}$. The time-dependence of $\hat{Z}(\omega)$ determined in eq. 2.8.84, $e^{i\omega_{fi}t}$, matches with the phase of the amplitude, leading to a non-vanishing second term in eq. 2.8.85. Performing the time differentiation in the last term of eq. 2.8.85 leads to

$$\frac{\partial\{\mathscr{L}_{fi}\}_T}{\partial t_\nu(\omega_{fi})} = \langle 0|\,\hat{L}_f[[\bar{H},\hat{R}_i],\hat{\tau}_\nu(\omega_{fi})]\,|0\rangle - \langle 0|\,\hat{Z}(\omega_{fi})\Big([\bar{H},\hat{\tau}_\nu(\omega_{fi})] - \omega_{fi}\hat{\tau}_\nu(\omega_{fi})\Big)\,|0\rangle = 0. \tag{2.8.86}$$

In the case of $i = f$, the same parameter $\eta = \Delta E_{\text{exc}}$ is found as seen for the single-state properties.

Once the functional has been made stationary with respect to the amplitudes. Note that the time averaging selects $\hat{Z}(\omega_{fi})$ as only non-vanishing contribution. This expression may be rewritten as $T_{fi} = \sum_{pq} D^{fi}_{pq}\mu_{pq}$, obtaining an expression for the one-electron *transition density* $\mathbf{D}^{fi}$.

The non-Hermiticity of the theory reflects on the fact that transition moments do not respect the symmetry $T_{fi} \neq T^*_{if}$, valid in the exact case. The oscillator strength f_{fi} is the measurable observable connected to transition dipole moments

$$f_{fi} = \frac{2}{3}(E_f - E_i)|T_{fi}|^2. \tag{2.8.87}$$

For EOM-CC theory, the dipole strength is calculated as $f_{fi} = \frac{2}{3}(E_f - E_i)T_{fi}T_{if}$. As a consequence, the EOM-CC approximation of the positive quantity $|T_{fi}|^2$ may result in a negative number, as $T_{fi}T_{if}$ can become negative for a non-Hermitian theory.[36] This problematic result is another limitation of EOM-CC theory.

Chapter 3

Unitary Coupled-Cluster Theory

This chapter deals with the formulation of a solution to the problems arising from the non-Hermitian character of Coupled-Cluster theory, which have been discussed in the last chapter. The first target of the discussion consists in the development of a theory with a Hermitian character, able to avoid the unphysical appearance of complex energies. In order to do so, the ansatz of unitary coupled-cluster theory is exploited.[48] The parameterisation of the wave function is discussed on the basis of the approximation suggested by Liu *et al.*[160] This theory is then adapted to treat the finite magnetic-field case, which is a novel development of UCC.

3.1 Unitary Coupled-Cluster ansatz

Unitary Coupled-Cluster (UCC) theory is formulated through a modification of the CC ansatz. The wave function is expressed through the exponential operator $\hat{U} = e^{\hat{\sigma}-\hat{\sigma}^\dagger}$. This operator satisfies the definition of a unitary operator, i.e., an operator satisfying $\hat{U}^\dagger\hat{U} = 1$ or equivalently $\hat{U}^\dagger = \hat{U}^{-1}$. This property is fulfilled by the defined $\hat{U}$ operator, as

$$\hat{U}^\dagger = (e^{\hat{\sigma}-\hat{\sigma}^\dagger})^\dagger = e^{\hat{\sigma}^\dagger-\hat{\sigma}} = \hat{U}^{-1}. \tag{3.1.1}$$

The Unitary Coupled Cluster (UCC) ansatz is therefore given by a unitary transformation of the reference determinant, and is written as

$$|\Psi_{\mathrm{UCC}}\rangle = e^{\hat{\sigma}-\hat{\sigma}^\dagger}\,|0\rangle\,, \tag{3.1.2}$$

where $|0\rangle$ is the Fermi vacuum; here the HF determinant is chosen. $\hat{\sigma}$ is an excitation operator of the form

$$\hat{\sigma} = \hat{\sigma}_1 + \hat{\sigma}_2 + \hat{\sigma}_3 + \ldots \qquad \hat{\sigma}_n = \frac{1}{(n!)^2}\sum \sigma_{ijk\ldots}^{abc\ldots}\{a^\dagger i b^\dagger j c^\dagger k \ldots\} = \sum_n \sigma_n \hat{\tau}_n. \tag{3.1.3}$$

Note that $\hat{\sigma}^\dagger$ is a de-excitation operator and does not commute with the excitation operators: $[\hat{\sigma}, \hat{\sigma}^\dagger] \neq 0$.

Analogously to CC, the unitary parameterisation is equivalent to FCI, in its untruncated form

$$e^{\hat{\sigma}-\hat{\sigma}^\dagger}\,|0\rangle = [1 + (\hat{\sigma}-\hat{\sigma}^\dagger) + \frac{1}{2}(\hat{\sigma}-\hat{\sigma}^\dagger)(\hat{\sigma}-\hat{\sigma}^\dagger) + \frac{1}{3!}(\hat{\sigma}-\hat{\sigma}^\dagger)(\hat{\sigma}-\hat{\sigma}^\dagger)(\hat{\sigma}-\hat{\sigma}^\dagger) + \ldots]\,|0\rangle\,. \tag{3.1.4}$$

It is not as straightforward as for CC to write the equivalent operator combinations, contributing to each FCI excitation operator; here only an idea of how this equivalence can be

established is provided, by presenting some selected terms contributing to the FCI operator at the lowest excitation level $\hat{C}_0$

$$\hat{C}_0 = 1 + \frac{1}{2}\sum_n \hat{\sigma}_n^\dagger \hat{\sigma}_n + \frac{1}{3!}\sum_{ij} \hat{\sigma}_i^\dagger \hat{\sigma}_j^\dagger \hat{\sigma}_{i+j} + \frac{1}{4!}\sum_{ijk} \hat{\sigma}_i^\dagger \hat{\sigma}_j^\dagger \hat{\sigma}_k^\dagger \hat{\sigma}_{i+j+k} + \dots \tag{3.1.5}$$

Every combination of excitation and de-excitation operators, with a global excitation level of 0 contribute. The same reasoning can be applied to the other excitation operators: $\hat{C}_n$ is given by the sum of all combination of excitation and de-excitation operators, whose overall excitation level is n. Comparing to the equivalence explained for CC theory in eq. 2.7.4, it appears that UCC has a higher level of complexity, but in its full expansion an exact equivalence to FCI can be established in the same way.

Inserting the UCC ansatz for the wave function Ψ_{UCC} into the Schrödinger equation yields

$$\hat{H}\left|\Psi_{\mathrm{UCC}}\right\rangle = E_{\mathrm{UCC}}\left|\Psi_{\mathrm{UCC}}\right\rangle \implies \hat{H}e^{\hat{\sigma}-\hat{\sigma}^\dagger}\left|0\right\rangle = E_{\mathrm{UCC}}e^{\hat{\sigma}-\hat{\sigma}^\dagger}\left|0\right\rangle. \tag{3.1.6}$$

The energy can be found by projection on the wave function $\langle\Psi_{\mathrm{UCC}}|$, which, unlike for standard CC, is the adjoint of the state $|\Psi_{\mathrm{UCC}}\rangle$

$$E_{\mathrm{UCC}} = \left\langle 0\right| e^{-(\hat{\sigma}-\hat{\sigma}^\dagger)}\hat{H}e^{\hat{\sigma}-\hat{\sigma}^\dagger}\left|0\right\rangle = \left\langle 0\right|\bar{H}\left|0\right\rangle. \tag{3.1.7}$$

This formulation involves the unitary transformation of the Hamiltonian $\bar{H} = e^{-(\hat{\sigma}-\hat{\sigma}^\dagger)}\hat{H}e^{\hat{\sigma}-\hat{\sigma}^\dagger}$, giving a Hermitian expression for the energy, $(e^{-(\hat{\sigma}-\hat{\sigma}^\dagger)})^\dagger = e^{\hat{\sigma}-\hat{\sigma}^\dagger}$. The energy values are therefore bound to be real.

In analogy to standard CC theory, the amplitudes are determined by projecting the Schrödinger equation on the excited determinants $\{\Phi_\mu\}$ (*amplitude equations*)

$$\left\langle\Phi_\mu\right|\bar{H}\left|0\right\rangle = 0. \tag{3.1.8}$$

One of the main advantages of the exponential parameterisation in CC is the size-extensivity; this property is still fulfilled by UCC. In the case of two non-interacting subsystems A and B, size-extensivity requires $E_{\mathrm{AB}} = E_{\mathrm{A}} + E_{\mathrm{B}}$, while the wave function is given by

$$\left|\Psi_{\mathrm{AB}}\right\rangle = e^{\hat{\sigma}_{\mathrm{A}}-\hat{\sigma}_{\mathrm{A}}^\dagger+\hat{\sigma}_{\mathrm{B}}-\hat{\sigma}_{\mathrm{B}}^\dagger}\left|0\right\rangle. \tag{3.1.9}$$

Recalling that for two operators $\hat{X}$, $\hat{Y}$

$$e^{\hat{X}+\hat{Y}} = e^{\hat{X}}e^{\hat{Y}} \Leftrightarrow [\hat{X},\hat{Y}] = 0, \tag{3.1.10}$$

the partitioning of the wave function in eq. 3.1.9 can be performed if $[\hat{\sigma}_{\mathrm{A}} - \hat{\sigma}_{\mathrm{A}}^\dagger, \hat{\sigma}_{\mathrm{B}} - \hat{\sigma}_{\mathrm{B}}^\dagger] = 0$. Although excitation and de-excitation operators usually do not commute, the orbitals of system A and of system B belong to two orthogonal spaces, and therefore the commutator vanishes

$$\left|\Psi_{\mathrm{AB}}\right\rangle = e^{\hat{\sigma}_{\mathrm{A}}-\hat{\sigma}_{\mathrm{A}}^\dagger+\hat{\sigma}_{\mathrm{B}}-\hat{\sigma}_{\mathrm{B}}^\dagger}\left|0\right\rangle = e^{\hat{\sigma}_{\mathrm{A}}-\hat{\sigma}_{\mathrm{A}}^\dagger}e^{\hat{\sigma}_{\mathrm{B}}-\hat{\sigma}_{\mathrm{B}}^\dagger}\left|0\right\rangle. \tag{3.1.11}$$

The Hamilton operator can be separated into $\hat{H}_{\mathrm{AB}} = \hat{H}_{\mathrm{A}} + \hat{H}_{\mathrm{B}}$, as the two systems are assumed to not interact. The energy of the system AB is

$$\begin{aligned} E_{\mathrm{AB}} &= \left\langle\Psi_{\mathrm{AB}}\right|\hat{H}i_{\mathrm{AB}}\left|\Psi_{\mathrm{AB}}\right\rangle = \left\langle 0\right| e^{-(\hat{\sigma}_{\mathrm{A}}-\hat{\sigma}_{\mathrm{A}}^\dagger)}e^{-(\hat{\sigma}_{\mathrm{B}}-\hat{\sigma}_{\mathrm{B}}^\dagger)}(\hat{H}_{\mathrm{A}}+\hat{H}_{\mathrm{B}})e^{\hat{\sigma}_{\mathrm{A}}-\hat{\sigma}_{\mathrm{A}}^\dagger}e^{\hat{\sigma}_{\mathrm{B}}-\hat{\sigma}_{\mathrm{B}}^\dagger}\left|0\right\rangle = \\ &= \left\langle 0\right| e^{\hat{\sigma}_{\mathrm{A}}-\hat{\sigma}_{\mathrm{A}}^\dagger}\hat{H}_{\mathrm{A}}e^{-(\hat{\sigma}_{\mathrm{A}}-\hat{\sigma}_{\mathrm{A}}^\dagger)}\left|0\right\rangle + \left\langle 0\right| e^{-(\hat{\sigma}_{\mathrm{B}}-\hat{\sigma}_{\mathrm{B}}^\dagger)}\hat{H}_{\mathrm{B}}e^{\hat{\sigma}_{\mathrm{B}}-\hat{\sigma}_{\mathrm{B}}^\dagger}\left|0\right\rangle = E_{\mathrm{A}} + E_{\mathrm{B}}. \end{aligned} \tag{3.1.12}$$

Thus, the unitary framework possesses the advantage of size-extensivity typical of the exponential parameterisation of standard CC theory.

3.1.1 Bernoulli expansion of the transformed Hamiltonian

In order to obtain the working equations for the energy and the amplitudes, the transformed Hamiltonian may be expanded; the BCH expansion here yields

$$\bar{H} = e^{-(\hat{\sigma}-\hat{\sigma}^\dagger)}\hat{H}e^{\hat{\sigma}-\hat{\sigma}^\dagger} = \hat{H} + [\hat{H},\hat{\sigma}] + [\hat{\sigma}^\dagger,\hat{H}] + \frac{1}{2}\{[[\hat{H},\hat{\sigma}],\hat{\sigma}] + [\hat{\sigma}^\dagger,[\hat{\sigma}^\dagger,\hat{H}]] + [\hat{H},[\hat{\sigma},\hat{\sigma}^\dagger]]\} + \dots \tag{3.1.13}$$

This expansion involves commutators as $[\hat{\sigma},\hat{\sigma}^\dagger]$, which do not vanish, resulting in a non-truncating series. This is the major difference to CC theory, as the BCH expansion of the CC similarity-transformed Hamiltonian truncates after the fourth commutator (see sec. 2.7).

For UCC, the major issue is about how to design a reasonable truncation scheme. Kutzelnigg approached the problem by developing a unitary version of CC in 1991.[233] Bartlett explored the truncation of the UCC ansatz by only considering terms up to a certain perturbative order in the BCH expansion;[49] these methods are named UCC(n), with n as the order of truncation.

More recent suggestions for truncating UCC have been explored by Taube *et al.*,[51] where an alternative to the BCH formulation is found in the Zassenhaus expansion. The latter has the advantage of decoupling excitation and de-excitation operators exactly; however, it does not yield tractable equations. Truncation of the exponential operator of the ground-state wave function opens two possible ways for the calculation of the energy: either the left state is defined through the inverse operator, yielding a connected formulation but breaking the variational condition, or through the adjoint operator, which however leads to an energy expression which cannot be written in a connected form, violating size-extensivity.[51]

In this thesis, the truncation scheme described in ref. 160 is adopted. As described in ref. 49, the expansion of the transformed Hamiltonian can be simplified by observing some major cancellation between commutators involving the Fock matrix and those involving the potential. This leads to a single commutator with the Fock matrix and a series of commutators with the potential in which the coefficients are given by the Bernoulli numbers. This result was already obtained by Kutzelnigg;[234,235] however, in the following the easier derivation described in ref. 160 is presented.

We first introduce the definition of a superoperator,[235] as it is needed to derive the Bernoulli expansion. Given the operator $\hat{D}$, the spectral theorem can be exploited to obtain its representation through the knowledge of its eigenvalues d_k and its eigenvectors $|v_k\rangle$, giving $\hat{D} = \sum_k d_k \hat{P}_k$. Here $\hat{P}_k$ is the orthogonal projector on the corresponding eigenvector v_k, $\hat{P}_k = |v_k\rangle\langle v_k|$. The superoperator $\hat{\mathscr{D}}$ associated to $\hat{D}$ is defined through the relation

$$\hat{\mathscr{D}}\hat{C} = [\hat{D},\hat{C}] = \sum_{k,l}(d_k - d_l)\hat{P}_k\hat{C}\hat{P}_l, \tag{3.1.14}$$

where $\hat{C}$ is an arbitrary operator. The power of a superoperator is defined through repeated applications

$$(\hat{\mathscr{D}})^n\hat{C} = [\hat{D},[\hat{D},\dots[\hat{D},\hat{C}]\dots]] = \sum_{k,l}(d_k - d_l)^n\hat{P}_k\hat{C}\hat{P}_l. \tag{3.1.15}$$

Therefore, the exponential of a superoperator results in a similarity transformation:

$$e^{\hat{\mathscr{D}}} = \sum_{k,l} e^{d_k - d_l}\hat{P}_k\hat{C}\hat{P}_l = (\sum_k e^{b_k}\hat{P}_k)\hat{C}(\sum_l e^{-b_l}\hat{P}_l) = e^{\hat{D}}\hat{C}e^{-\hat{D}} \tag{3.1.16}$$

It is therefore possible to define a superoperator $\hat{\mathscr{S}}$, associated to $-(\hat{\sigma}-\hat{\sigma}^\dagger)$, in order to rewrite the similarity transformed Hamiltonian as

$$\bar{H} = e^{-(\hat{\sigma}-\hat{\sigma}^\dagger)}\hat{H}e^{\hat{\sigma}-\hat{\sigma}^\dagger} = e^{\hat{\mathscr{S}}}\hat{H} = e^{\hat{\mathscr{S}}}\hat{F} + e^{\hat{\mathscr{S}}}\hat{V}. \tag{3.1.17}$$

Eq. 3.1.17 can be rewritten in terms of a polynomial function defined through the Taylor expansion of the exponential

$$\bar{H} = \hat{F} + \hat{X}(\hat{\mathscr{D}})\hat{\mathscr{D}}\hat{F} + e^{\hat{\mathscr{D}}}\hat{V}, \tag{3.1.18}$$

where $\hat{X}(\hat{\mathscr{D}}) = \sum_n \frac{1}{n!}\hat{\mathscr{D}}^{n-1} = 1 + \frac{1}{2}\hat{\mathscr{D}} + \frac{1}{6}\hat{\mathscr{D}}^2 + \dots$ For the superoperator applied on the Fock operator

$$e^{\hat{\mathscr{D}}}\hat{F} = \hat{F} + X(\hat{\mathscr{D}})\hat{\mathscr{D}}\hat{F} \qquad \Longrightarrow \qquad X(\hat{\mathscr{D}}) = \frac{e^{\hat{\mathscr{D}}} - 1}{\hat{\mathscr{D}}}. \tag{3.1.19}$$

The coefficients in the so-called Bernoulli series are defined through the exponential generating function[236]

$$\frac{x}{e^x - 1} = \sum_{n=0}^{\infty} B_n \frac{x^n}{n!}. \tag{3.1.20}$$

Comparing the exponential generating function to eq. 3.1.19, the connection to $X(\hat{\mathscr{D}})^{-1}$ is evident. Eq. 3.1.18 can be rewritten as

$$\hat{X}^{-1}(\hat{\mathscr{D}})(\bar{H} - \hat{F}) = \hat{\mathscr{D}}\hat{F} + \hat{X}^{-1}(\hat{\mathscr{D}})e^{\hat{\mathscr{D}}}\hat{V}. \tag{3.1.21}$$

The inversion X^{-1} therefore contains the Bernoulli coefficients in the expansion

$$X^{-1}(\hat{\mathscr{D}}) = 1 + \sum_n B_n \hat{\mathscr{D}}^n \qquad B_1 = -\frac{1}{2}, B_2 = \frac{1}{6}, B_3 = 0, B_4 = -\frac{1}{30}, \dots \tag{3.1.22}$$

The coefficients in the Bernoulli expansion in the convention that $B_1 = -\frac{1}{2}$ (note that there exists also a less used convention with $B_1 = \frac{1}{2}$) can be calculated recursively[236]

$$B_m = -\frac{1}{m+1} \sum_{j=0}^{m-1} \binom{m+1}{j} B_j. \tag{3.1.23}$$

It can be proven that, for odd n, with $n > 1$, the coefficients B_n vanish.
A recursive form of the Hamilton operator is obtained from eq. 3.1.21

$$(1 + \sum_n B_n \hat{\mathscr{D}}^n)(\bar{H} - \hat{F}) = \hat{\mathscr{D}}\hat{F} + \hat{X}^{-1}(\hat{\mathscr{D}})e^{\hat{\mathscr{D}}}\hat{V}. \tag{3.1.24}$$

The transformed Hamiltonian can be separated as $\bar{H} = \hat{F} + \bar{V}$, where $\bar{V}$ is defined to gather all contributions to the transformed Hamiltonian besides the Fock operator $\hat{F}$. An expression suitable for an iterative determination of $\bar{V}$ is obtained

$$\bar{V} = \hat{\mathscr{D}}\hat{F} + \hat{X}^{-1}(\hat{\mathscr{D}})e^{\hat{\mathscr{D}}}\hat{V} - \sum_{n \neq 0} B_n \hat{\mathscr{D}}^n \bar{V}. \tag{3.1.25}$$

Now, the definition by Kutzelnigg[234] of the *non-diagonal part* $\hat{O}_{\mathrm{ND}}$ of an operator $\hat{O}$ is introduced: it is defined as the joint set of excitation and de-excitation portions of the operator not containing number-conserving parts. The remaining part without $\hat{O}_{\mathrm{ND}}$ is the so-called *rest part* $\hat{O}_{\mathrm{R}} = \hat{O} - \hat{O}_{\mathrm{ND}}$.

The final form of the expansion is then found to be

$$\begin{aligned}
\bar{H} &= \bar{H}_0 + \bar{H}_1 + \bar{H}_2 + \bar{H}_3 + \dots \\
\bar{H}_0 &= F + V, \\
\bar{H}_1 &= [F, \tilde{\sigma}] + \frac{1}{2}[V, \tilde{\sigma}] + \frac{1}{2}[V_{\mathrm{R}}, \tilde{\sigma}], \\
\bar{H}_2 &= \frac{1}{12}[[V_{\mathrm{ND}}, \tilde{\sigma}], \sigma] + \frac{1}{4}[[V, \tilde{\sigma}]_{\mathrm{R}}, \tilde{\sigma}] + \frac{1}{4}[[V_{\mathrm{R}}, \tilde{\sigma}]_{\mathrm{R}}, \tilde{\sigma}], \\
\bar{H}_3 &= \frac{1}{24}[[[V_{\mathrm{ND}}, \tilde{\sigma}], \tilde{\sigma}]_{\mathrm{R}}, \sigma] + \frac{1}{8}[[[V, \tilde{\sigma}]_{\mathrm{R}}, \tilde{\sigma}]_{\mathrm{R}}, \tilde{\sigma}] + \frac{1}{8}[[[V_{\mathrm{R}}, \tilde{\sigma}]_{\mathrm{R}}, \tilde{\sigma}]_{\mathrm{R}}, \tilde{\sigma}], \\
&\quad - \frac{1}{24}[[[V, \tilde{\sigma}]_{\mathrm{R}}, \tilde{\sigma}], \tilde{\sigma}] - \frac{1}{24}[[[V_{\mathrm{R}}, \tilde{\sigma}]_{\mathrm{R}}, \tilde{\sigma}], \tilde{\sigma}],
\end{aligned} \tag{3.1.26}$$

where $\tilde{\sigma} = \hat{\sigma} - \hat{\sigma}^\dagger$ has been adopted.

Once the structure of the transformed Hamiltonian is defined, it may be inserted in the energy equation 3.1.7 for the calculation of the ground-state energy; the solution of the amplitude equations in eq. 3.1.8 yield the parameters of the ground-state wave function.

3.1.2 UCC for excited states

This section aims at describing excited states through UCC theory, adapting the formalism explained for EOM-CC to the UCC framework. The most intuitive parameterisation consists in applying an excitation operator on the UCC ground-state wave function, obtaining $|\Psi_k\rangle = \hat{R} e^{\hat{\sigma}-\hat{\sigma}^\dagger} |0\rangle$, with $\hat{R}$ defined as in eq. 2.7.15 as $\hat{R} = \sum_{ia} r_i^a \{\hat{a}^\dagger \hat{i}\} + \sum_{i<j,a<b} r_{ij}^{ab} \{\hat{a}^\dagger \hat{i} \hat{b}^\dagger \hat{j}\} + \dots$ An alternative is given by exciting the reference state and then applying the unitary transformation to it, obtaining $|\Psi_k\rangle = e^{\hat{\sigma}-\hat{\sigma}^\dagger} \hat{R} |0\rangle$. Unlike for CC theory, for UCC these two formulations are not equivalent, due to the fact that the exponential operator and the excitation operator $\hat{R}$ do not commute, i.e. $[e^{\hat{\sigma}-\hat{\sigma}^\dagger}, \hat{R}] \neq 0$. In order to decide which parameterisation should be adopted, the so-called *killer condition* can be considered.[237,238]

Every theory intended to describe excited states should satisfy the *killer condition*, meaning that any de-excitation of the ground state should vanish[237,238]

$$\hat{O}_k^\dagger |\Psi_{\mathrm{GS}}\rangle = 0 \qquad \forall k, \tag{3.1.27}$$

where $\hat{O}_k^\dagger = |\Psi_{\mathrm{GS}}\rangle \langle \Psi_k|$ is a de-excitation operator to the ground-state; k here labels the excited states. Therefore, the killer condition $|\Psi_{\mathrm{GS}}\rangle \langle \Psi_k | \Psi_{\mathrm{GS}}\rangle = 0 \ \forall k$ is satisfied if the excited states are all orthogonal or biorthogonal to the ground state.

UCC has been constructed to be a Hermitian theory, and the state $\langle \Psi_k|$ is given by taking the adjoint of the state $|\Psi_k\rangle$. For the first formulation of the Equation-Of-Motion (EOM) ansatz for UCC, $|\Psi_k\rangle = \hat{R} e^{\hat{\sigma}-\hat{\sigma}^\dagger} |0\rangle$ and $\langle \Psi_k| = \langle 0| e^{-(\hat{\sigma}-\hat{\sigma}^\dagger)} \hat{R}$, the killer condition is not satisfied, as

$$\langle \Psi_k | \Psi_{\mathrm{GS}}\rangle = \langle 0| e^{-(\hat{\sigma}-\hat{\sigma}^\dagger)} \hat{R}^\dagger e^{\hat{\sigma}-\hat{\sigma}^\dagger} |0\rangle . \tag{3.1.28}$$

The overlap $\langle \Psi_k | \Psi_{\mathrm{GS}}\rangle$ is not vanishing in the general case, as the commutator $[\hat{R}, e^{\hat{\sigma}-\hat{\sigma}^\dagger}] \neq 0$ does not allow the two operators to swap places. As suggested in ref. 237, the killer condition can be reestablished by introducing the similarity transformed operators $\tilde{R} = e^{\hat{\sigma}-\hat{\sigma}^\dagger} \hat{R} e^{-(\hat{\sigma}-\hat{\sigma}^\dagger)}$. With these transformed operators, the EOM ansatz is written as

$$|\Psi_k\rangle = \tilde{R} e^{\hat{\sigma}-\hat{\sigma}^\dagger} |0\rangle = e^{\hat{\sigma}-\hat{\sigma}^\dagger} \hat{R} e^{-(\hat{\sigma}-\hat{\sigma}^\dagger)} e^{\hat{\sigma}-\hat{\sigma}^\dagger} |0\rangle = e^{\hat{\sigma}-\hat{\sigma}^\dagger} \hat{R} |0\rangle . \tag{3.1.29}$$

With this ansatz, the killer condition becomes

$$\langle\Psi_k|\Psi_{\mathrm{GS}}\rangle = \langle 0|\, e^{-(\hat{\sigma}-\hat{\sigma}^\dagger)} e^{\hat{\sigma}-\hat{\sigma}^\dagger}\, \hat{R}\,|0\rangle = \langle 0|\,\hat{R}\,|0\rangle = 0. \tag{3.1.30}$$

The Schrödinger equation for excited states therefore is

$$\hat{H}\,|\Psi_k\rangle = E_k\,|\Psi_k\rangle \qquad \hat{H} e^{\hat{\sigma}-\hat{\sigma}^\dagger}\,\hat{R}\,|0\rangle = E_k e^{\hat{\sigma}-\hat{\sigma}^\dagger}\,\hat{R}\,|0\rangle\,, \tag{3.1.31}$$

and, by multiplying with $e^{-(\hat{\sigma}-\hat{\sigma}^\dagger)}$ on the left

$$\bar{H}\,\hat{R}\,|0\rangle = E_k \hat{R}\,|0\rangle \tag{3.1.32}$$

which is a CI-like problem. The excited states are found through diagonalisation of the transformed Hamiltonian matrix.

UCC is characterised by its Hermitian formalism and, unlike for CC theory, the left eigenstates are the adjoint of the right ones

$$\langle\Psi| = \langle 0|\,\hat{R}^\dagger e^{-(\hat{\sigma}-\hat{\sigma}^\dagger)}. \tag{3.1.33}$$

The orthonormality condition for different UCC excited states reads

$$\langle\Psi_k|\Psi_l\rangle = \langle 0|\,\hat{R}_k^\dagger \hat{R}_l\,|0\rangle = \delta_{kl}. \tag{3.1.34}$$

3.1.3 The UCC*n* methods

For the methods discussed here, the excitation space is chosen to include single and double excitations $\hat{\sigma} = \hat{\sigma}_1 + \hat{\sigma}_2$, defining an analogon to the CCSD method. In fact, it has been shown that UCCSD recovers a similar amount of correlation energy as standard CCSD.[239] The transformed Hamiltonian matrix has the following block structure

$$\bar{H} = \begin{pmatrix} \bar{H}_{\mathrm{SS}} & \bar{H}_{\mathrm{SD}} \\ \bar{H}_{\mathrm{DS}} & \bar{H}_{\mathrm{DD}} \end{pmatrix}. \tag{3.1.35}$$

It has been discussed already in section 3.1.1 that the expansion of the similarity transformed Hamiltonian matrix does not truncate. Therefore, a truncation scheme needs to be designed. In order to find a truncation criterion, orders in perturbation theory can be considered. It is shown hereafter that the σ_2-amplitudes are first order, while the σ_1-amplitudes are second order in perturbation theory.

The normal-ordered Hamiltonian $\hat{H}_{\mathrm{N}} = \hat{F}_{\mathrm{N}} + \hat{V}_{\mathrm{N}}$ is composed of the normal-ordered Fock operator $\hat{F}_{\mathrm{N}}$ and the potential $\hat{V}_{\mathrm{N}}$, which can be considered the perturbation. The similarity transformed Hamiltonian in the UCC framework thus is given by

$$e^{-(\hat{\sigma}-\hat{\sigma}^\dagger)}\hat{H}_{\mathrm{N}} e^{\hat{\sigma}-\hat{\sigma}^\dagger} = e^{-(\hat{\sigma}-\hat{\sigma}^\dagger)}\hat{F}_{\mathrm{N}} e^{\hat{\sigma}-\hat{\sigma}^\dagger} + e^{-(\hat{\sigma}-\hat{\sigma}^\dagger)}\hat{V}_{\mathrm{N}} e^{\hat{\sigma}-\hat{\sigma}^\dagger}. \tag{3.1.36}$$

In the Bernoulli expansion, there is only one commutator with the Fock matrix, which is

$$e^{-(\hat{\sigma}-\hat{\sigma}^\dagger)}\hat{F}_{\mathrm{N}} e^{\hat{\sigma}-\hat{\sigma}^\dagger} = \hat{F}_{\mathrm{N}} + [\hat{F}_{\mathrm{N}}, \hat{\sigma}-\hat{\sigma}^\dagger] = \hat{F}_{\mathrm{N}} + \sum_\mu \varepsilon_\mu \sigma_\mu \hat{\tau}_\mu - \sum_\mu \varepsilon_\mu \sigma_\mu^* \hat{\tau}_\mu^\dagger. \tag{3.1.37}$$

ε_μ are the orbital energies obtained from the canonical HF equation $\mathbf{FC} = \mathbf{C}\boldsymbol{\varepsilon}$. From the UCC amplitude equation, an expression for the amplitudes σ_μ is obtained

$$\langle\mu|\,\bar{H}_{\mathrm{N}}\,|0\rangle = \varepsilon_\mu\sigma_\mu + \langle\mu|\,\bar{V}_{\mathrm{N}}\,|0\rangle = 0 \implies \varepsilon_\mu\sigma_\mu = -\langle\mu|\,\bar{V}_{\mathrm{N}}\,|0\rangle\,. \tag{3.1.38}$$

The amplitudes may be expanded in perturbation orders

$$\sigma_\mu = \sigma_\mu^{(0)} + \sigma_\mu^{(1)} + \sigma_\mu^{(2)} + \sigma_\mu^{(3)} + \dots \tag{3.1.39}$$

Eq. 3.1.38 can be written for each perturbation order n, giving

$$\varepsilon_\mu \sigma_\mu^{(n)} = -\langle \mu | \, (e^{-(\hat{\sigma}-\hat{\sigma}^\dagger)} \hat{V}_\mathrm{N} e^{\hat{\sigma}-\hat{\sigma}^\dagger})^{(n)} \, |0\rangle \, . \tag{3.1.40}$$

For the first orders in perturbation, relations can be found in order to determine the contributions to the different excitation operators

$$\sigma_\mu^{(0)} = 0 \tag{3.1.41}$$

$$\varepsilon_\mu \sigma_\mu^{(1)} = -\langle \mu | \, (e^{-(\hat{\sigma}-\hat{\sigma}^\dagger)} \hat{V}_\mathrm{N} e^{\hat{\sigma}-\hat{\sigma}^\dagger})^{(1)} \, |0\rangle \rightarrow \hat{\sigma}_2^{(1)} \tag{3.1.42}$$

$$\varepsilon_\mu \sigma_\mu^{(2)} = -\langle \mu | \, (e^{-(\hat{\sigma}-\hat{\sigma}^\dagger)} \hat{V}_\mathrm{N} e^{\hat{\sigma}-\hat{\sigma}^\dagger})^{(2)} \, |0\rangle \rightarrow \hat{\sigma}_2^{(2)}, \hat{\sigma}_1^{(2)}, \hat{\sigma}_3^{(2)}. \tag{3.1.43}$$

To the excitation operators at first order, only double excitations contribute. The single excitations vanish at first order due to the Brillouin theorem, which states that the Hamiltonian matrix element between single excited determinants Φ_S and the ground state vanish, giving $\langle \Phi_\mathrm{S} | \, \hat{H} \, |0\rangle = 0$. At second order also single and triple excitations have to be considered. Truncating the excitation space at single and double excitations, in the following discussion $\hat{\sigma}_2$ is always considered to have a leading contribution at first order in perturbation theory and $\hat{\sigma}_1$ a leading contribution at second order in perturbation theory.

In this thesis, two different methods will be considered, UCC2 and UCC3, where the number expresses the order at which the amplitude equations and the energy expressions are truncated.

In the case of UCC3, it can be shown that the triple amplitudes are not needed in order to have excited-state energies correct up to third order, for excited states dominated by single excitations. This may be briefly discussed here. From the diagonalisation problem, the eigenvectors of the transformed Hamiltonian matrix can be found, in the single and double excitation space:

$$\begin{pmatrix} \bar{H}_\mathrm{SS} & \bar{H}_\mathrm{SD} \\ \bar{H}_\mathrm{DS} & \bar{H}_\mathrm{DD} \end{pmatrix} \begin{pmatrix} R_\mathrm{S} \\ R_\mathrm{D} \end{pmatrix} = E \begin{pmatrix} R_\mathrm{S} \\ R_\mathrm{D} \end{pmatrix}. \tag{3.1.44}$$

Substituting the expression for the double excitations in the single-excitation one, the following secular equation for the singles-singles block is obtained

$$(\bar{H}_\mathrm{SS} + \bar{H}_\mathrm{SD}(E - \bar{H}_\mathrm{DD})^{-1} \bar{H}_\mathrm{DS}) R_\mathrm{S} = E R_\mathrm{S}. \tag{3.1.45}$$

In order to have energies correct up to third order, $(\bar{H}_\mathrm{SS} + \bar{H}_\mathrm{SD}(E - \bar{H}_\mathrm{DD})^{-1} \bar{H}_\mathrm{DS})$ has to be truncated at third order. This implies the following truncation for the Hamilton matrix blocks:

$$\begin{pmatrix} \bar{H}_\mathrm{SS}^{(3)} & \bar{H}_\mathrm{SD}^{(2)} \\ \bar{H}_\mathrm{DS}^{(2)} & \bar{H}_\mathrm{DD}^{(1)} \end{pmatrix}. \tag{3.1.46}$$

In principle, if triple excitations were considered, also their contribution could be folded in the secular equation of the singles-singles block, giving an additional term of the form $\bar{H}_\mathrm{ST}(E - \bar{H}_\mathrm{TT})^{-1} \bar{H}_\mathrm{TS}$. As the amplitude equations 3.1.8 are satisfied for projection on singly- and doubly-excited determinants, $\bar{H}_\mathrm{ST}$ is given by three-body terms, giving at least second order in perturbation theory. The triples term $\bar{H}_\mathrm{ST}(E - \bar{H}_\mathrm{TT})^{-1} \bar{H}_\mathrm{TS}$ is at least of fourth order, thus not contributing to UCC3. Therefore, it has here been proven that triple excitations are not needed to obtain energies correct up to third order.[160]

In the case of UCC2, where the energies are exact up to second order, the secular equation gives the following truncation scheme of the Hamilton matrix blocks

$$\begin{pmatrix} \bar{H}^{(2)}_{\mathrm{SS}} & \bar{H}^{(1)}_{\mathrm{SD}} \\ \bar{H}^{(1)}_{\mathrm{DS}} & \bar{H}^{(0)}_{\mathrm{DD}} \end{pmatrix}. \tag{3.1.47}$$

With this approximation of the blocks of the Hamiltonian matrix (explicit expressions are found in sec. 4.3), it can be shown that the r^{ab}_{ij} amplitudes for the double excitations are completely determined by the amplitudes r^{a}_{i}. Therefore, the EOM-UCC2 matrix elements can be rewritten as a non-linear set of equations only dependent on the single-excitation amplitudes. For the description of states dominated by a double-excitation character, the UCC2 method is not applicable. In principle, the same could be said for UCC3 in the case of states dominated by a triple-excitation character. However, these states are not occurring in practical applications.

3.1.4 UCC2 and UCC3 amplitude equations

The full expressions of the Hamilton matrix elements can be found in section 4.3; here only the amplitude equations are reported, in order to show the differences in complexity of the various truncations. The red terms of the following expressions constitute the UCC2 amplitude equations. The whole expressions given by all terms are the complete amplitude equations for the UCC3 method.

$$\begin{aligned}
\bar{H}_{ai} &= f_{ai} + \sum_{jb} \langle aj||ib\rangle\, \sigma^{b}_{j} + \frac{1}{2}\sum_{jb} \langle ab||ij\rangle\, \sigma^{b*}_{j} + \frac{1}{2}\sum_{jbc} \langle aj||cb\rangle\, \sigma^{cb}_{ij} - \frac{1}{2}\sum_{jkb} \langle kj||ib\rangle\, \sigma^{ba}_{jk} \\
&+ \sum_{jklbc} \frac{1}{2} \langle al||ik\rangle\, \sigma^{bc*}_{jk}\sigma^{bc}_{jl} + \sum_{jkbcd} \frac{1}{2} \langle ad||ic\rangle\, \sigma^{bd*}_{jk}\sigma^{bc}_{jk} - \sum_{jklbc} \langle bl||ji\rangle\, \sigma^{bc*}_{jk}\sigma^{ca}_{kl} \\
&+ \sum_{jkbcd} \langle ab||dj\rangle\, \sigma^{bc*}_{jk}\sigma^{cd}_{ki} - \sum_{jklbc} \frac{1}{4} \langle bl||jk\rangle\, \sigma^{bc*}_{jk}\sigma^{ac}_{il} + \sum_{jkbcd} \frac{1}{4} \langle bd||jc\rangle\, \sigma^{bd*}_{jk}\sigma^{ac}_{ik} \\
&+ \sum_{jkbcd} \frac{1}{4} \langle bd||ic\rangle\, \sigma^{bd*}_{jk}\sigma^{ca}_{jk} - \sum_{jklbc} \frac{1}{4} \langle al||jk\rangle\, \sigma^{bc*}_{jk}\sigma^{cb}_{il} + \sum_{b} f_{ab}\sigma^{b}_{i} - \sum_{j} f_{ij}\sigma^{a}_{j} + \sum_{jb} f_{jb}\sigma^{ab}_{ij} = 0
\end{aligned} \tag{3.1.48}$$

$$\begin{aligned}
\bar{H}_{abij} &= \langle ab||ij\rangle - P(ab)\sum_{k} \langle ka||ji\rangle\, \sigma^{b}_{k} + P(ij)\sum_{c} \langle ab||ic\rangle\, \sigma^{c}_{j} + \frac{1}{2}\sum_{kl} \langle kl||ij\rangle\, \sigma^{ab}_{kl} \\
&+ \frac{1}{2}\sum_{cd} \langle ab||cd\rangle\, \sigma^{cd}_{ij} + P(ij)P(ab)\sum_{kc} \langle ak||ic\rangle\, \sigma^{bc}_{jk} + P(ij)P(ab)\sum_{klcd} \frac{1}{3} \langle kl||cd\rangle\, \sigma^{ac}_{ik}\sigma^{bd}_{jl} \\
&+ \sum_{klcd} \frac{1}{6} \langle kl||cd\rangle\, \sigma^{cd}_{ij}\sigma^{ab}_{kl} - P(ab)\sum_{klcd} \frac{1}{3} \langle kl||cd\rangle\, \sigma^{ad}_{ij}\sigma^{cb}_{kl} - P(ij)\sum_{klcd} \frac{1}{3} \langle kl||cd\rangle\, \sigma^{ab}_{il}\sigma^{dc}_{jk} \\
&+ P(ij)P(ab)\sum_{klcd} \frac{1}{3} \langle ad||il\rangle\, \sigma^{cd*}_{kl}\sigma^{bc}_{jk} + \sum_{klcd} \frac{1}{12} \langle cd||ij\rangle\, \sigma^{cd*}_{kl}\sigma^{ab}_{kl} + \sum_{klcd} \frac{1}{12} \langle ab||kl\rangle\, \sigma^{cd*}_{ij}\sigma^{cd}_{kl} \\
&- P(ab)\sum_{klcd} \frac{1}{6} \langle ad||ij\rangle\, \sigma^{cd*}_{kl}\sigma^{cb}_{kl} - P(ij)\sum_{klcd} \frac{1}{6} \langle ab||il\rangle\, \sigma^{cd*}_{kl}\sigma^{dc}_{jk} - P(ij)\sum_{klcd} \frac{1}{6} \langle cd||kj\rangle\, \sigma^{cd*}_{kl}\sigma^{ab}_{il} \\
&- P(ab)\sum_{klcd} \frac{1}{6} \langle bc||lk\rangle\, \sigma^{cd*}_{kl}\sigma^{ad}_{ij} + P(ab)\sum_{c} f_{bc}\sigma^{ac}_{ij} - P(ij)\sum_{k} f_{kj}\sigma^{ab}_{ik} = 0
\end{aligned} \tag{3.1.49}$$

The notation here defines $\bar{H}_{ai} = \langle \Phi_i^a | \bar{H} | 0 \rangle$ and $\bar{H}_{abij} = \left\langle \Phi_{ij}^{ab} \right| \bar{H} | 0 \rangle$. The differences in complexity are apparent: UCC2 only shows terms contracting two tensors at most, none of which contains the adjoint amplitude $\hat{\sigma}^\dagger$, while UCC3 possesses a large plethora of contributions involving three tensors, among which $\hat{\sigma}^\dagger$ has to be considered. The solution of these equations is more extensively explained in the implementation chapter 4.

3.1.5 UCC2 and UCC3 ground-state energy

The energy expression for the UCC method is obtained from

$$E_{\mathrm{UCC}} = \langle 0 | \bar{H} | 0 \rangle . \tag{3.1.50}$$

Looking at the Bernoulli expansion of the transformed Hamiltonian and taking into account that σ_2 is of first order in MP perturbation theory and σ_1 of second order, the relevant contributions to the transformed UCC3 Hamiltonian are

$$\bar{H}^0 = F + V, \tag{3.1.51}$$

$$\bar{H}^1 = [F, \sigma_1 + \sigma_2] + \frac{1}{2}[V, \sigma_1 + \sigma_2] + \frac{1}{2}[V_{\mathrm{R}}, \sigma_1 + \sigma_2], \tag{3.1.52}$$

$$\bar{H}^2 = \frac{1}{12}[[V_{\mathrm{N}}, \sigma_2], \sigma_2] + \frac{1}{4}[[V, \sigma_2]_{\mathrm{R}}, \sigma_2] + \frac{1}{4}[[V_{\mathrm{R}}, \sigma_2]_{\mathrm{R}}, \sigma_2]. \tag{3.1.53}$$

For the single commutators in $\bar{H}^1$, single excitations contribute for terms up to third order, while for the double commutators in $\bar{H}^2$, only double excitations are relevant for a third-order truncation. $\bar{H}^3$ is not needed here, as triple commutators are at least of fourth order in perturbation theory.

Note that for UCC2, $\bar{H}^0$ has the same form of eq. 3.1.51, $\bar{H}^1$ takes the form $\bar{H}^1 = [F, \sigma_1 + \sigma_2] + \frac{1}{2}[V, \sigma_2] + \frac{1}{2}[V_{\mathrm{R}}, \sigma_2]$, while $\bar{H}^2$ does not contribute.

From these expressions of the truncated transformed Hamiltonian, the final energy expression is

$$E_{\mathrm{UCC2/UCC3}} = \left(\left(\sum_{ia} F_{ia} \sigma_i^a + \frac{1}{8} \sum_{ijab} \langle ij || ab \rangle \, \sigma_{ij}^{ab} \right) + h.c. \right). \tag{3.1.54}$$

Note that UCC2 and UCC3 have the same energy expression, as all terms are of second order in perturbation theory. The terms coming from the double commutators do not contribute; for a more visual derivation of these equation it may be referred to sec. 4.2, where the exploitation of a diagrammatic formalism clarifies this statement. Naturally, the amplitudes in eq. 3.1.54 are obtained from the UCC2 or UCC3 amplitude equations.

From a computational point of view, UCC2 scales as $O(N^5)$ with system size, while UCC3 scales as $O(N^6)$, comparable to the CCSD method. For a more accurate discussion of the scaling properties of UCC2 and UCC3, see sec. 4.3 in the Implementation chapter (chapter 4), where the cost-determining terms are analysed.

3.1.6 Algebraic diagrammatic construction scheme and Unitary Coupled-Cluster theory

An alternative to UCC is given by the algebraic diagrammatic construction (ADC) scheme, which was originally formulated via the application of Green's function theory to the time-dependent Schrödinger equation.[240,241] It can be seen as an extension of the perturbation-theory approach exploited in Møller-Plesset (MP) theory[242] in order to describe excited

states.[243] The potential of ADC has grown considerably since the introduction of the so-called intermediate-state representation (ISR),[244–247] through which all matrices for energies and properties are expressed. In this frame, the ADC scheme solves a Hermitian eigenvalue problem

$$\mathbf{MY} = \mathbf{Y\Omega}, \qquad \mathbf{Y}^\dagger\mathbf{Y} = \mathbf{1}, \tag{3.1.55}$$

where $\mathbf{\Omega}$ is the diagonal matrix containing the excitation energies ω_n, $\mathbf{Y}$ is the eigenvector matrix, and $\mathbf{M}$ is the shifted Hamiltonian matrix, written in the ISR basis $\tilde{\Psi}_k$

$$M_{ij} = \left\langle \tilde{\Psi}_i \right| \hat{H} - E_0^{\mathrm{MP}n} \left| \tilde{\Psi}_j \right\rangle. \tag{3.1.56}$$

The different ADC schemes differ in the construction of the ISR basis, which are in general defined as excitations out of the correlated MPn ground-state wave function

$$\left| \tilde{\Psi}_k \right\rangle = \hat{\tau}_k \left| \Psi_{\mathrm{GS}}^{\mathrm{MP}n} \right\rangle. \tag{3.1.57}$$

The basis is then orthonormalised through a Gram-Schmidt orthonormalisation. Diagonalising the matrix $\mathbf{M}$ and solving the eigenvalue problem in eq. 3.1.55 leads to the excited states

$$|\Psi_n\rangle = \sum_j Y_{jn} \left| \tilde{\Psi}_j \right\rangle. \tag{3.1.58}$$

The order n in perturbation theory chosen for the MP wave function in eqs. 3.1.56 and 3.1.57 determines the different ADC methods, named consistently ADC(n). The ADC matrices have a well-defined order in each block; an example is given by the methods ADC(2) and ADC(3)

$$\mathbf{M}_{\mathrm{ADC(2)}} = \begin{pmatrix} M_{\mathrm{SS}}^{(2)} & M_{\mathrm{SD}}^{(1)} \\ M_{\mathrm{DS}}^{(1)} & M_{\mathrm{DD}}^{(0)} \end{pmatrix}, \qquad \mathbf{M}_{\mathrm{ADC(3)}} = \begin{pmatrix} M_{\mathrm{SS}}^{(3)} & M_{\mathrm{SD}}^{(2)} \\ M_{\mathrm{DS}}^{(2)} & M_{\mathrm{DD}}^{(1)} \end{pmatrix}. \tag{3.1.59}$$

Standard ADC schemes are single-reference methods; therefore, they should be applied only to molecular systems for which MP perturbation theory is expected to give trustworthy results.

Recently, the connection between ADC and CC theory was recognised in the particular variant of UCC described above:[160] the Bernoulli expansion of the unitarily transformed UCC Hamiltonian leads to the ADC terms.[59,160,248,249] Unlike ADC, the ground-state description of UCC is determined in a self-consistent way through the iterative procedure described before, analogous to CC. From a computational point of view, the ADC equations are obtained by substituting the amplitudes with the MPn guesses, without having to converge them iteratively.

At infinite order, these two methods are related by a unitary transformation, and yield the same results. For the truncated schemes, however, this transformation is no longer unitary and the results of UCC and ADC differ.[249,250]

3.2 Molecular properties with UCC Theory

In the following, UCC response theory is developed, following the approach discussed in sec. 2.8. To the knowledge of the author, the only existing studies on UCC properties exploit the expectation-value approach.[59] The formulation of UCC response theory offers an alternative to standard CC theory for the calculation of properties, of interest in particular for those systems, for which standard CC obtains physically wrong results, as in the case of negative oscillator strengths. This chapter is concerned with the formulation of UCC response theory for the calculation of properties, focusing on the analogies and differences to the CC approach.

3.2.1 Lagrange functional for EOM-UCC dipole moments

The theoretical approach developed in secs. 2.8.1 and 2.8.2 can be exploited to formulate EOM-UCC response theory. As a first consideration, it is important to notice that the truncated form of EOM-UCC is not variational. Therefore, the expectation-value approach and the differentiation of the energy are not equivalent, as the former does not contain the response of the wave function to the perturbation. In the following, response theory is developed.

Starting from the UCC parameterisation of excited states, $|\Psi\rangle = e^{\hat{\sigma}-\hat{\sigma}^\dagger}\hat{R}|0\rangle$ and $\langle\Psi| = \langle 0|\hat{R}^\dagger e^{-(\hat{\sigma}-\hat{\sigma}^\dagger)}$, the UCC energy is given by

$$E_{\mathrm{UCC}} = \langle 0|\hat{R}^\dagger e^{-(\hat{\sigma}-\hat{\sigma}^\dagger)}\hat{H}e^{\hat{\sigma}-\hat{\sigma}^\dagger}\hat{R}|0\rangle = \langle 0|\hat{R}^\dagger\bar{H}\hat{R}|0\rangle\,. \tag{3.2.1}$$

Both the right and the left eigenfunctions are described by additive operators and the expression in eq. 3.2.1 is size-extensive. Unlike EOM-CC, there is no need to introduce a commutator in the EOM-UCC energy.

This expression is stationary with respect to $\hat{R}$ (the proof is the same as for CC in eq. 2.8.30). The differentiation of the energy with respect to the perturbation ε gives

$$\frac{\mathrm{d}E_{\mathrm{UCC}}}{\mathrm{d}\varepsilon} = \langle 0|\hat{R}^\dagger\frac{\mathrm{d}\bar{H}}{\mathrm{d}\varepsilon}\hat{R}|0\rangle = \langle 0|\hat{R}^\dagger\frac{\mathrm{d}(e^{-(\hat{\sigma}-\hat{\sigma}^\dagger)}\hat{H}e^{\hat{\sigma}-\hat{\sigma}^\dagger})}{\mathrm{d}\varepsilon}\hat{R}|0\rangle\,. \tag{3.2.2}$$

As for CC theory, this expression requires the computation of the perturbed amplitudes $\frac{\mathrm{d}\hat{\sigma}}{\mathrm{d}\varepsilon}$ and $\frac{\mathrm{d}\hat{\sigma}^*}{\mathrm{d}\varepsilon}$, implying that for every perturbation, a different set of solving equations has to be formulated. Therefore the Lagrangian method is preferably exploited.

The construction of the appropriate functional needs to account for the Hermiticity of the theory, obtaining a Lagrangian fulfilling the relation $\mathscr{L}^*_{\mathrm{UCC}} = \mathscr{L}_{\mathrm{UCC}}$. As for CC, the constraints are the amplitude equations and the normalisation condition

$$\mathscr{L}_{\mathrm{UCC}} = \langle 0|\hat{R}^\dagger\bar{H}\hat{R}|0\rangle + \langle 0|\hat{Z}\bar{H}|0\rangle + \langle 0|\bar{H}\hat{Z}^\dagger|0\rangle - \eta\langle 0|\hat{R}^\dagger\hat{R}-1|0\rangle\,. \tag{3.2.3}$$

In the case of $\hat{R} = \hat{1}$, the Lagrange functional for the ground state is obtained.

The functional in eq. 3.2.3 can be used instead of the actual energy in order to calculate single-state properties. The stationarity conditions with respect to the amplitudes determine the $\hat{Z}$ multipliers:

$$\frac{\partial\mathscr{L}_{\mathrm{UCC}}}{\partial\sigma_\mu} = \langle 0|\hat{R}^\dagger\frac{\partial\bar{H}}{\partial\sigma_\mu}\hat{R}|0\rangle + \langle 0|\hat{Z}\frac{\partial\bar{H}}{\partial\sigma_\mu}|0\rangle + \langle 0|\frac{\partial\bar{H}}{\partial\sigma_\mu}\hat{Z}^\dagger|0\rangle\,, \tag{3.2.4}$$

$$\frac{\partial\mathscr{L}_{\mathrm{UCC}}}{\partial\sigma^*_\mu} = \langle 0|\hat{R}^\dagger\frac{\partial\bar{H}}{\partial\sigma^*_\mu}\hat{R}|0\rangle + \langle 0|\hat{Z}\frac{\partial\bar{H}}{\partial\sigma^*_\mu}|0\rangle + \langle 0|\frac{\partial\bar{H}}{\partial\sigma^*_\mu}\hat{Z}^\dagger|0\rangle\,. \tag{3.2.5}$$

Note that eq. 3.2.5, which determines $\hat{Z}^\dagger$, is the adjoint of eq. 3.2.4, the defining equation for $\hat{Z}$. Therefore, only one of these equations has to be actually solved, as the other one is automatically fulfilled. Differentiation with respect to the $\hat{R}$ amplitudes gives $\bar{H}\hat{R}|0\rangle = \eta\hat{R}|0\rangle$, which is satisfied for $\eta = \Delta E_{\mathrm{exc}}$.

Once the stationarity conditions are satisfied, the EOM-UCC properties are computed through partial differentiation of the UCC Lagrangian

$$\frac{\mathrm{d}\mathscr{L}_{\mathrm{UCC}}}{\mathrm{d}\varepsilon} = \frac{\partial\mathscr{L}_{\mathrm{UCC}}}{\partial\varepsilon} = \langle 0|\hat{R}^\dagger\bar{X}\hat{R}|0\rangle + \langle 0|\hat{Z}\bar{X}|0\rangle + \langle 0|\bar{X}\hat{Z}^\dagger|0\rangle\,. \tag{3.2.6}$$

The formalism is analogous to the modus operandi of standard CC theory, but the differentiation hides the difficulty of this approach. The differentiation of the unitarily transformed Hamilton operator can be written in detail

$$\frac{\mathrm{d}e^{-(\hat{\sigma}-\hat{\sigma}^\dagger)}\hat{H}e^{\hat{\sigma}-\hat{\sigma}^\dagger}}{\mathrm{d}\varepsilon} = \frac{\mathrm{d}e^{-(\hat{\sigma}-\hat{\sigma}^\dagger)}}{\mathrm{d}\varepsilon}\hat{H}e^{\hat{\sigma}-\hat{\sigma}^\dagger} + e^{-(\hat{\sigma}-\hat{\sigma}^\dagger)}\frac{\mathrm{d}\hat{H}}{\mathrm{d}\varepsilon}e^{\hat{\sigma}-\hat{\sigma}^\dagger} + e^{-(\hat{\sigma}-\hat{\sigma}^\dagger)}\hat{H}\frac{\mathrm{d}e^{\hat{\sigma}-\hat{\sigma}^\dagger}}{\mathrm{d}\varepsilon}. \tag{3.2.7}$$

The differentiation of the exponential operator is not at all trivial, which is clear through the series expansion

$$\frac{\mathrm{d}e^{\hat{\sigma}-\hat{\sigma}^\dagger}}{\mathrm{d}\varepsilon} = \frac{\mathrm{d}}{\mathrm{d}\varepsilon}\sum_{n=0}^{\infty}\frac{(\hat{\sigma}-\hat{\sigma}^\dagger)^n}{n!} = \cdots + \underbrace{(\hat{\sigma}-\hat{\sigma}^\dagger)\ldots(\hat{\sigma}-\hat{\sigma}^\dagger)\frac{\mathrm{d}}{\mathrm{d}\varepsilon}(\hat{\sigma}-\hat{\sigma}^\dagger)\ldots(\hat{\sigma}-\hat{\sigma}^\dagger)}_{n\text{ terms}} + \ldots \tag{3.2.8}$$

As excitation and de-excitation operators do not commute ($[\hat{\sigma},\hat{\sigma}^\dagger]\neq 0$), the derivative cannot be factorised in front of the series and the original exponential series is not regained

$$\frac{\mathrm{d}e^{\hat{\sigma}-\hat{\sigma}^\dagger}}{\mathrm{d}\varepsilon} \neq \frac{\mathrm{d}(\hat{\sigma}-\hat{\sigma}^\dagger)}{\mathrm{d}\varepsilon}(e^{\hat{\sigma}-\hat{\sigma}^\dagger}). \tag{3.2.9}$$

In order to differentiate the terms in eq. 3.2.3, it is necessary to differentiate the explicit, already truncated equations of the energy and the amplitude equations (for example in the UCC2 and UCC3 form), leading to different expressions, depending on the order of approximation.

3.2.2 FCI limit of EOM-UCC properties

In eq. 3.2.6, the two terms containing the Lagrange multipliers account for the effect of the perturbed amplitudes. As seen in the case of exact theory in sec. 2.8, these contributions vanish, due to the fact that the wave function is a solution of the Schrödinger equation. Therefore, in the limit of untrucated UCC (which is equivalent to FCI), in eq. 3.2.2 the term depending on the perturbed amplitudes, or equivalently, the terms containing the Lagrange multipliers in eq. 3.2.6 has to vanish.

Following the proof Stanton formulated for standard CC theory in ref. 224, this behaviour can be shown from the differentiation of the energy of an excited state

$$\begin{aligned}\frac{\partial E_{\mathrm{EOM-UCC}}}{\partial\varepsilon} = {}& \langle 0|\,\hat{R}^\dagger\frac{\partial e^{-(\hat{\sigma}-\hat{\sigma}^\dagger)}}{\partial\varepsilon}\hat{H}e^{\hat{\sigma}-\hat{\sigma}^\dagger}\hat{R}\,|0\rangle + \langle 0|\,\hat{R}^\dagger e^{-(\hat{\sigma}-\hat{\sigma}^\dagger)}\hat{H}\frac{\partial e^{\hat{\sigma}-\hat{\sigma}^\dagger}}{\partial\varepsilon}\hat{R}\,|0\rangle \\ & + \langle 0|\,\hat{R}^\dagger e^{-(\hat{\sigma}-\hat{\sigma}^\dagger)}\frac{\partial\hat{H}}{\partial\varepsilon}e^{\hat{\sigma}-\hat{\sigma}^\dagger}\hat{R}\,|0\rangle\,.\end{aligned} \tag{3.2.10}$$

The space of all possible Slater determinants can be partitioned as $|\Phi_p\rangle\oplus|\Phi_q\rangle$, where $|\Phi_p\rangle$ comprises all Slater determinants lying in the basis of $\bar{H}$ (i.e., $|0\rangle$, singly-exicted and doubly-excited determinants for UCC2 and UCC3), and $|\Phi_q\rangle$ comprises all other determinants. Note that in the exact limit, $|\Phi_q\rangle$ will reduce to the null space.

The first two terms in eq. 3.2.10 contain the differentiation of the exponential operator and can be reformulated introducing the resolution of identity $\hat{1} = |\Phi_p\rangle\langle\Phi_p| + |\Phi_q\rangle\langle\Phi_q|$,

$$\begin{aligned}&\langle 0|\,\hat{R}^\dagger\frac{\partial e^{-(\hat{\sigma}-\hat{\sigma}^\dagger)}}{\partial\varepsilon}e^{\hat{\sigma}-\hat{\sigma}^\dagger}\,|\Phi_p\rangle\langle\Phi_p|\,\bar{H}\hat{R}\,|0\rangle + \langle 0|\,\hat{R}^\dagger\bar{H}\,|\Phi_p\rangle\langle\Phi_p|\,e^{-(\hat{\sigma}-\hat{\sigma}^\dagger)}\frac{\partial e^{\hat{\sigma}-\hat{\sigma}^\dagger}}{\partial\varepsilon}\hat{R}\,|0\rangle + \\ &\langle 0|\,\hat{R}^\dagger\frac{\partial e^{-(\hat{\sigma}-\hat{\sigma}^\dagger)}}{\partial\varepsilon}e^{\hat{\sigma}-\hat{\sigma}^\dagger}\,|\Phi_q\rangle\langle\Phi_q|\,\bar{H}\hat{R}\,|0\rangle + \langle 0|\,\hat{R}^\dagger\bar{H}\,|\Phi_q\rangle\langle\Phi_q|\,e^{-(\hat{\sigma}-\hat{\sigma}^\dagger)}\frac{\partial e^{\hat{\sigma}-\hat{\sigma}^\dagger}}{\partial\varepsilon}\hat{R}\,|0\rangle\,.\end{aligned} \tag{3.2.11}$$

Using the fact that the eigenfunctions of $\bar{H}$ are defined in the space spanned by the $\{\Phi_p\}$ basis, the time-independent Schrödinger equations $\langle 0|\,\hat{R}^\dagger \bar{H}\,|\Phi_p\rangle = E_{\text{exc}}\,\langle 0|\,\hat{R}^\dagger\,|\Phi_p\rangle$ and $\langle \Phi_p|\,\bar{H}\hat{R}\,|0\rangle = E_{\text{exc}}\,\langle \Phi_p|\,\hat{R}\,|0\rangle$ may be exploited to simplify this equation. As the eigenvectors are defined only in the $|\Phi_p\rangle$ space, eq. 3.2.11 becomes

$$\begin{aligned} &E_{\text{exc}}\left[\langle 0|\,\hat{R}^\dagger \frac{\partial e^{-(\hat{\sigma}-\hat{\sigma}^\dagger)}}{\partial\varepsilon} e^{\hat{\sigma}-\hat{\sigma}^\dagger}\,\hat{R}\,|0\rangle + \langle 0|\,\hat{R}^\dagger e^{-(\hat{\sigma}-\hat{\sigma}^\dagger)} \frac{\partial e^{\hat{\sigma}-\hat{\sigma}^\dagger}}{\partial\varepsilon}\,\hat{R}\,|0\rangle\right] + \\ &\langle 0|\,\hat{R}^\dagger \frac{\partial e^{-(\hat{\sigma}-\hat{\sigma}^\dagger)}}{\partial\varepsilon} e^{\hat{\sigma}-\hat{\sigma}^\dagger}\,|\Phi_q\rangle\,\langle\Phi_q|\,\bar{H}\hat{R}\,|0\rangle + \langle 0|\,\hat{R}^\dagger \bar{H}\,|\Phi_q\rangle\,\langle\Phi_q|\,e^{-(\hat{\sigma}-\hat{\sigma}^\dagger)} \frac{\partial e^{\hat{\sigma}-\hat{\sigma}^\dagger}}{\partial\varepsilon}\,\hat{R}\,|0\rangle\,. \end{aligned} \tag{3.2.12}$$

The first two terms add to zero, as can be shown from the following relation

$$\frac{\partial e^{-(\hat{\sigma}-\hat{\sigma}^\dagger)}}{\partial\varepsilon} e^{\hat{\sigma}-\hat{\sigma}^\dagger} + e^{-(\hat{\sigma}-\hat{\sigma}^\dagger)} \frac{\partial e^{\hat{\sigma}-\hat{\sigma}^\dagger}}{\partial\varepsilon} = \frac{\partial}{\partial\varepsilon}(e^{-(\hat{\sigma}-\hat{\sigma}^\dagger)} e^{\hat{\sigma}-\hat{\sigma}^\dagger}) = 0. \tag{3.2.13}$$

The only terms left in eq. 3.2.12 are those projected on the orthogonal space to the one $\bar{H}$ is defined in

$$\langle 0|\,\hat{R}^\dagger \frac{\partial e^{-(\hat{\sigma}-\hat{\sigma}^\dagger)}}{\partial\varepsilon} e^{\hat{\sigma}-\hat{\sigma}^\dagger}\,|\Phi_q\rangle\,\langle\Phi_q|\,\bar{H}\hat{R}\,|0\rangle + \langle 0|\,\hat{R}^\dagger \bar{H}\,|\Phi_q\rangle\,\langle\Phi_q|\,e^{-(\hat{\sigma}-\hat{\sigma}^\dagger)} \frac{\partial e^{\hat{\sigma}-\hat{\sigma}^\dagger}}{\partial\varepsilon}\,\hat{R}\,|0\rangle\,. \tag{3.2.14}$$

In the exact case limit, the $|\Phi_q\rangle$ space reduces to the null space, making these contributions vanish.

The EOM-UCC response properties have the correct FCI limit in the case of untruncated expansion.

3.2.3 EOM-UCC transition dipole moments

The theory for transition dipole moments can be developed adapting the infrastructure discussed for CC theory to UCC theory. The UCC2 and UCC3 methods described in section 3.1.3 are not variational and the response of the wave function to the perturbation has to be included in the determination of properties. Following the definitions in sec. 2.8, Q_{fi} for the UCC parameterisation yields

$$Q_{fi} = \langle 0|\,\hat{R}_f^\dagger e^{-(\hat{\sigma}-\hat{\sigma}^\dagger)}(\hat{H} - i\frac{\partial}{\partial t}) e^{\hat{\sigma}-\hat{\sigma}^\dagger}\,\hat{R}_i e^{i\omega_{fi}t}\,|0\rangle - Q_f\,\langle 0|\,\hat{R}_f^\dagger \hat{R}_i e^{i\omega_{fi}t}\,|0\rangle\,. \tag{3.2.15}$$

Referring to the discussion in sec 2.8.1, the operators $\hat{R}_i$ and $\hat{R}_f^\dagger$, appearing in eq. 3.2.15 are additive, as the left states are the adjoint ones of the local operators for the right states. Therefore the expression is already size-extensive, without the need to introduce a commutator, as was suggested in eq. 2.8.15. The derivative approach shows one advantage, which should be remembered: being UCC2 and UCC3 based on the truncation at a given order in perturbation theory of the amplitude equations and of the Hamiltonian matrix, the truncation of $e^{-(\hat{\sigma}-\hat{\sigma}^\dagger)}(\hat{H} - i\frac{\partial}{\partial t}) e^{\hat{\sigma}-\hat{\sigma}^\dagger}$ is clearly defined. Therefore, a formulation of transition moments involving the Hamiltonian and the energy expression leads to a well-defined truncation in the properties. This formalism is therefore equivalent to a Bernoulli expansion and perturbative truncation of $e^{-(\hat{\sigma}-\hat{\sigma}^\dagger)}\hat{\mu}e^{\hat{\sigma}-\hat{\sigma}^\dagger}$. Another option could be to expand it with the BCH expansion, as done in ref. 59.

For the reverse transition, the quantity Q_{if} is obtained exchanging the indices of the initial and final states. In order to have a physically correct formulation, its form should permit its derivative to fulfill eq. 2.8.48. The following form satisfies these requirement

$$Q_{if} = \langle 0|\,\hat{R}_i^\dagger e^{-(\hat{\sigma}-\hat{\sigma}^\dagger)}(\hat{H} - i\frac{\partial}{\partial t}) e^{\hat{\sigma}-\hat{\sigma}^\dagger}\,\hat{R}_f e^{i\omega_{if}t}\,|0\rangle - Q_i\,\langle 0|\,\hat{R}_i^\dagger \hat{R}_f e^{i\omega_{if}t}\,|0\rangle\,. \tag{3.2.16}$$

Similarly to EOM-CC theory, the quasi-energy functional is stationary with respect to $\hat{R}$, but not with respect to $\hat{\sigma}$. From the definition in eq. 2.8.76, the transition dipole moment for EOM-UCC theory can be written as

$$T_{fi} = \{\langle 0| \hat{R}_f^\dagger \frac{\mathrm{d}\bar{H}}{\mathrm{d}\varepsilon(\omega_{fi})} \hat{R}_i e^{i\omega_{fi}t} |0\rangle\}_T. \tag{3.2.17}$$

The differentiation with respect to the perturbation of the transition frequency ω_{fi} is performed. The differentiation of eq. 3.2.17 requires the determination of the perturbed amplitudes $\frac{\partial \sigma_\mu}{\partial \varepsilon}$ and $\frac{\partial \sigma_\mu^*}{\partial \varepsilon}$. As before, the Lagrangian formalism is preferred. The constraints for the UCC Lagrange functional are the UCC amplitude equations and the orthogonality of the two excited states

$$\begin{aligned}\mathscr{L}_{fi} = &\langle 0| \hat{R}_f^\dagger e^{-(\hat{\sigma}-\hat{\sigma}^\dagger)} \hat{H} e^{\hat{\sigma}-\hat{\sigma}^\dagger} \hat{R}_i e^{i\omega_{fi}t} |0\rangle - Q_f \langle 0| \hat{R}_f^\dagger e^{i\omega_{fi}t} \hat{R}_i |0\rangle \\ &- \langle 0| \hat{Z}_{fi}(\omega) e^{-(\hat{\sigma}-\hat{\sigma}^\dagger)} (\hat{H} - i\frac{\partial}{\partial t}) e^{\hat{\sigma}-\hat{\sigma}^\dagger} |0\rangle - \langle 0| e^{-(\hat{\sigma}-\hat{\sigma}^\dagger)} (\hat{H} - i\frac{\partial}{\partial t}) e^{\hat{\sigma}-\hat{\sigma}^\dagger} \hat{Z}_{if}^\dagger(\omega) |0\rangle \\ &- \eta \langle 0| (\hat{R}_f^\dagger \hat{R}_i - \delta_{if}) e^{i\omega_{fi}t} |0\rangle .\end{aligned} \tag{3.2.18}$$

$\hat{Z}_{fi}$ and $\hat{Z}_{if}$ are de-excitation operators, formed with the Lagrange multipliers as amplitudes; these amplitudes will be called, respectively, ζ_μ and θ_μ

$$\hat{Z}_{fi} = \sum_{ia} \zeta_i^a \{\hat{i}^\dagger \hat{a}\} + \frac{1}{4} \sum_{ijab} \zeta_{ij}^{ab} \{\hat{i}^\dagger \hat{j}^\dagger \hat{b} \hat{a}\}, \qquad \hat{Z}_{if} = \sum_{ia} \theta_i^a \{\hat{i}^\dagger \hat{a}\} + \frac{1}{4} \sum_{ijab} \theta_{ij}^{ab} \{\hat{i}^\dagger \hat{j}^\dagger \hat{b} \hat{a}\}. \tag{3.2.19}$$

$\hat{Z}_{fi}^\dagger$ therefore is an excitation operator. Note that two sets of Lagrange multipliers are needed, as one would not be sufficient to satisfy the condition $\mathscr{L}_{fi} = \mathscr{L}_{if}^*$, which determines the symmetry in eq. 2.8.48.

The stationarity conditions are imposed to calculate the Lagrange multipliers

$$\begin{aligned} \frac{\partial \{\mathscr{L}_{fi}\}_T}{\partial \sigma_\mu} = 0 \qquad &\rightarrow \qquad \text{determines } \hat{Z}_{fi}, \\ \frac{\partial \{\mathscr{L}_{fi}\}_T}{\partial \sigma_\mu^*} = 0 \qquad &\rightarrow \qquad \text{determines } \hat{Z}_{if}^\dagger. \end{aligned} \tag{3.2.20}$$

Here both equations are needed, as the two sets $\hat{Z}_{fi}$ and $\hat{Z}_{if}$ are not one the adjoint of the other.
When $i = f$, the stationarity condition with respect to $\hat{R}_i$ gives $\eta = \Delta E_{\text{exc}}$, in agreement with eq. 3.2.3.

The time differentiation of the exponential operator is not easily carried out, as seen in eq. 3.2.9, and has to be consistently truncated for the different orders of approximation. A detailed analysis of the equations obtained can be found in sec. 4.5.5.

Once the stationarity conditions are solved, the transition dipole moments are obtained by means of partial differentiation of the Lagrange functional with respect to the perturbation

$$\begin{aligned} T_{fi} = \frac{\partial \{\mathscr{L}_{fi}\}_T}{\partial \varepsilon(\omega_{fi})} = &\{\langle 0| \hat{R}_i^\dagger e^{-(\hat{\sigma}-\hat{\sigma}^\dagger)} \hat{\mu} e^{\hat{\sigma}-\hat{\sigma}^\dagger} \hat{R}_f e^{i\omega_{if}t} |0\rangle\}_T - \{\langle 0| \hat{Z}_{fi}(\omega) e^{-(\hat{\sigma}-\hat{\sigma}^\dagger)} \hat{\mu} e^{\hat{\sigma}-\hat{\sigma}^\dagger} |0\rangle\}_T \\ &- \{\langle 0| e^{-(\hat{\sigma}-\hat{\sigma}^\dagger)} \hat{\mu} e^{\hat{\sigma}-\hat{\sigma}^\dagger} \hat{Z}_{if}^\dagger(\omega) |0\rangle\}_T. \end{aligned} \tag{3.2.21}$$

Also for the EOM-UCC transition dipole moments, eq. 3.2.21 can be recast into the form $T_{fi} = \sum_{pq} D_{pq}^{fi} \mu_{pq}$. The one-electron transition density matrix $\mathbf{D}^{fi}$, however, is specific for each UCCn truncation.

Transitions from the ground state

Adapting eq. 3.2.18 to the special case of transitions from the ground state gives the following form for the Lagrange functional

$$\begin{aligned}\mathscr{L}_{0i} = &\{\langle 0|\, e^{-(\hat{\sigma}-\hat{\sigma}^\dagger)}\hat{H}e^{\hat{\sigma}-\hat{\sigma}^\dagger}\hat{R}_i e^{i\omega_{0i}t}\,|0\rangle\}_T - Q_0\{\langle 0|\, e^{i\omega_{0i}t}\hat{R}_i\,|0\rangle\}_T \\ &- \{\langle 0|\,\hat{Z}_{0i}(\omega)e^{-(\hat{\sigma}-\hat{\sigma}^\dagger)}(\hat{H}-i\frac{\partial}{\partial t})e^{\hat{\sigma}-\hat{\sigma}^\dagger}\,|0\rangle\}_T - \{\langle 0|\, e^{-(\hat{\sigma}-\hat{\sigma}^\dagger)}(\hat{H}-i\frac{\partial}{\partial t})e^{\hat{\sigma}-\hat{\sigma}^\dagger}\hat{Z}^\dagger_{i0}(\omega)\,|0\rangle\}_T \\ &- \eta\,\langle 0|\,\hat{R}_i\,|0\rangle\,,\end{aligned} \tag{3.2.22}$$

where $\hat{R}^\dagger_f = 1$. It is noted that the two operators $\hat{R}_i$ and $\hat{Z}^\dagger_{i0}$ both multiply the similarity-transformed Hamiltonian on the right hand-side and the terms $\langle 0|\, e^{-(\hat{\sigma}-\hat{\sigma}^\dagger)}\hat{H}e^{\hat{\sigma}-\hat{\sigma}^\dagger}\hat{R}_i e^{i\omega_{0i}t}\,|0\rangle$ and $\langle 0|\, e^{-(\hat{\sigma}-\hat{\sigma}^\dagger)}\hat{H}e^{\hat{\sigma}-\hat{\sigma}^\dagger}\hat{Z}^\dagger_{i0}e^{i\omega_{0i}t}\,|0\rangle$ sum to give a contribution of the form $\langle 0|\, e^{-(\hat{\sigma}-\hat{\sigma}^\dagger)}\hat{H}e^{\hat{\sigma}-\hat{\sigma}^\dagger}(\hat{R}_i+\hat{Z}^\dagger_{i0})e^{i\omega_{0i}t}\,|0\rangle$. However, $\hat{R}_i$ is an eigenvector of the similarity-transformed Hamiltonian and the stationarity condition is fulfilled only for $\hat{Z}^\dagger_{i0} = 0$.

The condition involving the $\hat{Z}^\dagger_{i0}$ multipliers is not needed and therefore superfluous. Transitions from and to the ground state are described by a simpler Lagrangian, involving only one set of conditions

$$\begin{aligned}\mathscr{L}_{0i} = &\{\langle 0|\, e^{-(\hat{\sigma}-\hat{\sigma}^\dagger)}\hat{H}e^{\hat{\sigma}-\hat{\sigma}^\dagger}\hat{R}_i e^{i\omega_{0i}t}\,|0\rangle\}_T - Q_0\{\langle 0|\, e^{i\omega_{0i}t}\hat{R}_i\,|0\rangle\}_T \\ &- \{\langle 0|\,\hat{Z}_{0i}(\omega)e^{-(\hat{\sigma}-\hat{\sigma}^\dagger)}(\hat{H}-i\frac{\partial}{\partial t})e^{\hat{\sigma}-\hat{\sigma}^\dagger}\,|0\rangle\}_T - \eta\,\langle 0|\,\hat{R}_i\,|0\rangle\,,\end{aligned} \tag{3.2.23}$$

$$\begin{aligned}\mathscr{L}_{i0} = &\{\langle 0|\,\hat{R}^\dagger_i e^{-(\hat{\sigma}-\hat{\sigma}^\dagger)}\hat{H}e^{\hat{\sigma}-\hat{\sigma}^\dagger}e^{i\omega_{i0}t}\,|0\rangle\}_T - Q_0\{\langle 0|\,\hat{R}^\dagger_i e^{i\omega_{i0}t}\,|0\rangle\}_T \\ &- \{\langle 0|\, e^{-(\hat{\sigma}-\hat{\sigma}^\dagger)}(\hat{H}-i\frac{\partial}{\partial t})e^{\hat{\sigma}-\hat{\sigma}^\dagger}\hat{Z}^\dagger_{0i}(\omega)\,|0\rangle\}_T - \eta\,\langle 0|\,\hat{R}^\dagger_i\,|0\rangle\,.\end{aligned} \tag{3.2.24}$$

These two forms still satisfy the condition $\mathscr{L}_{0i} = \mathscr{L}^*_{i0}$.

Chapter 4

Implementation

This chapter discusses the features of the implementation of the expressions for energies and properties, showing the strategies by means of which the implementation has been made possibly efficient and low-scaling.

The CFOUR program package[251,252] provides all one- and two-electron integrals in the presence of a finite magnetic field, which are computed in a GIAO basis set. Furthermore, the MO coefficients from the HF SD are provided. The input for the CFOUR program specifies the settings for the geometry of the molecular system (in internal or Cartesian coordinates), the orientation of the magnetic field, the chosen basis set, the charge, and the multiplicity of the target state.

The necessary information is passed from the CFOUR output to QCUMBRE via an interface between the two program packages.

4.1 QCUMBRE

The theory discussed here has been implemented in the QCUMBRE package.[161] This program is written in C++[253] and has been developed to perform finite-field calculations with post-HF methods. It has been already pointed out that a finite-field calculation requires complex algebra. It has to be emphasized that a complex computation is much more expensive than a real one. In fact, the storage requirement of any quantity is increased by a factor of two, as both the real and the imaginary part of a number have to be stored. Furthermore, the permutational symmetry of integrals is no longer eight-fold but only four-fold ($\langle pq|rs\rangle = \langle qp|sr\rangle = \langle rs|pq\rangle^* = \langle sr|qp\rangle^*$). Finally, complex algebra formally implies an increase in computational cost of a factor four for multiplications. The QCUMBRE code is one

Figure 4.1: Logo of the QCUMBRE program package,[161] adapted for UCC.

of the few codes able to perform a complex-valued CC calculation.* The integrals and HF MO coefficients are provided through interfaces with the CFOUR program and the LONDON program.

In Flowchart 1, the structure of a QCUMBRE calculation is illustrated. First, an external HF-SCF calculation is performed, either with the CFOUR or with the LONDON program package. The aforementioned interface collects the relevant data from this calculation, i.e., all one- and two-electron integrals, to be used in the next steps of the calculation. QCUMBRE is then able to compute the ground-state energy and wave function for methods belonging to the CC and the UCC parameterisations, through the `SubCC` function. The program can then be asked to calculate a certain number of excited states, through the solution of the EOM-CC/EOM-UCC equations. This part is managed by `SubEOMCC`. Once the states have been computed, QCUMBRE can proceed to the treatment of molecular properties, both for the ground state (`SubCCProp`) and the excited states (`SubEOMProp`). The structure of each of these functions is explained in detail in the next sections, with reference to the new developments performed during this thesis.

A full list of the implemented methods and keywords in QCUMBRE may be found on the website (`https://www.qcumbre.org`). During this thesis, the following features were developed:

- implementation of UCC2 and UCC3 ground- and excited-state energies in a finite magnetic field – `SubCC` and `SubEOMCC` (sec. 4.3);
- implementation of ADC2, ADC2-x, ADC3 ground- and excited-state energies in a finite magnetic field – in `SubCC` and `SubEOMCC` (sec. 4.4);
- implementation of UCC2 and UCC3 ground- and excited-state dipole moments in a finite magnetic field – in `SubCCProp` and `SubEOMProp` (secs. 4.5.1-4.5.4);
- implementation of UCC2 and UCC3 ground- and excited-state transition dipole moments in a finite magnetic field – in `SubCCProp` and `SubEOMProp` (secs. 4.5.5-4.5.8);
- generation of output files for the calculation of MCD spectra (sec. 6.2);
- development of QED-UCC2 equations and their implementation (the latter performed by Laurenz Monzel), explained in sec. 7.2.

In the next sections, the implementation of the UCC method to compute energies and properties is discussed in detail. The full equations are given with the strategies applied to deal with the computational challenges these equations offer. In order to give a general idea of the implementation, flowcharts describing the structure of the calculations in QCUMBRE are provided. Before starting the discussion of the equations, an important section on a very powerful tool for their development is presented. The so-called *diagrammatic technique* is therefore discussed hereafter.

*Other complex codes are LONDON,[254] CFOUR,[251] BAGEL,[255] CHRONUS,[256] QUEST,[257] and TURBOMOLE.[258]

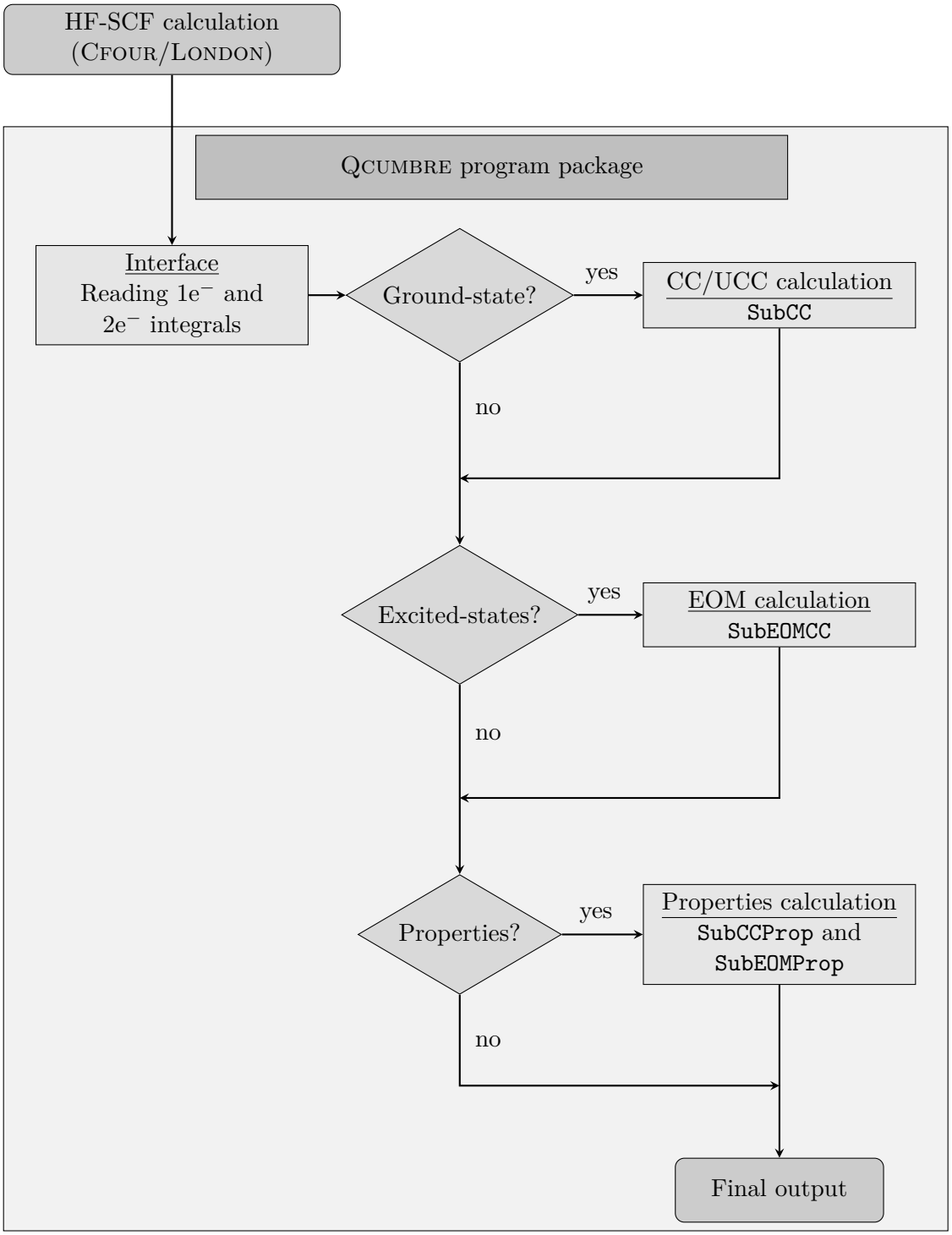

Flowchart 1: Flowchart illustrating the structure of a Qcumbre calculation.

4.2 Diagrammatic rules

A very useful and widely exploited tool for the derivation of CC equations is provided by the diagrammatic representation of the equations. This technique permits to find a simpler language for the evaluation of complicated terms, originating from the contraction of multiple operators, whose derivation through Wick's theorem would be lengthy and difficult. In this thesis the origin of the diagrammatic rules will not be discussed in depth, but only to the extent in which they differ from those for standard CC. A helpful reference for the explanation of the diagrammatic rules in CC may be found in ref. 259. In order to remember the differences in the assignment of coefficients in the Bernoulli expansion method with respect to the usual BCH one, the terms required for the UCC3 method are listed hereafter once more

$$\bar{H}^0 = F + V, \tag{4.2.1}$$

$$\bar{H}^1 = [F, \tilde{\sigma}_1 + \tilde{\sigma}_2] + \frac{1}{2}[V, \tilde{\sigma}_1 + \tilde{\sigma}_2] + \frac{1}{2}[V_{\mathrm{R}}, \tilde{\sigma}_1 + \tilde{\sigma}_2], \tag{4.2.2}$$

$$\bar{H}^2 = \frac{1}{12}[[V_{\mathrm{ND}}, \tilde{\sigma}_2], \tilde{\sigma}_2] + \frac{1}{4}[[V, \tilde{\sigma}_2]_{\mathrm{R}}, \tilde{\sigma}_2] + \frac{1}{4}[[V_{\mathrm{R}}, \tilde{\sigma}_2]_{\mathrm{R}}, \tilde{\sigma}_2]. \tag{4.2.3}$$

The *ND* part of operators or contractions of operators are given by pure excitation or de-excitations. For example, the terms contributing to the V_{ND} operator are $\langle ab||ij\rangle\,\{\hat{a}^\dagger\hat{b}^\dagger\hat{j}\hat{i}\}$ and $\langle ij||ab\rangle\,\{\hat{i}^\dagger\hat{j}^\dagger\hat{b}\hat{a}\}$. All other terms in V, as for example $\langle ak||ij\rangle\,\{\hat{a}^\dagger\hat{k}^\dagger\hat{j}\hat{i}\}$, belong to the *rest* part V_{R}. The CC diagrammatic rules can be used for the determination of the prefactor; on top of the known rules, four more steps need to be considered:

1. consider whether the $\hat{V}$ operator belongs to the non-diagonal or the rest part. The non-diagonal part of an operator is made of either pure excitations or pure de-excitations.

2. consider if the contractions $[\hat{V}, \tilde{\sigma}]$ belong to the non-diagonal or the rest part. This becomes relevant for understanding to which terms in eqs. 4.2.2 and 4.2.3 each diagram belongs to.

3. consider the prefactor (sum of prefactors) of the commutator to which the diagrams belongs. Calculate the ratio between this prefactor and the one present in the analogous term in the BCH expansion. This ratio needs to be multiplied to the prefactor calculated through the standard diagrammatic rules.

4. for terms belonging to eq. 4.2.3, observe whether the Hamiltonian is connected to only one or both $\tilde{\sigma}$ operators. If it is connected to only one of them, a further factor of $\frac{1}{2}$ needs to be multiplied, as only half of the terms in the commutator contribute to the diagram.

Some examples are shown in appendix A.

4.3 UCC ground- and excited-state energies

The calculation of the ground- and excited-state energies are managed, respectively, by `SubCC` and `SubEOMCC`, as seen in Flowchart 1. In Flowchart 2 and 3, their structure is shown.

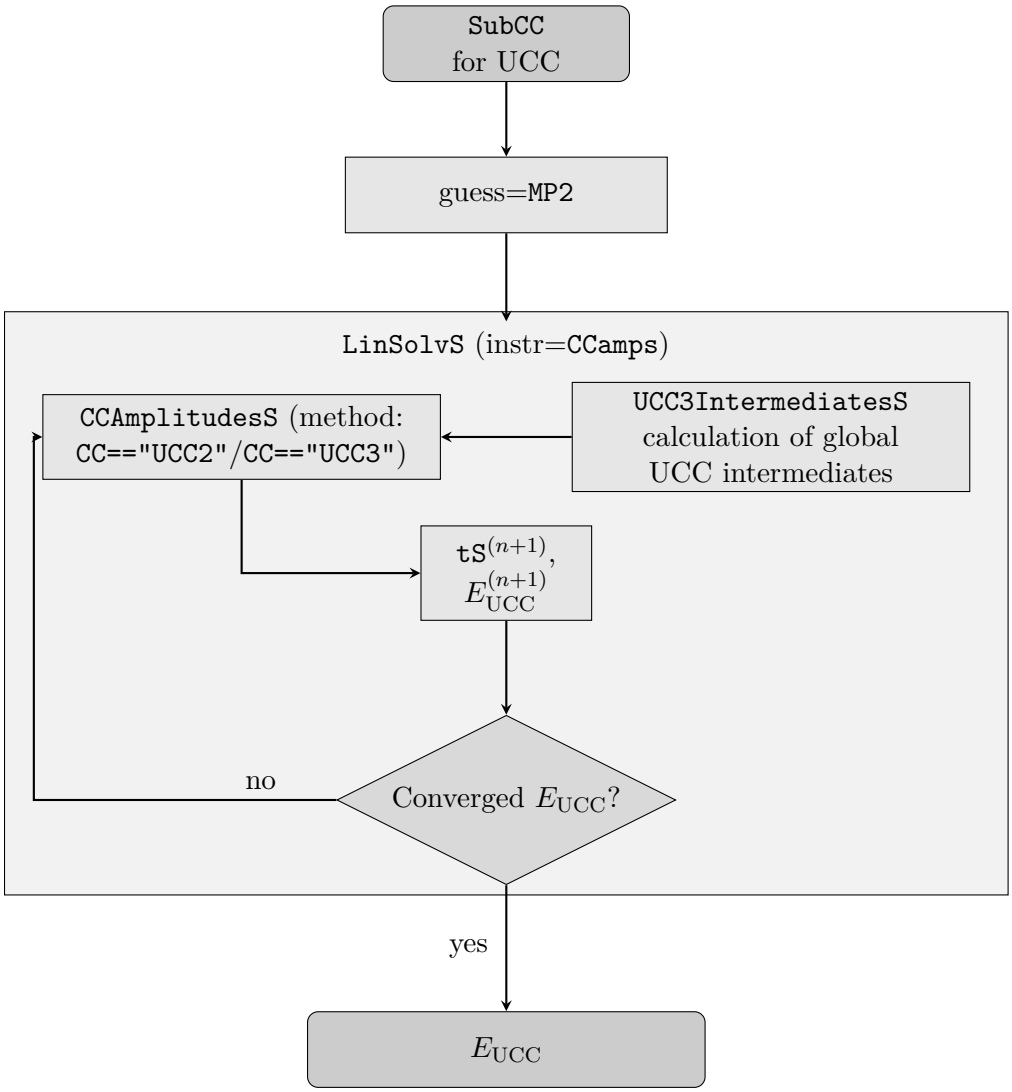

Flowchart 2: Flowchart illustrating a ground-state calculation in QCUMBRE.

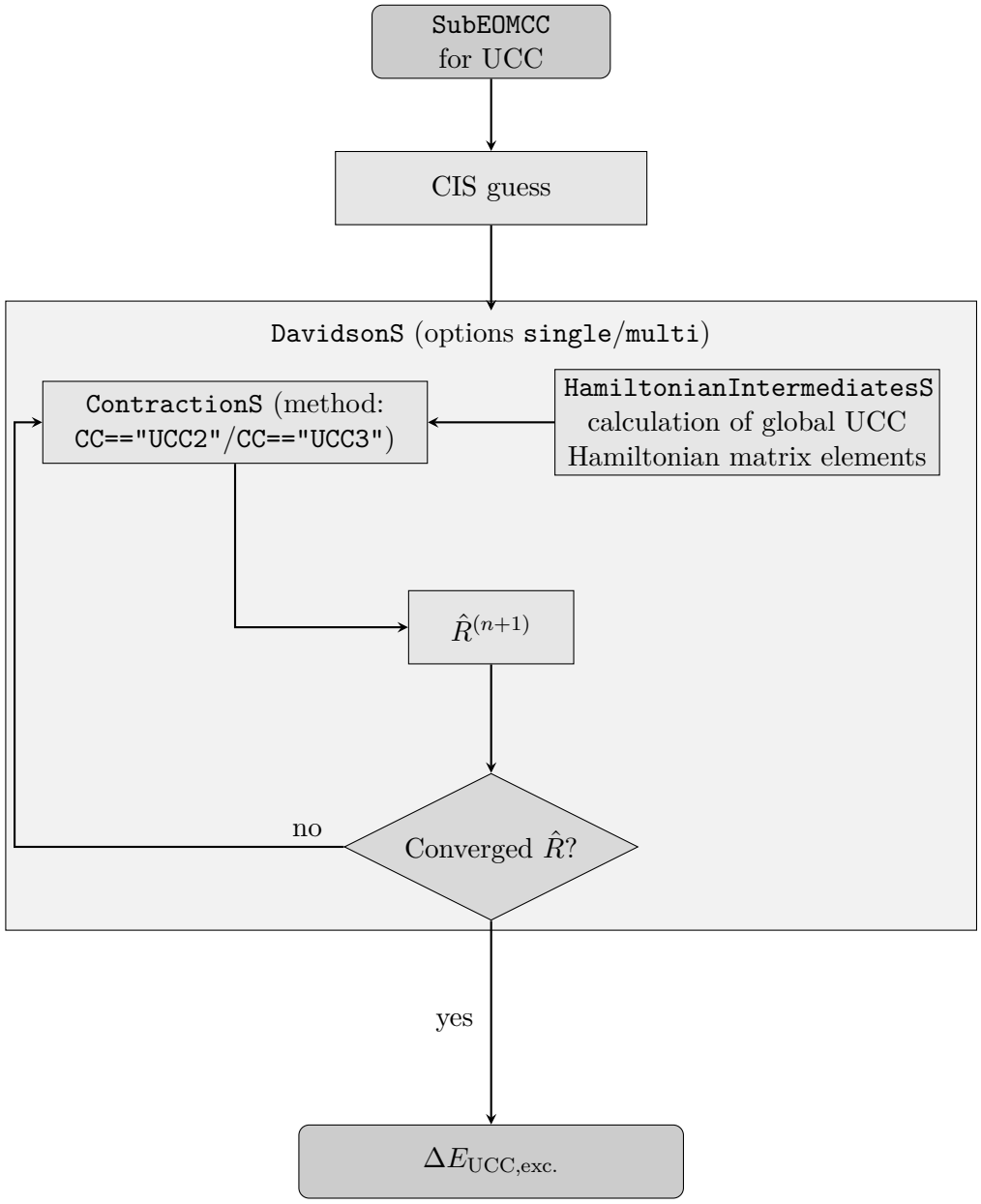

Flowchart 3: Flowchart illustrating an excited-state calculation in QCUMBRE.

Starting from `SubCC`, all CC or UCC calculation first needs to solve the amplitude equations iteratively. As for the CC equations, the initial guess for the σ-amplitudes is given by the MP2 guess, $\sigma_i^{a[0]} = 0$ and $\sigma_{ij}^{ab(0)} = \frac{\langle ab||ij\rangle}{\varepsilon_i+\varepsilon_j-\varepsilon_a-\varepsilon_b}$. The amplitude equations are then solved iteratively using the solver in QCUMBRE, encoded in the function `LinSolvS`. The solution is obtained by exploiting the DIIS (direct inversion of the iterative subspace) technique.[260] This method allows the solution of a quasi-linear equation of the kind $\mathbf{A}(\mathbf{x})\mathbf{x} = \mathbf{b}$ without having to assemble the matrix itself, as it is constructed such as to require only the product vector $\mathbf{A}(\mathbf{x})\mathbf{x}$. The solver can be given the instruction `CCamps` to calculate the amplitudes. In particular, the terms of the amplitude equations are calculated in the function `CCAmplitudesS`. The definition of intermediate contractions allows to keep the scaling of the equations as low as possible. The detailed discussion of these intermediates is provided later in this section. These intermediates are calculated in `UCC3IntermediatesS` and passed to `CCAmplitudes`.

Once the amplitudes have been calculated in the nth iteration, the energy is computed with eq. 3.1.7 and compared to the previous iteration: if $\left|E_{\mathrm{UCC}}^{(n+1)} - E_{\mathrm{UCC}}^{(n)}\right| < \tau$, with τ a given threshold specified in the input as `convergence-criterium`, the amplitudes are considered converged and the energy of the ground state is found.

In Flowchart 3, the structure of `SubEOMCC` is shown. It has been discussed in sec. 3.1.2 that the r_μ amplitudes are calculated via diagonalisation of the transformed Hamiltonian matrix, where the Davidson algorithm[261–264] is used. The function `DavidsonS` provides the possibility to compute single or multiple roots simultaneously (further details may be found in ref. 207). An EOM-UCC calculation is preceded by a Configuration Interaction with Single excitations (CIS) calculation, providing the initial guess for the single-excitation amplitudes $\hat{R}_1$, while all other amplitudes are set to zero. The EOM-UCC equations are calculated in the function `ContractionS`. The scaling is kept as low as possible through the definition of intermediates, calculated through the function `HamiltonianIntermediatesS`. The $\hat{R}$ operators parameterising the EOM-UCC states are determined through the Davidson algorithm. `SubEOMCC` then computes the excitation energy $\Delta E_{\mathrm{UCC,exc.}}$.

The structure of the algorithms and functions used in the calculation of UCC ground- and excited-state energies has been discussed; now further details on the implemented equations are provided. Particular attention is given to the scaling of the terms, and the aforementioned intermediate contractions are discussed in more detail.

The amplitude equations for the UCC2 and UCC3 approximations have been listed in section 3.1.3, showing the different complexity of these two approaches. Here the focus is placed on the implementation strategy, which should ensure the lowest scaling possible. The UCC2 equations can be implemented following their written expression, as they are constructed from two tensors at most. In addition, UCC3 involves contractions of three tensors and some intermediate quantities need to be defined. This step-wise implementations ensures a lower scaling and a cheaper computation in terms of time and memory. From here on, the Einstein convention for sums over repeated indices is assumed.

The intermediate quantities given by contractions of $\hat{\sigma}_2^\dagger$ and $\hat{\sigma}_2$ are widely used in the UCC equations; they are therefore defined as global variables in the `main` file of QCUMBRE and their expressions are calculated by the function `UCC3IntermediatesS`. These intermediates are

$$Z_{ab} = \sigma_{kl}^{ca*}\sigma_{kl}^{cb}, \qquad Z_{ij} = \sigma_{ki}^{ab*}\sigma_{jk}^{ba}, \qquad Z_{iabj} = \sigma_{jk}^{ac*}\sigma_{ki}^{cb}, \qquad Z_{ijkl} = \sigma_{ij}^{ab*}\sigma_{kl}^{ab}. \tag{4.3.1}$$

The correct scaling is achieved by defining some more intermediates for the UCC3 amplitude

equations

$$\begin{aligned}
U_{ai} &= \langle bi||jk\rangle\, \sigma_{jk}^{ba*},\\
V_{ai} &= \langle cb||aj\rangle\, \sigma_{ij}^{cb*},\\
R_{ijka} &= \langle bd||ka\rangle\, \sigma_{ij}^{bd*},\\
UWS_{iabj} &= \langle ia||bj\rangle + \frac{1}{3}[\langle ki||cb\rangle\, \sigma_{jk}^{ac} + \langle ac||jk\rangle\, \sigma_{ki}^{cb*}],\\
UWS_{ijkl} &= \frac{1}{2}\langle ij||kl\rangle + \frac{1}{6}\langle ij||cd\rangle\, \sigma_{kl}^{cd} + \frac{1}{12}\langle cd||kl\rangle\, \sigma_{ij}^{cd*},\\
UFS_{ab} &= \frac{1}{3}\langle kl||cb\rangle\, \sigma_{kl}^{ca} + \frac{1}{6}\langle ac||lk\rangle\, \sigma_{lk}^{bc*},\\
UFS_{ij} &= \frac{1}{3}\langle kj||cd\rangle\, \sigma_{ki}^{cd} + \frac{1}{6}\langle cd||ki\rangle\, \sigma_{kj}^{cd*}.
\end{aligned} \tag{4.3.2}$$

These intermediates are directly calculated in the function in which the amplitude equations are solved, `CCAmplitudesS`.

With these definitions, the amplitude equations for UCC3 read

$$\begin{aligned}
\bar{H}_{ai} = f_{ai} &+ \langle aj||ib\rangle\, \sigma_j^b + \frac{1}{2}\langle ab||ij\rangle\, \sigma_j^{b*} + \frac{1}{2}\langle aj||cb\rangle\, \sigma_{ij}^{cb} - \frac{1}{2}\langle kj||ib\rangle\, \sigma_{jk}^{ba} - \frac{1}{2}\langle al||ik\rangle\, Z_{kl}\\
&+ \frac{1}{2}\langle ad||ic\rangle\, Z_{dc} - \langle bl||ji\rangle\, Z_{jl}^{ba} + \langle ab||dj\rangle\, Z_{ji}^{bd} - \frac{1}{4}(U_{cl} - V_{cl})\sigma_{il}^{ac} + \frac{1}{4}R_{ijka}\sigma_{jk}^{ca}\\
&- \frac{1}{4}\langle al||jk\rangle\, Z_{jkli} + f_{ab}\sigma_i^b - f_{ij}\sigma_j^a + f_{jb}\sigma_{ij}^{ab} = 0,
\end{aligned} \tag{4.3.3}$$

$$\begin{aligned}
\bar{H}_{abij} = &-P(ab)\langle ka||ji\rangle\, \sigma_k^b + P(ij)\langle ab||ic\rangle\, \sigma_j^c - P(ab)\frac{1}{6}\langle ad||ij\rangle\, Z_{db} - P(ij)\frac{1}{6}\langle ab||il\rangle\, Z_{lj}\\
&+ P(ij)P(ab)UWS_{ladi}\sigma_{jl}^{bd} + UWS_{klij}\sigma_{kl}^{ab} + \frac{1}{2}\langle ab||cd\rangle\, \sigma_{ij}^{cd} + \frac{1}{12}\langle ab||kl\rangle\, Z_{klij}\\
&- P(ab)UFS_{bd}\sigma_{ij}^{ad} - P(ij)UFS_{jl}\sigma_{il}^{ab} + \langle ab||ij\rangle + P(ab)f_{bc}\sigma_{ij}^{ac} - P(ij)f_{kj}\sigma_{ik}^{ab} = 0.
\end{aligned} \tag{4.3.4}$$

From this reformulation, it appears that UCC3 scales formally as CCSD, as the only term scaling as $\sim N_{\mathrm{v}}^4 N_{\mathrm{o}}^2$ is the same particle-particle ladder term $\frac{1}{2}\langle ab||cd\rangle\, \sigma_{ij}^{cd}$. However, for the terms scaling as $\sim N_{\mathrm{v}}^3 N_{\mathrm{o}}^3$, besides the ones present for CCSD, $P(ij)P(ab)\langle ak||ic\rangle\, \sigma_{jk}^{bc}$ and $P(ij)P(ab)\frac{1}{3}\langle kl||cd\rangle\, \sigma_{ik}^{ac}\sigma_{jl}^{bd}$, there is one more, $P(ij)P(ab)\frac{1}{3}\langle ad||il\rangle\, \sigma_{kl}^{cd*}\sigma_{jk}^{bc}$. UCC3 therefore still scales as $\sim N^6$, though being more expensive than CCSD for the solution of the amplitude equations.

Expressions for the iterative determination of the amplitudes are obtained from the amplitude equations $\bar{H}_{ai} = 0$ and $\bar{H}_{abij} = 0$. By moving the diagonal part of eq. 4.3.3 and 4.3.4 to the right hand-side, the amplitudes of iteration n+1 are obtained from the amplitudes of iteration n from

$$\sigma_i^{a[n+1]} = \frac{\bar{H}_{ai}^{[n]} - \mathrm{diag}[\sum_b f_{ab}\sigma_i^{b[n]} - \sum_j f_{ij}\sigma_j^{a[n]}]}{\varepsilon_i - \varepsilon_a}, \tag{4.3.5}$$

$$\sigma_{ij}^{ab[n+1]} = \frac{\bar{H}_{ab,ij}^{[n]} - \mathrm{diag}[P(ab)\sum_c f_{bc}\sigma_{ij}^{ac[n]} - P(ij)\sum_k f_{kj}\sigma_{ik}^{ab[n]}]}{\varepsilon_i + \varepsilon_j - \varepsilon_a - \varepsilon_b}. \tag{4.3.6}$$

Moving to the treatment of the excited states with UCC theory, the eigenvectors of the transformed Hamiltonian in eq. 3.1.44 need to be determined in order to find the excitation

operator $\hat{R}$, parameterising the excited state. For UCC2, the eigenvector equation for the eigenvectors of the transformed Hamiltonian are

$$\Delta E_{\text{exc}} r_i^a = \bar{H}^{(2)}_{ad} r_i^d - \bar{H}^{(2)}_{li} r_l^a + \bar{H}^{(2)}_{ladi} r_l^d + \frac{1}{2}\bar{H}^{(1)}_{alde} r_{il}^{de} - \frac{1}{2}\bar{H}^{(1)}_{lmid} r_{lm}^{ad} + \frac{1}{4}\bar{H}^{(1)}_{klacdi} r_{kl}^{cd}, \tag{4.3.7}$$

$$\begin{aligned}\Delta E_{\text{exc}} r_{ij}^{ab} = {} & P(ij)\bar{H}^{(1)}_{abdj} r_i^d - P(ab)\bar{H}^{(1)}_{lbij} r_l^a + \bar{H}^{(1)}_{abk,ijc} r_k^c + P(ab)\bar{H}^{(0)}_{ad} r_{ij}^{db} - P(ij)\bar{H}^{(0)}_{lj} r_{il}^{ab} \\ & + \frac{1}{2}\bar{H}^{(0)}_{abde} r_{ij}^{de} + \frac{1}{2}\bar{H}^{(0)}_{lmij} r_{lm}^{ab} - P(ab)P(kl)\bar{H}^{(0)}_{ladi} r_{jl}^{db},\end{aligned} \tag{4.3.8}$$

where $\bar{H}^{(n)}$ indicates the transformed Hamiltonian truncated at order n. For UCC3 the eigenvectors are determined from the following equations

$$\Delta E_{\text{exc}} r_i^a = \bar{H}^{(3)}_{ad} r_i^d - \bar{H}^{(3)}_{li} r_l^a + \bar{H}^{(3)}_{ladi} r_l^d + \frac{1}{2}\bar{H}^{(2)}_{alde} r_{il}^{de} - \frac{1}{2}\bar{H}^{(2)}_{lmid} r_{lm}^{ad} + \frac{1}{4}\bar{H}^{(2)}_{kla,cdi} r_{kl}^{cd}, \tag{4.3.9}$$

$$\begin{aligned}\Delta E_{\text{exc}} r_{ij}^{ab} = {} & P(ij)\bar{H}^{(2)}_{abdj} r_i^d - P(ab)\bar{H}^{(2)}_{lbij} r_l^a + \bar{H}^{(2)}_{abk,ijc} r_k^c + P(ab)\bar{H}^{(1)}_{ad} r_{ij}^{db} - P(ij)\bar{H}^{(1)}_{lj} r_{il}^{ab} \\ & + \frac{1}{2}\bar{H}^{(1)}_{abde} r_{ij}^{de} + \frac{1}{2}\bar{H}^{(1)}_{lmij} r_{lm}^{ab} - P(ab)P(kl)\bar{H}^{(1)}_{ladi} r_{jl}^{db}.\end{aligned} \tag{4.3.10}$$

The equations are very similar to the EOM-CCSD ones,[22] but a few differences may be noted. The three-body term $\bar{H}^{(1)}_{klacdi}$ is not present in standard CC theory; this might be understood from the diagrammatic formalism, as no $\bar{H}$ term could possibly have four or more lines below the vertex, except for the single two-body operator. The other difference to standard EOM-CC theory is the absence of the contraction with $\bar{H}_{\text{occ-virt}}$ terms: the unitarily transformed Hamiltonian is self-adjoint and therefore $\bar{H}_{ia} = \bar{H}^*_{ai} = 0$ and $\bar{H}_{ijab} = \bar{H}^*_{abij} = 0$.

Furthermore, it has to be accounted for the correct truncation order of the transformed Hamiltonian blocks. Their expressions at a given perturbation order are

$$\begin{aligned}\bar{H}^{(3)}_{ia,bj} = {} & \langle ai||cb\rangle \sigma_j^c + \langle ca||bj\rangle \sigma_i^{c*} - \langle ki||jb\rangle \sigma_k^a - \langle ia||kj\rangle \sigma_k^{b*} + \frac{1}{2}\langle ac||jk\rangle \sigma_{ik}^{bc*} + \frac{1}{2}\langle ik||bc\rangle \sigma_{jk}^{ac} \\ & + \underbrace{\left[\frac{1}{4}\langle il||mk\rangle \sigma_{mk}^{bc*} + \frac{1}{4}\langle ed||bc\rangle \sigma_{il}^{ed*} - \frac{1}{2}\big(\langle ld||kb\rangle \sigma_{ki}^{cd*} + \langle id||kc\rangle \sigma_{lk}^{db*}\big)\right]}_{S_{il}^{bc}} \sigma_{jl}^{ac} \\ & + \underbrace{\left[\frac{1}{4}\langle mk||jl\rangle \sigma_{mk}^{ac} + \frac{1}{4}\langle ac||ed\rangle \sigma_{jl}^{ed} - \frac{1}{2}\big(\langle ka||ld\rangle \sigma_{kj}^{cd} + \langle kc||jd\rangle \sigma_{lk}^{da}\big)\right]}_{S_{jl}^{ac*}} \sigma_{il}^{bc*} \\ & - \frac{1}{4}\langle id||bj\rangle \underbrace{\sigma_{kl}^{ca}\sigma_{kl}^{cd*}}_{Z_{da}} - \frac{1}{4}\langle ia||bl\rangle \underbrace{\sigma_{jk}^{dc}\sigma_{kl}^{cd*}}_{Z_{lj}} - \langle ia||kc\rangle \underbrace{\sigma_{jl}^{cd}\sigma_{kl}^{bd*}}_{Z_{kj}^{bc}} - \frac{1}{4}\langle ai||jd\rangle \underbrace{\sigma_{kl}^{cb*}\sigma_{kl}^{cd}}_{Z_{bd}} \\ & - \frac{1}{4}\langle al||jb\rangle \underbrace{\sigma_{ik}^{dc*}\sigma_{kl}^{cd}}_{Z_{il}} - \langle kc||jb\rangle \underbrace{\sigma_{il}^{cd*}\sigma_{kl}^{ad}}_{Z_{ik}^{ca}} + \langle ik||lj\rangle \underbrace{\sigma_{km}^{ac}\sigma_{lm}^{bc*}}_{Z_{lk}^{ba}} + \langle ad||cb\rangle \underbrace{\sigma_{jk}^{ce}\sigma_{ik}^{de*}}_{Z_{ij}^{dc}} \\ & + \frac{1}{2}\langle ka||bl\rangle \underbrace{\sigma_{kj}^{cd}\sigma_{il}^{cd*}}_{Z_{ilkj}} + \frac{1}{2}\langle ic||dj\rangle \underbrace{\sigma_{kl}^{cb*}\sigma_{kl}^{ad}}_{Z_{cbad}},\end{aligned} \tag{4.3.11}$$

$$\begin{aligned}\bar{H}^{(3)}_{ij} = f_{ij} &+ \langle ik||ja\rangle\,\sigma^{a}_{k} + \langle ia||jk\rangle\,\sigma^{a*}_{k} + \frac{1}{4}\langle ik||ab\rangle\,\sigma^{ab}_{jk} + \frac{1}{4}\langle ab||jk\rangle\,\sigma^{ab*}_{ik} + \frac{1}{2}\langle ic||al\rangle\,\underbrace{\sigma^{ab}_{jk}\sigma^{bc*}_{kl}}_{Z^{ca}_{lj}} \\ &+ \frac{1}{2}\langle al||jc\rangle\,\underbrace{\sigma^{ab*}_{ik}\sigma^{bc}_{kl}}_{Z^{ac}_{il}} + \frac{1}{8}\langle im||kl\rangle\,\underbrace{\sigma^{ab}_{jm}\sigma^{ab*}_{kl}}_{Z_{kljm}} + \frac{1}{8}\langle kl||jm\rangle\,\underbrace{\sigma^{ab*}_{im}\sigma^{ab}_{kl}}_{Z_{imkl}} - \frac{1}{2}\langle im||jl\rangle\,\underbrace{\sigma^{ab*}_{kl}\sigma^{ab}_{km}}_{Z_{lm}} \\ &+ \frac{1}{2}\langle ic||jb\rangle\,\underbrace{\sigma^{ab}_{kl}\sigma^{ac*}_{kl}}_{Z_{cb}} - f_{ib}\sigma^{a}_{i} - f_{ai}\sigma^{b*}_{i},\end{aligned} \tag{4.3.12}$$

$$\begin{aligned}\bar{H}^{(3)}_{ab} = f_{ab} &+ \langle ai||bc\rangle\,\sigma^{c}_{i} + \langle ac||bi\rangle\,\sigma^{c*}_{i} - \frac{1}{4}\langle ij||bc\rangle\,\sigma^{ac}_{ij} - \frac{1}{4}\langle ac||ij\rangle\,\sigma^{bc*}_{ij} - \frac{1}{2}\langle kd||bj\rangle\,\underbrace{\sigma^{ca}_{ik}\sigma^{cd*}_{ij}}_{Z^{da}_{jk}} \\ &- \frac{1}{2}\langle aj||kd\rangle\,\underbrace{\sigma^{cb*}_{ik}\sigma^{cd}_{ij}}_{Z^{bd}_{kj}} + \frac{1}{8}\underbrace{\langle fd||cb\rangle\,\sigma^{fd*}_{ij}}_{R^{*}_{ijcb}}\sigma^{ac}_{ij} + \frac{1}{8}\underbrace{\langle ca||fd\rangle\,\sigma^{bc*}_{ij}}_{R_{ijca}}\sigma^{fd}_{ij} + \frac{1}{2}\langle ad||bc\rangle\,\underbrace{\sigma^{fc}_{ij}\sigma^{fd*}_{ij}}_{Z_{dc}} \\ &- \frac{1}{2}\langle ka||jb\rangle\,\underbrace{\sigma^{cd}_{ik}\sigma^{cd*}_{ij}}_{Z_{jk}} + f_{ia}\sigma^{a}_{j} + f_{aj}\sigma^{a*}_{i},\end{aligned} \tag{4.3.13}$$

$$\bar{H}^{(2)}_{ibc,ajk} = P(jk)[-\sum_{l}\langle il||aj\rangle\,\sigma^{cb}_{kl}] + P(bc)[\sum_{d}\langle ib||ad\rangle\,\sigma^{dc}_{jk}], \tag{4.3.14}$$

$$\bar{H}^{(2)}_{ci,ab} = \langle ci||ab\rangle + P(ab)\sum_{jd}\langle cd||aj\rangle\,\sigma^{bd*}_{ij} + \frac{1}{2}\sum_{kj}\langle ci||jk\rangle\,\sigma^{ab*}_{jk} - f_{cj}\sigma^{ba*}_{ji}, \tag{4.3.15}$$

$$\bar{H}^{(2)}_{jk,ia} = \langle jk||ia\rangle + P(jk)\sum_{lb}\langle jb||il\rangle\,\sigma^{ab*}_{kl} + \frac{1}{2}\sum_{bc}\langle bc||ia\rangle\,\sigma^{bc*}_{jk} + f_{bi}\sigma^{ab*}_{kj}. \tag{4.3.16}$$

$$\bar{H}^{(1)}_{ij,kl} = \langle ij||kl\rangle\,, \qquad \bar{H}^{(1)}_{ab,cd} = \langle ab||cd\rangle\,, \tag{4.3.17}$$

$$\bar{H}^{(1)}_{ab} = F_{ab}, \qquad \bar{H}^{(1)}_{ij} = F_{ij}, \qquad \bar{H}^{(1)}_{iabj} = \langle ia||bj\rangle\,. \tag{4.3.18}$$

The computation of these matrix elements is performed in `HamiltonianIntermediatesS`. Further intermediate quantities are needed to ensure a lower scaling, given by

$$\begin{aligned}S_{abij} &= \frac{1}{4}\langle ij||mk\rangle\,\sigma^{ab*}_{mk} + \frac{1}{4}\langle ed||ab\rangle\,\sigma^{ed*}_{ij} - \frac{1}{2}(\langle jc||ka\rangle\,\sigma^{cb*}_{ki} + \langle id||kb\rangle\,\sigma^{da*}_{jk}), \\ R_{ijab} &= \langle ab||cd\rangle\,\sigma^{cd}_{ij}, \\ Z_{abcd} &= \sigma^{ab*}_{ij}\sigma^{cd}_{ij}.\end{aligned} \tag{4.3.19}$$

The terms of eqs. 4.3.7-4.3.10 are calculated in `ContractionS`. Intermediate contractions are needed for the three-body term, written as

$$\begin{aligned}\bar{H}^{(2)}_{kla,cbi}r^{cb}_{kl} &= -\langle ak||ij\rangle\,\underbrace{\sigma^{cb*}_{jl}r^{cb}_{kl}}_{Q_{jk}} + \langle al||ij\rangle\,\underbrace{\sigma^{cb*}_{jk}r^{cb}_{kl}}_{-Q_{jl}} + \langle da||ci\rangle\,\underbrace{\sigma^{db*}_{kl}r^{cb}_{kl}}_{Q_{dc}} - \langle da||bi\rangle\,\underbrace{\sigma^{dc*}_{kl}r^{cb}_{kl}}_{-Q_{db}} = \\ &= -2\langle ak||ij\rangle\,Q_{jk} + 2\langle da||ci\rangle\,Q_{dc}.\end{aligned} \tag{4.3.20}$$

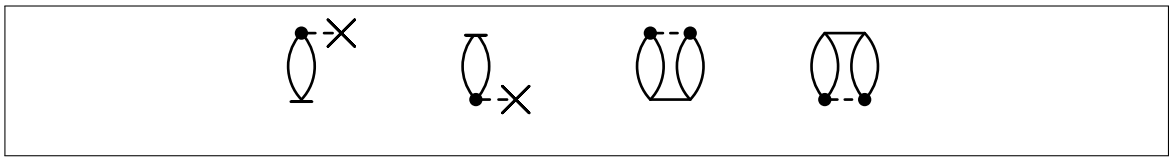

Diagrams 1: Diagrams describing the UCC energy; these are the same both in the UCC2 and UCC3 framework. The continuous lines depict the $\hat{\sigma}$ operator, the dashed line with a cross is the Fock operator, while the dashed line with two vertices symbolizes the operator $\hat{V}$.

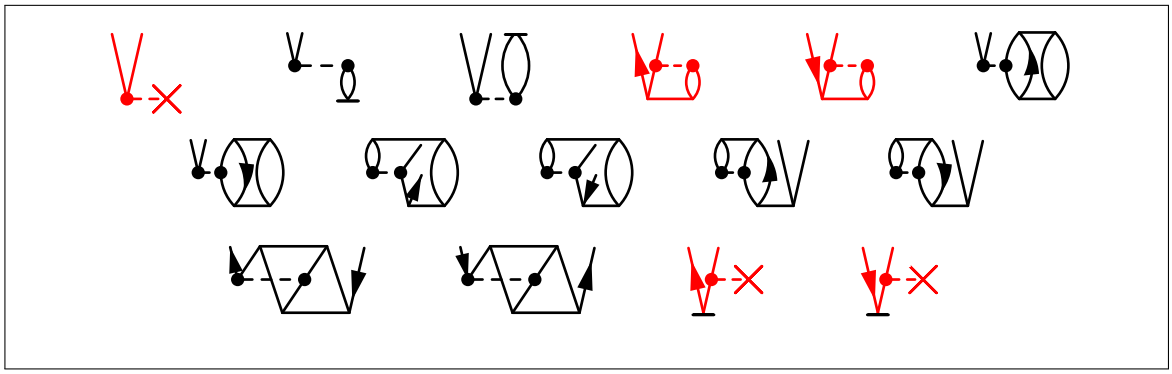

Diagrams 2: Diagrams describing the UCC amplitude equation $\bar{H}_{ai} = 0$. The same conventions for the operators as in diags. 1 are adopted. The red diagrams are those contributing to the UCC2 approximation, while all terms are needed for the UCC3 one.

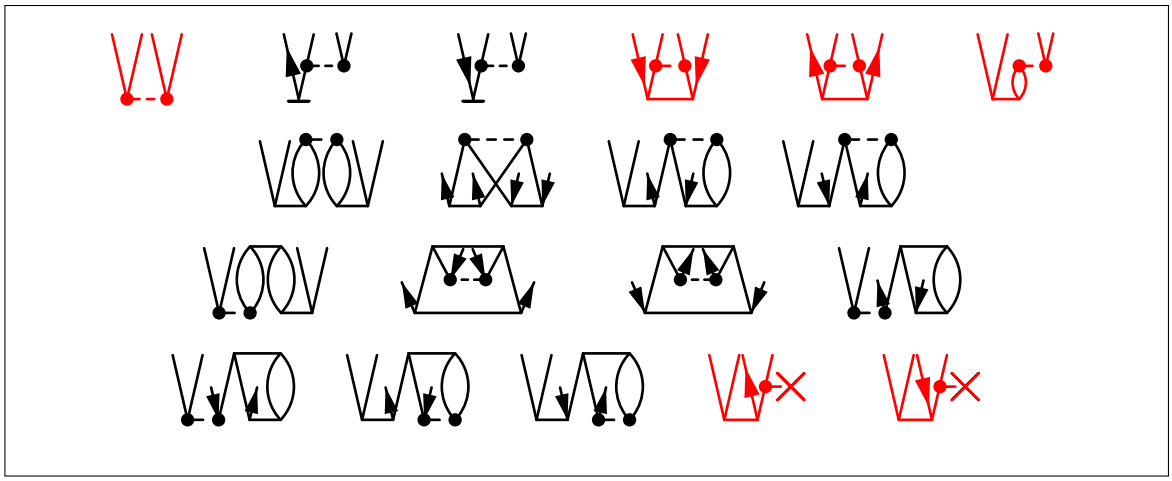

Diagrams 3: Diagrams describing the UCC amplitude equation $\bar{H}_{abij} = 0$. The same conventions for the operators as in diags. 1 are adopted. The red diagrams are those contributing to the UCC2 approximation, while all terms are needed for the UCC3 one.

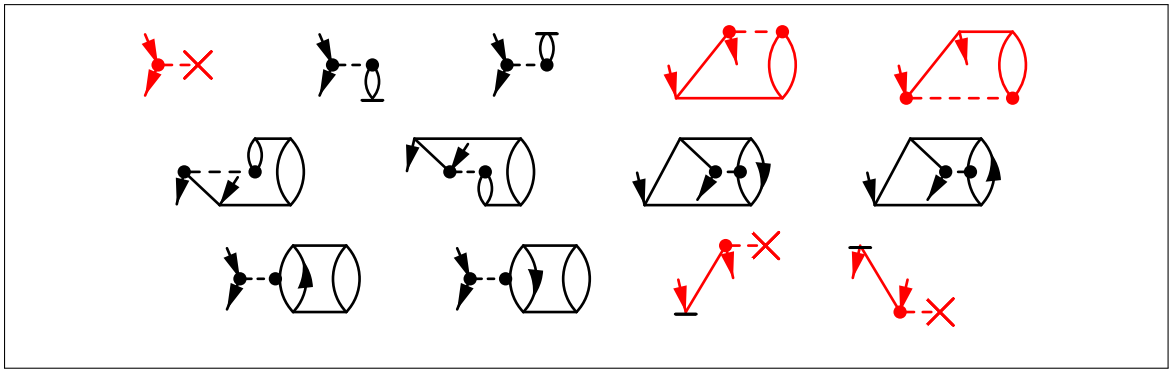

Diagrams 4: Diagrams of the contributions to the transformed Hamiltonian matrix element $\bar{H}_{ij}$. The red diagrams contribute to the UCC2 element $\bar{H}^{(2)}_{ij}$, while all diagrams contribute to the UCC3 block $\bar{H}^{(3)}_{ij}$.

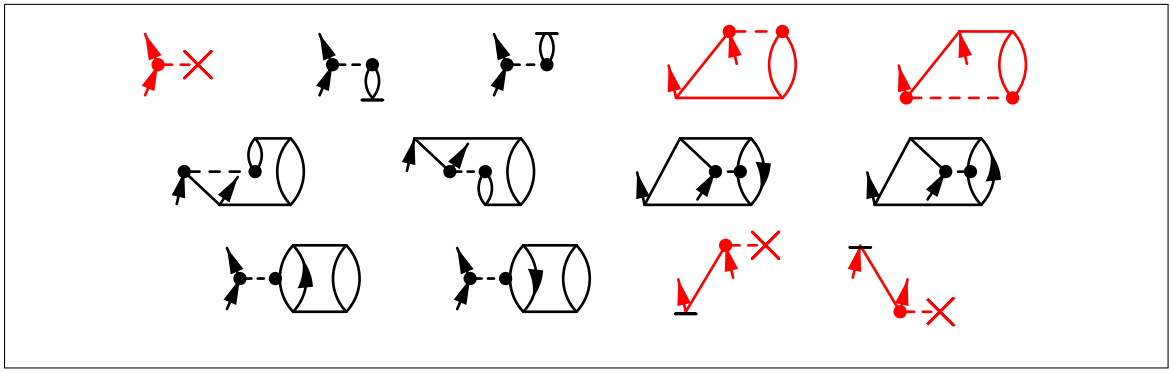

Diagrams 5: Diagrams of the contributions to the transformed Hamiltonian matrix element $\bar{H}_{ab}$. The red diagrams contribute to the UCC2 element $\bar{H}^{(2)}_{ab}$, while all diagrams contribute to the UCC3 block $\bar{H}^{(3)}_{ab}$.

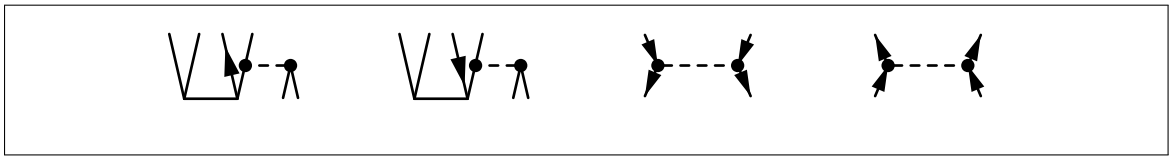

Diagrams 6: Diagrams of the contributions to the transformed Hamiltonian matrix elements for the UCC3 method $\bar{H}^{(1)}_{ibcajk}$, $\bar{H}^{(1)}_{ijkl}$, $\bar{H}^{(1)}_{abcd}$. The corresponding elements for UCC2 are vanishing, as none of these terms is of zeroth order, in order to satisfy $\bar{H}^{(0)}_{ibcajk}$, $\bar{H}^{(0)}_{ijkl}$, $\bar{H}^{(0)}_{abcd}$.

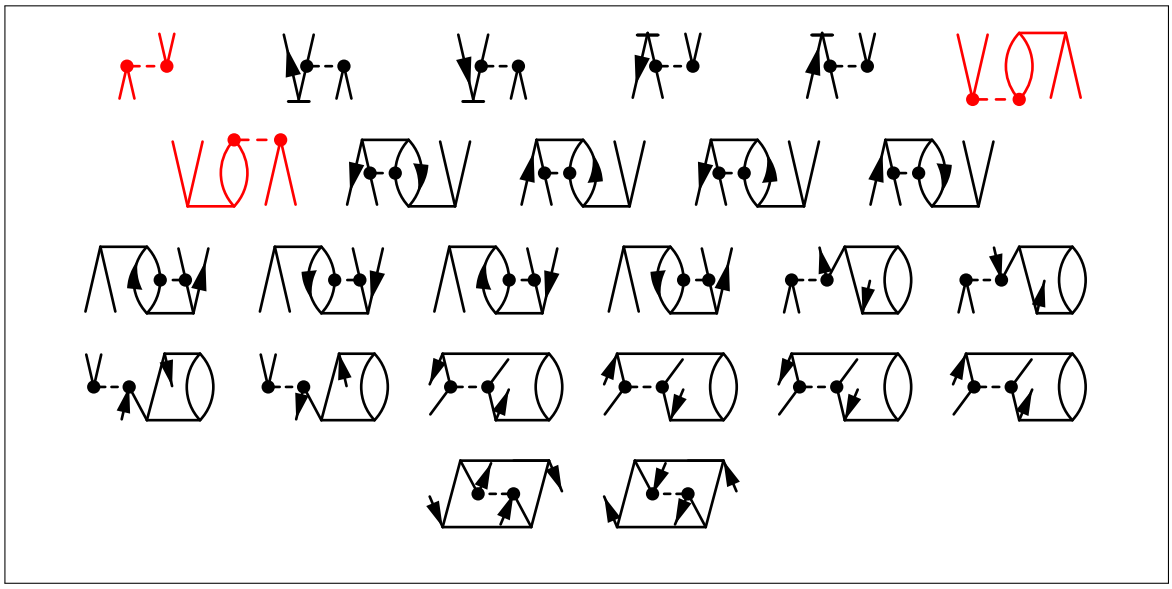

Diagrams 7: Diagrams of the contributions to the transformed Hamiltonian matrix element $\bar{H}_{iabj}$. The red diagrams contribute to the UCC2 element $\bar{H}^{(2)}_{iabj}$, while all diagrams contribute to the UCC3 block $\bar{H}^{(3)}_{iabj}$.

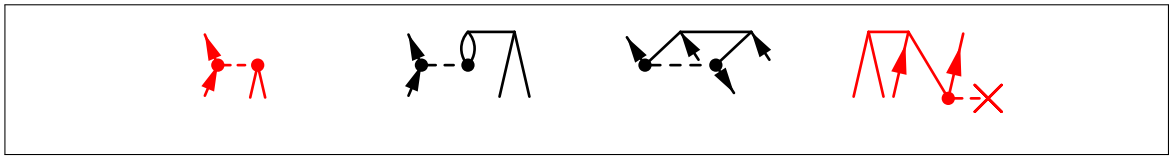

Diagrams 8: Diagrams of the contributions to the transformed Hamiltonian matrix element $\bar{H}_{ciab}$. The red diagrams contribute to the UCC2 element $\bar{H}^{(1)}_{ciab}$, while all diagrams contribute to the UCC3 block $\bar{H}^{(2)}_{ciab}$.

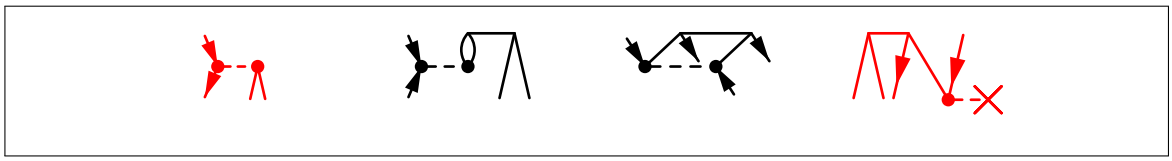

Diagrams 9: Diagrams of the contributions to the transformed Hamiltonian matrix element $\bar{H}_{jkia}$. The red diagrams contribute to the UCC2 element $\bar{H}^{(1)}_{jkia}$, while all diagrams contribute to the UCC3 block $\bar{H}^{(2)}_{jkia}$

The computational cost for a EOM-UCC3 calculation scales as for a EOM-CCSD calculation, $\sim N^6$. The solution of the UCC3 amplitude equation has the same scaling given by the $N_{\text{virt}}^4 N_{\text{occ}}^2$ term, but it has one more $N_{\text{virt}}^3 N_{\text{occ}}^3$ term. However, the construction of the similarity-transformed Hamiltonian matrix is more expensive than for EOM-CCSD, as there are three additional terms scaling as $N_{\text{virt}}^4 N_{\text{occ}}^2$ compared to the CCSD equations: in eq. 4.3.11, $\frac{1}{4}\langle ed||bc\rangle \sigma_{il}^{ed*}\sigma_{jl}^{ac}$ and its adjoint $\frac{1}{4}\langle ac||ed\rangle \sigma_{jl}^{ed}\sigma_{il}^{bc*}$, $\langle ad||cb\rangle \sigma_{jk}^{ce}\sigma_{ik}^{de*}$ and $\frac{1}{2}\langle ic||dj\rangle \sigma_{kl}^{cb*}\sigma_{kl}^{ad}$ are the three most expensive terms.

In Diagrams 1-9, the diagrammatic representation of the UCC3 terms is shown, where the red ones are those contributing to the lower-order UCC2 expressions.

4.4 ADC implementation

In ref. 160, the connection between ADC and UCC has been shown: the working equations for the similarity-transformed Hamiltonian are the same, with the important difference that the amplitudes in ADC are not determined iteratively through the amplitude equations, but are provided by a perturbative approximation and are not modified during the whole computation. In Qcumbre, different flavours of ADC have been implemented. The ADC amplitudes are computed by the function `AdcAmplitudes`, and $\sigma_{ij}^{ab[2]}$ is named `tS2`, and $\sigma_i^{a[2]}$ `tS1`, respectively. The leading contribution $\sigma_{ij}^{ab[1]}$ is named `tS` and calculated with the MP2 initial guess.

For the strict version of ADC2, the transformed Hamiltonian blocks have the same expression as for UCC2. However, the amplitudes are given by the MP2 guess

$$\sigma_i^a = 0, \qquad \sigma_{ij}^{ab} = \frac{\langle ab||ij\rangle}{\varepsilon_i + \varepsilon_j - \varepsilon_a - \varepsilon_b}. \tag{4.4.1}$$

A modified version of ADC2-strict is ADC2-x, a variation defined not to improve the description of the single-excited states but to give a diagnostic for the double-excited ones.[265] In this case, the transformed Hamiltonian matrix has an additional first-order contribution in the doubles-doubles block, with the form

$$\mathbf{M}_{\text{ADC(2)}} = \begin{pmatrix} M_{\text{SS}}^{(2)} & M_{\text{SD}}^{(1)} \\ M_{\text{DS}}^{(1)} & M_{\text{DD}}^{(0)} + C^{(1)} \end{pmatrix}, \tag{4.4.2}$$

where the additional part is given by the term

$$\begin{aligned} C_{abkl,a'b'k'l'}^{(1)} =& \delta_{kk'}\delta_{ll'}\langle ab||a'b'\rangle + \delta_{aa'}\delta_{bb'}\langle kl||k'l'\rangle - P(a'b')P(k'l')(\delta_{bb'}\delta_{ll'}\langle ak'||a'k\rangle \\ &+ \delta_{bb'}\delta_{kk'}\langle al'||a'l\rangle\delta_{aa'}\delta_{ll'}\langle bk'||b'k\rangle + \delta_{aa'}\delta_{kk'}\langle bl'||b'l\rangle). \end{aligned} \tag{4.4.3}$$

The ADC3 amplitudes are obtained through perturbation theory: σ_i^a has only a second-order contribution, while σ_{ij}^{ab} has both a first- and a second-order part.

$$\sigma_{ij}^{ab[1]} = \frac{\langle ab||ij\rangle}{\varepsilon_i + \varepsilon_j - \varepsilon_a - \varepsilon_b}, \tag{4.4.4}$$

$$\sigma_{ij}^{ab[2]} = \frac{1}{2}\sum_{kl}\frac{\langle kl||ij\rangle\sigma_{kl}^{ab[1]}}{\varepsilon_i + \varepsilon_j - \varepsilon_a - \varepsilon_b} + \frac{1}{2}\sum_{cd}\frac{\langle ab||cd\rangle\sigma_{ij}^{cd[1]}}{\varepsilon_i + \varepsilon_j - \varepsilon_a - \varepsilon_b} + P(ij)P(ab)\sum_{kc}\frac{\langle ak||ic\rangle\sigma_{jk}^{bc[1]}}{\varepsilon_i + \varepsilon_j - \varepsilon_a - \varepsilon_b}, \tag{4.4.5}$$

$$\sigma_i^{a[2]} = \frac{1}{2}\sum_{jbc}\frac{\langle aj||cb\rangle\sigma_{ij}^{cb[1]}}{\varepsilon_i - \varepsilon_a} - \frac{1}{2}\sum_{jkb}\frac{\langle kj||ib\rangle\sigma_{jk}^{ba[1]}}{\varepsilon_i - \varepsilon_a}. \tag{4.4.6}$$

In the construction of the Hamiltonian matrix elements, attention must be paid to the correct inclusion of the amplitudes to the right order. To clarify this statement, two terms of the $\bar{H}_{ij}$ block are discussed as an example:

$$\begin{aligned} &\frac{1}{4}\sum_{kab}\langle ik||ab\rangle\,\sigma_{jk}^{ab} \xrightarrow[ADC3]{} \frac{1}{4}\sum_{kab}\langle ik||ab\rangle\,(\sigma_{jk}^{ab[1]}+\sigma_{jk}^{ab[2]}),\\ &\frac{1}{2}\sum_{lac}\langle ic||al\rangle\sum_{bk}\sigma_{jk}^{ab}\sigma_{kl}^{bc*} \xrightarrow[ADC3]{} \frac{1}{2}\sum_{lac}\langle ic||al\rangle\sum_{bk}\sigma_{jk}^{ab[1]}\sigma_{kl}^{bc*[1]}. \end{aligned} \tag{4.4.7}$$

The equations for the determination of the ADC3 excited states are written with the same terms as the equations for the calculation of the UCC3 excited states. The difference between the two methods is given by the amplitudes $\hat{\sigma}_1$ and $\hat{\sigma}_2$ used.

4.4.1 Validation

The implementation for the zero-field case has been validated by comparing the results on some test molecules with results by the authors of ref. 160, both for the ground state and the excited states. As an intermediate debugging step, the results of the ADC2 and ADC3 implementation have been compared to those by Liu *et al.* The QCUMBRE implementation is also able to exploit point-group symmetry; its correctness has been validated by checking the consistency of the results when calculating molecular systems of higher symmetry without symmetry and with various Abelian subgroups.

As the implementation in a complex code in the presence of an external magnetic field is a new development of the theory, the validation needs to account for correct results in the case of a complex Hamiltonian. The finite-field Hamiltonian itself was already implemented in the QCUMBRE package and tested extensively for all methods. The correct treatment of complex values in UCC has been validated by ensuring the Hermiticity of each part of the implemented equations to hold.

4.5 Response properties implementation

As stated in the theory chapter 2, the calculation of molecular properties is of major importance for the application of an electronic-structure method, as these are quite easily comparable with experiment. Therefore, not only the energy for ground and excited states, but also single-state and transition properties were implemented in QCUMBRE in the present work.

4.5.1 Ground-state dipole moments UCC2

The following discussion focuses on the implementation of the Lagrange method for the calculation of ground-state dipole moments. From sec. 3.2.1, the Lagrange functional considered for ground-state properties is

$$\mathscr{L}_{\mathrm{UCC}} = \langle 0|\,\bar{H}\,|0\rangle + \langle 0|\,\hat{\Lambda}\bar{H}\,|0\rangle + \langle 0|\,\bar{H}\hat{\Lambda}^{\dagger}\,|0\rangle\,, \tag{4.5.1}$$

where $\hat{\Lambda}$ are the Lagrange multipliers imposing the amplitude equations as constraints. In Flowchart 4, the calculation of ground-state dipole moments with UCC in QCUMBRE is shown.

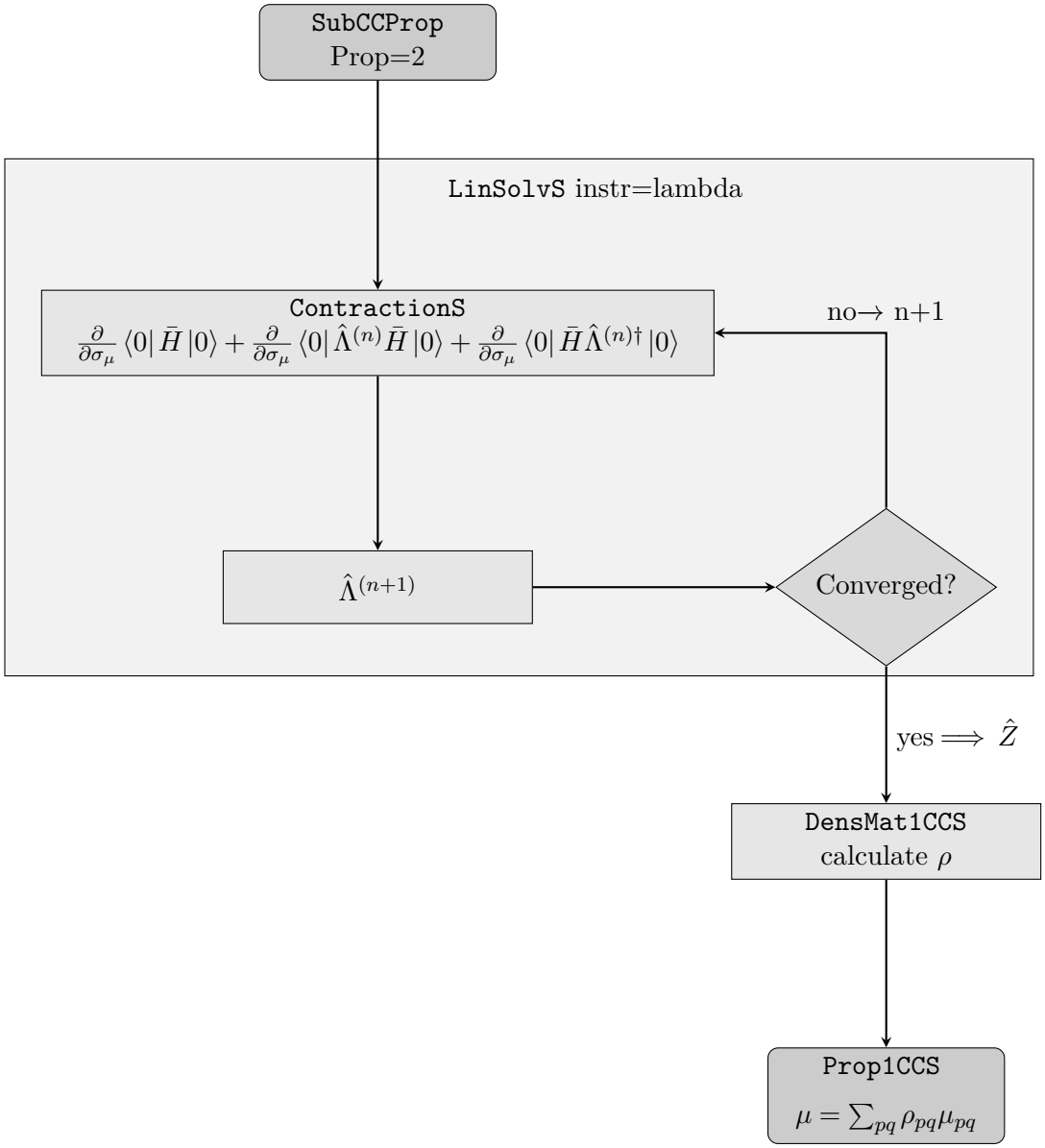

Flowchart 4: Flowchart illustrating how ground-state response properties are calculated in QCUMBRE.

In order to compute dipole moments with the response-theory approach, the keyword `prop=2` is passed to the function `SubCCProp`. The so-called Λ-equations are solved iteratively, through the already explained solver `LinSolvS`. The instruction `lambda`, passed to the solver, allows to access the Λ-equations, which are calculated in `ContractionS`. Once the Lagrange multipliers are converged, the density matrix ρ is computed through the function `DensMat1CCS`. The final result for the dipole moment $\mu = \sum_{pq} \mu_{pq}\rho_{pq}$ is given by exploiting the function `Prop1CCS`, which contracts the density matrix with the dipole integrals obtained by means of a CFOUR calculation.

A deeper understanding of the implementation may be gained by analysing the single terms in the equations, thereby focusing on efficiency. Once more, intermediates are exploited, giving a step-wise calculation of the terms which allows to keep the scaling as low as possible.

For single-state properties, the discussion should start from the implementation of the Lagrange functional for the ground state. The stationarity condition in eq. 3.2.3 is

$$\frac{\partial \mathscr{L}}{\partial \sigma_\nu} = \frac{\partial E}{\partial \sigma_\nu} + \sum_\mu \lambda_\mu \frac{\partial \bar{H}_\mu}{\partial \sigma_\nu} + \sum_\mu \lambda_\mu^* \frac{\partial \bar{H}_\mu^*}{\partial \sigma_\nu} = 0. \tag{4.5.2}$$

Differentiation with respect to the single-excitation amplitudes provides the first stationarity condition

$$\frac{\partial \mathscr{L}}{\partial \sigma_m^e} = (f + \mu\cdot\varepsilon)_{me} + \lambda_m^a (f + \mu\cdot\varepsilon)_{ae} - \lambda_i^e (f + \mu\cdot\varepsilon)_{im} = 0. \tag{4.5.3}$$

Differentiation with respect to the double-excitation amplitudes yields the second stationarity condition

$$\begin{aligned}\frac{\partial \mathscr{L}}{\partial \sigma_{mn}^{ef}} =& \frac{1}{8}\langle mn||ef\rangle + \frac{1}{4}P(mn)\lambda_m^a \langle an||ef\rangle - \frac{1}{4}P(ef)\lambda_i^f \langle nm||ie\rangle + \frac{1}{4}P(ef)P(mn)\lambda_m^e f_{jb} \\ &+ \frac{1}{4}\Bigg(\frac{1}{2}\sum_{ij}\lambda_{ij}^{ef}\langle mn||ij\rangle + \frac{1}{2}\lambda_{mn}^{ab}\langle ab||ef\rangle + P(ef)P(mn)\lambda_{im}^{ae}\langle an||if\rangle \\ &+ P(ef)(f+\mu\cdot\varepsilon)_{bf}\lambda_{mn}^{eb} - P(mn)(f+\mu\cdot\varepsilon)_{nj}\lambda_{mj}^{ef}\Bigg) = 0.\end{aligned} \tag{4.5.4}$$

For dipole moments, the differentiation is performed at $\varepsilon = 0$. As $f_{ai} = 0$, while f_{ab} and f_{ij} are diagonal: the iterative procedure returns $\lambda_i^a = 0 \ \forall i,a$ from eq. 4.5.3. Substituting this result in eq. 4.5.4, the amplitude equation for λ_2 becomes

$$\begin{aligned}&\frac{1}{8}\langle mn||ef\rangle + \frac{1}{4}\Bigg(\frac{1}{2}\sum_{ij}\lambda_{ij}^{ef}\langle mn||ij\rangle + \frac{1}{2}\sum_{ab}\lambda_{mn}^{ab}\langle ab||ef\rangle + P(ef)P(mn)\sum_{ia}\lambda_{im}^{ae}\langle an||if\rangle \\ &+ P(ef)\sum_b (f+\mu\cdot\varepsilon)_{bf}\lambda_{mn}^{eb} - P(mn)\sum_j (f+\mu\cdot\varepsilon)_{nj}\lambda_{mj}^{ef}\Bigg) = 0.\end{aligned} \tag{4.5.5}$$

Multiplying by a factor 8 and introducing the new variable $\bar{\lambda} = 2\lambda$, it can be observed that an equation identical in form to the double-excitation amplitude equation for UCC2 is obtained

$$\begin{aligned}&\langle mn||ef\rangle + \frac{1}{2}\sum_{ij}\bar{\lambda}_{ij}^{ef}\langle mn||ij\rangle + \frac{1}{2}\sum_{ab}\bar{\lambda}_{mn}^{ab}\langle ab||ef\rangle + P(ef)P(mn)\sum_{ia}\bar{\lambda}_{im}^{ae}\langle an||if\rangle \\ &+ P(ef)\sum_b (f+\mu\cdot\varepsilon)_{bf}\bar{\lambda}_{mn}^{eb} - P(mn)\sum_j (f+\mu\cdot\varepsilon)_{nj}\bar{\lambda}_{mj}^{ef} = 0.\end{aligned} \tag{4.5.6}$$

Therefore, $\bar{\lambda}$ is equal to σ^*, implying $\lambda = \frac{1}{2}\sigma^*$. In the particular case of a field-free UCC2 calculation, the response-theory approach delivers the same result as in ref. 59, where the expectation value of the dipole moment is considered. Note that this is not a general result, but is a peculiarity of this low approximation order.

The expressions of stationarity conditions are calculated in `ContractionS`. The diagonal part of eq. 4.5.3 and 4.5.4 is isolated and the λ-amplitudes are computed through the same iterative procedure as used for the UCC amplitudes in eqs. 4.3.5-4.3.6, exploiting the DIIS algorithm.[260] The initial guess provided to the solver is the inhomogeneous part of eq. 4.5.6, $\langle mn||ef\rangle$.

The stationarity condition $\frac{\partial \mathscr{L}}{\partial \sigma_\mu^*} = 0$ is not discussed, as the Hermitian form of the Lagrange functional leads to the symmetry $\frac{\partial \mathscr{L}}{\partial \sigma_\mu^*} = \left(\frac{\partial \mathscr{L}}{\partial \sigma_\mu}\right)^* = 0$; this property defines the λ^*-equations which are the adjoints of eqs. 4.5.3-4.5.4. The set of Lagrange multipliers is therefore well-defined and satisfies both stationarity conditions.

Once the Lagrange multipliers λ_μ are calculated, the ground-state dipole moment is obtained through partial differentiation of the Lagrangian, as in eq. 3.2.6. The final expression of the dipole moment is

$$\begin{aligned}\mu =&\mu_{ia}\sigma_i^a + \mu_{ai}\sigma_i^{a*} + \lambda_i^a(\mu_{ai} + \mu_{ab}\sigma_i^b - \mu_{ij}\sigma_j^a) + \lambda_i^{a*}(\mu_{ia} + \mu_{ba}\sigma_i^{b*} - \mu_{ji}\sigma_j^{a*}) \\ &+ \frac{1}{4}\lambda_{ij}^{ab}(\mu_{bc}\sigma_{ij}^{ac} - \mu_{ac}\sigma_{ij}^{bc} - \mu_{kj}\sigma_{ik}^{ab} + \mu_{ki}\sigma_{jk}^{ab}) + \frac{1}{4}\lambda_{ij}^{ab*}(\mu_{cb}\sigma_{ij}^{ac*} - \mu_{ca}\sigma_{ij}^{bc*} - \mu_{jk}\sigma_{ik}^{ab*} + \mu_{ik}\sigma_{jk}^{ab*}).\end{aligned} \tag{4.5.7}$$

Dipole moments may be expressed as $\mu = \mu_{pq}\rho_{pq}$, where $\boldsymbol{\rho}$ is the one-electron density matrix. It is advantageous to have an expression for the density matrix, as the latter can be used for the determination of all one-electron properties expressed in general as $X = \sum_{pq} x_{pq}\rho_{pq}$. The density matrix has the following matrix elements

$$\rho_{ia} = \sigma_i^a + \lambda_i^{a*} + \lambda_j^b\sigma_{ij}^{ab}, \qquad \rho_{ai} = \rho_{ia}^*, \tag{4.5.8}$$

$$\rho_{ij} = -\lambda_i^a\sigma_j^a - \lambda_j^{a*}\sigma_i^{a*} - \frac{1}{2}\lambda_{kj}^{ab}\sigma_{ki}^{ab} - \frac{1}{2}\lambda_{ki}^{ab*}\sigma_{kj}^{ab*}, \tag{4.5.9}$$

$$\rho_{ab} = \lambda_i^a\sigma_i^b + \lambda_i^{b*}\sigma_i^{a*} + \frac{1}{2}\lambda_{ij}^{ca}\sigma_{ij}^{cb} + \frac{1}{2}\lambda_{ij}^{cb*}\sigma_{ij}^{ca*}. \tag{4.5.10}$$

In this work, response theory is compared to the so-called *expectation-value* approach. This terminology is used to indicate the results obtained from eqs. 4.5.8-4.5.10, with $\lambda = 0$, corresponding to the partial differentiation of the energy. Note that in ref. 248 the expectation value of the dipole moment operator is calculated with a BCH expansion, which does not correspond to the expansion in the energy expression. This approach is motivated by the fact that the dipole-moment operator does not provide cancellation relations leading to the Bernoulli expansion, based on the amplitude equations. It can be argued that the definition of the property operators should be connected to the differentiation of the energy expression. Thus, here the Bernoulli expansion is adopted for the expectaion-value calculations.

The dipole integrals are calculated by Cfour and passed to Qcumbre; the density matrices are computed in `DensMat1CCS`. They are contracted with the dipole integrals by the routine `Prop1CCS`. For UCC, only *unrelaxed* dipole moments are calculated, meaning that it is here neglected that also the HF orbitals respond to the perturbation.

4.5.2 Ground-state dipole moments UCC3

The code structure for UCC3 is the same as for UCC2, but the equations are more involved, due to the higher number of terms which need to be differentiated. Differentiating the UCC3

Lagrangian with respect to the single-excitation amplitudes, the first stationarity condition is obtained

$$\begin{aligned}\frac{\partial \mathscr{L}}{\partial \sigma_i^a} &= (f+\mu\cdot\varepsilon)_{ia} + \lambda_j^b \langle bi||ja\rangle + \lambda_i^b (f+\mu\cdot\varepsilon)_{ba} - \lambda_j^a (f+\mu\cdot\varepsilon)_{ji} \\ &+ \frac{1}{4}\Big(-2\lambda_{jk}^{ba}\langle ib||kj\rangle + 2\lambda_{ji}^{bc}\langle bc||ja\rangle \Big) + \frac{1}{2}\lambda_j^{b*}\langle ba||ji\rangle^* = 0.\end{aligned} \tag{4.5.11}$$

Differentiation with respect to the double-excitation amplitudes yields the second stationarity condition

$$\begin{aligned}
&\frac{\partial \mathscr{L}}{\partial \sigma_{ij}^{ab}} = \frac{1}{2}\langle ij||ab\rangle + P(ij)\lambda_i^c\langle cj||ab\rangle - P(ab)\lambda_k^b\langle ji||ka\rangle - P(ij)\underbrace{\lambda_l^c\langle cj||lk\rangle}_{T_{jk}}\sigma_{ik}^{ab*} \\
&+ P(ab)\underbrace{\lambda_k^c\langle cd||kb\rangle}_{T_{db}}\sigma_{ij}^{ad*} - P(ij)P(ab)\underbrace{\lambda_k^b\langle cj||lk\rangle}_{T_{jcbl}}\sigma_{il}^{ac*} + P(ab)P(ij)\underbrace{\lambda_j^c\langle cd||bk\rangle}_{T1_{jdbk}}\sigma_{ik}^{ad*} \\
&- \frac{1}{4}P(ab)P(ij)\lambda_i^a\underbrace{(\langle cj||lk\rangle\sigma_{lk}^{cb*} + \langle cd||kb\rangle\sigma_{kj}^{cd*})}_{SI_{bj}} + \frac{1}{2}P(ab)\lambda_k^b\underbrace{\langle cd||ka\rangle\sigma_{ij}^{cd*}}_{Sint_{ijka}} \\
&- \frac{1}{2}P(ij)\underbrace{\lambda_i^c\langle cj||lk\rangle}_{T_{ijlk}}\sigma_{kl}^{ab*} + P(ab)P(ij)\lambda_i^a f_{jb} + \frac{1}{2}\lambda_{kl}^{ab}\langle ij||kl\rangle + \frac{1}{2}\lambda_{ij}^{cd}\langle cd||ab\rangle \\
&+ P(ab)P(ij)\lambda_{ik}^{ac}\langle cj||kb\rangle + \frac{2}{3}P(ij)P(ab)\lambda_{il}^{ad}\underbrace{\langle kj||cb\rangle\sigma_{kl}^{cd}}_{SI_{ldbj}} + \frac{1}{6}\lambda_{kl}^{ab}\underbrace{\sigma_{kl}^{cd}\langle ij||cd\rangle}_{SI_{klij}^*} \\
&+ \frac{1}{6}\underbrace{\lambda_{ij}^{cd}\sigma_{kl}^{cd}}_{LS_{ijkl}}\langle kl||ab\rangle - \frac{1}{3}P(ab)\underbrace{\lambda_{kl}^{cb}\sigma_{kl}^{cd}}_{LS_{bd}}\langle ij||ad\rangle - \frac{1}{3}P(ab)\lambda_{ij}^{ad}\underbrace{\langle kl||cb\rangle\sigma_{kl}^{cd}}_{Sint_{db}} \\
&- \frac{1}{3}P(ij)\underbrace{\lambda_{ki}^{cd}\sigma_{kl}^{cd}}_{LS_{il}}\langle jl||ba\rangle - \frac{1}{3}P(ij)\lambda_{il}^{ab}\underbrace{\langle kj||cd\rangle\sigma_{kl}^{cd}}_{Sint_{lj}} + \frac{1}{3}P(ij)P(ab)\lambda_{ik}^{ac}\underbrace{\langle cd||kl\rangle\sigma_{jl}^{bd*}}_{SI_{jbck}^*} \\
&+ \frac{1}{12}\lambda_{kl}^{ab}\underbrace{\langle cd||kl\rangle\sigma_{ij}^{cd*}}_{SI_{ijkl}} + \frac{1}{12}\underbrace{\lambda_{ij}^{cd}\langle cd||kl\rangle}_{LI_{ijkl}}\sigma_{kl}^{ab*} - \frac{1}{6}P(ab)\underbrace{\lambda_{kl}^{cb}\langle cd||kl\rangle}_{LI_{bd}}\sigma_{ij}^{ad*} \\
&- \frac{1}{6}P(ij)\underbrace{\lambda_{ki}^{cd}\langle cd||kl\rangle}_{LI_{il}}\sigma_{jl}^{ba*} - \frac{1}{6}P(ij)\lambda_{il}^{ab}\underbrace{\langle cd||kl\rangle\sigma_{kj}^{cd*}}_{Sint_{jl}^*} - \frac{1}{6}P(ab)\lambda_{ij}^{ad}\underbrace{\langle cd||kl\rangle\sigma_{kl}^{cb*}}_{Sint_{bd}^*} \\
&+ P(ab)f_{cb}\lambda_{ij}^{ac} - P(ij)f_{jk}\lambda_{ik}^{ab} \\
&+ \Big(-P(ij)\underbrace{\lambda_k^c\langle cl||kj\rangle}_{T_{lj}}\sigma_{il}^{ab} + P(ab)\underbrace{\lambda_k^d\langle bd||ck\rangle}_{T_{bc}}\sigma_{ij}^{ac} - P(ab)P(ij)\underbrace{\lambda_k^c\langle al||ik\rangle}_{T_{laci}}\sigma_{jl}^{bc} \\
&+ P(ab)P(ij)\underbrace{\lambda_k^c\langle ca||di\rangle}_{T1_{kadi}}\sigma_{jk}^{bd} - \frac{1}{2}P(ab)\underbrace{\lambda_k^c\sigma_{kl}^{cb}}_{LS_{bl}}\langle al||ij\rangle + \frac{1}{2}P(ij)\underbrace{\lambda_k^d\sigma_{jk}^{cd}}_{LS_{cj}}\langle ab||ic\rangle \\
&+ \underbrace{\lambda_k^d\sigma_{ij}^{cd}}_{LS_{ijkc}}\langle ab||kc\rangle - \underbrace{\lambda_k^c\langle cl||ij\rangle}_{T_{klij}}\sigma_{kl}^{ba} + \frac{1}{3}P(ab)P(ij)\underbrace{\lambda_{kl}^{cd}\sigma_{il}^{ad}}_{LS_{kcai}}\langle cb||kj\rangle
\end{aligned} \tag{4.5.12}$$

$$+\frac{1}{12}\underbrace{\lambda_{kl}^{cd}\sigma_{ij}^{cd}}_{LS_{klij}}\langle ab||kl\rangle+\frac{1}{12}\underbrace{\lambda_{kl}^{cd}\langle cd||ij\rangle}_{LI_{klij}}\sigma_{kl}^{ab}-\frac{1}{6}P(ab)\underbrace{\lambda_{kl}^{cd}\langle cb||kl\rangle}_{LI_{db}}\sigma_{ij}^{ad}$$
$$-\frac{1}{6}P(ij)\underbrace{\lambda_{kl}^{cd}\langle cd||kj\rangle}_{LI_{lj}}\sigma_{il}^{ab}-\frac{1}{6}P(ij)\underbrace{\lambda_{kl}^{cd}\sigma_{kj}^{cd}}_{LS_{lj}}\langle ab||il\rangle-\frac{1}{6}P(ab)\underbrace{\lambda_{kl}^{cd}\sigma_{kl}^{cb}}_{LS_{db}}\langle ad||ij\rangle\Big)^{*}=0.$$

In order to keep the scaling of these equations as low as possible, the implementation of the terms in eq. 4.5.2 is performed by defining intermediate quantities, which are directly listed in the equation. The algorithm for the calculation of the ground-state dipole moments for UCC3 is the same as the one described for UCC2. Rearrangement of the equation leads to the computation of the set of Lagrange parameters.

The partial differentiation of the UCC3 Lagrangian yields the same density matrices as for UCC2 (eqs. 4.5.8-4.5.10), calculated in `DensMat1CCS`. Contracting with the dipole moment integrals calculated by CFOUR, the UCC3 dipole moments can be computed.

4.5.3 Excited-states dipole moments with UCC2

Calculation of excited-state dipole moments is performed by the function `SubEOMProp`, whose structure is shown in Flowchart 5. The keyword `prop=2` ensures that the response-theory approach is exploited. For the implementation of the terms contributing to the stationarity condition in eq. 3.2.4, the equation is split into a homogeneous and an inhomogeneous part, giving

$$\frac{\partial\mathscr{L}_{\mathrm{UCC}}}{\partial\sigma_\mu}=\underbrace{\langle 0|\,\hat{R}^\dagger\frac{\partial\bar{H}}{\partial\sigma_\mu}\hat{R}\,|0\rangle}_{\text{inhomog.}}+\underbrace{\langle 0|\,\hat{Z}\frac{\partial\bar{H}}{\partial\sigma_\mu}\,|0\rangle+\langle 0|\,\frac{\partial\bar{H}}{\partial\sigma_\mu}\hat{Z}^\dagger\,|0\rangle}_{\text{homog.}}. \tag{4.5.13}$$

This partition is motivated by the fact that the inhomogeneous part does not depend on the Lagrange multipliers and is therefore calculated outside the iterative procedure solving for the ζ parameters. The function `ContractionZetaS` computes the differentiated inhomogeneous term $\langle 0|\,\hat{R}^\dagger\frac{\partial\bar{H}}{\partial\sigma_\mu}\hat{R}\,|0\rangle$. The listed instructions `left=right, freq=0` specify that a single-state property is being targeted.
The $\hat{Z}$-equations are then solved iteratively, through the solver `LinSolvS`. The instruction `instr=Zvec` allows the solver to call the function `ContractionZvecS`, where the homogeneous part of the stationarity condition in eq. 4.5.13 is computed. Once the Lagrange multipliers have been determined iteratively, the density matrix for the excited state is computed: the function `DensMat1EOM_UCC` computes the $\hat{R}$-dependent part of the density matrices, while the function `DensMat1InterS_UCC` computes the $\hat{Z}$-dependent part. Finally, the dipole moments are computed by contracting the dipole integrals obtained from the CFOUR calculation with the density matrix. This step is performed by the function `Prop1CCS`.

A full understanding of the complexity of the implementation can be gained by analysing the equations in full detail. A complete discussion of the implemented terms follows, also focusing on the intermediates which need to be defined in order to ensure a low scaling.

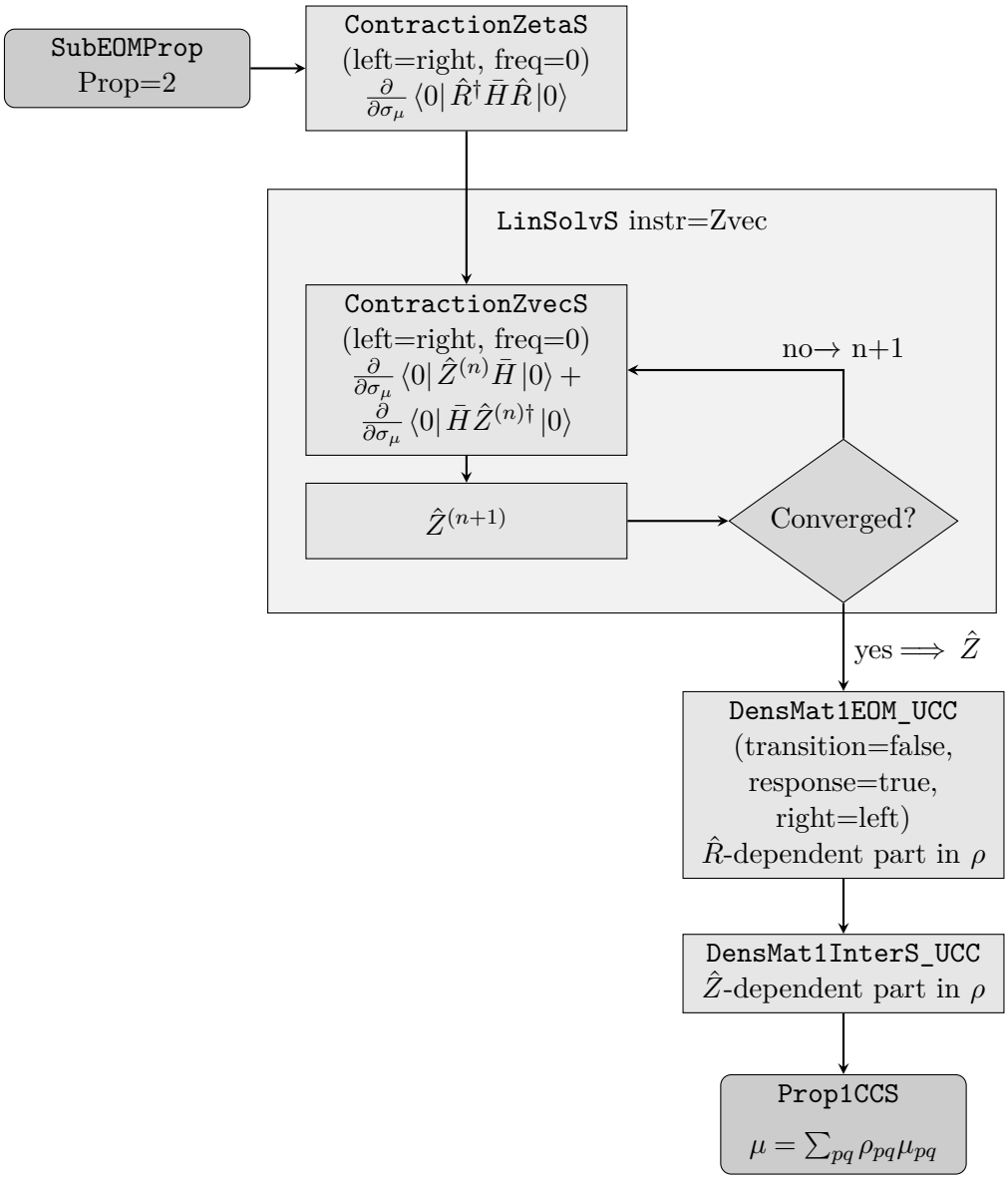

Flowchart 5: Flowchart illustrating how single-state excited-state response properties are calculated in QCUMBRE.

Excited-state dipole moments are obtained by differentiating the Lagrangian in eq. 3.2.3 and imposing the stationarity conditions in eqs. 3.2.4 and 3.2.5. The differentiation of the amplitude equations is the same as discussed for the ground-state dipole moments. The term $\langle 0|\,\hat{R}^\dagger \bar{H} \hat{R}\,|0\rangle$ can be split into a ground-state contribution, already calculated, and the one specific for the excited state

$$\langle 0|\,\hat{R}^\dagger \bar{H} \hat{R}\,|0\rangle = \langle 0|\,\hat{R}^\dagger [\bar{H}, \hat{R}]\,|0\rangle + \langle 0|\,\bar{H}\,|0\rangle\,. \tag{4.5.14}$$

The additional term which needs to be differentiated yields

$$\frac{\partial\,\langle 0|\,\hat{R}^\dagger [\bar{H}, \hat{R}]\,|0\rangle}{\partial \sigma^e_m} = -f_{mb} r^{e*}_i r^b_i - f_{ie} r^{a*}_m r^a_j, \tag{4.5.15}$$

$$\begin{aligned}\frac{\partial\,\langle 0|\,\hat{R}^\dagger [\bar{H}, \hat{R}]\,|0\rangle}{\partial \sigma^{ab}_{ij}} &= -\frac{1}{2} P(ab)\,\langle ij||cb\rangle \underbrace{r^{a*}_l r^c_l}_{R_{ca}} - \frac{1}{2} P(ij)\,\langle kj||ab\rangle \underbrace{r^{d*}_i r^d_k}_{R_{ik}} \\ &+ \frac{1}{2} P(ij)P(ab) \underbrace{\langle kj||cb\rangle\, r^c_k}_{RI_{bj}} r^{a*}_i - P(ij) f_{ic} \underbrace{r^{ab*}_{kj} r^c_k}_{RR_{abcj}} - P(ab) f_{kb} \underbrace{r^{ac*}_{ij} r^c_k}_{-RR_{ijka}}\,.\end{aligned} \tag{4.5.16}$$

These terms are calculated in `ContractionZetaS` in QCUMBRE.

The ζ-equations are found by requiring $\frac{\partial \mathscr{L}}{\partial \sigma^a_i} = 0$, adding the contributions in eqs. 4.5.3 and 4.5.15, and $\frac{\partial \mathscr{L}}{\partial \sigma^{ab}_{ij}} = 0$, adding the contributions in eqs. 4.5.4 and 4.5.16. The $\hat{Z}$ operator is determined in an iterative procedure using the solver in `LinSolv`, with the same strategy as for the σ-amplitudes: the diagonal part of the ζ-equations is isolated and an expression for its amplitudes defined.

Once the $\hat{Z}$ operator has been determined, the dipole moments are calculated via the expressions obtained by partial differentiation of the Lagrangian. An additional term $\Delta\mu_I$ needs to be calculated on top of the contributions already calculated for the ground-state dipole moment, given by

$$\frac{\mathrm{d}\mathscr{L}}{\mathrm{d}\varepsilon} = \frac{\partial \mathscr{L}}{\partial \varepsilon} = \mu_{\mathrm{GS}} + \Delta\mu_I$$

$$\begin{aligned}\Delta\mu_I = \frac{\partial\,\langle 0|\,\hat{R}^\dagger_I [\bar{H}, \hat{R}_I]\,|0\rangle}{\partial \varepsilon} &= r^{a*}_i \Big((\mu_{ab} - \mu_{jb}\sigma^a_j - \mu_{aj}\sigma^{b*}_j) r^b_i - (\mu_{ji} + \mu_{jb}\sigma^b_i + \mu_{bi}\sigma^{b*}_j) r^a_j \\ &+ \frac{1}{2}(-\mu_{aj}\sigma^{cb*}_{jl}) r^{cb}_{il} - \frac{1}{2}(\mu_{ci}\sigma^{bc*}_{lj}) r^{ab}_{jl} \Big) + \frac{1}{4} r^{ab*}_{ij} \Big(P(ij)(-\mu_{kc}\sigma^{ab}_{kj}) r^c_i - P(ab)(\mu_{kc}\sigma^{bc}_{ji}) r^a_k \\ &+ 2(\mu_{ac} - \mu_{kc}\sigma^a_k - \mu_{ak}\sigma^{c*}_k) r^{cb}_{ij} - 2(\mu_{kj} + \mu_{kc}\sigma^c_j + \mu_{cj}\sigma^{c*}_k) r^{ab}_{ik} \Big)\end{aligned} \tag{4.5.17}$$

The one-electron density matrices are formulated

$$\begin{aligned}\rho_{ia} &= \sigma^a_i + \zeta^{a*}_i + \zeta^b_j \sigma^{ab}_{ij} - r^{b*}_j \sigma^b_i r^a_j - r^{b*}_j \sigma^a_j r^b_i + \frac{1}{2} r^{bc*}_{jk} \sigma^{cb}_{ik} r^a_j + \frac{1}{2} r^{bc*}_{jk} \sigma^{ca}_{jk} r^b_i \\ \rho_{ij} &= -\zeta^a_i \sigma^a_j - \zeta^{a*}_j \sigma^{a*}_i - \frac{1}{2} \zeta^{ab}_{kj} \sigma^{ab}_{ki} - \frac{1}{2} \zeta^{ab*}_{ki} \sigma^{ab*}_{kj} - r^{a*}_j r^a_i - \frac{1}{2} r^{ab*}_{kj} r^{ab}_{ki} \\ \rho_{ab} &= \zeta^a_i \sigma^b_i + \zeta^{b*}_i \sigma^{a*}_i + \frac{1}{2} \zeta^{ca}_{ij} \sigma^{cb}_{ij} + \frac{1}{2} \zeta^{cb*}_{ij} \sigma^{ca*}_{ij} + r^{a*}_i r^b_j + \frac{1}{2} r^{ac*}_{ij} r^{bc}_{ij}.\end{aligned} \tag{4.5.18}$$

The expressions corresponding to μ_{GS} are calculated in `DensMat1InterS_UCC`, while the $\Delta\mu_I$ part is included in `DensMat1EOM_UCC`.

4.5.4 Excited-state dipole moments with UCC3

Going to UCC3, the structure of the calculation of excited-state dipole moments is the same as the one shown in Flowchart 4 for UCC2. The detailed equations, however, are more involved and a detailed discussion of the additional terms arising at this order of approximation is given hereafter.

As for UCC2, the inhomogeneous part of eq. 4.5.13 needs to be implemented. The expression is quite lengthy and has to be factorised with intermediates, in order to keep the scaling as low as possible. Equations for the singles amplitude ζ_i^a are found by imposing the sum of eq. 4.5.11 and of the following expression to vanish

$$\begin{aligned}\frac{\partial \langle 0|\hat{R}_I^\dagger[\bar{H},\hat{R}_I]|0\rangle}{\partial \sigma_i^a} &= (\underbrace{r_j^{c*}}_{RR_{bc}}\langle ci||ba\rangle - f_{ib}\underbrace{r_j^{a*}}_{RR_{ba}})r_j^b - r_j^b(\langle ji||ka\rangle \underbrace{r_k^{b*}}_{RR_{kj}} + f_{ja}\underbrace{r_i^{b*}}_{RR_{ij}}) \\ &+ (\underbrace{\langle cj||ab\rangle}_{RL_{ca}} r_i^{c*} - \underbrace{\langle ij||kb\rangle}_{RL_{ik}} r_k^{a*})r_j^b.\end{aligned} \tag{4.5.19}$$

Equations for the amplitudes ζ_{ij}^{ab} are defined by ensuring that the sum of eq. 4.5.2 and of the following differentiation vanishes

$$\begin{aligned}\frac{\partial \langle 0|\hat{R}_I^\dagger[\bar{H},\hat{R}_I]|0\rangle}{\partial \sigma_{ij}^{ab}} &= -\frac{1}{2}P(ab)(\langle ij||cb\rangle + \underbrace{P(ij)\langle id||ck\rangle \sigma_{jk}^{bd*} + \frac{1}{2}\langle dg||bc\rangle \sigma_{ij}^{gd*}}_{Int1_{ijcb}})\underbrace{r_l^{a*}r_l^c}_{RR_{ca}} \\ &+ \frac{1}{2}(-P(ab)P(ij)\langle cj||kb\rangle \underbrace{\sigma_{ik}^{ad*}}_{RRS_{ikac}} - \langle ec||ba\rangle \underbrace{\sigma_{ij}^{de*}}_{-RRS_{ijec}} + 2P(ab)\underbrace{\langle ce||db\rangle}_{RRS_{eb}}\sigma_{ij}^{ae*} \\ &- 2P(ij)\underbrace{\langle jc||kd\rangle}_{RRS_{jk}}\sigma_{ik}^{ab*})\underbrace{r_l^{c*}r_l^d}_{RR_{dc}} - \frac{1}{2}P(ij)(\langle kj||ab\rangle + \underbrace{P(ab)\langle kc||al\rangle \sigma_{jl}^{bc*} + \frac{1}{2}\langle kj||ml\rangle \sigma_{ml}^{ab*}}_{Int2_{kjab}})\underbrace{r_i^{d*}r_k^d}_{RR_{ik}} \\ &+ \frac{1}{2}(P(ab)P(ij)\langle cj||kb\rangle \underbrace{\sigma_{li}^{ca*}}_{SRR_{kica}} + \langle ij||km\rangle \underbrace{\sigma_{lm}^{ab*}}_{SRR_{kmab}} - 2P(ij)\underbrace{\langle lj||km\rangle}_{SRR_{jm}}\sigma_{im}^{ab*} \\ &+ 2P(ab)\underbrace{\langle lc||kb\rangle}_{SRR_{cb}}\sigma_{ij}^{ac*})\underbrace{r_k^{d*}r_l^d}_{RR_{kl}} + \frac{1}{2}P(ij)P(ab)\cdot \\ &\underbrace{(\langle kj||cb\rangle + \frac{1}{2}\langle kj||ml\rangle \sigma_{ml}^{cb*} + \frac{1}{2}\langle ed||cb\rangle \sigma_{kj}^{ed*} - \langle jd||lc\rangle \sigma_{kl}^{db*} - \langle kd||lb\rangle \sigma_{lj}^{cd*})}_{Int3_{kjcb}\rightarrow Int3R_{bj}} r_i^{a*}r_k^c \\ &+ \frac{1}{2}P(ab)(\underbrace{\langle ij||km\rangle}_{RL1^*_{jima}}\underbrace{\sigma_{lm}^{db*}}_{RS_{bm}} - P(ij)\underbrace{\langle ic||kb\rangle}_{LR^*_{baci}}\underbrace{\sigma_{lj}^{dc*}}_{RS_{cj}} - \underbrace{\langle lc||dk\rangle}_{RL_{ck}\rightarrow RLR_{ca}}\sigma_{ji}^{bc*} \\ &- 2P(ij)\underbrace{\langle ic||kd\rangle}_{L_{cida}}\underbrace{\sigma_{lj}^{cb*}}_{RS_{djcb}} + 2P(ij)\underbrace{\langle li||mk\rangle}_{R_{kila}}\underbrace{\sigma_{mj}^{db*}}_{L_{ljkb}} + 2\underbrace{\langle lc||bk\rangle}_{RL_{dcbk}\rightarrow RLS2_{ijkb}}\sigma_{ij}^{cd*})r_k^{a*}r_l^d \\ &+ \frac{1}{2}P(ij)(\underbrace{\langle ce||ab\rangle}_{LR1^*_{baei}}\underbrace{\sigma_{kj}^{de*}}_{RS_{ej}} - P(ab)\underbrace{\langle jc||la\rangle}_{RL^*_{jila}}\underbrace{\sigma_{kl}^{db*}}_{RS_{bl}} - \underbrace{\langle kc||dl\rangle}_{RL_{cl}\rightarrow RLR_{il}}\sigma_{jl}^{ba*}\end{aligned}$$

$$
\begin{aligned}
&-2P(ab)\underbrace{\langle kc||la\rangle}_{L_{ljkb}}\underbrace{\sigma_{lj}^{db*}}_{R_{kila}}+2P(ab)\underbrace{\langle ce||ad\rangle}_{L1_{cida}}\underbrace{\sigma_{kj}^{eb*}}_{RS_{djcb}}+2\underbrace{\langle jc||dl\rangle}_{LR_{kljc}\rightarrow LRS2_{abcj}}\sigma_{kl}^{ba*})r_i^{c*}r_k^d\\
&-\frac{1}{2}(P(ij)\underbrace{\langle cj||kd\rangle}_{RL_{dj}^*\rightarrow RLR_{lj}^*}\sigma_{li}^{ba*}+P(ab)\underbrace{\langle cl||kb\rangle}_{RL_{bl}^*\rightarrow RLR_{bd}^*}\sigma_{ij}^{ad*})r_k^{c*}r_l^d+\\
&+(P(ab)P(ij)\langle dj||cb\rangle\underbrace{r_{ki}^{da*}}_{RR_{daci}}+\langle ij||cl\rangle\underbrace{r_{kl}^{ab*}}_{RR_{abcl}}-P(ij)f_{ic}\underbrace{r_{kj}^{ab*}}_{RR_{abcj}})r_k^c\\
&-(P(ab)P(ij)\langle kj||lb\rangle\underbrace{r_{li}^{ca*}}_{RR_{lika}}+\langle kd||ab\rangle\underbrace{r_{ij}^{cd*}}_{RR_{ijkd}}+P(ab)f_{kb}\underbrace{r_{ij}^{ac*}}_{-RR_{ijka}})r_k^c\\
&+(-P(ij)\underbrace{\langle kj||cl\rangle}_{RL_{jl}}r_{il}^{ab*}+P(ab)\underbrace{\langle kd||ca\rangle}_{RL_{da}}r_{ij}^{db*})r_k^c.
\end{aligned}
\tag{4.5.20}
$$

The terms dyed with the same colour are contracted to form the intermediates of the corresponding colour: the red terms are contracted as well as the blue ones; the arrows between two intermediates stand for a contraction of the intermediate on the left with the term of the same colour of the final intermediate. As an example, the following term can be discussed

$$
-\frac{1}{2}(P(ij)\underbrace{\langle cj||kd\rangle}_{RL_{dj}^*\rightarrow RLR_{lj}^*}\sigma_{li}^{ba*})r_k^{c*}r_l^d. \tag{4.5.21}
$$

The integral in red, $\langle cj||kd\rangle$, is contracted with the $\hat{R}$ amplitude in red, r_k^{c*}, to yield the intermediate quantity in red, RL_{dj}^*. This intermediate is contracted with the $\hat{R}$ amplitude in blue, r_l^d to give the intermediate quantity in blue, RLR_{lj}^*. This stepwise contraction scheme allows to keep the scaling of the equations as low as possible.

The terms in eq. 4.5.20 are calculated in the subroutine `ContractionZetaS`. The ζ_μ are obtained by solving the linear system with the solver in `LinSolvS`. With the obtained Lagrange parameters, the excited-state density matrices are computed, which have the same expression as for UCC2 (eq. 4.5.18).

After the calculation of the excited state eigenvectors, response properties are computed with the input keyword `properties=2`. The inhomogeneous part of the $\hat{Z}$-equation, $\frac{\partial}{\partial\sigma_\mu}\langle 0|\hat{R}^\dagger\bar{H}\hat{R}|0\rangle$, is first calculated and provides the initial guess to the solver. For the ground state, the inhomogeneous part is given only by $\frac{\partial}{\partial\sigma_\mu}\langle 0|\bar{H}|0\rangle$. The terms obtained from the differentiation of the amplitude equations are added to the inhomogeneous part of the equation and the ζ_μ-amplitudes converged iteratively. Afterwards the density matrices can be computed and contracted with the dipole integrals to obtain the dipole moments. Flowchart 5 displays this algorithm in QCUMBRE.

4.5.5 Transition dipole moments with UCC2

At first, transitions between two excited states are discussed; the special case of transitions from the ground state are treated at the end of this section. In Flowchart 6, the algorithm for the calculation of transition dipole moments in the case of UCC2 is displayed. The function `SubEOMProp` is called with the keyword `prop=2`, which ensures that response theory is used. Recalling the structure of eq. 3.2.18, two stationarity conditions are needed, determining the $\hat{Z}_{fi}$ and the $\hat{Z}_{if}$ multipliers, respectively. Analogously to the calculation of excited-state dipole moments, the stationarity conditions may be divided into an inhomogeneous and a homogenous part.

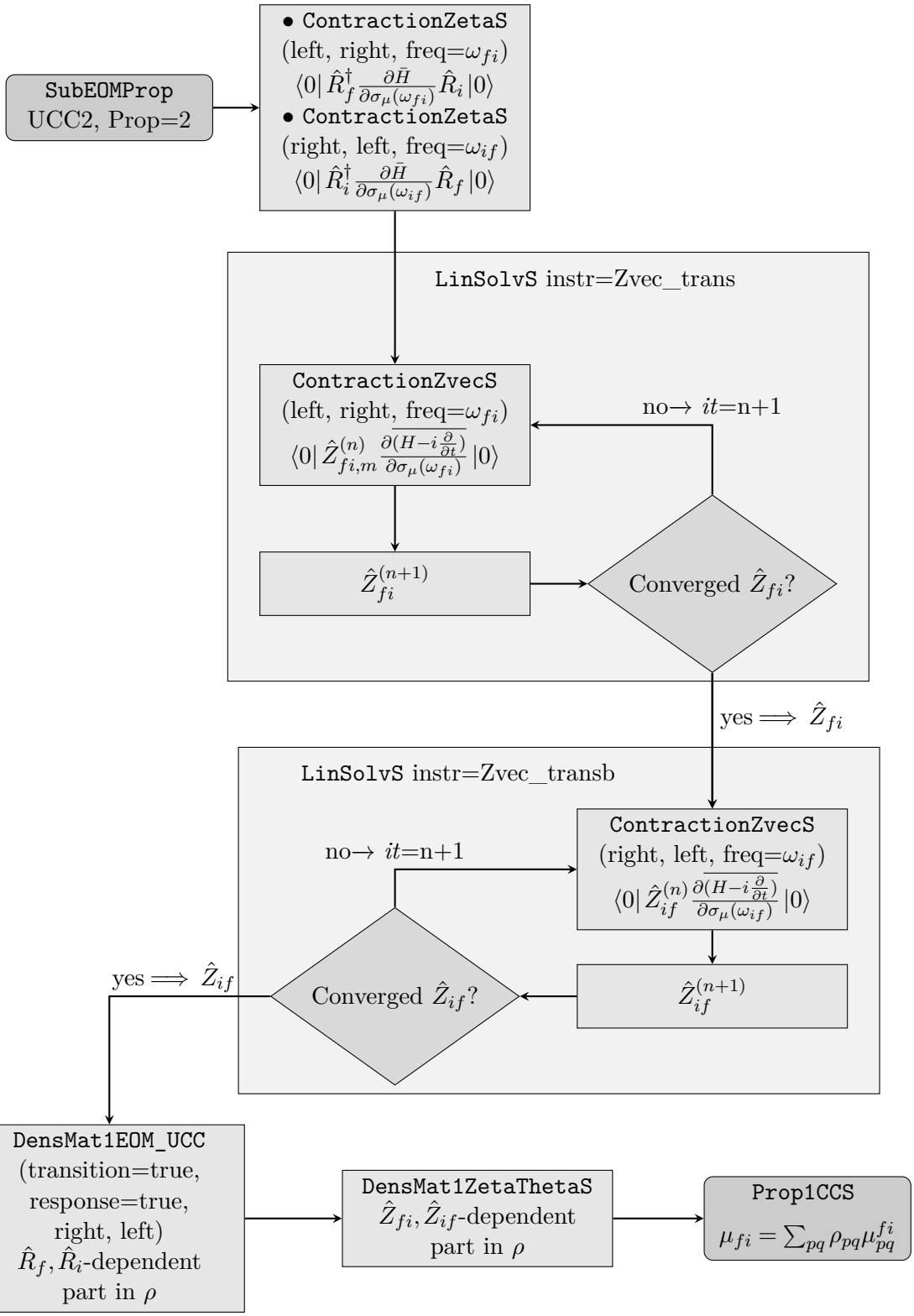

Flowchart 6: Flowchart illustrating how transition dipole moments between two excited states are calculated with UCC2 in Qcumbre.

The inhomogeneous parts $\langle 0|\,\hat{R}_f^\dagger \frac{\partial \bar{H}}{\partial \sigma_\mu(\omega_{fi})}\hat{R}_i\,|0\rangle$ and $\langle 0|\,\hat{R}_i^\dagger \frac{\partial \bar{H}}{\partial \sigma_\mu(\omega_{fi})}\hat{R}_f\,|0\rangle$ are both calculated by the function `ContractionZetaS`, called once with the instruction `left, right, freq=`ω_{fi} and once with the instruction `right, left, freq=`$-\omega_{fi}$, respectively.
It was discussed in sec. 3.2.1 that the stationarity conditions for the UCC2 method are decoupled, i.e. they can be solved separately. In QCUMBRE, first the solver `LinSolvS` is called to calculate $\hat{Z}_{fi}$: the homogenous part of its defining equation is calculated with the function `ContractionZvecS`. After reaching convergence, `LinSolvS` is called once more to solve for the multipliers $\hat{Z}_{if}$, calculating the corresponding homogeneous part exploiting once again `ContractionZvecS`. Having found both sets of Lagrange multipliers, the density matrix of the transition can be computed. The part dependent on the operators $\hat{R}_i$ and $\hat{R}_f$ is computed through the function `DensMat1_UCC`, to which the instructions `transition` and `response` are conveyed. The function `DensMat1ZetaThetaS` adds the density-matrix terms which depend on the Lagrange mulitpliers. Finally, the function `Prop1CCS` contracts the calculated density matrix with the dipole integrals provided by CFOUR. The structure of the algorithm has been explained, in order to give an overview over the implementation of the transition dipole moments in QCUMBRE. A more complete discussion it possible via an analysis of the implemented terms. Therefore, the discussion now becomes more technical and is concerned with the implementation of the discussed equations.

Its time-dependent form, imposed as constraint in the Lagrangian in eq. 3.2.18, is

$$\langle \mu|\, e^{-(\hat{\sigma}-\hat{\sigma}^\dagger)}(\hat{H} - i\frac{\partial}{\partial t})e^{\hat{\sigma}-\hat{\sigma}^\dagger}\,|0\rangle = 0. \tag{4.5.22}$$

The terms which contribute on top of those discussed in the excited-state dipole case, coming from the time-independent Schrödinger equation, are computed by expanding the exponential operators in a Taylor series.

$$\langle \mu|\,\bar{H}\,|0\rangle = i\,\langle \mu|\,[1-(\hat{\sigma}-\hat{\sigma}^\dagger)+\frac{1}{2}(\hat{\sigma}-\hat{\sigma}^\dagger)(\hat{\sigma}-\hat{\sigma}^\dagger)]\frac{\partial}{\partial t}[(\hat{\sigma}-\hat{\sigma}^\dagger)+\frac{1}{2}(\hat{\sigma}-\hat{\sigma}^\dagger)(\hat{\sigma}-\hat{\sigma}^\dagger)]\,|0\rangle\,, \tag{4.5.23}$$

where $\bar{H} = e^{-(\hat{\sigma}-\hat{\sigma}^\dagger)}\hat{H}e^{\hat{\sigma}-\hat{\sigma}^\dagger}$ is the unitarily transformed Hamiltonian, truncated at the UCC2 level of theory.

The single-excitation operator $\hat{\sigma}_1$ is second order in perturbation theory; the double-excitation one $\hat{\sigma}_2$ is first order. Only operator combinations up to second order may contribute in the UCC2 amplitude equation: $\hat{\sigma}_1$, $\hat{\sigma}_1^\dagger$, $\hat{\sigma}_2$, $\hat{\sigma}_2^\dagger$, $\hat{\sigma}_2\hat{\sigma}_2$, $\hat{\sigma}_2^\dagger\hat{\sigma}_2$, $\hat{\sigma}_2\hat{\sigma}_2^\dagger$, $\hat{\sigma}_2^\dagger\hat{\sigma}_2^\dagger$. The only possible contributions are given by $\hat{\sigma}_1$, $\hat{\sigma}_2$, as the remaining combinations cannot match the excitation level of the single- or double-excitation amplitude equations (Φ_1 and Φ_2 are the single- and double-excited projection manifold)

$$\langle \Phi_1|\,\bar{H}\,|0\rangle = i\,\langle \Phi_1|\,\frac{\partial \hat{\sigma}_1}{\partial t}\,|0\rangle \tag{4.5.24}$$

$$\langle \Phi_2|\,\bar{H}\,|0\rangle = i\,\langle \Phi_2|\,\frac{\partial \hat{\sigma}_2}{\partial t}\,|0\rangle\,. \tag{4.5.25}$$

For the UCC2 truncation scheme, the Lagrangian is

$$\begin{aligned}\mathscr{L}_{fi} =& \{\langle 0|\,\hat{R}_f^\dagger e^{-(\hat{\sigma}-\hat{\sigma}^\dagger)}\hat{H}e^{\hat{\sigma}-\hat{\sigma}^\dagger}\hat{R}_i e^{i\omega_{fi}t}\,|0\rangle\}_T - Q_f\{\langle 0|\,\hat{R}_f^\dagger e^{i\omega_{fi}t}\hat{R}_i\,|0\rangle\}_T \\ &+ \{\langle 0|\,\hat{Z}_{fi}(\omega)(\bar{H} - i\frac{\partial \hat{\sigma}}{\partial t})\,|0\rangle\}_T + \{\langle 0|\,(\bar{H} + i\frac{\partial \hat{\sigma}^\dagger}{\partial t})\hat{Z}_{if}^\dagger(\omega)\,|0\rangle\}_T.\end{aligned} \tag{4.5.26}$$

The transition dipole moment can be defined by the partial derivative of the functional in eq. 4.5.26 with respect to the perturbation, at the specific frequency ω_{fi}, corresponding to

the energy difference of the two states (resonance condition)

$$\frac{\partial \mathscr{L}_{fi}}{\partial \varepsilon(\omega_{fi})} = \{\langle 0|\, \hat{R}_f^\dagger \bar{\mu} \hat{R}_i e^{i\omega_{fi}t}\, |0\rangle\}_T + \{\langle 0|\, \hat{Z}_{fi}(\omega_{fi}) \bar{\mu}\, |0\rangle\}_T + \{\langle 0|\, \bar{\mu} \hat{Z}_{if}^\dagger(\omega_{fi})\, |0\rangle\}_T. \tag{4.5.27}$$

Considering a perturbation oscillating with frequency ω_{fi}, $\hat{\mu} \sim e^{-i\omega_{fi}t}$, time averaging selects only the components $\hat{Z}_{fi}(\omega_{fi}) \sim e^{i\omega_{fi}t}$ and $\hat{Z}_{if}^\dagger(\omega_{fi}) \sim e^{i\omega_{fi}t}$, while all other contributions oscillating with a different frequency are averaged out.

Recalling the definition of the $\hat{Z}_{fi}$ and $\hat{Z}_{if}$ amplitudes as in eq. 3.2.19, the stationarity conditions $\frac{\partial \mathscr{L}_{fi}}{\partial \zeta_\mu(\omega_{fi})} = 0$ and $\frac{\partial \mathscr{L}_{fi}}{\partial \theta_\mu(\omega_{fi})} = 0$ return the UCC amplitude equations, which are already satisfied. Stationarity with respect to the amplitudes $\sigma_\mu(\omega_{fi}) \sim e^{-i\omega_{fi}t}$ leads to the determination of the $\zeta_\mu(\omega_{fi})$ coefficients,

$$\begin{aligned}\frac{\partial \mathscr{L}_{fi}}{\partial \sigma_\mu} = &\{\langle 0|\, \hat{R}_f^\dagger \frac{\partial \bar{H}}{\partial \sigma_\mu} \hat{R}_i e^{i\omega_{fi}t}\, |0\rangle\}_T + \{\langle 0|\, \hat{Z}_{fi}(\omega_{fi}) \frac{\partial \bar{H}}{\partial \sigma_\mu}\, |0\rangle\}_T + \{\langle 0|\, \frac{\partial \bar{H}}{\partial \sigma_\mu} \hat{Z}_{if}^\dagger(\omega_{fi})\, |0\rangle\}_T \\ &- i\{\langle 0|\, \hat{Z}_{fi}(\omega_{fi}) \frac{\partial}{\partial \sigma_\mu} \frac{\partial \hat{\sigma}}{\partial t}\, |0\rangle\}_T = 0.\end{aligned} \tag{4.5.28}$$

It can be observed that in the last term, the time averaging selects $\sigma \sim e^{-i\omega_{fi}t}$.
Stationarity with respect to $\sigma_\mu^*(\omega_{fi}) \sim e^{-i\omega_{fi}t}$ leads to equations for the determination of $\theta_\mu(\omega_{fi})$

$$\begin{aligned}\frac{\partial \mathscr{L}_{fi}}{\partial \sigma_\mu^*} = &\{\langle 0|\, \hat{R}_f^\dagger \frac{\partial \bar{H}}{\partial \sigma_\mu^*} \hat{R}_i e^{i\omega_{fi}t}\, |0\rangle\}_T + \{\langle 0|\, \hat{Z}_{fi}(\omega_{fi}) \frac{\partial \bar{H}}{\partial \sigma_\mu^*}\, |0\rangle\}_T + \{\langle 0|\, \frac{\partial \bar{H}}{\partial \sigma_\mu^*} \hat{Z}_{if}^\dagger(\omega_{fi})\, |0\rangle\}_T \\ &+ i\{\langle 0|\, \frac{\partial}{\partial \sigma_\mu^*} \frac{\partial \hat{\sigma}^\dagger}{\partial t} \hat{Z}_{if}^\dagger(\omega_{fi})\, |0\rangle\}_T = 0.\end{aligned} \tag{4.5.29}$$

In the last term, time averaging selects $\sigma^\dagger \sim e^{-i\omega_{fi}t}$.
From this analysis, the stationarity conditions are

$$\begin{aligned}\frac{\partial \mathscr{L}_{fi}}{\partial \sigma_\mu} = &\{\langle 0|\, \hat{R}_f^\dagger \frac{\partial \bar{H}}{\partial \sigma_\mu} \hat{R}_i e^{i\omega_{fi}t}\, |0\rangle\}_T + (\langle 0|\, \hat{Z}_{fi}(\omega_{fi}) \frac{\partial \bar{H}}{\partial \sigma_\mu}\, |0\rangle + \langle 0|\, \frac{\partial \bar{H}}{\partial \sigma_\mu} \hat{Z}_{if}^\dagger(\omega_{fi})\, |0\rangle \\ &- \omega_{fi} \langle 0|\, \hat{Z}_{fi}(\omega_{fi}) \hat{\tau}_\mu\, |0\rangle) = 0,\end{aligned} \tag{4.5.30}$$

$$\begin{aligned}\frac{\partial \mathscr{L}_{fi}}{\partial \sigma_\mu^*} = &\{\langle 0|\, \hat{R}_f^\dagger \frac{\partial \bar{H}}{\partial \sigma_\mu^*} \hat{R}_i e^{i\omega_{fi}t}\, |0\rangle\}_T + (\langle 0|\, \hat{Z}_{fi}(\omega_{fi}) \frac{\partial \bar{H}}{\partial \sigma_\mu^*}\, |0\rangle + \langle 0|\, \frac{\partial \bar{H}}{\partial \sigma_\mu^*} \hat{Z}_{if}^\dagger(\omega_{fi})\, |0\rangle \\ &+ \omega_{fi} \langle 0|\, \hat{\tau}_\mu^\dagger \hat{Z}_{if}^\dagger(\omega_{fi})\, |0\rangle) = 0.\end{aligned} \tag{4.5.31}$$

For a Hermitian theory, eq. 2.8.48 must hold, implying $\frac{\partial \mathscr{L}_{if}}{\partial \sigma_\mu} = (\frac{\partial \mathscr{L}_{fi}}{\partial \sigma_\mu^*})^*$.

$$\begin{aligned}\frac{\partial \mathscr{L}_{if}}{\partial \sigma_\mu} = &\{\langle 0|\, \hat{R}_i^\dagger \frac{\partial \bar{H}}{\partial \sigma_\mu} \hat{R}_f e^{i\omega_{if}t}\, |0\rangle\}_T + (\langle 0|\, \hat{Z}_{if}(\omega_{if}) \frac{\partial \bar{H}}{\partial \sigma_\mu}\, |0\rangle + \langle 0|\, \frac{\partial \bar{H}}{\partial \sigma_\mu} \hat{Z}_{fi}^\dagger(\omega_{if})\, |0\rangle \\ &- \omega_{if} \langle 0|\, \hat{Z}_{if}(\omega_{if}) \hat{\tau}_\mu\, |0\rangle) = 0,\end{aligned} \tag{4.5.32}$$

which is satisfied by the formulation in eq. 4.5.26 of the Lagrange functional.

The stationarity condition in eq. 4.5.30 is divided into a homogeneous and an inhomogeneous part. The inhomogeneous part, consisting of the first term in the first line and the second term in the second line, is calculated in `ContractionZetaS`. The first term is the same as for the excited-state dipole moments, where the $\hat{R}$ operators correspond to the two

different states between which the transition is considered. The solution of eq. 4.5.30 leads to the determination of $\hat{Z}_{fi}$; the DIIS algorithm is used.[260] The initial guess provided for the vector of Lagrange multipliers is the inhomogeneous part of the equation.

Eq. 4.5.31 determines the Lagrange multipliers $\hat{Z}^{\dagger}_{if}$. From a computational point of view, however, it is preferred to calculate the amplitudes of $\hat{Z}_{if}$ via eq. 4.5.32. Therefore, the second set of Lagrange multipliers $\hat{Z}_{if}$ is obtained through the same function as $\hat{Z}_{fi}$, changing the order of the states and the sign of the transition energy in the input. As the two stationarity conditions are decoupled, they are each calculated independently via the solver in `LinSolvS`.
Once the Lagrange multipliers have been determined, the transition dipole moments are computed through the transition densities

$$\begin{aligned}
\rho_{ia} &= \theta^{a*}_{i} + \zeta^{b}_{j}\sigma^{ab}_{ij} - \mathfrak{r}^{b*}_{j}\sigma^{b}_{i}r^{a}_{j} - \mathfrak{r}^{b*}_{j}\sigma^{a}_{j}r^{b}_{i} + \frac{1}{2}\mathfrak{r}^{bc*}_{jk}\sigma^{cb}_{ik}r^{a}_{j} + \frac{1}{2}\mathfrak{r}^{bc*}_{jk}\sigma^{ca}_{jk}r^{b}_{i},\\
\rho_{ai} &= \zeta^{a}_{i} + \theta^{b*}_{j}\sigma^{ab*}_{ij} - \mathfrak{r}^{b}_{j}\sigma^{b*}_{i}r^{a*}_{j} - \mathfrak{r}^{b}_{j}\sigma^{a*}_{j}r^{b*}_{i} + \frac{1}{2}\mathfrak{r}^{bc}_{jk}\sigma^{cb*}_{ik}r^{a*}_{j} + \frac{1}{2}\mathfrak{r}^{bc}_{jk}\sigma^{ca*}_{jk}r^{b*}_{i},\\
\rho_{ij} &= -\zeta^{a}_{i}\sigma^{a}_{j} - \theta^{a*}_{j}\sigma^{a*}_{i} - \frac{1}{2}\zeta^{ab}_{kj}\sigma^{ab}_{ki} - \frac{1}{2}\theta^{ab*}_{ki}\sigma^{ab*}_{kj} - \mathfrak{r}^{a*}_{j}r^{a}_{i} - \frac{1}{2}\mathfrak{r}^{ab*}_{kj}r^{ab}_{ki},\\
\rho_{ab} &= \zeta^{a}_{i}\sigma^{b}_{i} + \theta^{b*}_{i}\sigma^{a*}_{i} + \frac{1}{2}\zeta^{ca}_{ij}\sigma^{cb}_{ij} + \frac{1}{2}\theta^{cb*}_{ij}\sigma^{ca*}_{ij} + \mathfrak{r}^{a*}_{i}r^{b}_{j} + \frac{1}{2}\mathfrak{r}^{ac*}_{ij}r^{bc}_{ij}.
\end{aligned} \tag{4.5.33}$$

The character $\mathfrak{r}$ is employed for the excitation amplitudes of the left state. These expressions are calculated in `DensMat1EOM_UCC`, where the option `transition=true` allows to consider two different states as left and right states in the transition.

4.5.6 Transition dipole moments with UCC3

It was discussed in sec. 3.2.1 that the stationarity conditions coming from the Lagrangian for the computation of transition dipole moments in the UCC3 approximation are coupled, while they are not coupled in the UCC2 framework. Therefore, the calculation of UCC3 transition dipole moments follows a different scheme, shown in Flowchart 7. The inhomogeneous parts of the stationarity conditions are calculated through two calls of the function `ContractionZetaS`, one for the $\Psi_i \rightarrow \Psi_f$ transition and one for the $\Psi_f \rightarrow \Psi_i$ one. The iterative solution of the equations for $\hat{Z}_{fi}$ and $\hat{Z}_{if}$ is complicated by the fact that the equations are coupled. The algorithm for the calculation of UCC3 transition moments consists of a complicated loop structure: the first loop contains in each macroiteration another loop structure, consisting of microiterations. This algorithm is visualised in Flowchart 7:

1. the inhomogeneous parts are calculated as before in `ContractionZetaS`;

2. in each macroiteration m, `LinSolvS` is called to determine $\hat{Z}^{(n+1)}_{fi,m}$, in function of $\hat{Z}^{(n)}_{fi,m}$ and $\hat{Z}^{(n)}_{if,m}$ (`instr=Zvec_trans`). The stationarity equation is the sum of the inhomogenous part and of the homogeneous one, the latter calculated with `ContractionZvecS`, with a transition frequency ω_{fi};

3. in the same macroiteration m, `LinSolvS` is called to determine $\hat{Z}^{(n+1)}_{if,m}$, in function of the newly computed $\hat{Z}_{fi,m+1}$ and $\hat{Z}^{(n)}_{if,m}$ (`instr=Zvec_transb`). The homogeneous part of the stationarity condition is provided by `ContractionZvecS`, where the order of the states is reverted and the transition frequency set to ω_{if}.

4. at the end of the macroiteration, the differences $\left|\hat{Z}_{fi,m+1} - \hat{Z}_{fi,m}\right|$ and $\left|\hat{Z}_{if,m+1} - \hat{Z}_{if,m}\right|$ are calculated; if at least one of the two parameters $\hat{Z}_{fi}$ and $\hat{Z}_{if}$ is not converged, the algorithm proceeds to the next macroiteration.

The computation of the density-matrix elements needed for the transition dipole moments is performed with the same procedure described before for UCC2. The part of the density matrix dependent on $\hat{R}_i$ and $\hat{R}_f$ is calculated via the function `DensMat1EOM_UCC`, while the part of the density matrices depending on the Lagrange multipliers is calculated by `DensMat1ZetaThetaS`. The function `Prop1CCS` contracts the density matrix with the dipole integrals provided by the CFOUR calculation.

The discussed overview is needed to give a general understanding of the challenges of the UCC implementation. The full details of the implemented equations is presented hereafter, focusing on the particular challenges this approximation order brings to the computation

$$\begin{aligned}
\langle\mu|\,\bar{H}\,|0\rangle = i\,\langle\mu|\,[1 - (\hat{\sigma} - \hat{\sigma}^\dagger) + \frac{1}{2}(\hat{\sigma} - \hat{\sigma}^\dagger)(\hat{\sigma} - \hat{\sigma}^\dagger) - \frac{1}{6}(\hat{\sigma} - \hat{\sigma}^\dagger)(\hat{\sigma} - \hat{\sigma}^\dagger)(\hat{\sigma} - \hat{\sigma}^\dagger)] \\
\frac{\partial}{\partial t}[(\hat{\sigma} - \hat{\sigma}^\dagger) + \frac{1}{2}(\hat{\sigma} - \hat{\sigma}^\dagger)(\hat{\sigma} - \hat{\sigma}^\dagger) + \frac{1}{6}(\hat{\sigma} - \hat{\sigma}^\dagger)(\hat{\sigma} - \hat{\sigma}^\dagger)(\hat{\sigma} - \hat{\sigma}^\dagger)]\,|0\rangle \\
= i\,\langle\mu|\,(\dot{\sigma} - \dot{\sigma}^\dagger) - \frac{1}{2}(\hat{\sigma} - \hat{\sigma}^\dagger)(\dot{\sigma} - \dot{\sigma}^\dagger) + \frac{1}{2}(\dot{\sigma} - \dot{\sigma}^\dagger)(\hat{\sigma} - \hat{\sigma}^\dagger) + \frac{1}{6}(\dot{\sigma} - \dot{\sigma}^\dagger)(\hat{\sigma} - \hat{\sigma}^\dagger)(\hat{\sigma} - \hat{\sigma}^\dagger) \\
- \frac{1}{3}(\hat{\sigma} - \hat{\sigma}^\dagger)(\dot{\sigma} - \dot{\sigma}^\dagger)(\hat{\sigma} - \hat{\sigma}^\dagger) + \frac{1}{6}(\hat{\sigma} - \hat{\sigma}^\dagger)(\hat{\sigma} - \hat{\sigma}^\dagger)(\dot{\sigma} - \dot{\sigma}^\dagger)\,|0\rangle\,,
\end{aligned} \tag{4.5.34}$$

where $\bar{H}$ is the transformed Hamiltonian truncated following the UCC3 scheme. Operator combinations up to third order are $\hat{\sigma}_1$, $\hat{\sigma}_2$, $\hat{\sigma}_1\hat{\sigma}_2$, $\hat{\sigma}_2\hat{\sigma}_2\hat{\sigma}_2$ and all combination of their adjoint operators.

$$\begin{aligned}
\langle\Phi_1|\,\bar{H}\,|0\rangle = & i\,\langle\Phi_1|\,\dot{\sigma}_1\,|0\rangle + \frac{i}{2}\,\langle\Phi_1|\,-\dot{\sigma}_1^\dagger(\omega_{fi})\hat{\sigma}_2(0) + \hat{\sigma}_1^\dagger(0)\dot{\sigma}_2(\omega_{fi})\,|0\rangle = \\
& \omega_{fi}\,\langle\Phi_1|\,\hat{\sigma}_1\,|0\rangle + \frac{\omega_{fi}}{2}\,\langle\Phi_1|\,\hat{\sigma}_1^\dagger(0)\hat{\sigma}_2(\omega_{fi}) - \hat{\sigma}_1^\dagger(\omega_{fi})\hat{\sigma}_2(0)\,|0\rangle
\end{aligned} \tag{4.5.35}$$

For the projection on a doubly-excited determinant, the only two combinations up to third-order are $\sigma_2^\dagger\sigma_2\sigma_2$ and $\sigma_2\sigma_2^\dagger\sigma_2$

$$\begin{aligned}
\langle\Phi_2|\,\bar{H}\,|0\rangle = & i\,\langle\Phi_2|\,\dot{\sigma}_2\,|0\rangle - i\,\langle\Phi_2|\,\frac{1}{6}\dot{\sigma}_2^\dagger\hat{\sigma}_2\hat{\sigma}_2 - \frac{1}{3}\hat{\sigma}_2^\dagger\dot{\sigma}_2\hat{\sigma}_2 + \frac{1}{6}\hat{\sigma}_2^\dagger\hat{\sigma}_2\dot{\sigma}_2\,|0\rangle \\
& - i\,\langle\Phi_2|\,\frac{1}{6}\dot{\sigma}_2\hat{\sigma}_2^\dagger\hat{\sigma}_2 - \frac{1}{3}\hat{\sigma}_2\dot{\sigma}_2^\dagger\hat{\sigma}_2 + \frac{1}{6}\hat{\sigma}_2\hat{\sigma}_2^\dagger\dot{\sigma}_2\,|0\rangle\,.
\end{aligned} \tag{4.5.36}$$

The amplitudes can be expressed through their Fourier expansion

$$\sigma = \sum_k \sigma(\omega_k)e^{-i\omega_k t} \qquad \sigma^* = \sum_k \sigma(\omega_k)^* e^{i\omega_k t} \tag{4.5.37}$$

$$\hat{\sigma}\hat{\sigma}^\dagger = \sum_{kl} \hat{\sigma}(\omega_k)\hat{\sigma}^\dagger(\omega_l)e^{-i(\omega_k - \omega_l)t}. \tag{4.5.38}$$

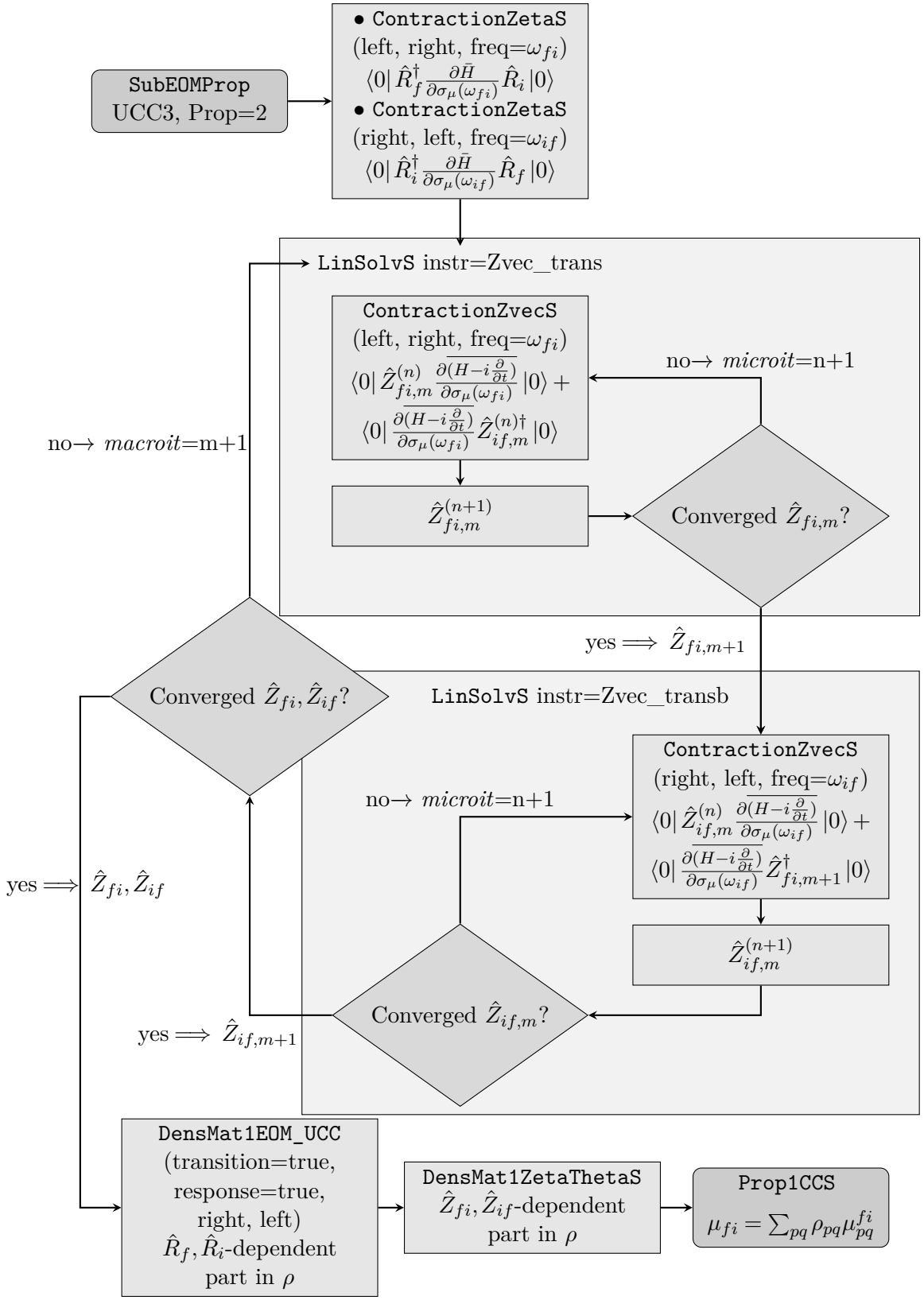

Flowchart 7: Flowchart illustrating how transition dipole moments between two excited states are calculated with UCC3 in QCUMBRE.

Considering that differentiation is performed with respect to $\sigma_\mu(\omega_{fi})$, the only relevant terms are

$$\begin{aligned}
&\langle\Phi_2|\,\bar{H}\,|0\rangle = i\,\langle\Phi_2|\,\dot{\sigma}_2\,|0\rangle - i\,\langle\Phi_2|\,\frac{1}{6}\dot{\hat{\sigma}}_2^\dagger\hat{\sigma}_2\hat{\sigma}_2 - \frac{1}{3}\hat{\sigma}_2^\dagger\dot{\hat{\sigma}}_2\hat{\sigma}_2 + \frac{1}{6}\hat{\sigma}_2^\dagger\hat{\sigma}_2\dot{\hat{\sigma}}_2\,|0\rangle \\
&- i\,\langle\Phi_2|\,\frac{1}{6}\dot{\hat{\sigma}}_2\hat{\sigma}_2^\dagger\hat{\sigma}_2 - \frac{1}{3}\hat{\sigma}_2\dot{\hat{\sigma}}_2^\dagger\hat{\sigma}_2 + \frac{1}{6}\hat{\sigma}_2\hat{\sigma}_2^\dagger\dot{\hat{\sigma}}_2\,|0\rangle = \\
&= \omega_{fi}\,\langle\Phi_2|\,\hat{\sigma}_2(\omega_{fi}) - \frac{1}{6}\hat{\sigma}_2(\omega_{fi})\hat{\sigma}_2^\dagger(0)\hat{\sigma}_2(0) + \frac{1}{3}\hat{\sigma}_2(0)\hat{\sigma}_2^\dagger(\omega_{fi})\hat{\sigma}_2(0) - \frac{1}{6}\hat{\sigma}_2(0)\hat{\sigma}_2^\dagger(0)\hat{\sigma}_2(\omega_{fi}) \\
&- \frac{1}{6}\hat{\sigma}_2(\omega_{fi})\hat{\sigma}_2^\dagger(0)\hat{\sigma}_2(0) + \frac{1}{3}\hat{\sigma}_2(0)\hat{\sigma}_2^\dagger(\omega_{fi})\hat{\sigma}_2(0) - \frac{1}{6}\hat{\sigma}_2(0)\hat{\sigma}_2^\dagger(0)\hat{\sigma}_2(\omega_{fi})\,|0\rangle\,.
\end{aligned} \tag{4.5.39}$$

The terms entering the stationarity condition may be listed here

$$\begin{aligned}
\frac{\partial\mathscr{L}_{fi}}{\partial\sigma_1(\omega_{fi})} &\to -\omega_{fi}\,\langle 0|\,\hat{Z}_{fi}\hat{\tau}_1\,|0\rangle + \frac{\omega_{if}}{2}\,\langle 0|\,\hat{\sigma}_2^\dagger\hat{\tau}_1\hat{Z}_{if}^\dagger\,|0\rangle \\
\frac{\partial\mathscr{L}_{fi}}{\partial\sigma_2(\omega_{fi})} &\to -\omega_{fi}\,\langle 0|\,\hat{Z}_{fi}\hat{\tau}_2\,|0\rangle + \frac{\omega_{fi}}{2}\,\langle 0|\,\hat{Z}_{fi}(-\hat{\sigma}_1^\dagger\hat{\tau}_2)\,|0\rangle \\
&\quad + \omega_{fi}\,\langle 0|\,\hat{Z}_{fi}(\frac{1}{6}\hat{\tau}_2\hat{\sigma}_2^\dagger\hat{\sigma}_2 - \frac{1}{3}\hat{\sigma}_2^\dagger\hat{\tau}_2\hat{\sigma}_2 + \frac{1}{6}(\hat{\sigma}_2^\dagger\hat{\sigma}_2\hat{\tau}_2 + \hat{\sigma}_2\hat{\sigma}_2^\dagger\hat{\tau}_2))\,|0\rangle \\
&\quad + \omega_{if}\,\langle 0|\,(-\frac{1}{3}\hat{\sigma}_2^\dagger\hat{\tau}_2\hat{\sigma}_2^\dagger + \frac{1}{6}\hat{\sigma}_2^\dagger\hat{\sigma}_2^\dagger\hat{\tau}_2)\hat{Z}_{if}^\dagger\,|0\rangle\,,
\end{aligned} \tag{4.5.40}$$

which written out explicitely are

$$\begin{aligned}
&\frac{\partial\mathscr{L}_{fi}}{\partial\sigma_1(\omega_{fi})} \to -\omega_{fi}\zeta_i^a + \frac{\omega_{if}}{2}\sigma_{ij}^{ab*}\theta_j^{b*} \\
&\frac{\partial\mathscr{L}_{fi}}{\partial\sigma_2(\omega_{fi})} \to -\omega_{fi}\zeta_{ij}^{ab} - \frac{\omega_{fi}}{2}P(ij)P(ab)\zeta_i^a\sigma_j^b \\
&-\omega_{fi}\Big\{\frac{1}{6}\Big(-\frac{1}{2}P(ab)\underbrace{\sigma_{kl}^{cd}\sigma_{kl}^{ad*}}_{Z_{ac}}\zeta_{ij}^{cb} - \frac{1}{2}P(ij)\underbrace{\sigma_{kl}^{cd}\sigma_{il}^{cd*}}_{Z_{ik}}\zeta_{kj}^{ab} - \frac{1}{2}P(ab)\underbrace{\sigma_{kl}^{cd}\zeta_{kl}^{ad}}_{LS_{ac}}\sigma_{ij}^{cb*} \\
&-\frac{1}{2}P(ij)\underbrace{\sigma_{kl}^{cd}\zeta_{il}^{cd}}_{LS_{ik}}\sigma_{kj}^{ab*} + P(ij)P(ab)\underbrace{\sigma_{kl}^{cd}\sigma_{ik}^{ac*}}_{Z_{ladi}}\zeta_{jl}^{bd} + \frac{1}{4}\sigma_{kl}^{ab*}\underbrace{\sigma_{kl}^{cd}\zeta_{ij}^{cd}}_{LS_{ijkl}} + \frac{1}{4}\underbrace{\sigma_{ij}^{cd*}\sigma_{kl}^{cd}}_{Z_{ijkl}}\zeta_{kl}^{ab}\Big)\Big\} \\
&+\omega_{if}\Big\{\frac{1}{6}\Big(-\frac{1}{2}P(ij)\sigma_{ik}^{ab*}\underbrace{\sigma_{jl}^{cd*}\theta_{kl}^{cd*}}_{xLS_{kj}^*} - \frac{1}{2}P(ab)\sigma_{ij}^{ac*}\underbrace{\sigma_{kl}^{bd*}\theta_{kl}^{cd*}}_{xLS_{cb}^*} + P(ij)P(ab)\sigma_{il}^{ad*}\underbrace{\sigma_{jk}^{bc*}\theta_{kl}^{cd*}}_{xLS_{lbdj}^*} \\
&+\frac{1}{4}\sigma_{kl}^{ab*}\underbrace{\theta_{kl}^{cd*}\sigma_{ij}^{cd*}}_{xLS_{klij}^*}\Big)\Big\}.
\end{aligned} \tag{4.5.41}$$

As a final comment on the discussion on transition dipole moments, it has to be noted that in the literature the transition moments are obtained from the calculation of residues of the response functions.[37] However, this study has not dealt with the formulation of a response function for UCC properties. From preliminary considerations it is very likely that the poles do not correspond to the excitation energies (as is the case for the CC response function). This chapter will refrain from further discussions on the pole structure of the UCC response function, as these go beyond the aims of the present investigation.

4.5.7 Transitions from the ground state with UCC

The discussed implementation applies to transitions between two excited states. Transitions from and to the ground state are described by the modified Lagrange functionals in eq. 3.2.24-3.2.23. Here, the case $\hat{R}_f = 1$ is discussed, as the opposite transition is obtained by the adjoint Lagrangian.

The first term, $\langle 0| e^{-(\hat{\sigma}-\hat{\sigma}^\dagger)} \hat{H} e^{\hat{\sigma}-\hat{\sigma}^\dagger} \hat{R}_i |0\rangle$ has the same form as $\langle 0| e^{-(\hat{\sigma}-\hat{\sigma}^\dagger)} \hat{H} e^{\hat{\sigma}-\hat{\sigma}^\dagger} \hat{Z}^\dagger |0\rangle$, which was discussed as a constraint in the previous sections. Differentiation with respect to $\hat{\sigma}$ and $\hat{\sigma}^\dagger$ gives the same terms as for the adjoint of the amplitude equation, with the replacement of the θ-amplitudes with the r-amplitudes. Their computation is performed in `ContractionZetaS`, where `gs_left=true` identifies the case $\hat{R}_f = 1$ and `gs_right=true` the case $\hat{R}_i = 1$. Only one constraint is needed here, which is calculated in `ContractionZvecS` with `instr=Zvec_trans`. The Lagrange multipliers are calculated via an iterative procedure in `LinSolvS`.

The transition density matrix elements are calculated by means of the partial differentiation of the Lagrangian

$$\begin{aligned}
\rho_{ia} &= r_i^a + \zeta_j^b \sigma_{ij}^{ab} \\
\rho_{ai} &= r_j^b \sigma_{ij}^{ab*} + \zeta_i^{a*} \\
\rho_{ij} &= -r_i^a \sigma_j^{a*} - \frac{1}{2} r_{kj}^{ab} \sigma_{ki}^{ab*} - \frac{1}{2} \zeta_{ki}^{ab} \sigma_{kj}^{ab} - \zeta_j^a \sigma_i^a \\
\rho_{ab} &= r_i^b \sigma_i^{a*} + \frac{1}{2} r_{ij}^{cb} \sigma_{ij}^{ca*} + \frac{1}{2} \zeta_{ij}^{ca} \sigma_{ij}^{cb} + \zeta_i^a \sigma_i^b .
\end{aligned} \tag{4.5.42}$$

The transition density matrix for transitions from the ground state is calculated in `DensMat1EOM_UCC`, where `gs_left=true` specifies this particular case.

4.5.8 Expectation-value properties

In QCUMBRE, the possibility of calculating properties without the response of the amplitudes is also available, by choosing, in the input file, the keyword `properties=1`. For UCC there are different options for the calculation of properties without the response of amplitudes. From eq. 3.2.2, single-state dipole moments are defined as

$$\mu_I = \frac{\partial}{\partial \varepsilon} \langle 0| \hat{R}_I^\dagger e^{-(\hat{\sigma}-\hat{\sigma}^\dagger)} \hat{H} e^{\hat{\sigma}-\hat{\sigma}^\dagger} \hat{R}_I |0\rangle = \langle 0| \hat{R}_I^\dagger e^{-(\hat{\sigma}-\hat{\sigma}^\dagger)} \hat{\mu} e^{\hat{\sigma}-\hat{\sigma}^\dagger} \hat{R}_I |0\rangle . \tag{4.5.43}$$

In this expression, the only operator explicitly dependent on the electric field is the Hamilton operator, which differentiated corresponds to the dipole operator $\frac{\partial \hat{H}}{\partial \varepsilon} = -\hat{\mu}$. The Bernoulli expansion of the energy expression is based on the cancellation of commutators through substitution of the amplitude equation into the BCH expansion. The partial differentiation of the energy expression with respect to the electric field therefore leads to a Bernoulli expansion of the dipole operator. On the other hand, starting from the expectation value of the dipole operator, no amplitude equation is given for this operator and the BCH expansion can be maintained.[59] The two formalisms are equivalent in the limit of the full expansion, but differ when truncated.

In this thesis, when comparing to the expectation-value approach, the first choice of having a Bernoulli expansion of the properties operator has been made. This choice is motivated by the fact that the expression of the density matrices should be consistent with the energy formulation, as the density matrices are obtained through differentiation from the energy expression.

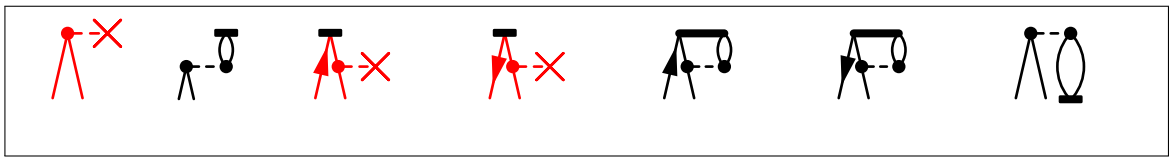

Diagrams 10: Diagrams of the terms arising from the differentiation $\frac{\partial \mathscr{L}}{\partial \sigma_i^a}$ in the Λ-equations. The thicker line represents the Lagrange multipliers. These terms are the same for the excited-state properties, where the Lagrangian multiplier was named $\hat{Z}$. These diagrams also describe the differentiation of the constraints for the transition dipole moments; in this case the thick line on the bottom is $\hat{Z}_{if}^{\dagger}$, while the thick line on the top represents $\hat{Z}_{fi}$. The red diagrams are those contributing to the UCC2 approximation, while all diagrams are needed in the UCC3 method.

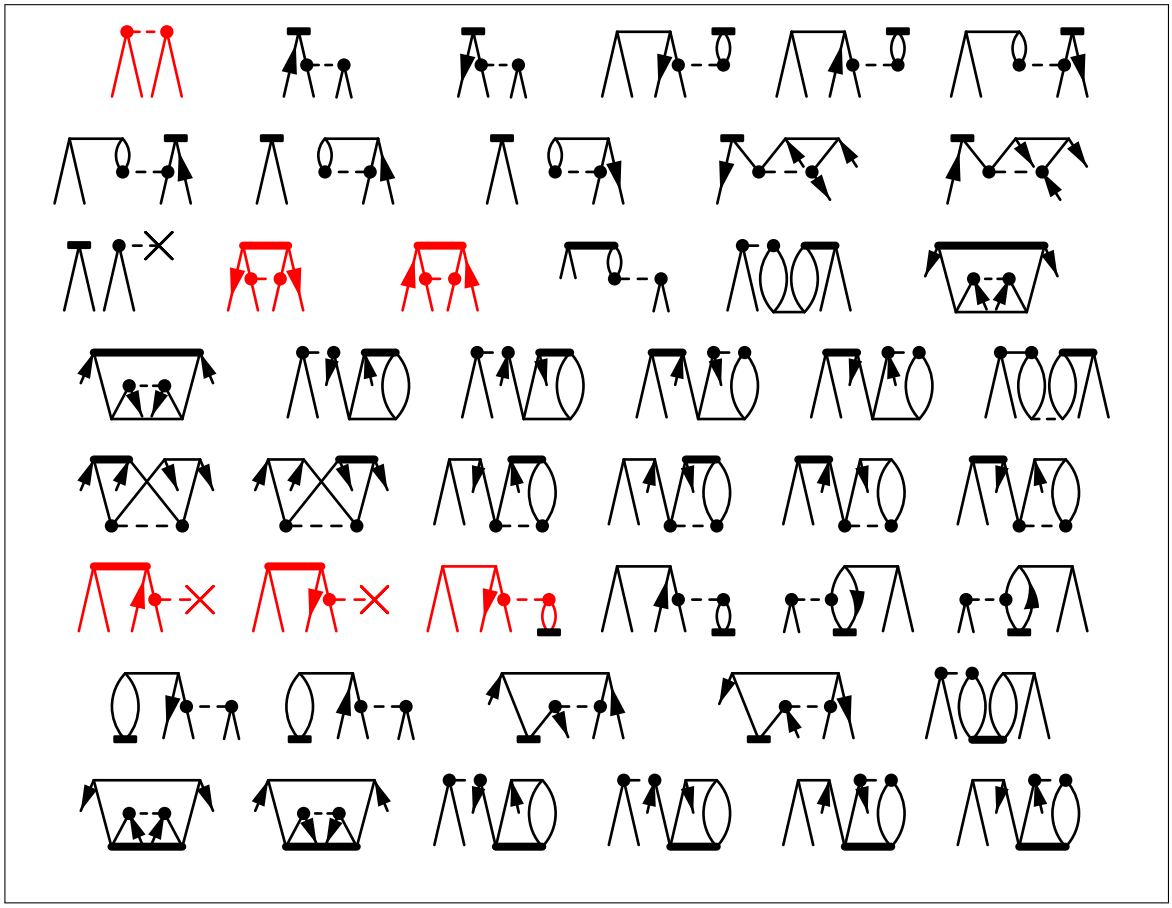

Diagrams 11: Diagrams of the terms arising from the differentiation $\frac{\partial \mathscr{L}}{\partial \sigma_{ij}^{ab}}$ in the Λ-equations. The thicker line represents the Lagrange multipliers $\hat{\Lambda}$. These terms are the same for the excited-state properties, where the Lagrangian multiplier was named $\hat{Z}$. These diagrams also describe the differentiation of the constraints for the transition dipole moments; in this case the thick line on the bottom is $\hat{Z}_{if}^{\dagger}$, while the thick line on the top represents $\hat{Z}_{fi}$. The red diagrams are those contributing to the UCC2 approximation, while all diagrams are needed in the UCC3 method.

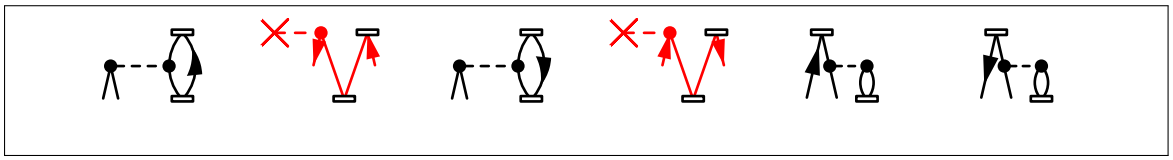

Diagrams 12: Diagrams depicting the terms arising from the differentiation of the inhomogeneous frequency-independent term with respect to the single-excitation amplitudes: $\frac{\partial \langle 0|\hat{R}_I^\dagger \bar{H} \hat{R}_I|0\rangle}{\partial \bar{\sigma}_i^a}$. The double lines represent the EOM-UCC eigenvectors $\hat{R}$; in the case of transition dipole moments, the double lines on top represent $\hat{R}_f$ and those on the bottom $\hat{R}_i$. The red diagrams are the only ones needed in the UCC2 approximation; all diagrams are needed for the correct response treatment in the UCC3 framework.

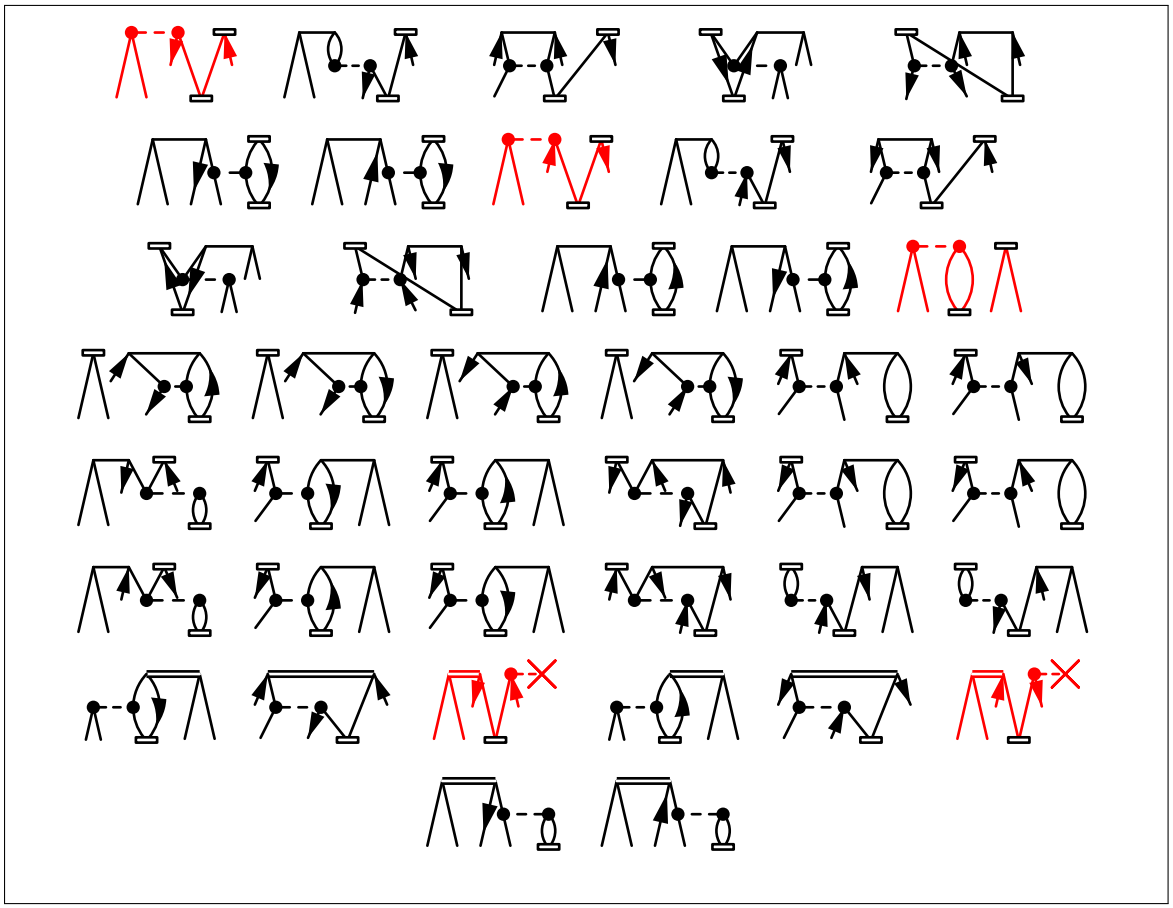

Diagrams 13: Diagrams depicting the terms arising from the differentiation of the inhomogeneous frequency-independent term with respect to the single-excitation amplitudes: $\frac{\partial \langle 0|\hat{R}_I^\dagger \bar{H} \hat{R}_I|0\rangle}{\partial \bar{\sigma}_{ij}^{ab}}$. The double lines represent the EOM-UCC eigenvectors $\hat{R}$; in the case of transition dipole moments, the double lines on top represent $\hat{R}_f$ and those on the bottom $\hat{R}_i$. The red diagrams are the only ones needed in the UCC2 approximation; all diragrams are needed for the correct response treatment in the UCC3 framework.

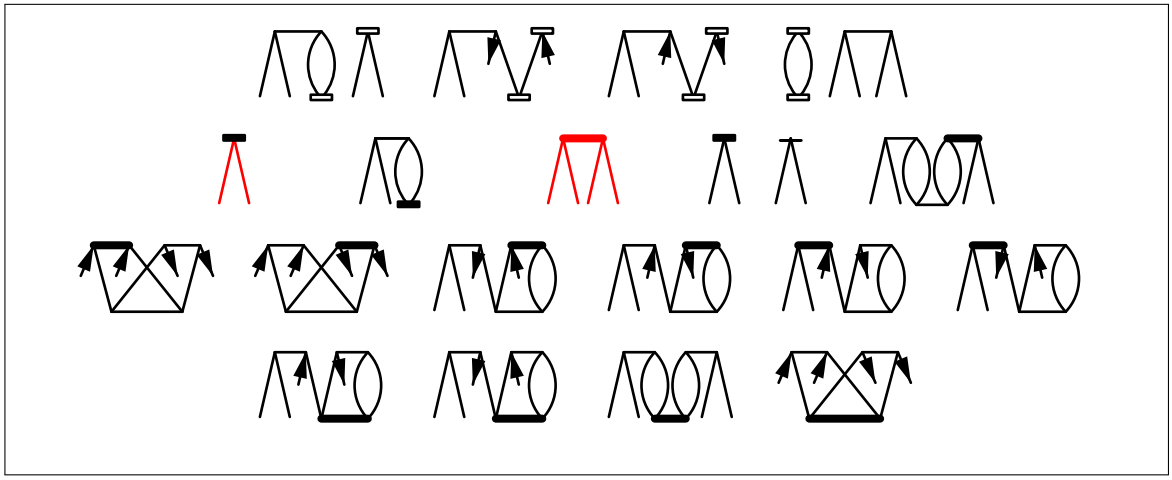

Diagrams 14: Diagrams describing the frequency-dependent terms, necessary in the time-dependent framework for the correct treatment of transition dipole moments. The first row collects the additional terms to the inhomogeneous part, the other rows show the additional terms to the differentiation of the constraints.

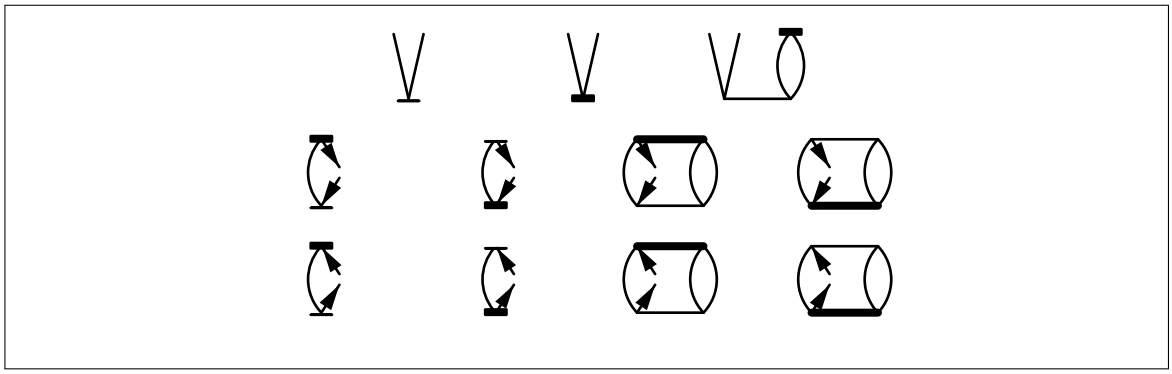

Diagrams 15: Diagrams illustrating the one-electron ground-state density matrix, in the UCC framework. These are the same for UCC2 and UCC3. The thicker line represents the $\hat{\Lambda}$-amplitudes.

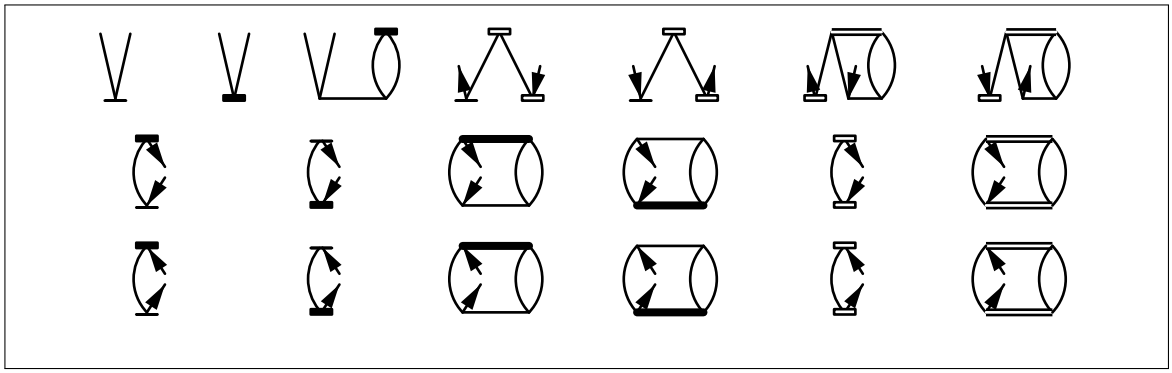

Diagrams 16: Diagrams illustrating the one-electron excited-state density matrix, in the UCC framework. These are the same for UCC2 and UCC3. The thicker line represents the $\hat{Z}$-amplitudes, while the double lines symbolize the EOM-UCC eigenvectors. In the case of transition density matrices, the same diagrams may be drawn, with the exception of the first one in the first line.

With the chosen truncation scheme, the density matrices for the expectation-value approach neglect the terms coming from the response of the amplitudes to the perturbation. These density matrices are obtained by skipping the routines adding the constraints to the Lagrange functionals. The density matrices are directly calculated in `DensMat1`, through the various routines described for the single-state and transition properties. The properties are computed by contracting the one-electron density matrix with the dipole integrals passed from the CFOUR calculation.

Note that in the following discussion, the expectation-value approach will often be referred to as *EOM approach*. This is based on a notation established in the literature.[60–63,114]

4.5.9 Validation of implementation of molecular properties

The implementation of ground-state dipole moments has been validated by comparing results of the Lagrange-functional approach to the results obtained by performing the differentiation of the energy via the calculation of finite differences

$$\frac{\mathrm{d}E}{\mathrm{d}\varepsilon} = \lim_{\varepsilon_1 - \varepsilon_2 \to 0} \frac{E(\varepsilon_1) - E(\varepsilon_2)}{\varepsilon_1 - \varepsilon_2}. \tag{4.5.44}$$

The possibility of switching on an electric field after the SCF calculation has been implemented in QCUMBRE. This option is specified in the input through the keyword `electric-field-strength`, where the three Cartesian components in atomic units may be entered (being used only for debugging, this keyword is only implemented for calculations not exploiting symmetry). The electric field contribution $-\hat{\mu}\cdot\varepsilon$ is added to the Fock operator after the HF calculation; the properties are therefore unrelaxed, meaning that the relaxation of the HF orbitals with respect to the perturbation is neglected. The differentiation of the energy through finite differences could be applied to the validation of the excited-state dipole moments results. The routine `ContractionZvecS`, which calculates the terms coming from the differentiation of the amplitude equations, has the same expressions as `ContractionS`, involved in the calculation of the ground state. Ensuring that the ground state dipole moment is the same using the function `SubCCProp` and the function `SubEOMProp`, the correctness of the implementation of the inhomogeneous part is proven.

The transition dipole moments cannot be obtained differentiating an observable quantity; thus, a different method for debugging was chosen. As seen in section 2.8.1, dipole moments may equivalently be computed through the perturbed amplitudes $\frac{\partial \sigma_\mu}{\partial \varepsilon}$ and $\frac{\partial \sigma_\mu^*}{\partial \varepsilon}$. The possibility of calculating transition dipole moments via perturbed amplitudes has therefore been implemented in QCUMBRE, though only for debugging reasons; the logic behind it is briefly explained here.

The perturbed amplitudes $\frac{\partial \sigma_\mu}{\partial \varepsilon}$ are determined through equations obtained by differentiating the amplitude equations. They are calculated in `ContractionAmplDeriv`, by using the solver `LinSolvS`, where the three possible orientations of the electric field are specified through the instructions `instr=en_deriv_x`, `instr=en_deriv_y`, `instr=en_deriv_z`. The guess vectors for the perturbed amplitudes are constructed from the part of the amplitude equation independent from the perturbed amplitudes, that is

$$\begin{aligned} \left(\frac{\partial \sigma_i^a}{\partial \varepsilon}\right)_{\text{guess}} &= \mu_{ai} + \mu_{ab}\sigma_i^b - \mu_{ji}\sigma_j^a + \mu_{jb}\sigma_{ij}^{ab} \\ \left(\frac{\partial \sigma_{ij}^{ab}}{\partial \varepsilon}\right)_{\text{guess}} &= P(ab)\mu_{ac}\sigma_{ij}^{cb} - P(ij)\mu_{ki}\sigma_{kj}^{ab}. \end{aligned} \tag{4.5.45}$$

The guess vectors are provided by the function `guess_amp_deriv` in QCUMBRE. The correct implementation of the perturbed amplitude equations has been tested debugging the

calculation of ground-state dipole moments by means of perturbed amplitudes against the calculation of ground-state dipole moments by means of the Lagrange functional approach.

For the inhomogeneous part, the expressions for the calculation of excited-state dipole moments via perturbed amplitudes have also been implemented. The routine `DerivedHamiltonianIntermediates` computes the perturbed Hamiltonian matrix elements $\frac{\mathrm{d}\bar{H}_{ij}}{\mathrm{d}\varepsilon}$, $\frac{\mathrm{d}\bar{H}_{ab}}{\mathrm{d}\varepsilon}$, $\frac{\mathrm{d}\bar{H}_{iabj}}{\mathrm{d}\varepsilon}$, $\frac{\mathrm{d}\bar{H}_{ijka}}{\mathrm{d}\varepsilon}$, $\frac{\mathrm{d}\bar{H}_{abci}}{\mathrm{d}\varepsilon}$, $\frac{\mathrm{d}\bar{H}_{ai}}{\mathrm{d}\varepsilon}$, $\frac{\mathrm{d}\bar{H}_{abij}}{\mathrm{d}\varepsilon}$. These are passed to the routine `DerivedEOMS`, where the expression $\frac{\partial\bar{H}}{\partial\varepsilon}\hat{R}\,|0\rangle$ is computed. This part can then be contracted with the adjoint state in order to obtain $\langle 0|\,\hat{R}^{\dagger}\frac{\partial\bar{H}}{\partial\varepsilon}\hat{R}\,|0\rangle$.

By means of these steps, the algorithm calculating dipole moments via the perturbed amplitudes has been debugged against the algorithm calculating dipole moments via the Lagrangian approach. It is a preliminary necessary step, in order to have a trustworthy method for the validation of transition dipole moments. The debugging strategy consisted in calculating transition dipole moments exploiting both the Lagrangian method and the perturbed-amplitudes approach and checking the results to be coincident.

The debugging strategy applied to transition dipole moments is graphically shown in Flowchart 8. For the perturbed-amplitudes algorithm, both $\frac{\partial\sigma_{\mu}(\omega_{fi})}{\partial\varepsilon}$ and $\frac{\partial\sigma^{*}_{\mu}(\omega_{fi})}{\partial\varepsilon}$ have to be calculated. The terms of the Fourier expansion contributing to the transition moment are pairs of complex-conjugate amplitudes, as both are oscillating as $\sim e^{i\omega_{fi}t}$. The solution of coupled equations is performed with the `LinSolvS2` solver, which has been constructed in analogy to `LinSolvS` during this thesis. For transition dipole moments, two sets of perturbed amplitudes are requested, $\frac{\partial\sigma_{\mu}(\omega_{fi})}{\partial\varepsilon}$, called `dtS` in QCUMBRE, and $\frac{\partial\sigma_{\mu}(\omega_{if})}{\partial\varepsilon}$, the adjoint amplitude of $\frac{\partial\sigma^{*}_{\mu}(\omega_{fi})}{\partial\varepsilon}$, named `dtSx`. These two quantities are found by solving the perturbed amplitude equations, which (in the case of UCC3) are coupled.

Each set of amplitudes is calculated via an iterative procedure solving the perturbed-amplitude equations in `ContractionAmplDerivUCC3`, where the instructions given in the input of `LinSolvS2` permit to run both calculations with the same routine:

- the $\frac{\partial\sigma_{\mu}(\omega_{fi})}{\partial\varepsilon}$ amplitudes, referred to as `dtS` in QCUMBRE, are calculated by the function `ContractionAmplDerivUCC3`. The instruction `instr1=trans_deriv_I` (`I=x,y,z`) is used to specify the direction of the electric field. During this calculation, the amplitudes $\frac{\partial\sigma^{*}_{\mu}(\omega_{fi})}{\partial\varepsilon}$, referred to as `dtSx` in QCUMBRE, enter as parameters in the equations. The transition frequency is fixed to ω_{fi};

- the $\frac{\partial\sigma_{\mu}(\omega_{if})}{\partial\varepsilon}$ amplitudes, referred to as `dtSx` in QCUMBRE, are calculated through the function `ContractionAmplDerivUCC3`. The instruction `instr2=trans_deriv_I+` (`I=x,y,z`) conveys the information on the orientation of the electric field. Here, the amplitudes $\frac{\partial\sigma^{*}_{\mu}(\omega_{fi})}{\partial\varepsilon}$, stored as `dtS`, enter the equations parameterically. The transition frequency is fixed to ω_{if}.

Summarizing, the sets of amplitudes $\texttt{dtS}^{(n+1)}$ and $\texttt{dtSx}^{(n+1)}$ are calculated from the guesses $\texttt{dtS}^{(n)}$ and $\texttt{dtSx}^{(n)}$ of the previous iteration. The two expressions are computed simultaneously and the differences with respect to the previous iteration are compared to the convergence threshold.
The transition dipole moments via perturbed amplitudes are calculated by contracting the output of the routine `DerivedEOMS`, which accounts for $\frac{\partial\bar{H}}{\partial\varepsilon}\hat{R}_i\,|0\rangle$, with the operator $\hat{R}^{\dagger}_f$, in order to find $\langle 0|\,\hat{R}^{\dagger}_f\frac{\partial\bar{H}}{\partial\varepsilon}\hat{R}_i\,|0\rangle$. This result has been checked to be the same as the transition dipole moment obtained through the Lagrangian approach, both in the absence and presence of an external magnetic field.

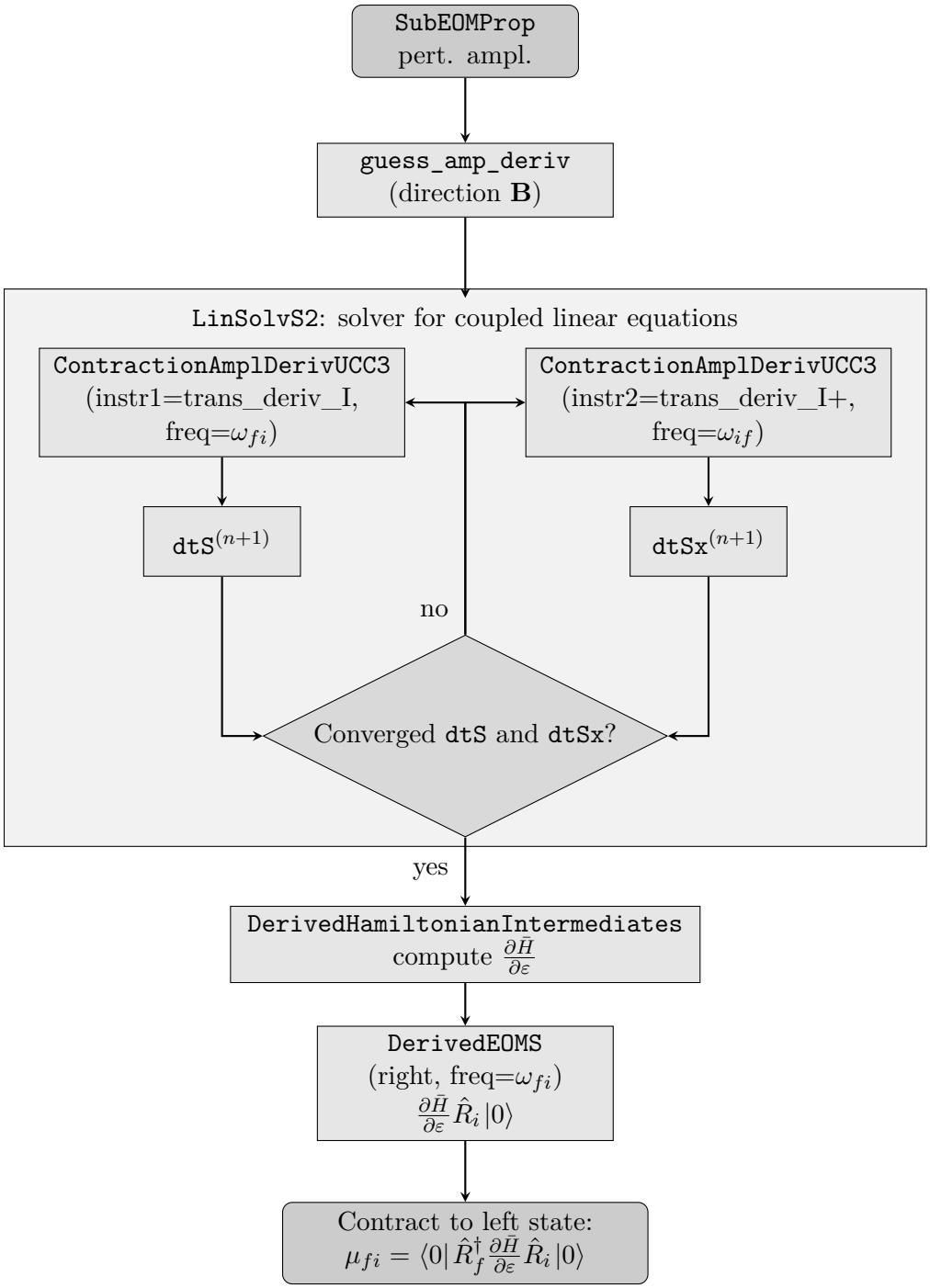

Flowchart 8: Flowchart illustrating how the calculation of transition moments with perturbative amplitudes is performed in QCUMBRE.

Chapter 5

Results

In the previous chapters, the theory and implementation of the unitary coupled-cluster method were explained and validated. This chapter investigates whether UCC theory represents a valid alternative to CC theory, both in the calculation of molecular energies and properties. In particular, a comparison is drawn between the UCC3 and CCSD approximations, as these share the same excitation space (single and double excitations) and the same scaling of the computational cost with system size ($\sim N^6$).

5.1 Molecular energies

The first important result discussed in this chapter is the solution given by UCC theory to the occurrence of complex energies in the CC framework. The validation of the UCC method is here performed through various subsequent steps: first, the energy values obtained with UCC2 and UCC3 are compared to the FCI results for two-electron systems, both with and without a magnetic field. The EOM-UCC3 and EOM-CCSD results are compared for LiH in a perpendicular magnetic field, which allows to investigate the agreement of the excited-state energies in a rather simple case, and CH^+, which is chosen to investigate the accuracy of EOM-UCC2 and EOM-UCC3 for the calculation of states possessing a double-excitation character.
Next UCC results for molecules, which in the CC framework have complex energy values, are analysed. First, the water molecule in a magnetic field is discussed with a focus on whether the imaginary part of the CCSD energy has a physical interpretation. Then, a discussion of the excited states of $B(OH)_3$, characterised by a complex Abelian point group follows in sec. 5.1.5.

5.1.1 Hydrogen molecule and HeH^+ cation

A first assessment of the accuracy of UCC is performed by comparing UCC2 and UCC3 energies with the results obtained by means of FCI for the two-electron systems H_2 and HeH^+. It may be emphasized that for the two systems CCSD is equivalent to FCI, while the same is not true for UCC2 and UCC3. In the tables 5.1 and 5.2, the ground-state and the excitation energies of the lowest excited states of H_2 and HeH^+ are displayed, computed using the uncontracted aug-cc-pVXZ (X=T,Q,5) basis sets for H_2 and the uncontracted aug-cc-pVXZ (X=T,Q) basis sets for HeH^+. Note that the decontraction is essential to provide enough flexibility for the description of the deformations of the orbitals due to the magnetic field. The chosen bond lengths are $R_{H-H} = 1.423\,a_0$ (0.735 Å) and $R_{He-H} = 1.5\,a_0$ (7.938 Å).[272]

H_2					
aug-cc-pVTZ	FCI	UCC3	UCC2	ΔE_{UCC3}	ΔE_{UCC2}
1^1A_g	-1.1728	-1.1726	-1.1735	-0.0002	0.0006
2^1A_g	-0.6930	-0.6949	-0.6838	0.0019	-0.0092
1^1B_{1g}	-0.1557	-0.1595	-0.1367	0.0038	-0.0190
1^1B_{2g}	-0.5141	-0.5159	-0.5042	0.0018	-0.0098
1^1A_u	0.1303	0.1274	0.1448	0.0029	-0.0145
1^1B_{1u}	-0.7084	-0.7101	-0.6988	0.0017	-0.0096
1^1B_{2u}	-0.6455	-0.6475	-0.6344	0.0019	-0.0112
aug-cc-pVQZ					
1^1A_g	-1.1738	-1.1736	-1.1745	-0.0002	0.0006
2^1A_g	-0.6939	-0.6958	-0.6849	0.0019	-0.0091
1^1B_{1g}	-0.3009	-0.3033	-0.2888	0.0024	-0.0121
1^1B_{2g}	-0.5504	-0.5521	-0.5415	0.0018	-0.0089
1^1A_u	-0.1369	-0.1387	-0.1273	0.0018	-0.0095
1^1B_{1u}	-0.7091	-0.7108	-0.6996	0.0017	-0.0094
1^1B_{2u}	-0.6627	-0.6647	-0.6526	0.0019	-0.0102
aug-cc-pV5Z					
1^1A_g	-1.1742	-1.1740	-1.1748	-0.0002	0.0006
2^1A_g	-0.6946	-0.6965	-0.6857	0.0019	-0.0089
1^1B_{1g}	-0.3832	-0.3853	-0.3730	0.0021	-0.0101
1^1B_{2g}	-0.5692	-0.5709	-0.5607	0.0017	-0.0085
1^1A_u	-0.2655	-0.2672	-0.2568	0.0017	-0.0087
1^1B_{1u}	-0.7092	-0.7109	-0.6999	0.0017	-0.0093
1^1B_{2u}	-0.6714	-0.6733	-0.6616	0.0019	-0.0097
HeH^+					
aug-cc-pVTZ	FCI	UCC3	UCC2	ΔE_{UCC3}	ΔE_{UCC2}
1^1A_1	-2.9758	-2.9757	-2.9761	-0.0001	0.0003
2^1A_1	-2.0343	-2.0362	-2.0131	0.0019	-0.0213
3^1A_1	-1.7645	-1.7658	-1.7518	0.0013	-0.0127
1^1B_2	-1.7988	-1.8001	-1.7841	0.0013	-0.0148
aug-cc-pVQZ					
1^1A_1	-2.9776	-2.9775	-2.9779	-0.0001	0.0003
2^1A_1	-2.0356	-2.0375	-2.0146	0.0019	-0.0209
3^1A_1	-1.7652	-1.7666	-1.7526	0.0014	-0.0126
1^1B_2	-1.8025	-1.8039	-1.7883	0.0014	-0.0142

Table 5.1: Ground- and excited-state energies calculated for the H_2 molecule and the HeH^+ cation, for $B = 0$. For H_2, the ground state and the first excited states of each irreducible representation in the D_{2h} representation are shown (for states belonging to different irreducible representations but degenerate in the energy, only one state shown). For HeH^+, the ground state and the lowest three excited states are shown. Calculations have been performed with the FCI, UCC3, and UCC2 methods, with basis sets from the aug-cc-pVXZ (X=T,Q,5) series.[266–271] The energy differences are calculated as $\Delta E = E_{\mathrm{FCI}} - E_{\mathrm{UCC}}$; all energies are given in Hartree.

Table 5.2 shows the results for the field-free case. For the H_2 molecule, the computational point group of the calculation is D_{2h} and the lowest state of each irreducible representation was calculated (the states 1^1B_{3g} and 1^1B_{3u} are here omitted, as they are degenerate with the states 1^1B_{2g} and 1^1B_{2u}). As expected, the UCC3 method offers more accurate results, i.e., closer to the FCI calculation, for all states and basis sets in comparison to UCC2. The energy of the ground state 1^1A_g is overestimated by the UCC2 method, while it is underestimated by UCC3. The opposite trend is observed for all excited states, where the UCC3 method overestimates the FCI results. Similar trends can be observed for the HeH^+ calculations. For both molecules, the basis-set convergence of the results is observed for all three methods, when going to larger basis sets. For the H_2 molecule, the basis-set convergence is rather slow, where variations up to 0.1 E_h are observed (state 1^1A_u) when going from the unc-aug-cc-pVQZ to the unc-aug-cc-pV5Z basis set. The convergence is better for the energy values investigated for HeH^+, where most variations are smaller than 1 mE_h, when going from the unc-aug-cc-pVTZ to the unc-aug-cc-pVQZ basis set. The discrepancies with respect to FCI are rather constant: the magnitude of the UCC2 error decreases by at most 1 mE_h from unc-aug-cc-pVQZ to unc-aug-cc-pV5Z basis set for H_2, while it decreases by only 0.6 mE_h for HeH^+. The magnitude of the UCC3 error is constant for the investigated states when going to larger basis sets, with changes of at most 0.1 mE_h. Considering variations of 1 mE_h as the standard for chemical accuracy,[273] the UCC3 results are accurate in comparison to FCI. Overall, the errors of UCC3 are smaller by a factor of approximately 5 than the errors of the UCC2 results.

Next, the finite-field case is discussed for a magnetic field of $B = 0.1\,B_0$, oriented perpendicularly to the bond axis. This strength was chosen in order to have a field strong enough to observe a sizable effect on the electronic structure. In a magnetic field of perpendicular orientation, H_2 belongs to the point group C_{2h}, while HeH^+ has C_s symmetry. For both molecules, the ground state and the lowest-lying excited singlet states are analysed in table 5.2. In agreement to the results of the field-free case, the errors of UCC3 are smaller by a factor of approximately 5 than the errors observed for UCC2. However, the errors between the UCCn approximations and FCI remain constant, as observed for the field-free case. In addition, in the magnetic field, similar trends for the basis-set convergence are observed as for the field-free case.

5.1.2 Lithium hydride

The investigation on the accuracy of UCC2 and UCC3 is continued using the CCSD results as a reference.

The magnetic field is chosen to vary up to 0.6 B_0. The geometries have been taken from ref. 115 and the same orientation with respect to the molecule (perpendicular to the bond axis) has been used. In fig. 5.1b, the energies of the first four singlet states are shown as a function of the field strength, calculated at the CCSD, UCC2, and UCC3 levels of theory, using the uncontracted aug-cc-pVDZ basis set.[266–271] For the ground state only small discrepancies between the three methods are observed. The mean energy difference between the CCSD and the UCC2 results is -0.84 mE_h, while the mean energy difference between the CCSD and the UCC3 results is 0.32 mE_h. For excited states the UCC2 method gives higher energies with respect to UCC3 and CCSD, and lies always above the corresponding CCSD and UCC3 results. In the field-free case, the $1^1\Pi$ state is degenerate; the magnetic field causes the lifting of the degeneracy, giving the two distinct states $2^1A'$ and $1^1A''$. These two states are therefore allowed to cross. The third excited state shows some mixing with a higher-lying state not displayed here (but shown in ref. 115), around 0.1 B_0. The mean excitation energy differences with respect to CCSD are one order of magnitude larger for the

H_2					
aug-cc-pVTZ	FCI	UCC3	UCC2	ΔE_{UCC3}	ΔE_{UCC2}
$1A_g$	-1.1685	-1.1682	-1.1691	-0.0003	0.0006
$1B_u$	-0.6374	-0.6393	-0.6263	0.0019	-0.0111
$1A_u$	-0.7230	-0.7247	-0.7130	0.0017	-0.0099
$2A_u$	-0.6094	-0.6111	-0.5996	0.0017	-0.0098
aug-cc-pVQZ					
$1A_g$	-1.1695	-1.1692	-1.1701	0.0003	0.0006
$1B_u$	-0.6535	-0.6554	-0.6434	0.0019	-0.0101
$1A_u$	-0.7247	-0.7265	-0.7151	0.0018	-0.0096
$2A_u$	-0.6175	-0.6193	-0.6080	0.0017	-0.0095
aug-cc-pV5Z					
$1A_g$	-1.1698	-1.1696	-1.1705	-0.0002	0.0007
$1B_u$	-0.6613	-0.6632	-0.6516	0.0019	-0.0097
$1A_u$	-0.7251	-0.7268	-0.7155	0.0018	-0.0095
$2A_u$	-0.6210	-0.6227	-0.6116	0.0017	-0.0094
HeH^+					
aug-cc-pVTZ	FCI	UCC3	UCC2	ΔE_{UCC3}	ΔE_{UCC2}
$1A'$	-2.9739	-2.9738	-2.9742	-0.0001	0.0003
$2A'$	-2.0377	-2.0396	-2.0166	0.0019	-0.0211
$3A'$	-1.7880	-1.7894	-1.7734	0.0013	-0.0146
$4A'$	-1.7471	-1.7485	-1.7340	0.0013	-0.0132
$1A''$	-1.7936	-1.7950	-1.7789	0.0013	-0.0148
aug-cc-pVQZ					
$1A'$	-2.9757	-2.9756	-2.9760	-0.0001	0.0003
$2A'$	-2.0390	-2.0409	-2.0182	0.0019	-0.0208
$3A'$	-1.7907	-1.7921	-1.7765	0.0014	-0.0142
$4A'$	-1.7483	-1.7496	-1.7353	0.0013	-0.0130
$1A''$	-1.7971	-1.7985	-1.7829	0.0014	-0.0143

Table 5.2: Ground- and excited-state energies calculated for the H_2 molecule and the HeH^+ cation, in a magnetic field of $B = 0.1\ \mathrm{B}_0$ directed perpendicular to the bond axis. For H_2, the ground state and the first excited states of each irreducible representation in the D_{2h} representation are shown (for states belonging to different irreducible representations but degenerate in the energy, only one state shown). For HeH^+, the ground state and the lowest three excited states are shown. Calculations have been performed with the FCI, UCC3, and UCC2 methods, with basis sets from the aug-cc-pVXZ (X=T,Q,5) series. The energy differences are calculated as $\Delta E = E_{\mathrm{FCI}} - E_{\mathrm{UCC}}$; all energies are given in Hartree.

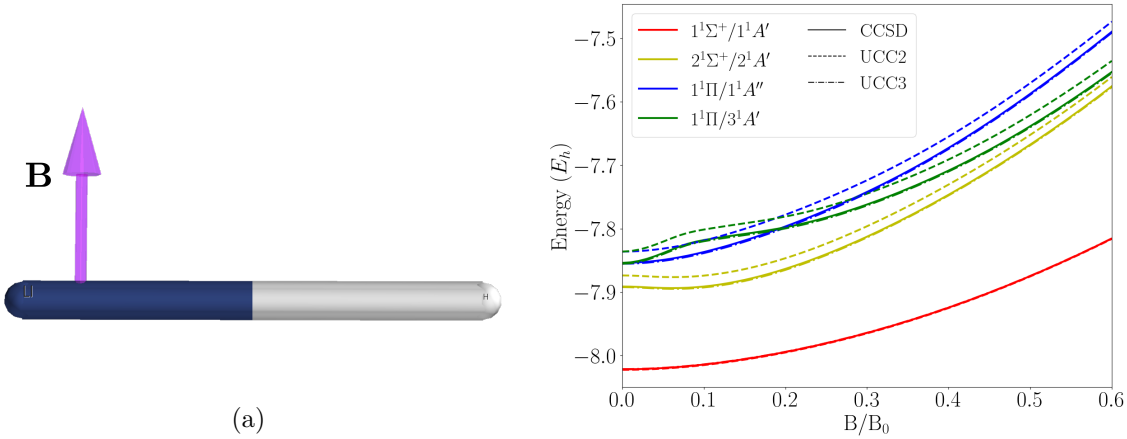

(a) (b)

Figure 5.1: The LiH molecule in a varying magnetic field perpendicular to its bond axis. The bond length is taken from ref. 115. Figure 5.1b shows the ground and excited states energies.

UCC2 method than for UCC3, giving in the UCC2 case 17 mE_h for the $2^1A'$, 18 mE_h for the $1^1A''$ and 17 mE_h for the $3^1A'$, while the mean energy difference between the CCSD and the UCC3 results is -0.82 mE_h for the $2^1A'$, -1.6 mE_h for the $1^1A''$ and -1.5 mE_h for the $3^1A'$. The UCC3 errors are of the order of the fixed standard for chemical accuracy (about 1 mE_h).

From the plot in fig. 5.1, the CCSD and UCC3 results are practically indistinguishable for all investigated magnetic field strengths, showing that the accuracy of the results does not depend significantly on the magnetic field. This investigation completes the discussion of sec. 5.1.1, as the example shows that the good agreement of the CCSD and UCC3 results is independent of the chosen magnetic field strength.

5.1.3 Methylidyne ion

In ref. 114, the behaviour of the methylidinium cation CH^+, in a strong magnetic field directed in various orientations with respect to the bond axis has been investigated, at the CCSDT and CCSD levels of theory. The calculations have been performed with the uncontracted cc-pVDZ basis set.[266–271] The molecular geometry was adopted from ref. 114, where the ground state had been optimised at the CCSD/unc-cc-pVDZ level in absence of the magnetic field. The magnetic field B varies between 0 and 1 B$_0$ and various orientations of the field with respect to the bond axis are explored.

From this first analysis, it appears that CCSD and UCC3 results agree in the description of the ground- and excited-state energies, showing energy differences at most of the order of 1 mE_h. The UCC2 approximation shows larger deviations when compared to the UCC3 and CCSD excited-state results. Therefore, the use of UCC3 instead of CCSD to study a molecular system is a valid choice. The UCC2 method can be used for a qualitative investigation, but its results cannot be used for an accurate quantitative investigation. The increasing accuracy with higher-order UCC approximations could be expected.

In the following discussion, the $^1\Sigma^+$ state has been taken as reference for the EOM calculations. It is described by the single closed-shell configuration $1\sigma^2 2\sigma^2 3\sigma^2$. With respect to this ground state, the three lowest-lying singlet excited states are considered. In the absence of a magnetic field, these are the two degenerate $1^1\Pi$ states (with the configuration

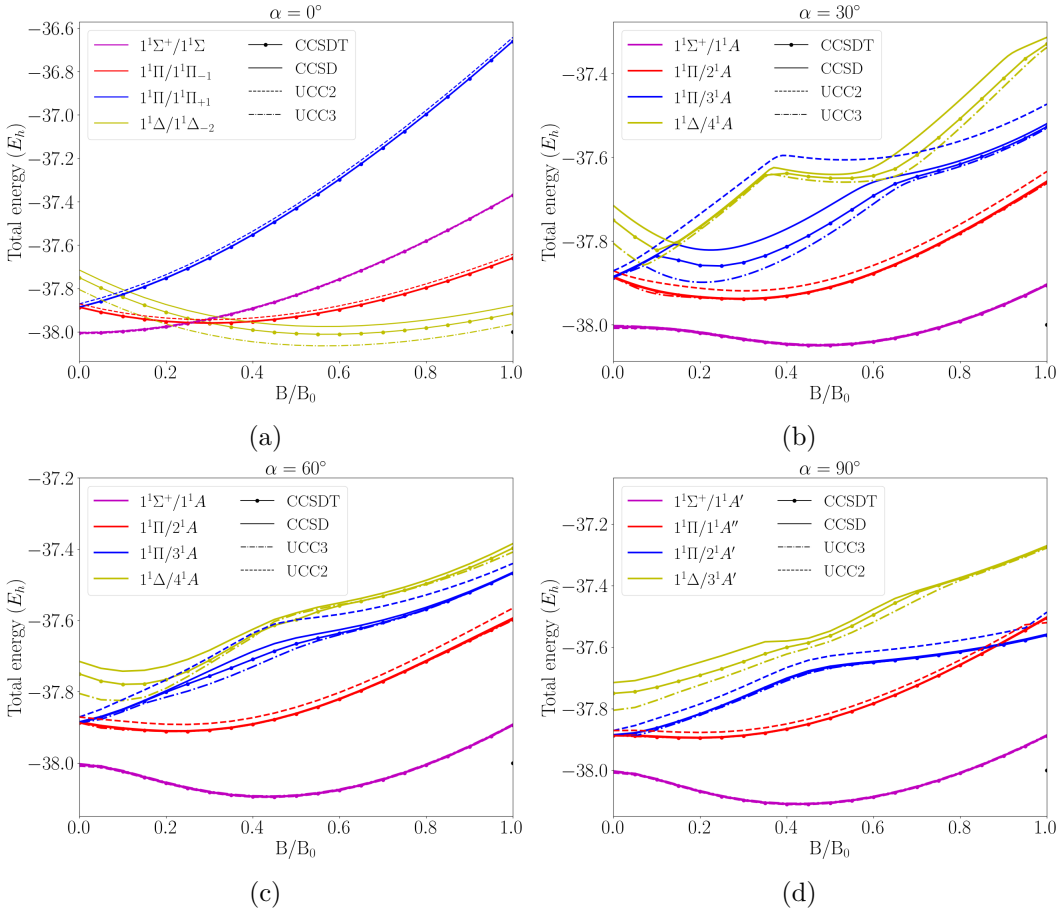

Figure 5.2: Ground state and low-lying excited singlet states for CH^+ in a magnetic field B of increasing strength (between 0 and 1 B_0) and an orientation of $\alpha = 0, \alpha = \pi/6, \alpha = \pi/3, \alpha = \pi/2$ with respect to the bond axis. The symmetry labels are composed by two terms, referring first to the $C_{\infty v}$ point group for the field-free case and then to the actual point group on the right in the magnetic field, respectively.

$\alpha = 0$	$\Delta E_{\mathrm{CCSD}}/\mathrm{m}E_{\mathrm{h}}$	$\Delta E_{\mathrm{UCC3}}/\mathrm{m}E_{\mathrm{h}}$	$\Delta E_{\mathrm{UCC2}}/\mathrm{m}E_{\mathrm{h}}$
$1^1\Sigma^+/1^1\Sigma$	1.71	3.13	-2.42
$1^1\Pi/1^1\Pi_{-1}$	2.95	0.47	17.55
$1^1\Pi/1^1\Pi_{+1}$	2.95	0.47	17.55
$1^1\Delta/1^1\Delta_{-2}$	35.59	-53.23	-
$\alpha = \pi/6$			
$1^1\Sigma^+/1^1A$	1.98	2.77	-0.38
$1^1\Pi/2^1A$	2.30	-1.05	20.91
$1^1\Pi/3^1A$	23.78	-19.28	100.37
$1^1\Delta/4^1A$	22.75	-16.63	-
$\alpha = \pi/3$			
$1^1\Sigma^+/1^1A$	1.82	2.81	-1.00
$1^1\Pi/2^1A$	2.36	-0.60	21.26
$1^1\Pi/3^1A$	8.29	-7.85	43.98
$1^1\Delta/4^1A$	19.96	-11.94	-
$\alpha = \pi/2$			
$1^1\Sigma^+/1^1A'$	1.79	2.83	-1.21
$1^1\Pi/1^1A''$	2.11	2.70	15.80
$1^1\Pi/2^1A'$	2.93	-1.93	36.82
$1^1\Delta/3^1A'$	20.99	-23.23	-

Table 5.3: CH^+ in a magnetic field: mean differences for the energies (in mE_h) of ground and the three lowest-lying excited singlet states of each symmetry for CCSD and UCC3 with respect to the reference value of the CCSDT calculation. The mean value has been calculated computing $\Delta E_{\mathrm{Method}} = E_{\mathrm{Method}} - E_{\mathrm{CCSDT}}$ over the range of varying magnetic field strengths between 0 and 1 B_0 and taking the arithmetic average of these values. The symmetry labels are composed by two terms, referring first to the $C_{\infty v}$ point group for the field-free case and then to the actual point group on the right in the magnetic field, respectively.

$1\sigma^2 2\sigma^2 3\sigma^1 1\pi^1$) and the degenerate $1^1\Delta$ state (with the configuration $1\sigma^2 2\sigma^2 1\pi^2$). The latter has a predominant double-excitation character with respect to the $^1\Sigma^+$ reference. It is well-known that states dominated by a double-excitation cannot be described accurately by CCSD.[114] In the following discussion, it is analysed how UCC3 compares to the CCSDT reference. A similar accuracy to CCSD is expected. The development of the states with respect to the strength of the magnetic field is shown in fig. 5.2, while the mean energy deviations from the CCSDT reference results are reported in tab. 5.3.

In fig. 5.2a, the magnetic field is oriented parallel to the bond axis. In this orientation, the molecular point group is lowered from $C_{\infty v}$ of the field-free case to C_∞. As the states all belong to different irreducible representations, they can cross without mixing. This leads for example to a change in the ground state when going to higher field strengths, around 0.3 B_0. The ground-state shows a quadratic dependence on the magnetic field, while the spin-Zeeman and orbital-Zeeman terms do not contribute to first order in the magnetic field. The two degenerate Π states are split into their components $1^1\Pi_{-1}$ and $1^1\Pi_{+1}$ by the orbital-Zeeman term. The lower $1^1\Pi_{-1}$ state is stabilised by the orbital-Zeeman term for field strengths up to 0.35 B_0, while the diamagnetic term dominates for higher magnetic-field strengths. Referring to table 5.3, the average difference of the computed ground-state energy with respect to the CCSDT value is about 3 mE_h and 2 mE_h for UCC3 and CCSD, respectively. For the states originating from the originally degenerate $^1\Pi$ states, UCC3 shows a better accuracy than CCSD, with an average energy difference of about 0.5 mE_h for UCC3 and almost 3 mE_h for CCSD. UCC2, on the other hand, shows an overestimation of the electronic energies of states $1^1\Pi_{-1}$ and $1^1\Pi_{+1}$, with mean differences of almost 18 mE_h. Major differences are found for the $1^1\Delta_{-2}$ state: from ref. 114 it is already known that CCSD overestimates the energy by an almost constant amount for all field strengths considered here, and a mean deviation with respect to the CCSDT results of 35.59 mE_h. This behaviour is caused by the doubly-excited character of the $1^1\Delta_{-2}$ state, as it cannot be accurately described in the space of single and double excitations. The same inaccuracy is shared with UCC3, which has a mean deviation of -53 mE_h. Here UCC3 underestimates the energy for all investigated field strengths, though correctly reproducing the shape of the CCSDT line. Analogously to the perturbative CC2 method,[274] UCC2 is unable to describe doubly-excited states as explained in the theory chapter (sec. 3.1.3). Hence, the $1^1\Delta_{-2}$ state is therefore completely missing in the UCC2 results.

In fig. 5.2b the magnetic field is oriented at an angle of $\alpha = \pi/6$ with respect to the bond axis. In this setting, the reduction of the molecular symmetry to C_1 symmetry leads to avoided crossings, as all states belong to the same irreducible representation. The state resulting from the $1^1\Sigma^+$ state (purple line) remains lowest in energy when increasing the magnetic field strength. It mixes with the first excited state, as can be inferred from the slight curvature of the purple line for magnetic field strengths up to 0.3 B_0. The ground state is well described by the methods considered here, with mean differences of 2 mE_h for CCSD, 3 mE_h for UCC3 and even less, -0.4 mE_h for UCC2, respectively. For the analysed orientations, the originally degenerate $1^1\Pi$ states are split due to the presence of the magnetic field. The $1^1\Pi_{-1}$ state (described by the red curve) is always lower in energy than $1^1\Pi_{+1}$; the mean differences with respect to the CCSDT reference are about 2 mE_h for CCSD, -1 mE_h for UCC3 and 20 mE_h for UCC2, respectively. Therefore, the description is good for CCSD and UCC3, while UCC2 overestimates the energy of this excited state.

The most interesting features are observed for the two higher-lying excited states: for $\alpha = \pi/6$ the two states 3^1A and 4^1A (the blue and the yellow lines in fig. 5.2b), originating from $1^1\Pi_{+1}$ and $1^1\Delta_{-2}$ in the field-free case, are mixing, resulting in an avoided crossing. For field strengths up to 0.1 B_0, the 3^1A state has a predominant double-excitation character,

which is then passed to the 4^1A state at the first avoided crossing. The 3^1A state acquires the double-excitation character back after the second avoided crossing. The presence of a double-excitation character influences the accuracy of the UCC3 and CCSD results, as both methods are not able to accurately describe states with a predominant double-excitation character. Furthermore, the avoided crossings are observed at different field strengths, at 0.10 B_0 and 0.65 B_0 for CCSDT, at 0.14 B_0 and 0.60 B_0 for CCSD, and at 0.07 B_0 and 0.67 B_0 for UCC3. As for the parallel case, CCSD overestimates the CCSDT energy, with a mean difference of 23.78 mE_h,[114] while UCC3 underestimates it, with a mean difference of −19.28 mE_h. UCC2, on the other hand, is not able to describe the double-excitation character at all and just follows the state which is dominated by a singly-excited character. For this method, the description of the state is qualitatively wrong. The same behaviour has been described in ref. 274 for CC2. The feature at about 0.4 B_0 indicates that the 4^1A state also appears to mix with higher-lying states. A second mixing with a higher-lying state is observed for the CCSD results at field strengths larger than 0.9 B_0.

In the interval 0 B_0-0.2 B_0, the UCC3 energy of state 2^1A differs from the other methods by a slightly larger amount than for the rest of the curve (about 8 mE_h). The analysis shows that this state possesses a very small, but non-negligible, component with a double-excitation character when described at the UCC3 level of theory. This influence originates from the avoided crossing discussed above, which for UCC3 lies at lower energies than for the other methods. The proximity to this avoided crossing causes a slight double-excitation contribution in the description of state 2^1A, which is absent in the results of the other methods analysed here.

In fig. 5.2c, the magnetic field is oriented with an angle $\alpha = \pi/3$ with respect to the bond axis. As for the previous orientation, the ground state and the first excited state (purple and red lines) are accurately described by CCSD, UCC2, and UCC3, and the mean differences remain of the same order as for the orientations discussed previously. The two higher-lying states are still presenting an avoided crossing and are mixing, though not as evidently as for $\alpha = \pi/6$. The 3^1A state acquires the doubly-excited character after the first avoided crossing, at about 0.2 B_0. The singly-excited character is restored at higher field strengths. For state 4^1A, in the right part of the spectrum the accuracy increases for CCSD and UCC3. This may be due to the mixing with higher-lying states, to which the double-excitation character may be passed. For this orientation, UCC3 shows smaller mean deviations from the CCSDT reference than CCSD (see table 5.3). In particular the 4^1A state has a mean difference of 19.96 mE_h for the CCSD method, while the for UCC3 it is almost half of it, −11.94 mE_h. For the UCC2 results, an overestimation of the CCSDT reference energy is observed for 2^1A and 3^1A, with mean deviations of 21.26 mE_h and 43.98 mE_h, respectively. UCC2 cannot describe the state with predominant double-excitation character 4^1A.

In fig. 5.2d, the results for the perpendicular orientation are shown. In this case, the molecular symmetry is lowered to C_{2h}. Here, states $1^1A''$ and $2^1A'$ are allowed to cross in the strong-field region. No avoided crossing is observed, and an accurate reproduction of the three lowest-lying singlet states both by CCSD and UCC3 is observed, with mean differences of the same order of magnitude for both methods, about 3 mE_h. In this case, the double-excitation character of the $3^1A'$ state is only partially passed to the lower-lying $2^1A'$ state. For the $3^1A'$ state the same discrepancies as for the other orientations are observed. CCSD overestimates the energies, on average by 20.99 mE_h, while UCC3 underestimates them, on average by −23.23 mE_h. The UCC2 results show the same trends observed for the orientations previously discussed, with mean deviations of 15.80 mE_h for the $1^1A''$ state and 36.82 mE_h for the $2^1A'$ state.

As for the general behaviour, CCSD and UCC3 both show systematic problems for the

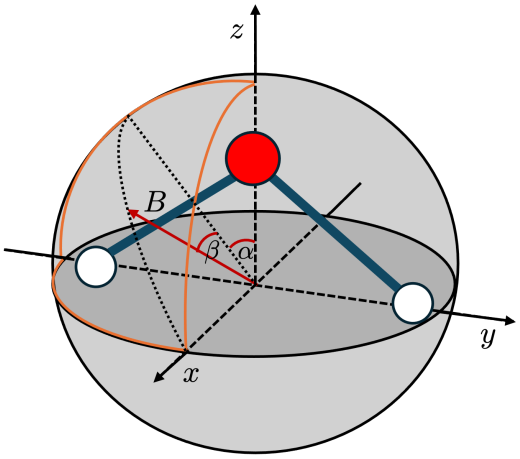

Figure 5.3: Water molecule in a magnetic field of B=0.5 B_0, whose orientation is allowed to vary corresponding to the polar coordinates α and β.

description of states with a double-excitation character, while they accurately reproduce the CCSDT results for singly-excited states. UCC2 proves to be a good approximation for states dominated by a single excitation, while it leads to qualitatively wrong results in cases with a double-excitation component.

5.1.4 Water molecule

Overall it is found that the comparison of UCC3 and CCSD results showed that these methods possess a similar accuracy. In ref. 35, the occurrence of complex energy eigenvalues in CC calculations has been analysed, showing that the unphysical complex energies are common to all non-linear molecules. In the aforementioned reference, the discussion focuses on the water molecule in a magnetic field of B=0.5 B_0. The direction of the field is varied on the surface of the positive octant of the unit sphere (fig. 5.3) and described by the two polar coordinates α, β. For the CCSD ground-state calculations, the imaginary part in the energy eigenvalues vanishes only if the direction of the magnetic field is aligned to one of the symmetry axes of the point group of the molecule in the field-free case, as derived in ref. 35. The use of a Hermitian expression for the energy eliminates the imaginary part by construction, leading to purely real energies. In this chapter the ground state and the first three excited singlet states of water are investigated. The aim is to investigate the magnitude of the imaginary part for the CC method not only for the ground state, as in ref. 35, but also for excited states, and to discuss whether a imaginary value is connected to the accuracy of the real part of the energy.[275] The calculations have been performed with the uncontracted cc-pVTZ[266–270] basis set, adopting the geometry from ref. 35.

The real parts of the ground- and excited-state CCSD energies and the corresponding UCC3 energies are plotted in fig. 5.4 as a function of the two polar coordinates α, β. As the underlying HF calculation is the same for both methods, the correlation energy for the ground state and the excitation energies from the ground state for the excited states are plotted. For the investigated states, the qualitative shape of the surfaces describing the ground-state energy obtained with UCC3 and CCSD is the same for both methods.

In fig. 5.4a, the (real) energy surfaces for the ground state are plotted, obtained with UCC3 and CCSD. The qualitative shape of the surfaces is the same. Fig. 5.5a shows the difference $\Delta E = E_{\mathrm{UCC3}} - E_{\mathrm{CCSD}}$ between the energy surfaces obtained with CCSD and UCC theory is plotted as a colour map. The regions characterised by very small differences are

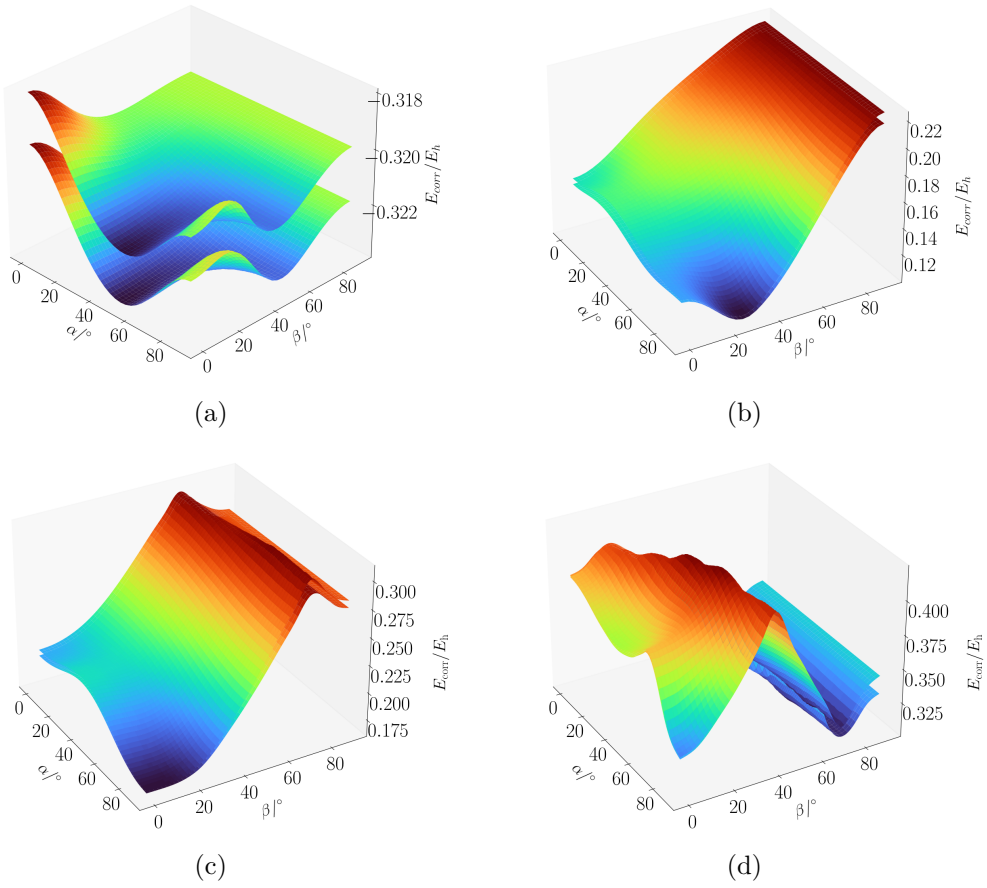

Figure 5.4: Correlation energy of the ground state (fig. 5.4a) and excitation energies of the first three excited states (figs. 5.4b-5.4d) of the water molecule in a magnetic field of B=0.5 B_0 as a function of its orientation, as pictured in fig. 5.3, calculated at the CCSD and UCC3 level of theory, using the unc-cc-pVTZ basis set.

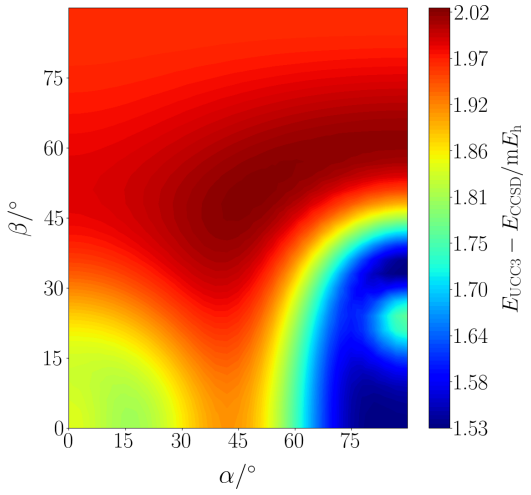

(a) $\Delta E = E_{\mathrm{UCC3}} - E_{\mathrm{CCSD}}$:
– $\max \Delta E = 2.028\mathrm{m}E_{\mathrm{h}}$ $(48°, 51°)$,
– $\min \Delta E = 1.531\mathrm{m}E_{\mathrm{h}}$ $(81°, 0°)$.

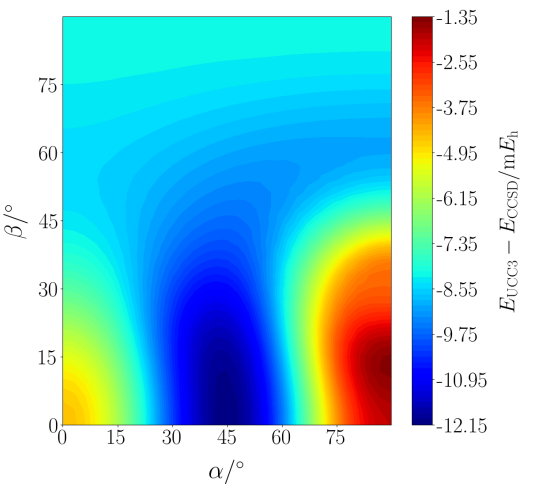

(b) $\Delta E = E_{\mathrm{UCC3}} - E_{\mathrm{CCSD}}$:
– $\max \Delta E = -1.431\mathrm{m}E_{\mathrm{h}}$ $(90°, 12°)$,
– $\min \Delta E = -12.133\mathrm{m}E_{\mathrm{h}}$ $(45°, 0°)$.

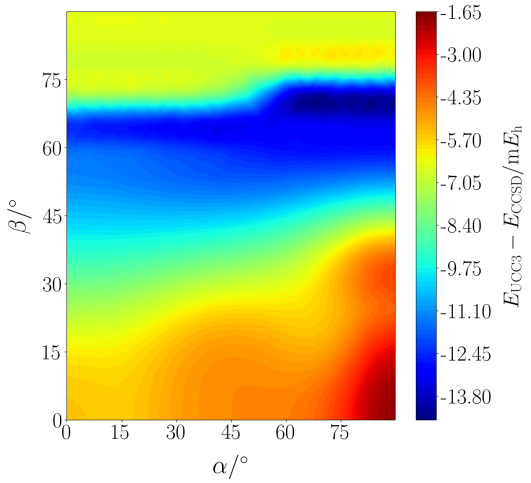

(c) $\Delta E = E_{\mathrm{UCC3}} - E_{\mathrm{CCSD}}$:
– $\max \Delta E = -1.797\mathrm{m}E_{\mathrm{h}}$ $(90°, 0°)$,
– $\min \Delta E = -13.792\mathrm{m}E_{\mathrm{h}}$ $(90°, 72°)$.

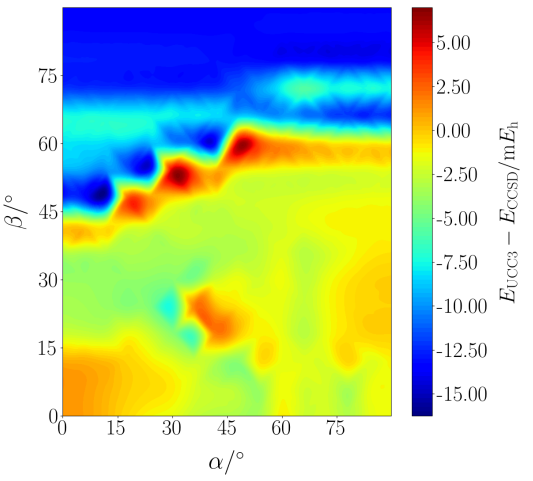

(d) $\Delta E = E_{\mathrm{UCC3}} - E_{\mathrm{CCSD}}$:
– $\max \Delta E = 5.535\mathrm{m}E_{\mathrm{h}}$ $(48°, 60°)$,
– $\min \Delta E = -14.721\mathrm{m}E_{\mathrm{h}}$ $(12°, 48°)$.

Figure 5.5: Energy differences, calculated as $E_{\mathrm{UCC3}} - E_{\mathrm{CCSD}}$, for the ground (fig. 5.5a) and first three excited states (figs. 5.5b-5.5d) of the water molecule in a magnetic field of B=0.5 B_0 as a function of its orientation, as pictured in fig. 5.3.

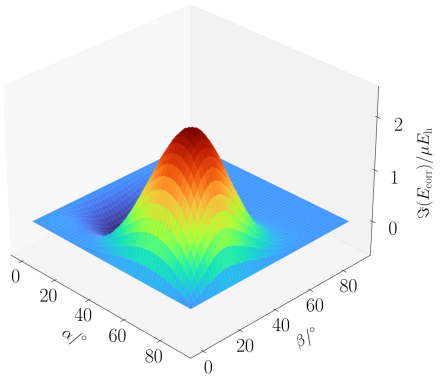

(a) Imaginary ground-state energy:
– $\max(\mathrm{Im}\{E_{\mathrm{CCSD}}\}) = 2.50\mu E_{\mathrm{h}}$ $(66°, 24°)$.

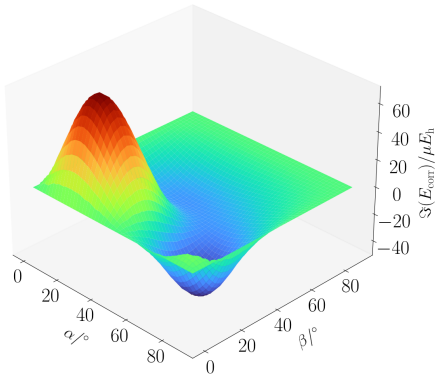

(b) Imaginary energy of Ψ_1:
– $\max(\mathrm{Im}\{E_{\mathrm{CCSD}}\}) = 69.87\mu E_{\mathrm{h}}$ $(21°, 18°)$,
– $\min(\mathrm{Im}\{E_{\mathrm{CCSD}}\}) = -48.31\mu E_{\mathrm{h}}$ $(69°, 24°)$.

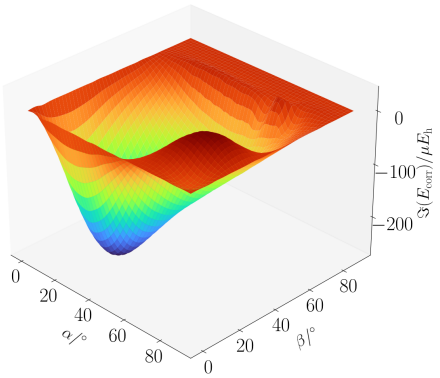

(c) Imaginary energy of Ψ_2:
– $\max(\mathrm{Im}\{E_{\mathrm{CCSD}}\}) = 38.25\mu E_{\mathrm{h}}$ $(72°, 24°)$,
– $\min(\mathrm{Im}\{E_{\mathrm{CCSD}}\}) = -266.87\mu E_{\mathrm{h}}$ $(24°, 24°)$.

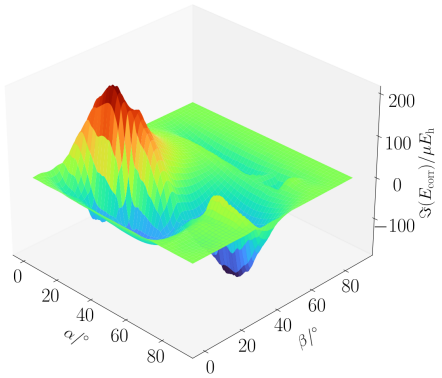

(d) Imaginary energy of Ψ_3:
– $\max(\mathrm{Im}\{E_{\mathrm{CCSD}}\}) = 182.48\mu E_{\mathrm{h}}$ $(18°, 24°)$,
– $\min(\mathrm{Im}\{E_{\mathrm{CCSD}}\}) = -171.70\mu E_{\mathrm{h}}$ $(72°, 42°)$.

Figure 5.6: Imaginary part of the energy surfaces of the ground and first three excited states of the water molecule in a magnetic field of B=0.5 B_0 as a function of its orientation, as pictured in fig. 5.3, calculated at the CCSD level of theory. The maximum and minimum values of the imaginary part of the CCSD energy is indicated below each figure, where the positions of minima and maxima are indicated as coordinates (α, β).

coloured in blue, while those with larger differences are coloured in red. In this particular case, it is observed that the energy difference $\Delta E = E_{\mathrm{UCC3}} - E_{\mathrm{CCSD}}$ has only positive values, therefore showing that the UCC3 energy is here always larger than the real part of the CCSD energy. The maximum energy difference is $2.02\,\mathrm{m}E_\mathrm{h}$, at about $\alpha = 48°$ and $\beta = 51°$, while the minimum energy difference of $1.53\,\mathrm{m}E_\mathrm{h}$ is found at about $\alpha = 81°$ and $\beta = 0°$. The imaginary part of the CCSD energy is plotted in fig. 5.6a.[35] The maximal absolute value of the imaginary contribution to the energy is of about 2.5 μE_h, situated at $\alpha = 66°$ and $\beta = 24°$. Comparing to the behaviour of the real part of the energy (fig. 5.4a) and to the difference plot (fig. 5.5a), there seems to be no correlation to the magnitude of the imaginary part.

Figs. 5.4b-5.4c show the surfaces given by the real part of the energy values of the first three excited singlet states, Ψ_1, Ψ_2 and Ψ_3. From these plots, it is noted that the states have avoided crossings, which can occur as all states have the same C_1 symmetry for a generic orientation of the magnetic field. The ground state has an avoided crossing with the first excited state Ψ_1 in the region around $\alpha = 80°$ and $\beta = 25°$ (figs. 5.4a and 5.4b). The excited states Ψ_2 and Ψ_3 (figs. 5.4c and 5.4d) also exhibit an avoided crossing, visible at around $\beta = 80°$, where the two surfaces are very close to each other for both methods. The third state is also mixing with the states above, which are not shown here. This mixing is visible at the crest at about $\beta = 40°$.
For all three states, the surfaces obtained with the CCSD and the UCC3 methods are qualitatively agreeing. A better evaluation of their differences is gained through the colour-map plots in figs. 5.5b-5.5d: for Ψ_1 and Ψ_2, the difference $\Delta E = E_{\mathrm{UCC3}} - E_{\mathrm{CCSD}}$ always takes negative values, stating that the CCSD surface lies above the UCC3 one for these two states. The energy difference for the state Ψ_3 takes both positive values on one side of the crest, negative values on the other side. For Ψ_1, the maximum absolute difference value is found to be about $\Delta E = -12.13\,\mathrm{m}E_\mathrm{h}$, at $\alpha = 45°$ and $\beta = 0°$, a region which is not related to the avoided crossing. The minimum absolute difference is found at $\alpha = 90°$ and $\beta = 12°$, where $\Delta E = -1.43\,\mathrm{m}E_\mathrm{h}$. The maximal ΔE values for the states Ψ_2 and Ψ_3 are found around the avoided crossing between the second and the third excited state. For Ψ_2, the maximum absolute energy difference is $\Delta E = -13.79\,\mathrm{m}E_\mathrm{h}$ at $\alpha = 90°$ and $\beta = 0°$, while the minimal discrepancy between the two methods is $\Delta E = -1.80\,\mathrm{m}E_\mathrm{h}$ at $\alpha = 90°$ and $\beta = 72°$. For the state Ψ_3, the energy difference has no constant sign throughout the surface: the largest positive value of $\Delta E = 5.54\,\mathrm{m}E_\mathrm{h}$ is obtained at $\alpha = 48°$ and $\beta = 60°$, while the largest negative value (the largest absolute difference) of $\Delta E = -14.72\,\mathrm{m}E_\mathrm{h}$ is observed at $\alpha = 12°$ and $\beta = 48°$. Importantly, it is observed that the description of the excited states shows energy differences between the two methods that are larger by one order of magnitude compared to the ground state.

While the magnitude of the imaginary part of the ground-state energy may seem negligible, this is no longer the case for the excited states: for the state Ψ_1, fig. 5.6b shows that the imaginary part reaches positive values up to $69.87\,\mu E_\mathrm{h}$ (at $\alpha = 21°$ and $\beta = 18°$) and negative values up to $-48.31\,\mu E_\mathrm{h}$ (at $\alpha = 69°$ and $\beta = 24°$). For excited states Ψ_2 and Ψ_3, the occurrence of complex eigenvalues becomes even more evident. In fig. 5.6c, a negative imaginary part of $-266\,\mu E_\mathrm{h}$ is observed at $\alpha = 24°$ and $\beta = 24°$, while for the third excited state a maximum value of the imaginary part of $182\,\mu E_\mathrm{h}$ is found at $\alpha = 18°$ and $\beta = 24°$. The magnitude of the imaginary parts therefore reaches 1/10 of the energy difference between the UCC3 and CCSD surfaces and is an effect which cannot be neglected.

However, there is no obvious interpretation which can be given to these complex eigenvalues, as from all plots it is observed that there is no correlation between large ΔE values and large imaginary parts. Furthermore, the imaginary parts cannot be related to avoided

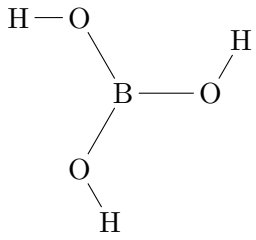

Figure 5.7: Boric acid $B(OH)_3$, exhibiting C_{3h} symmetry.

crossings, as they are observed also far from the avoided crossings. For this system, UCC3 gives results which are qualitatively very similar to CCSD, without the difficulties coming from complex energy values. In the cases for which CCSD leads to complex energy values, UCC3 should therefore be preferred.

5.1.5 Boric acid

Systems with a complex Abelian point group are characterised by excited states belonging to pairs of complex-conjugate irreducible representations. These states are pairwise degenerate and have a complex wave function. However, real linear combinations of the complex wave functions may be formed, in order to enable a treatment using a code based on real-valued wave functions. However, the non-Hermitian expression of the energy in EOM-CC theory leads to complex-conjugate energy values rather than truly degenerate results for the states belonging to the complex irreducible representations. The corresponding states are therefore not found with real EOM-CC codes. It is however possible to find them if complex EOM-CC codes, when available, are employed. As stated before, a computation involving complex algebra is more memory requiring and computationally expensive and hence for cases without a magnetic field, when the complex wave function cannot be avoided, the possibility to use a real program is preferable. Therefore, a formalism calculating the energy via the expectation value of a Hermitian operator, like UCC theory, is preferred. Note that the computation of the ground state, which is described by a real irreducible representation, does not pose any problems for the CC method in the field-free case.

Boric acid $B(OH)_3$ is an example of a system whose symmetry is described through a complex Abelian point group, C_{3h} (fig. 5.7). In addition, this symmetry remains the same when the molecule is in an external magnetic field, oriented perpendicularly to the molecular plane. The point group C_{3h} possesses two real irreducible representations, A' and A'', and two pairs of complex-conjugate ones, E'_1, E'_2 and E''_1, E''_2. The investigations focuses on the $B(OH)_3$ molecule, first in the field-free case and then in a perpendicular magnetic field with strength up to 0.8 B_0. The geometry used for all calculations was fixed to the optimised field-free geometry obtained at the CCSD/unc-aug-cc-pVDZ[266–270] level of theory: $R_{BO} = 2.6018\ a_0$, $R_{OH} = 1.8181\ a_0$ and $\angle BOH = 68.23°$. The energies of the ground state and the first excited state of each irreducible representation have been calculated with the QCUMBRE program package, using the unc-aug-cc-pVDZ basis set, at the CC3,[207,274] CCSD, CISD[207] and UCC3 levels of theory.

The results for CCSD, CC3, CISD, and UCC3 energies in the field-free case are given in table 5.4,* showing the excitation energies of the lowest excited states of the irreducible representations A', A'', E' and E'', at the CCSD, CC3, CISD, and UCC3 levels of theory. The energies of the states of the two real irreducible representations A' and A'' are real for

*The results for the CC3, CCSD, and CISD methods in table 5.4 and figs. 5.8-5.9 are taken from ref. 207.

Methods	Energies			
	A'	A''	E'	E''
CCSD	0.356378	0.332552	$0.364306 \pm 0.000047i$	$0.301831 \pm 0.000051i$
CC3	0.354183	0.331149	$0.362247 \pm 0.000004i$	$0.298958 \pm 0.000011i$
UCC3	0.366560	0.338875	0.373787	0.308129
CISD	0.255217	0.232414	0.263483	0.201056

Table 5.4: Excitation energies (E_h) of the lowest singlet states $1A'$, $1A''$, $1E'$ and $1E''$, at the CCSD, CC3, UCC3, and CISD levels of theory, with the unc-aug-cc-pVDZ basis set.[266–270] For CCSD and CC3, the energies are pairs of complex-conjugate numbers.

all methods, while for the complex irreducible representations E' and E'', the CC results consist in pairs of complex-conjugate values. The UCC3 results, on the other hand, correctly describe the degeneracy. The discrepancies between the CCSD and CC3 results is of the order of 0.001 E_h, while the differences between the CC3 and UCC3 values are of the order of 0.01 E_h. The two CC methods CC3 and CCSD therefore show a better agreement, which could be explained by the fact that they are different truncations of the same ansatz for the wave function and contributions to infinite order in perturbation theory. Furthermore, the CISD results are shown in table 5.4. The discrepancies of the CISD results with respect to the CC3 results is of the order of 0.1 E_h, larger than for the other inspected methods. Even though the energy in the CISD framework is calculated through Hermitian operators, it is much less accurate than UCC3. For a computation with a real code, the UCC3 method is therefore preferred to CISD. In the following discussion, in order to account for the large differences in correlation energies observed for CISD with respect to CC3, the CISD results have been shifted in order to coincide to the CCSD energies at $B = 0$.

In fig. 5.8, the total energy of the ground state is displayed as a function of the magnetic field strength. The energy rises in an increasing magnetic field, due to the diamagnetic term. The ground state is a closed-shell singlet state and therefore the spin-Zeeman term vanishes. In the left panel, the analysis of the real part shows superimposed and practically indistinguishable curves for the CCSD, CISD, and UCC3 methods, while the inclusion of triple excitations shifts the CC3 energy to slightly lower values, on average about 0.03 E_h below CCSD and UCC3. However, for both the CC3 and CCSD methods, a non-vanishing imaginary part arises in a magnetic field (right panel of fig. 5.8). For field strengths below 0.3 B_0, $\mathrm{Im}\{E_\mathrm{GS}\}$ is of the order of $\approx 10^{-5}\,E_\mathrm{h}$. Around 0.7 B_0, however, both CCSD and CC3 show an increase in the imaginary part of the total energy, up to a maximum of $\approx 0.34\,\mathrm{m}E_\mathrm{h}$ and $\approx 0.09\,\mathrm{m}E_\mathrm{h}$, respectively. It is observed that the imaginary part decreases with the inclusion of triple excitations, in agreement with the expectation that the imaginary part should diminish when going towards the FCI limit. The occurrence of complex energies does not seem to provide particular insight into the accuracy of the real part, as a large imaginary part in the CC energy does not correspond to noticeable features in the difference between the real part of the energies obtained with the CC and UCC methods, respectively.

Similar to the ground-state energy, in fig. 5.9 the excitation energies for the first excited singlet states of each irreducible representation are plotted as function of the magnetic field strength. For each figure, the left panel compares the real part of the excitation energies, computed with the four methods. In fig. 5.9a, the states ${}^1A'$ and ${}^1A''$, in fig. 5.9b, the states ${}^1E'_1$ and ${}^1E'_2$ and in fig. 5.9c, the states ${}^1E''_1$ and ${}^1E''_2$ are shown. The behaviour of the excitation energies of these states is more complicated than for the energies of the ground state, both in the case of the real and the imaginary parts. In particular, it is observed that the imaginary part of the CCSD energies is larger than the corresponding imaginary

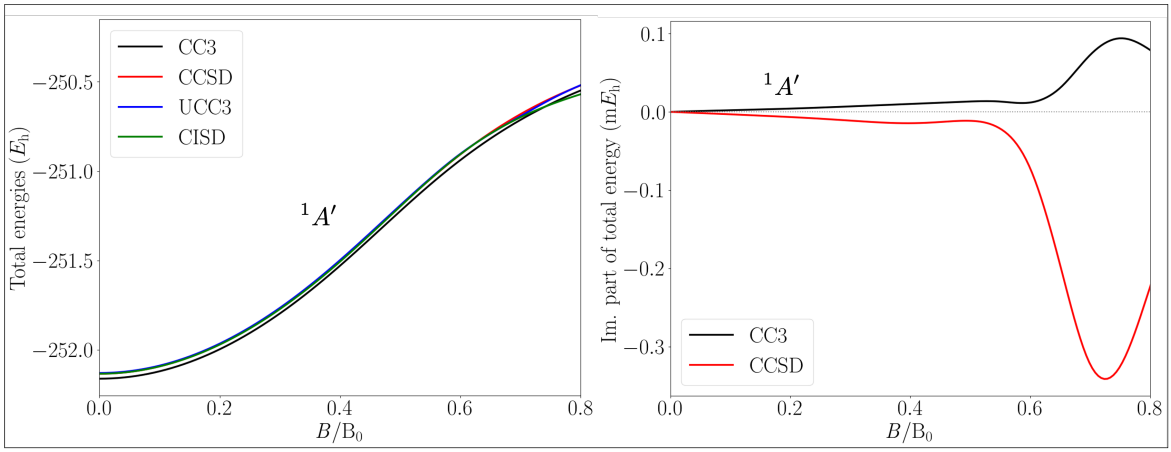

Figure 5.8: Total energy of the ground state of the boric acid $B(OH)_3$, in an external magnetic field, directed perpendicularly to the molecular plane. The field strength varies in the interval of 0 B_0-0.8 B_0. The left panel shows the comparison between the real parts of the energies computed at the CC3, CISD, CCSD, and UCC3 levels of theory. The right panel shows the non-vanishing imaginary parts of the CC energies.

part of the CC3 energies, but these values are unrelated to each other and show maxima and minima at different field strengths. The states $^1E_1''$,$^1E_2''$, characterised by the HOMO-LUMO transition, are the energetically lowest excited states. As discussed before, the states belonging to the representations of dimension 2, E' and E'', start off as a degenerate pair and are split by the magnetic field. All states experience a decrease in the excitation energy when going to higher magnetic-field strengths. In all plots, the three methods are in good agreement with each other for field strengths up to 0.5 B_0, while qualitative differences are observed for higher field strengths.

In fig. 5.9a, the energies of the states $^1A'$ and $^1A''$ are shown as a function of the magnetic field strength. For field strengths larger than 0.2 B_0, the $^1A'$ state becomes lower in energy than the $^1A''$ state. Major differences are observed in the magnetic-field range between 0.55 B_0 and 0.75 B_0. A double-excitation character is observed from the inspection of the amplitudes of the $^1A''$ state obtained with the CC3 method. As CC3 includes triple excitations, it is the most accurate among the considered methods for the description of states with a double-excitation character. The double-excitation character is described also by the UCC3 method, while it is absent in the CCSD results. The lowering in energy at about 0.7 B_0, found by CC3, is differently described by UCC3, CISD, and CCSD. The discrepancy with respect to CC3 might stem from the fact that the other methods, due to the limitation of the excitation space to singles and doubles, do not describe the double-excitation character well. For the $^1A'$ state, the lowering in energy is common to both CISD and UCC3. However, in this region UCC3 is also observed to acquire a partial double-excitation character, which is absent in the CC3 results. Therefore, the shape of the $^1A'$ curve differs from those obtained with the other methods, which describe the $^1A'$ state via a single excitation. On the right panel of fig. 5.9a, the corresponding imaginary parts of the CC3 and CCSD results are shown. For the states belonging to the real irreducible representations, $^1A'$ and $^1A''$, the excitation energies in the field-free case are real. The plotted imaginary values in the right panel of fig. 5.9a therefore start from 0 E_h. For CCSD, the maximum of $|\mathrm{Im}\{E_{exc}\}|$ of 1.8 mE_h is obtained for the $^1A''$ state, while the same state for CC3 has a maximum of $|\mathrm{Im}\{E_{exc}\}|$ of 0.4 mE_h. It is observed that the largest values of $|\mathrm{Im}\{E_{exc}\}|$ for the CC3 results are found at the field strengths at which the largest double-excitation character is found. The maxima and

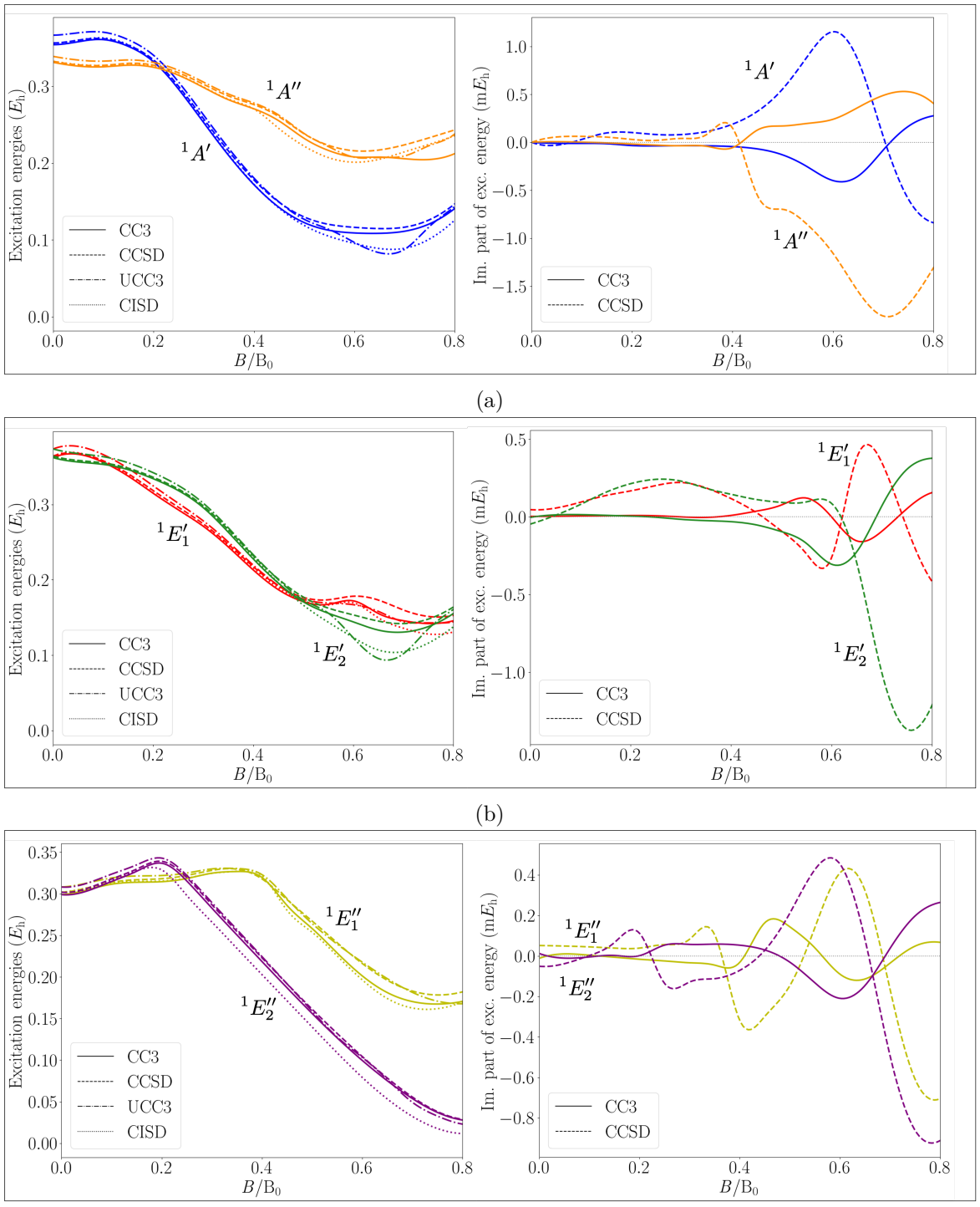

Figure 5.9: Excitation energies of low-lying singlet states of each irreducible representation for $B(OH)_3$, in an external magnetic field, directed perpendicularly to the molecular plane. The field strength varies in the interval 0 B_0-0.8 B_0. In the left column, the comparison between the real parts of the energies computed at the CC3, CCSD, CISD, and UCC3 levels of theory is shown. In the right column, the non-vanishing imaginary parts of the CC energies are shown.

minima for CCSD are found at similar field strengths. The CCSD results, even though not predicting a significant double-excitation character, still seem to exhibit a large imaginary part in these regions.
For the irreducible representation E' (fig. 5.9b), the same behaviour as in fig. 5.9a can be observed for magnetic fields larger than 0.55 B_0. The $^1E'_1$ state acquires a double-excitation character. As a consequence, major differences in the results are observed between 0.55 B_0 and 0.70 B_0. Here the CC3 and UCC3 result exhibits a double-excitation character, while CCSD exhibits only a single-excitation character. For the $^1E'_2$ state, the CC3 and UCC3 results possess a double-excitation character between 0.60 B_0 and 0.75 B_0. From the right panel, it is observed that the two states have complex-conjugate energy values in the field-free case, as expected. In the finite field, the energies do no longer occur as pairs on complex-conjugate values. The imaginary part is no longer negligible at higher magnetic-field strengths, especially in the range 0.4 B_0-0.8 B_0. In particular, the maximum of $|\mathrm{Im}\{E_{\mathrm{exc}}\}|$ for the $^1E'_1$ state is 0.53 mE_h for CCSD and 0.16 mE_h for CC3, while for the $^1E'_2$ state is 1.37 mE_h for CCSD and 0.38 mE_h for CC3. As for fig. 5.9b is it observed that the maxima of $|\mathrm{Im}\{E_{\mathrm{exc}}\}|$ for the CC3 energies are found in correspondence to the presence of a double-excitation character of the states.

In fig. 5.9c, the energies of the two lowest-lying states belonging to the irreducible representation E'' are shown. Here no major discrepancies are observed. The avoided crossings occur at 0.2 B_0 for the $^1E''_2$ state and 0.4 B_0 for the $^1E''_1$ state. Both states possess a small double-excitation character (however not predominating over the single-excitation character), observed in the CC3 and UCC3 results, while it is absent for CCSD. The maximum of $|\mathrm{Im}\{E_{\mathrm{exc}}\}|$ for the $^1E''_1$ state is 0.71 mE_h for CCSD and 0.16 mE_h for CC3, while for the $^1E''_2$ is 0.91 mE_h for CCSD and 0.27 mE_h for CC3. The maxima of $|\mathrm{Im}\{E_{\mathrm{exc}}\}|$ are found once more in correspondence to the largest double-excitation character for CC3. The maxima of $|\mathrm{Im}\{E_{\mathrm{exc}}\}|$ for the CCSD energies are found in approximately nearby field strengths.

In summary, UCC seems to be a good solution to find degenerate excited states of a complex Abelian point group, without having to resort to the use of a complex code.
The problems arising from the non-Hermiticity of the CC theory are evident in the finite-field case, due to large imaginary components in particular for excited states and show a complicated behaviour as a function of the magnetic field strength. It has been observed that the largest values of the imaginary parts are found where a partial double-excitation character in the description of the excited states is found. From this study, it seems that there could exist a correlation between a large imaginary part in the energy values and the presence of double excitations in the parameterisation of the states. As the quality of the CCSD but actually even of the CC3 results is not clear when large imaginary components occur, the UCC3 approach may be the better choice.

5.2 Molecular properties

In this section, molecular property results obtained by means of UCC theory are discussed. In particular, the focus is on the analysis of the differences between property values obtained by means of the EOM approach and of the response-theory approach. The UCC results are compared to CCSD results. First, the results for the two-electron systems discussed in sec. 5.1.1, H_2 and HeH^+ are shown. Then, the properties of the water molecule and the LiH molecule in a magnetic field are analysed.
As CC can yield negative transition probabilities (also in the field-free case), the applicability of UCC is explored. Negative transition probabilities can occur even when the energy results are real.[36] As negative probabilities cannot be connected to oscillator strengths, they do not

offer any meaningful interpretation. Hence, the use of UCC is explored as an alternative. Two systems for which negative CC transition probabilities occur, the silicon dication and the CH^+ cation, will be discussed in this section.*

5.2.1 Hydrogen molecule and HeH^+ cation

The importance of including the response of the wave function parameters to the perturbation in the calculation of properties is assessed through a comparison of results obtained via the response-theory approach (sec. 3.2.1) and the EOM approach (sec. 4.5.8) with FCI results. For a first evaluation, results for the hydrogen molecule H_2 and the HeH^+ cation are analysed. For both molecules, the same bond lengths as in sec. 5.1.1 have been used.

In table 5.5, transition dipole moments between the lowest singlet states of the hydrogen molecule are displayed. A magnetic field of 0.1 B_0 is chosen, directed perpendicularly to the bond axis. Only transitions with a non-vanishing transition dipole moment are reported here. For the calculation, the uncontracted augmented Dunning basis sets aug-cc-pVXZ (X=T,Q,5) were adopted.[266–271] The basis-set convergence is rather slow, in particular for the transition between excited states. The transition dipole moments from the ground state (the $1A_g$ state) are smaller than the ones between excited states. For this molecule, the EOM approach always overestimates the transition dipole moment, as can be seen by the negative $\Delta\mu_{\mathrm{EOM}} = |\mu_{\mathrm{FCI}}|^2 - |\mu_{\mathrm{EOM}}|^2$ values. On the other hand, the inclusion of the response of the amplitudes leads to an underestimation of the transition dipole moments, as $\Delta\mu_{\mathrm{resp.}} = |\mu_{\mathrm{FCI}}|^2 - |\mu_{\mathrm{resp.}}|^2 > 0$. In order to assess the importance of the inclusion of the response effects in the calculation of properties, the last column in table 5.5 shows the difference $\Delta = |\Delta\mu_{\mathrm{resp.}}| - |\Delta\mu_{\mathrm{EOM}}|$. Negative values of Δ mean that response-theory results are more accurate (i.e., closer to FCI results) than EOM results while positive values of Δ mean response-theory results are less accurate than EOM results. Except for the transition $1A_g \rightarrow 1A_u$, Δ is negative, showing that response theory is more accurate in these cases. The discrepancies between the two methods is two orders of magnitude larger for the transitions between excited states, up to 0.2 $e^2a_0^2$, compared to the discrepancies for the transitions from the ground state, up to 0.008 $e^2a_0^2$. Therefore, for practical applications, the EOM approach for similar calculations of transition dipole moments from the ground state is sufficient. It is interesting to observe that the perturbed amplitudes have such a large effect on the UCC3 transition dipole moments.

The HeH^+ ion is investigated in a magnetic field of 0.1 B_0, oriented perpendicularly to the bond axis. The system is characterised by the point group C_s.

In table 5.6 the dipole moments of the ground state $1A'$ and the lowest excited singlet states are listed. For the analysed basis sets, the differences with respect to FCI are smaller for the response theory results than for the EOM results, in most cases by an order of magnitude. The differences between the FCI and the UCC3 dipole moments computed with the EOM approach take values up to 0.288 $e^2a_0^2$, while the differences between the FCI and the UCC3 dipole moments computed with the response-theory approach take values up to 0.028 $e^2a_0^2$. For all excited states, the dipole moment obtained through the response-theory approach is closer to the FCI result. The ground-state dipole moment is very accurately reproduced already by the UCC3-EOM approximation.

In table 5.7 the transition dipole moments between the considered states are displayed. In agreement with the results discussed for the hydrogen molecule, the EOM treatment of

*In this section, dipole moments and transition dipole moments are discussed. With a slight abuse of notation, the quantity $|\mu|^2$ will be referred to as dipole moment, and the quantity $|\mu_{IJ}|^2 = \mu_{IJ} \cdot \mu_{JI}$ will be referred to as transition dipole moment for the transition from state I to state J. In both cases, the squared norm of the vectors is meant.

aug-cc-pVTZ	$\lvert\mu_{\mathrm{FCI}}\rvert^2$	$\lvert\mu_{\mathrm{resp.}}\rvert^2$	$\lvert\mu_{\mathrm{EOM}}\rvert^2$	$\Delta\mu_{\mathrm{resp.}}$	$\Delta\mu_{\mathrm{EOM}}$	Δ
$1A_g \to 1A_u$	0.995	0.978	1.010	0.017	−0.015	0.002
$1A_g \to 2A_u$	0.973	0.962	0.992	0.011	−0.019	−0.008
$1A_g \to 1B_u$	1.063	1.053	1.078	0.010	−0.015	−0.005
$2A_g \to 1A_u$	6.053	5.816	6.512	0.236	−0.460	−0.223
$2A_g \to 2A_u$	3.803	3.669	3.986	0.134	−0.182	−0.048
$2A_g \to 1B_u$	2.371	2.226	2.675	0.145	−0.304	−0.159
aug-cc-pVQZ						
$1A_g \to 1A_u$	0.993	0.976	1.008	0.017	−0.015	0.002
$1A_g \to 2A_u$	0.959	0.948	0.976	0.011	−0.017	−0.006
$1A_g \to 1B_u$	0.948	0.939	0.961	0.009	−0.013	−0.004
$2A_g \to 1A_u$	5.829	5.594	6.278	0.235	−0.450	−0.215
$2A_g \to 2A_u$	4.337	4.166	4.610	0.171	−0.273	−0.102
$2A_g \to 1B_u$	3.471	3.287	3.832	0.184	−0.361	−0.177
aug-cc-pV5Z						
$1A_g \to 1A_u$	0.997	0.980	1.012	0.018	−0.015	0.003
$1A_g \to 2A_u$	0.946	0.935	0.962	0.011	−0.016	−0.004
$1A_g \to 1B_u$	0.874	0.866	0.886	0.008	−0.012	−0.004
$2A_g \to 1A_u$	5.669	5.434	6.116	0.235	−0.447	−0.213
$2A_g \to 2A_u$	4.731	4.542	5.052	0.190	−0.321	−0.131
$2A_g \to 1B_u$	4.376	4.165	4.778	0.211	−0.402	−0.191

Table 5.5: Transition dipole moments between the first excited singlet states of the H_2 molecule in a magnetic field of 0.1 B_0 directed perpendicularly to the bond axis. The UCC3 results have been calculated with the response-theory formulation ($\mu_{\mathrm{resp.}}$) and in the expectation-value formulation (μ_{EOM}). The discrepancies with respect to the FCI reference values are calculated as $\Delta\mu_{\mathrm{resp.}} = \lvert\mu_{\mathrm{FCI}}\rvert^2 - \lvert\mu_{\mathrm{resp.}}\rvert^2$ and $\Delta\mu_{\mathrm{EOM}} = \lvert\mu_{\mathrm{FCI}}\rvert^2 - \lvert\mu_{\mathrm{EOM}}\rvert^2$. The difference between the absolute values of the errors is defined as $\Delta = \lvert\Delta\mu_{\mathrm{resp.}}\rvert - \lvert\Delta\mu_{\mathrm{EOM}}\rvert$. The calculations have been performed with different basis sets. The atomic units $e^2a_0^2$ are adopted here.

aug-cc-pVTZ	$\lvert\mu_{\mathrm{FCI}}\rvert^2$	$\lvert\mu_{\mathrm{resp.}}\rvert^2$	$\lvert\mu_{\mathrm{EOM}}\rvert^2$	$\Delta\mu_{\mathrm{resp.}}$	$\Delta\mu_{\mathrm{EOM}}$	Δ
$1A'$	0.116	0.107	0.121	0.010	−0.005	0.005
$2A'$	0.807	0.779	1.095	0.028	−0.289	−0.261
$3A'$	0.268	0.273	0.385	−0.005	−0.117	−0.112
$4A'$	0.534	0.518	0.452	0.017	0.082	−0.066
$1A''$	0.406	0.410	0.522	−0.005	−0.116	−0.111
aug-cc-pVQZ						
$1A'$	0.117	0.107	0.122	0.010	−0.005	0.005
$2A'$	0.802	0.774	1.090	0.028	−0.288	−0.260
$3A'$	0.204	0.210	0.320	−0.006	−0.116	−0.110
$4A'$	0.548	0.531	0.466	0.017	0.082	−0.065
$1A''$	0.319	0.325	0.433	−0.005	−0.114	−0.109

Table 5.6: Single-state dipole moments of the ground state and the first excited singlet states of the HeH^+ molecule in a magnetic field of 0.1 B_0 directed perpendicularly to the bond axis. The UCC3 results have been calculated with the response-theory formulation ($\mu_{\mathrm{resp.}}$) and in the expectation-value formulation (μ_{EOM}). The discrepancies with respect to the FCI reference values are calculated $\Delta\mu_{\mathrm{resp.}} = |\mu_{\mathrm{FCI}}|^2 - |\mu_{\mathrm{resp.}}|^2$ and $\Delta\mu_{\mathrm{EOM}} = |\mu_{\mathrm{FCI}}|^2 - |\mu_{\mathrm{EOM}}|^2$. The difference between the absolute values of the errors is defined as $\Delta = |\Delta\mu_{\mathrm{resp.}}| - |\Delta\mu_{\mathrm{EOM}}|$. All quantities are computed in atomic units. The calculations have been performed with different basis sets. The atomic units $e^2a_0^2$ are adopted here.

properties overestimates the transition dipole moments, with differences with respect to FCI up to $|\Delta\mu_{\mathrm{EOM}}| = 0.123\, e^2a_0^2$, while the inclusion of the response of the amplitudes leads to weaker transitions, with differences with respect to FCI up to $\Delta\mu_{\mathrm{resp}} = 0.046\, e^2a_0^2$. The transitions from the ground state $1A'$ are weaker than those between excited states. As for H_2, it is noticed that the transitions from the ground state have the smallest discrepancies with respect to the FCI reference calculations, of the order of $10^{-3}\, e^2a_0^2$.

In summary, as a general consideration, UCC3 response theory has been shown to reproduce better the FCI results than the EOM approach to the calculation of properties. The differences between the two approaches is larger for dipole moments of excited states and transition dipole moments between excited states. For properties involving the ground state, the discrepancies in the results of the two methods is of the order of $10^{-3}\, e^2a_0^2$, indicating that for these properties the EOM approach is a good alternative.

5.2.2 Water molecule

In this section, the properties of the water molecule are investigated, in a magnetic field of strength varying between 0 B_0 and 0.4 B_0. Preliminary investigations to this study showed that the water molecule dissociates for magnetic-field strengths larger than 0.4 B_0; this observation motivates the chosen range of magnetic-field strengths. The geometry was taken from ref. 248, where the bond lengths are $R_{\mathrm{OH}} = 0.957$ Å and the angle $\angle\mathrm{HOH} = 104.5°$. Calculations were performed with the uncontracted aug-cc-pVDZ basis set.[266–268,270]

The characterisation of the water molecule is discussed for three different orientations of the field, as shown in the left panels of fig. 5.10. In fig. 5.10a, the magnetic field is oriented perpendicularly to the molecular plane; in fig. 5.10c, the magnetic field is oriented along the bisector of the angle $\angle$HOH; in fig. 5.10b the magnetic field lies in the molecular plane, perpendicular to the orientations described for figs. 5.10a and 5.10c. In order to analyse single-state and transition properties of the system in a strong magnetic field, first the ener-

aug-cc-pVTZ	$\lvert\mu_{\mathrm{FCI}}\rvert^2$	$\lvert\mu_{\mathrm{resp.}}\rvert^2$	$\lvert\mu_{\mathrm{EOM}}\rvert^2$	$\Delta\mu_{\mathrm{resp.}}$	$\Delta\mu_{\mathrm{EOM}}$	$\Delta_{\mathrm{resp.}}$
$1A' \to 2A'$	0.657	0.645	0.665	0.012	−0.009	0.003
$1A' \to 3A'$	0.300	0.298	0.303	0.001	−0.003	−0.002
$1A' \to 4A'$	0.077	0.077	0.078	0.001	−0.001	−0.000
$1A' \to 1A''$	0.346	0.345	0.350	0.001	−0.004	−0.002
$2A' \to 3A'$	0.248	0.238	0.310	0.011	−0.062	−0.051
$2A' \to 4A'$	0.448	0.442	0.446	0.006	0.002	0.004
$2A' \to 1A''$	0.154	0.148	0.193	0.006	−0.038	−0.032
$3A' \to 4A'$	2.358	2.314	2.480	0.044	−0.122	−0.078
$3A' \to 1A''$	0.171	0.167	0.188	0.004	−0.017	−0.013
$4A' \to 1A''$	2.053	2.015	2.149	0.038	−0.096	−0.058
aug-cc-pVQZ						
$1A' \to 2A'$	0.656	0.644	0.665	0.012	−0.008	0.003
$1A' \to 3A'$	0.301	0.299	0.304	0.001	−0.003	−0.002
$1A' \to 4A'$	0.072	0.071	0.073	0.001	−0.001	0.000
$1A' \to 1A''$	0.340	0.339	0.344	0.001	−0.003	−0.002
$2A' \to 3A'$	0.230	0.220	0.290	0.010	−0.059	−0.049
$2A' \to 4A'$	0.455	0.449	0.454	0.006	0.001	0.005
$2A' \to 1A''$	0.138	0.132	0.173	0.006	−0.035	−0.030
$3A' \to 4A'$	2.490	2.444	2.613	0.046	−0.123	−0.077
$3A' \to 1A''$	0.175	0.171	0.192	0.004	−0.017	−0.013
$4A' \to 1A''$	2.284	2.243	2.387	0.042	−0.103	−0.061

Table 5.7: Transition dipole moment between the first excited singlet states of the HeH^+ molecule in a magnetic field of 0.1 B_0 directed perpendicularly to the bond axis. The UCC3 results have been calculated with the response-theory formulation ($\mu_{\mathrm{resp.}}$) and in the expectation-value formulation (μ_{EOM}). The discrepancies with respect to the FCI reference values are calculated as $\Delta\mu_{\mathrm{resp.}} = \lvert\mu_{\mathrm{FCI}}\rvert^2 - \lvert\mu_{\mathrm{resp.}}\rvert^2$ and $\Delta\mu_{\mathrm{EOM}} = \lvert\mu_{\mathrm{FCI}}\rvert^2 - \lvert\mu_{\mathrm{EOM}}\rvert^2$. The difference between the absolute values of the errors is defined as $\Delta = \lvert\Delta\mu_{\mathrm{resp.}}\rvert - \lvert\Delta\mu_{\mathrm{EOM}}\rvert$. The calculations have been performed with different basis sets. The atomic units $e^2a_0^2$ are adopted here.

gies of the first three singlet states with respect to the magnetic-field strength are discussed. They are plotted in the right panels of fig. 5.10, for each orientation. Results have been obtained at the CCSD, UCC2, and UCC3 levels of theory. For the three inspected orientations, UCC2, UCC3, and CCSD show very small differences in the results for the ground state $1^1A'$ energy (black lines in fig. 5.10). In detail, defining $\Delta E_{\mathrm{UCCn}} = \overline{(E_{\mathrm{UCCn}} - E_{\mathrm{CCSD}})}$ the mean differences of the UCC2 and UCC3 versus the CCSD results, the discrepancies differ by an approximate factor of 2, i.e. $\Delta E_{\mathrm{UCC2}}(1^1A') = -0.0028\,E_\mathrm{h}$ and $\Delta E_{\mathrm{UCC3}}(1^1A') = 0.0013\,E_\mathrm{h}$. The excited states may be analysed in detail. For the lowest two excited singlet states, the qualitative description of the state shows a good agreement of the three methods. The energy of these excited states increases in the increasing magnetic field, due to the contribution of the diamagnetic term of the finite-field Hamiltonian (eq. 2.3.12). For all states, UCC2 yields smaller energies than CCSD. For larger field strengths, the energy difference become smaller. Comparing UCC3 to CCSD, for all three plots in fig. 5.10 the UCC3 energies are larger than the CCSD energies, giving a discrepancy which is smaller than for the UCC2 results. In detail, $\Delta E_{\mathrm{UCC2}}(1^1A'') = -0.0113\,E_\mathrm{h}$ and $\Delta E_{\mathrm{UCC3}}(1^1A'') = 0.0062\,E_\mathrm{h}$, and $\Delta E_{\mathrm{UCC2}}(2^1A'') = -0.0137\,E_\mathrm{h}$, while $\Delta E_{\mathrm{UCC3}}(2^1A'') = 0.0065\,E_\mathrm{h}$. As for the ground state, the UCC2 and UCC3 results differ by an approximate factor of 2.
The investigation on the ground- and excited-state energies is necessary for the analysis of the dipole and transition dipole moments.

Dipole moments of water

The analysis of contributions to the dipole moment for each orientation requires some considerations of point group theory and the symmetry of the states. In order for the integral $\langle\Psi_a|\,\hat{\mu}\,|\Psi_b\rangle$ not to vanish, the product of the representations of Ψ_a, μ, Ψ_b must contain the total symmetric irreducible representation:

$$\Gamma_a \otimes \Gamma_\mu \otimes \Gamma_b \supseteq \Gamma_{id}. \tag{5.2.1}$$

In the first orientation (fig. 5.10a), where the magnetic field is perpendicular to the molecular plane, the system has C_s symmetry and the states Ψ_1 and Ψ_2 both have A'' symmetry, while the ground state has ${}^1A'$ symmetry. The two excited states show an avoided crossing at about 0.2 B_0.
Orienting the field perpendicularly to the bisector of the angle ∠HOH, along the molecular plane, as shown in fig. 5.10b, the system belongs to the point group C_s. Here Ψ_1 has A' symmetry, while Ψ_2 has A'' symmetry and no mixing between the states is allowed. Therefore, the two states do not interact and they increase in a rather parallel manner when increasing the magnetic field strength, which is clearly visible in the right panel of fig. 5.10b. The configuration in which the magnetic field is oriented along the bisector of the bond angle (fig. 5.10c) is described through the point group C_2. Ψ_1 belongs to the irreducible representation B, while Ψ_2 has A symmetry. Again, no mixing can therefore occur here, which is visible in the right panel of fig. 5.10c.

The corresponding electronic dipole moments (i.e., dipole moments without the nuclear contribution) are shown in fig. 5.11 as function of the field strength for the three orientations. The left column shows the properties at the EOM level, while the right one accounts for the response of the amplitudes of the wave function. All lines are essentially parallel and present the same qualitative description of dipole moments. In fig. 5.11a the major changes in magnitude of the dipole moments in the region around 0.2 B_0 is due to the avoided crossing of the states $1^1A''$ and $2^1A''$ observed in the energy plots. Looking at fig. 5.11, it is observed that the agreement between CCSD and UCC3 is much better in the response-theory

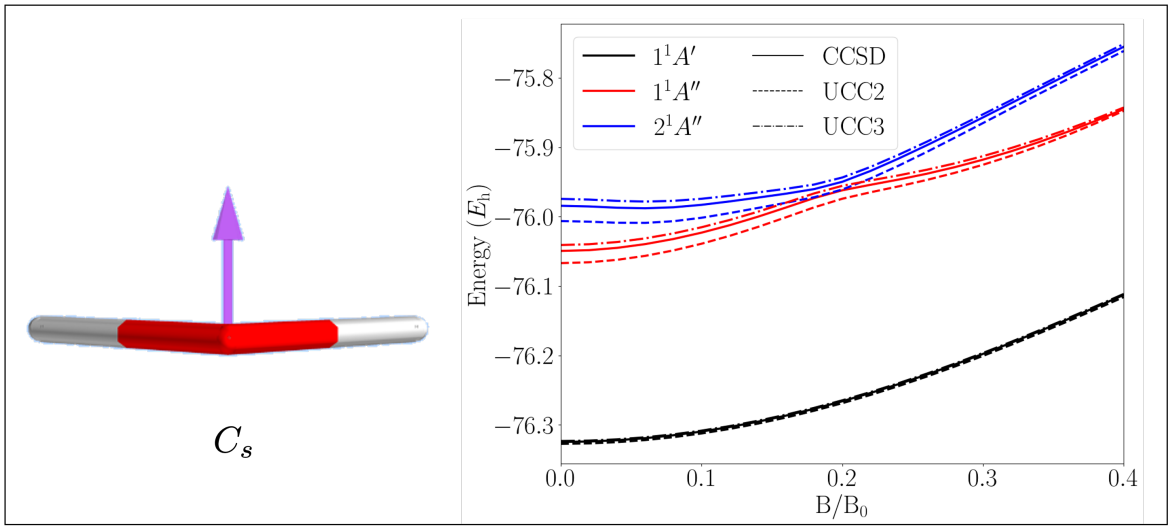

(a)

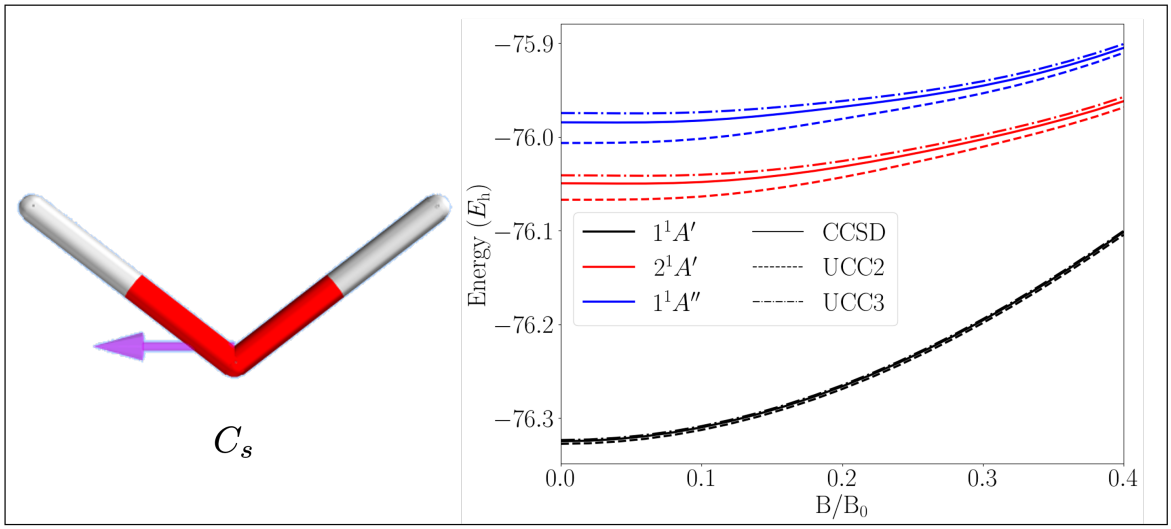

(b)

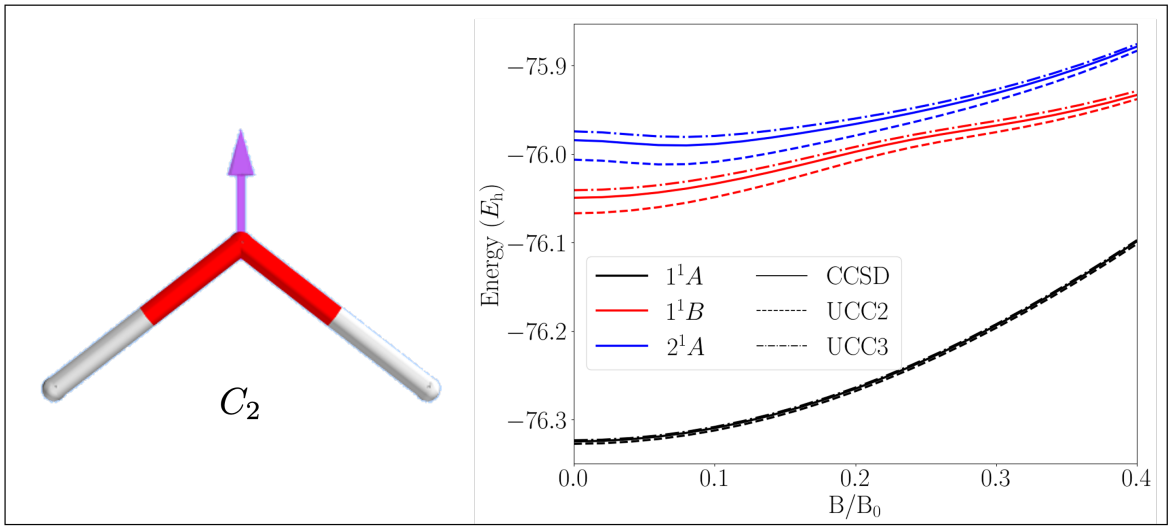

(c)

Figure 5.10: On the left, the different orientations of the magnetic field with respect to the water molecule are shown. On the right, the corresponding energies of the ground state and the first two excited states are displayed.

Fig. 5.10a	$\Delta\mu_{\mathrm{CCSD}}/e^2a_0^2$	$\Delta\mu_{\mathrm{UCC2}}/e^2a_0^2$	$\Delta\mu_{\mathrm{UCC3}}/e^2a_0^2$
$1^1A'$	0.0000	0.0154	0.0325
$1^1A''$	0.0008	0.0078	−0.2978
$2^1A''$	0.0099	0.0098	−0.3017
Fig. 5.10b			
$1^1A'$	0.0000	0.0159	0.0366
$2^1A'$	−0.0072	0.0068	−0.3436
$1^1A''$	−0.0008	0.0078	−0.3184
Fig. 5.10c			
1^1A	0.0000	0.0153	0.0315
1^1B	0.0083	0.0090	−0.2621
2^1A	0.0056	0.0087	−0.2749

Table 5.8: Differences between electronic dipole moments obtained with the EOM and response-theory approach, calculated as $\Delta\mu = |\mu_{\mathrm{resp}}|^2 - |\mu_{\mathrm{EOM}}|^2$. All results are given in atomic units ($e^2a_0^2$). The orientation of the magnetic field is indicated in the corresponding panel in fig. 5.10.

framework (the mean difference between the two methods in the response-theory framework is about $-0.016\,e^2a_0^2$ for the ground state, about $-0.076\,e^2a_0^2$ for the excited states, while it is of about $0.017\,e^2a_0^2$ for the ground state, about $0.247\,e^2a_0^2$ for the excited states in the EOM framework), whereas the UCC2 results are always larger than the CCSD and UCC3 results (the mean difference with respect to the CCSD results is of about $0.003\,e^2a_0^2$ for the ground state, about $0.397\,e^2a_0^2$ for the excited states in the response-theory case, while for the EOM-approach the mean difference yields about $-0.012\,e^2a_0^2$ for the ground state and about $0.390\,e^2a_0^2$ for the excited states). Table 5.8 shows the mean values of the discrepancies between the results obtained with the two property schemes, obtained as $\Delta\mu = |\mu_{\mathrm{resp}}|^2 - |\mu_{\mathrm{EOM}}|^2$. The mean value has been computed by dividing the range of the magnetic field, between 0 and 0.4 B_0, into 100 equally spaced points. In the CC framework, the ground-state dipole moments give the same result both with the EOM and the response-theory approach, as the Lagrange functional for the CC ground-state dipole moment coincides with the EOM parameterisation of the left hand-side ground state.[259] The mean differences $\Delta\mu_{\mathrm{UCC2}}$ (less than $0.01\,e^2a_0^2$ for the excited states dipole moments) are smaller than the mean differences $\Delta\mu_{\mathrm{UCC3}}$ (about $0.30\,e^2a_0^2$ for the excited states dipole moments). The inclusion of the amplitude relaxation has a larger effect on the UCC3 results than on the UCC2 results, giving a much better agreement with the CCSD results, as it is shown in the plots.

In summary, it can be stated that the inclusion of the response of the wave function to the perturbation is important in the UCC3 case to obtain dipole moments which are close to the CCSD results up to $0.08\,e^2a_0^2$. For UCC2, the inclusion of the response of the wave function does not lead to an increase in accuracy.

Transition moments of water

In fig. 5.12, the transition moments from the ground state to the two excited states ($1^1A' \to 1^1A''$ and $1^1A' \to 2^1A''$) and the transition $1^1A'' \to 1^1A''$ are analysed. The left panel shows the results obtained in the EOM framework, while the right one shows results obtained with response theory. In table 5.9, a quantitative analysis of the mean differences between response theory and EOM transition moments is presented. For all orientations of the magnetic field, the transition from the ground state to the first excited state (black lines in fig. 5.12) is

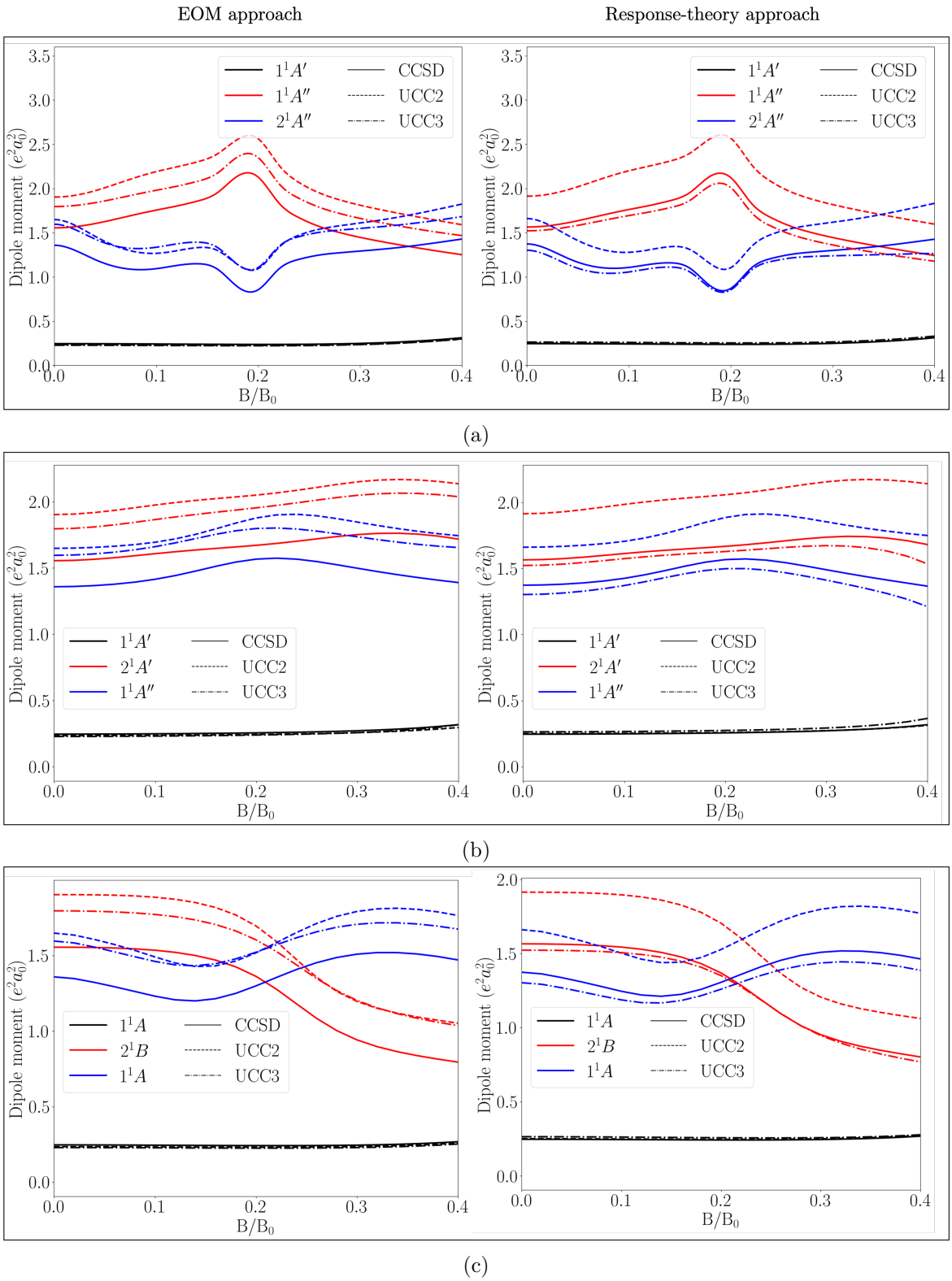

Figure 5.11: Electronic contribution to the dipole moments of the ground state and the lowest two excited states of H_2O in a strong magnetic field. For fig. 5.11a, fig. 5.11b, and fig. 5.11c, the magnetic field is oriented as shown in fig. 5.10a, fig. 5.10b, and fig. 5.10c, respectively. The left panels refer to calculations with the EOM approach, while the right panel refers to calculations performed with the response-theory approach.

fig. 5.10a	$\Delta\mu_{\mathrm{CCSD}}/e^2a_0^2$	$\Delta\mu_{\mathrm{UCC2}}/e^2a_0^2$	$\Delta\mu_{\mathrm{UCC3}}/e^2a_0^2$
$1^1A' \to 1^1A''$	-0.0002	0.0000	0.0004
$1^1A' \to 2^1A''$	0.0001	0.0000	0.0017
$1^1A'' \to 2^1A''$	-0.1271	-0.0237	-0.6525
fig. 5.10b			
$1^1A' \to 2^1A'$	-0.0005	0.0000	-0.0012
$1^1A' \to 1^1A''$	-0.0004	0.0000	-0.0025
$2^1A' \to 1^1A''$	-0.1469	-0.0247	-0.8822
fig. 5.10c			
$1^1A \to 1^1B$	0.0001	0.0000	0.0016
$1^1A \to 2^1A$	0.0001	0.0000	0.0001
$1^1B \to 2^1A$	-0.1429	-0.0243	-0.8397

Table 5.9: Differences between transition dipole moments obtained with the EOM and response-theory approach, calculated as $\Delta\mu = \Delta\mu = |\mu_{\mathrm{resp}}|^2 - |\mu_{\mathrm{EOM}}|^2$. All results are given in atomic units ($e^2a_0^2$). The orientation of the magnetic field is indicated through the corresponding figure in fig. 5.10.

stronger (i.e. larger values of $|\mu_{ij}|^2$) than to the second excited state (red lines). The lines are nearly coincident in most cases and the consideration of the response of the wave function to the perturbation does not affect the final result much, i.e., the differences including the response of amplitudes are negligible, of the order of $10^{-4}\ e^2a_0^2$.

As the ground state is totally symmetric, it can be shown that the allowed components for transitions in the field-free case are:

- $1^1A' \to 1^1A''$: only the μ_x component does not vanish;
- $1^1A' \to 2^1A''$: all components vanish, explaining the fact that the red lines in fig. 5.12 all start from zero.

In fig. 5.12a, the transition dipole moments are plotted as function of the magnetic field strength, with the field oriented perpendicularly to the molecular plane (fig. 5.10a). The two excited states both have A'' representation, and only the μ_z-component contributes to the transition dipole moment from the ground state, with A' symmetry. The transition $1^1A' \to 1^1A''$ is very similar for all methods, with mean deviations between UCC2 and CCSD of $-0.0010\ e^2a_0^2$ for the EOM approach and of $-0.0007\ e^2a_0^2$ for the response-theory approach. Mean deviations between the UCC3 and the CCSD transition dipole moments are even smaller: $-7\cdot10^{-5}\ e^2a_0^2$ for the EOM approach and of $0.0005\ e^2a_0^2$ for the response-theory approach. The transition $1^1A' \to 2^1A''$ shows larger but still quite small deviations; mean deviations between UCC3 and CCSD of $-0.0029\ e^2a_0^2$ for the EOM approach and of $-0.0012\ e^2a_0^2$ for the response-theory approach. The deviations in the UCC2 case are larger by an approximate factor of 5 with respect to the UCC3 case. Mean deviations between the UCC2 and the CCSD transition dipole moments are of $0.0054\ e^2a_0^2$ for the EOM approach and of $0.0053\ e^2a_0^2$ for the response-theory approach. The drastic changes in the magnitude occur around 0.2 B_0, where the two states are mixing.

In fig. 5.12b, for the transition $1^1A' \to 1^1A''$ only contributions involving the components μ_x, μ_y are allowed by symmetry, and the strength of the transition moment decreases in stronger magnetic fields. For $1^1A' \to 2^1A''$, only the μ_z component can contribute and increases for higher field strengths. In strong magnetic fields, UCC3 predicts somewhat larger, at most of $0.0324\ e^2a_0^2$, transition dipole moments. The mean differences between the

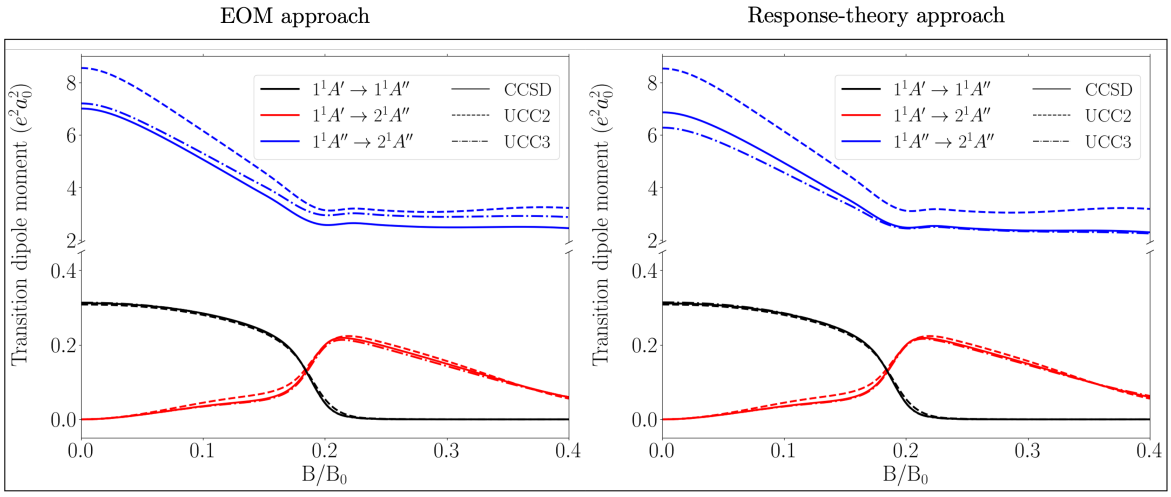

(a) H_2O in an increasing magnetic field directed along the bisector.

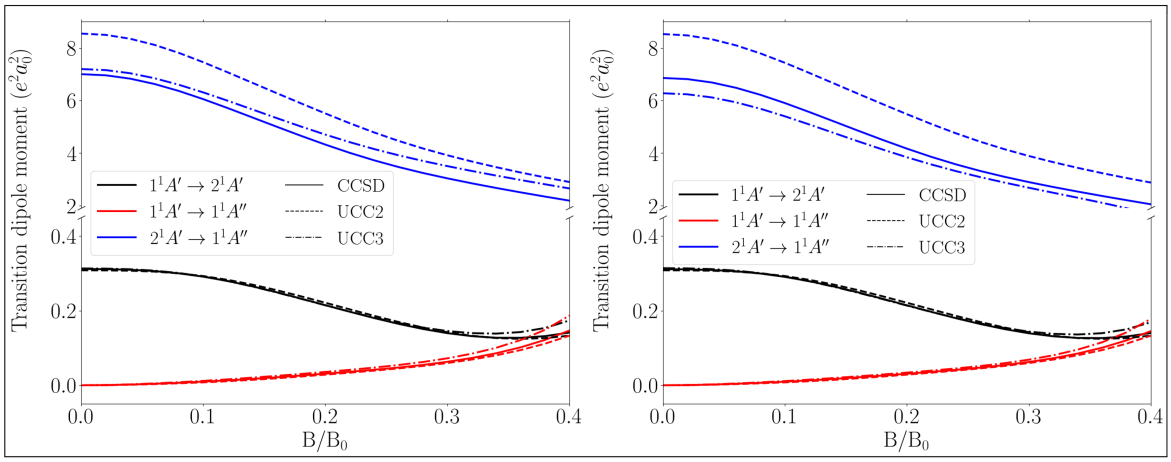

(b) H_2O in an increasing magnetic field directed along the plane.

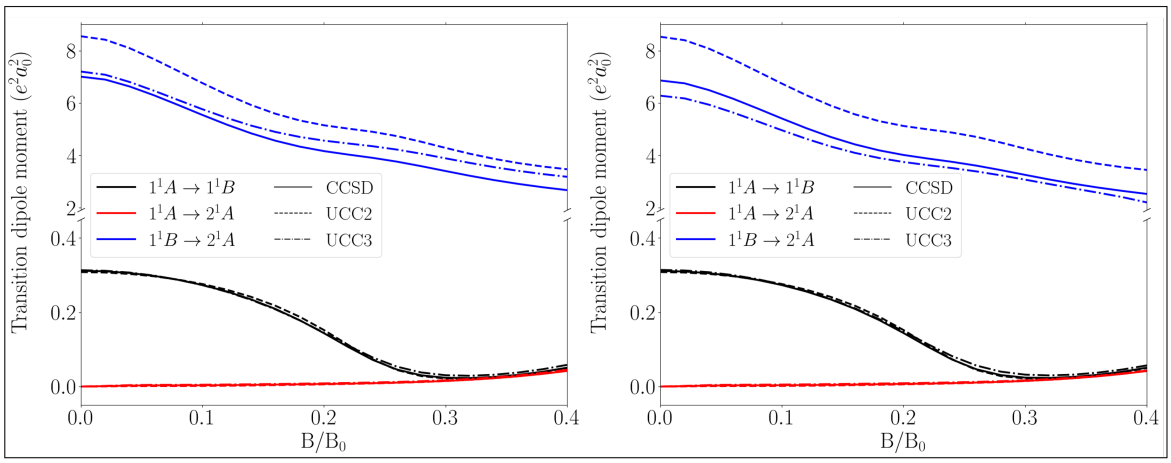

(c) H_2O in an increasing magnetic field directed along the perpendicular plane.

Figure 5.12: Transition moment from the ground state to the first two excited states of H_2O in a strong magnetic field of different orientations. For fig. 5.12a, fig. 5.12b, and fig. 5.12c, the magnetic field is oriented as shown in fig. 5.10a, fig. 5.10b, and fig. 5.10c, respectively. The left panels refer to calculations with the EOM approach, while the right panels refer to calculations performed with the response-theory approach.

UCC2 and CCSD results is of the order of $10^{-3}\, e^2a_0^2$, while the mean differences between the UCC3 and CCSD results is of the order of $10^{-4}\, e^2a_0^2$.

In fig. 5.12c, the transition moments for $1^1A' \to 1^1A''$ decrease in the increasing strong magnetic field. For the transition $1^1A' \to 2^1A''$ only transitions involving the component μ_z are allowed; the transition becomes slightly but not significantly stronger for high magnetic-field strengths (up to values of $|\mu_{ij}|^2 = 0.0418\, e^2a_0^2$). All three methods give the a qualitatively similar description of the dipole moment. The mean differences between the UCC2 and CCSD results is of the order of $10^{-3}\, e^2a_0^2$, while the mean differences between the UCC3 and CCSD results is of the order of $10^{-4}\, e^2a_0^2$.

The most intense transition is $1^1A'' \to 2^1A''$, plotted with the blue curves in fig. 5.12.

- field-free case: only μ_y is allowed;
- figs. 5.12a: μ_x, μ_y are allowed;
- figs. 5.12b: only μ_z is allowed;
- figs. 5.12c: μ_x, μ_y are allowed.

For this transition, the largest differences between response-theory results and EOM results are obtained. This observation agrees with the results obtained in the previous section (sec. 5.2.1), where the transitions between excited states showed the largest discrepancies between the EOM and the response-theory results. The transition dipole moments for $1^1A'' \to 2^1A''$ have absolute mean deviations between the response-theory and the EOM results of up to $0.88\, e^2a_0^2$ for UCC3, $0.02\, e^2a_0^2$ for UCC2 and $0.15\, e^2a_0^2$ for CCSD (in the orientation in fig. 5.10b). UCC2 has smaller discrepancies between the results obtained with the two approaches, due to the lower order of approximation of the method. Considering the symmetry of the states, the contributing components are predicted:
For all orientations, UCC2 considerably overestimates the transition dipole moment (the mean difference with respect to the CCSD results is $0.8780\, e^2a_0^2$ for the EOM approach, and $0.9814\, e^2a_0^2$ for the response-theory approach), compared to both CCSD and UCC3. The latter methods compare well to each other, especially when exploiting response theory. The mean difference of UCC3 results with respect to the CCSD results is $0.3256\, e^2a_0^2$ for the EOM approach, and $-0.1998\, e^2a_0^2$ for the response-theory approach. As seen for the transitions from the ground state, CCSD does not show major differences between the left and the right column of fig. 5.12, while the relaxation of the wave function amplitudes plays a non-negligible role for UCC3, where the discrepancies are much more relevant.

As a general consideration, it may be observed that the importance of including the response of the wave function to the perturbation is essential for UCC3 theory.

5.2.3 Lithium hydride

The comparison between UCC3 and CCSD can be continued through a discussion of the LiH molecule, whose ground- and lowest excited states have been discussed in sec. 5.1.2. UCC2 results are also shown, to investigate the effect of the truncation scheme on the results.

In fig. 5.13a the calculated dipole moments of the lowest four singlet states are plotted against the magnetic field. The molecular properties discussed in this section are all calculated considering the relaxation of the amplitudes. The description of the ground-state dipole moment (red line in the plot) is mostly agreeing for UCC3 and CCSD, where the maximal difference in magnitude is $0.20\, e^2a_0^2$. At larger magnetic field strengths, the UCC2 method shows a significant deviation from the other methods, giving a dipole moment larger by at most $0.41\, e^2a_0^2$ with respect to CCSD and UCC3. Major differences are observed for

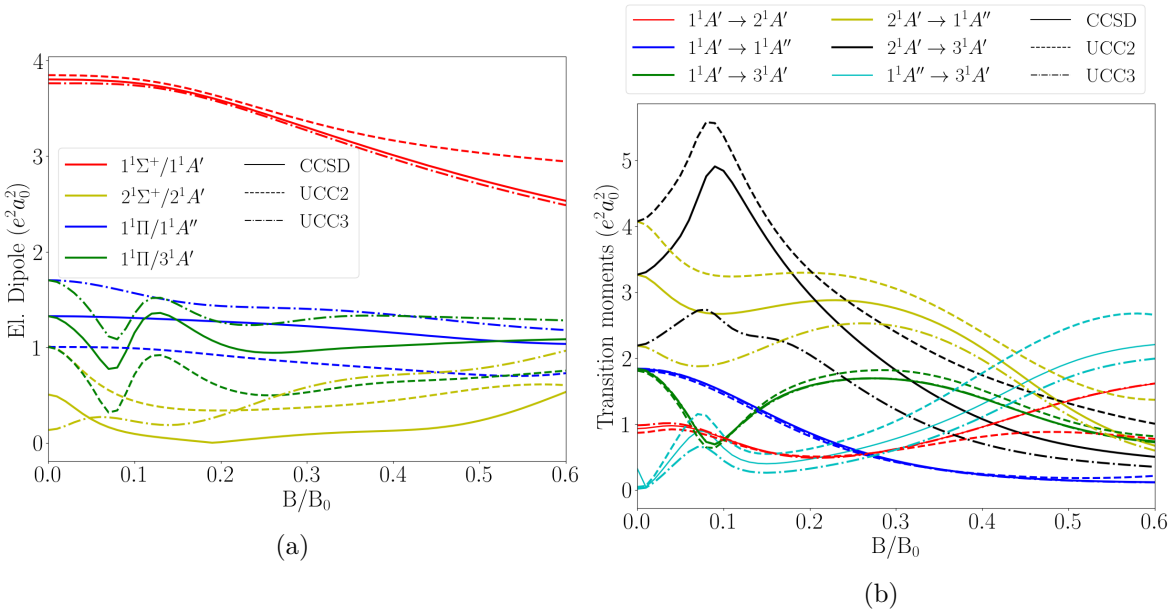

Figure 5.13: The LiH molecule in a varying magnetic field perpendicular to its bond axis. The bond length has been optimised as in ref. 115. Fig. 5.13a shows the dipole moments of the ground and lower excited states are shown. In fig. 5.13b, all transition moments between the analysed states are shown.

the excited states, where larger shifts occur. For the lowest excited state, $2^1A'$, the shape of the dipole moment is qualitatively different between the three methods. By analysing the direction of the electronic contribution to the dipole moment, it is noted that the CCSD and the UCC2 dipole moments are pointing in the opposite direction than the UCC3 one for field strengths smaller than 0.2 $e^2a_0^2$. The lines of the CCSD and the UCC3 calculation become parallel but shifted to each other, if the CCSD line is mirrored around the x-axis. The dipole moments of the former degenerate 1Π states present the same shape for all three methods, with the UCC2 results shifted to smaller values and the UCC3 ones to higher values. For both methods, the maximum difference with respect to CCSD is of about 0.3 $e^2a_0^2$, but is on average smaller for UCC3 than UCC2. The avoided crossing observed in fig. 5.1b at about 0.1 B$_0$ affecting state $3^1A'$ is evident in the huge change in magnitude of the dipole moments around that field strength (green line).
Concluding the analysis of the description of the dipole moments, the shape of the lines is not always the same for the three methods: it is fairly comparable for CCSD and UCC2, while major differences are found for UCC3. In particular, different directions of the dipole moment are obtained with different methods.

The transition dipole moments between the investigated states are pictured in fig. 5.13b. The same behaviour as for the water molecule is observed. For transitions involving the electronic ground state (red, blue and green lines in the plot), the three methods present very small differences. The transitions between excited states are more affected by the specific electronic method used. In agreement with the observations discussed for the dipole moments, the UCC2 results are always larger than the CCSD results, while UCC3 gives the smallest transition dipole moment. For the transition involving the state $3^1A'$ (green, black and light blue lines), the presence of the avoided crossing around 0.1 B$_0$ is noticeable in an abrupt change in magnitude of the properties. As in the $B = 0$ case, state $1^1\Pi/1^1A''$ and $1^1\Pi/3^1A'$ are degenerate, also the transitions $1^1A' \rightarrow 1^1A''$ (blue) with $1^1A' \rightarrow 3^1A'$ (green)

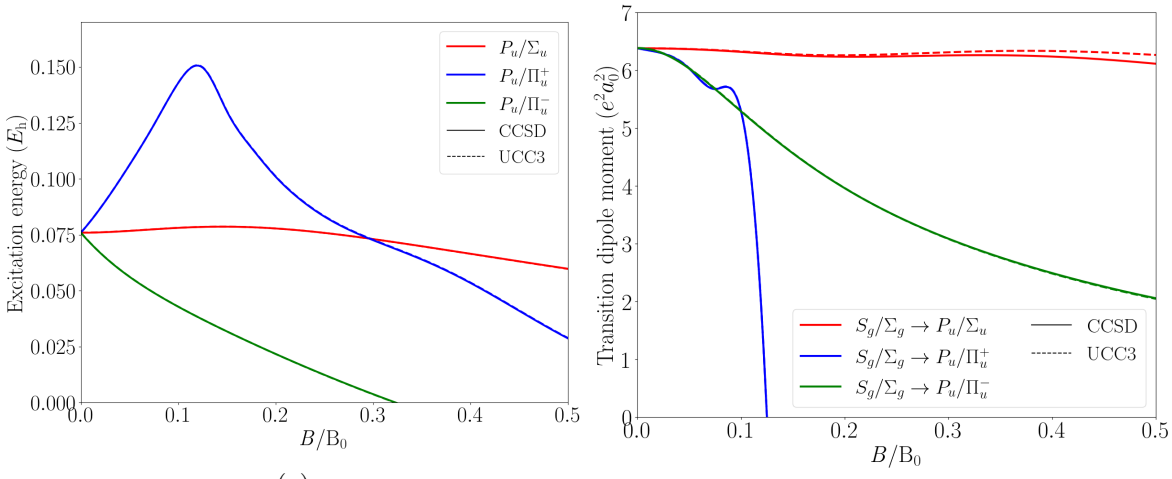

Figure 5.14: On the left, the excitation energies of the sodium atom in a varying magnetic field. On the right, the transition dipole moments from the ground state to the considered excited states are shown. The labelling of the states refers to the computational point group, C_{4h}.

and $2^1A' \to 1^1A''$ (yellow) with $2^1A' \to 3^1A'$ (black) depart from the same starting value.

The investigations on the systems H_2O and LiH allows to formulate some general observations concerning the comparison between CCSD and UCC3. The agreement between the two methods is much better when the response-theory approach is exploited. It is observed that both for the calculation of dipole and transition dipole moments, the UCC3 results are changing by a larger extent when including the response of the wave function to the perturbation. The lower order of approximation characterising UCC2 leads to a general overestimation of the single-state and transition dipole moments. The inclusion of the response of the wave function to the perturbation is essential for UCC3 to get more accurate results, which in general have smaller magnitude than the CCSD ones. With these considerations, the UCC3 response theory can be exploited to calculate the properties of molecules which exhibit unphysical results when treated at the CC level of theory.

5.2.4 Sodium atom

The last system here discussed as a benchmark for the accuracy of the UCC3 method is the sodium atom.[98,114] In this section, the discussion focuses on the splitting of the degenerate P_u states. These, when in a magnetic field, undergo orbital-Zeeman splitting, giving the states $\Pi_u^+, \Pi_u^-, \Sigma_u$. The magnetic field is chosen to vary up to 0.5 B_0, a magnitude which is realistic for a magnetic white dwarf star. Calculations have been performed with the uncontracted aug-cc-pCVTZ basis set,[266–268] both at the CCSD and at the UCC3 level of theory. For the transition dipole moment calculations, response theory has been exploited.

In fig. 5.14a, the excitation energies of the Π-states are plotted. It can be observed that the magnetic field leads to splitting of the degenerate states. The upper component is observed to have a maximum at about 0.15 B_0, after which the excitation energy decreases for this component as well. The lower component is crossing the ground state at 0.325 B_0; for larger field strengths, its excitation energy becomes negative. From the plot, it appears that the energy calculations performed with CCSD and UCC3 agree, as the lines lie on top of each other.

In fig. 5.14b, the transition dipole moments from the ground state to the considered excited states are plotted. Starting from the same value for the field-free case, the transition dipole moment $S_g/\Sigma_g \rightarrow P_u/\Sigma_u$ remains basically constant for the considered field strengths. For magnetic fields larger than 0.25 B_0, the results differ slightly, with larger values for the UCC3 calculation (the largest difference here is 0.153 $e^2a_0^2$). The transition $S_g/\Sigma_g \rightarrow P_u/\Pi_u^+$ abruptly goes to zero after the observed turnover in the excitation energy. For all transitions, the agreement between the two methods is very good.

The discussion of this atom of astrochemical relevance shows that UCC3 is a valid method for the study of properties in a strong magnetic field. In fact, these calculations show comparable results as those in ref. 98, and could be used as an interpretation tool for astrochemical spectra of magnetic white dwarf stars.

5.2.5 Si^{2+} ion

In this section, the UCC method is exploited to analyse the silicon dication, which has been observed among others in the spectra of white dwarf stars since the early 1980s.[276] In particular, the investigation of this section focuses on the discussion of a particular transition, which in the CC framework is characterised by a negative transition probability. First, the silicon dication Si^{2+} is considered in the field-free case; then, the discussion will be continued considering a magnetic field up to 0.4 B_0. All calculations are performed with the uncontracted aug-cc-pCVTZ basis set,[266–268] at the CCSD and UCC3 levels of theory. For the calculation of the desired states, the modified Davidson algorithm described in ref. 207 was exploited to determine multiple roots simultaneously. For the property calculation, the response-theory approach has been applied.

The Si^{2+} dication has a ground-state configuration given by [Ne] $3s^2$. Here the transitions $^1\Pi_u$([Ne] $3s^1$ $3p^1$) $\rightarrow$ $1^1\Sigma_g$([Ne] $3p^2$) and $^1\Pi_u$([Ne] $3s^1$ $3p^1$) $\rightarrow$ $2^1\Sigma_g$([Ne] $3s^1$ $4s^1$) are considered, as these transition are reported to be quite intense in the NIST database.[277] However, the S_g states are characterised differently by the two methods. In the CCSD case, both states, i.e. 1^1S_g and 2^1S_g, have a mixed configuration, with contributions from [Ne] $3s^1$ $4s^1$ and [Ne] $3p^2$.
On the other hand, the UCC3 calculation clearly distinguishes the two states 1^1S_g([Ne] $3p^2$) and 2^1S_g([Ne] $3s^1$ $4s^1$), which are not mixing. Looking at the data in the NIST database, it is observed that the states are also found to be mixing, but by a smaller extent (NIST reports a leading percentage of the [Ne] $3p^2$ component in the 1^1S_g state of about 82%, while the CCSD calculations gives a weight of 60% to the leading EOM vectors describing the double excitation). The excitation energies computed at the CCSD and UCC3 level of theory are compared to the experimental data in tab. 5.10. The state $^1\Pi_u$([Ne] $3s^1$ $3p^1$) is accurately described both by CCSD and by UCC3, with higher accuracy for CCSD. The two Σ_g states compare rather badly to the experimental data, as the CCSD method overestimates the mixing between the states, while the larger energetic difference between the two states found with UCC3 leads to results quite distant from the NIST results. This behaviour is not very surprising, as for both methods the restriction of the excitation space to single and double excitations implies that the description of doubly-excited states is rather bad. For a better description, methods as CC3 and its unitary analogue should be exploited and/or developed.

The transition $^1\Pi_u$([Ne] $3s^1$ $3p^1$) $\rightarrow$ $2^1\Sigma_g$([Ne] $3s^1$ $4s^1$) is observed at 1312.6 Å, while the calculated values are 1316.3 Å for CCSD and 1320.7 Å for UCC3. However, the calculated transition probability $\mu_{IJ} \cdot \mu_{JI}$ is negative for CCSD, therefore providing an example of an unphysical result due to the non-Hermiticity of CC theory. The magnitude of the UCC3 oscillator strength, a dimensionless quantity defined as $f_{ij} = \frac{2m_e}{3\hbar^2}\Delta E_{IJ}|\mu_{IJ}|^2$ (where m_e is

	NIST	CCSD	UCC3
$3s^1\ 3p^1$	82884.41	82940.47	81708.59
$3p^2$	153444.23	157486.33	136086.70
$3s^1\ 4s^1$	159069.61	158911.99	157426.21

Table 5.10: Excitation energies from the ground state of the NIST database[277] are compared to the excitation energies obtained with the CCSD and UCC3 methods, computed with the uncontracted aug-cc-pCVTZ basis set. All data are reported in cm^{-1}.

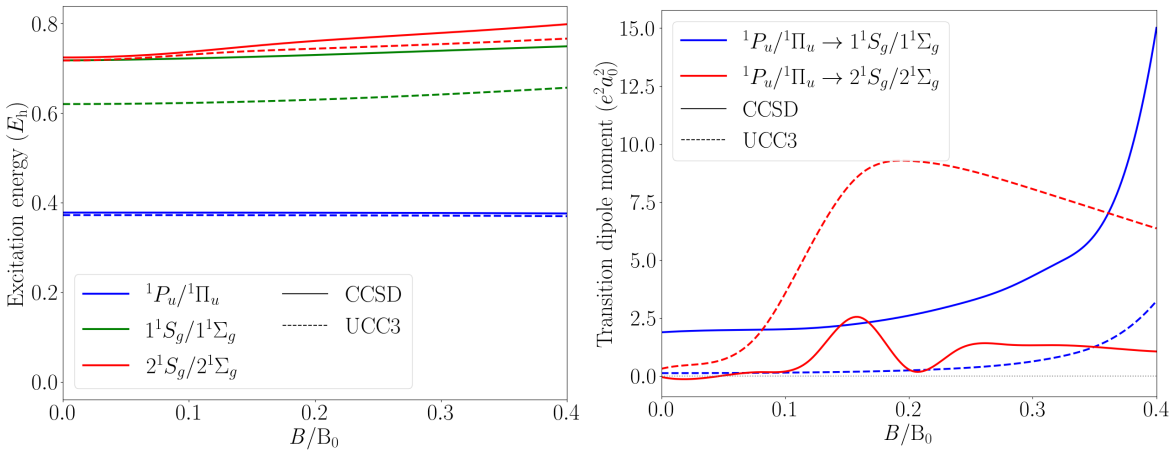

(a) (b)

Figure 5.15: On the left, the excitation energies of the $^1P_u/^1\Pi_u$, $1^1S_g/1^1\Sigma_g$ and $2^1S_g/2^1\Sigma_g$ states of the Si^{2+} atom, in a varying magnetic field, are shown. On the right, the transition dipole moment $^1\Pi_u([Ne]\ 3s^1\ 3p^1) \to {}^1\Sigma_g([Ne]\ 3s^1\ 4s^1)$ is displayed. Calculations exploit the CCSD and UCC3 response-theory approach for the investigation of molecular properties.

the mass of the electron),* is 0.072 and can be compared to the data reported in the NIST database, 0.057. While the UCC3 transition energy is further away when compared to CCSD; Both UCC3 and CCSD oscillator dipoles are of the same order of magnitude. Moreover, the oscillator strength at UCC3 is close to the experimental value while the CCSD predictions are unphysical.

The transition $^1\Pi_u([Ne]\ 3s^1\ 3p^1) \to 1^1\Sigma_g([Ne]\ 3p^2)$ is reported at 1417.2 Å, while the calculated values are 1341.5 Å for CCSD and 1839.0 Å for UCC3. Neither of them is in good agreement with the experimental data. The comparison of the transition dipole moments with the NIST database, which reports an oscillator strength of 0.218, shows that CCSD cannot give an accurate description of the transition, as CCSD gives an oscillator strength of 0.427 and UCC3 0.021. The transition $^1\Pi_u([Ne]\ 3s^1\ 3p^1) \to {}^1\Sigma_g([Ne]\ 3s^1\ 4s^1)$ can be discussed when the Silicon dication is in a finite field, up to 0.4 B_0. In fig. 5.15a, the energy of the excited states $^1P_u/^1\Pi_u$, $1^1S_g/1^1\Sigma_g$ and $2^1S_g/2^1\Sigma_g$ are plotted as a function of the magnetic-field strength. For the $^1\Pi_u$ state the difference between the two methods remains small. The differences in the description of the excited states Σ_g lead to a large shift of the excited state energies, though maintaining a parallel evolutions. In fig. 5.15b, the transition dipole moments $^1\Pi_u([Ne]\ 3s^1\ 3p^1) \to 2^1\Sigma_g([Ne]\ 3s^1\ 4s^1)$ and $^1\Pi_u([Ne]\ 3s^1\ 3p^1) \to 1^1\Sigma_g([Ne]\ 3p^2)$ are plotted.

Starting from the transition $^1\Pi_u([Ne]\ 3s^1\ 3p^1) \to 2^1\Sigma_g([Ne]\ 3s^1\ 4s^1)$, the red lines in the

*In atomic units, $m_e = 1$ and $\hbar = 1$

plot, it is clearly shown that the CCSD method gives unphysical results on the left side of the plot, up to 0.3 B_0. One has to note that the plotted quantity is $|\mu_{IJ}|^2 = \mu_{IJ} \cdot \mu_{JI}$. Due to the fact that CCSD has different parameterisations for the right and left eigenstates, the relation $\mu_{IJ} \neq \mu_{JI}$ holds, allowing for the unphysical results $|\mu_{IJ}|^2 < 0$ to occur. This is an example of the limitations of the non-Hermitian CC theory when studying systems in a magnetic field. The negative and oscillating results are found for transitions for which the μ_{IJ} value is very far from being the adjoint of μ_{JI}, being opposite in sign or various orders of magnitude different. The UCC3 results are real and their value is increasing in a stronger magnetic field.

The transition $^1\Pi_u([\mathrm{Ne}]\ 3s^1\ 3p^1) \rightarrow 1^1\Sigma_g([\mathrm{Ne}]\ 3p^2)$ is plotted in blue for CCSD and UCC3. It is shown that the lines have a similar behaviour, but are shifted with higher values for the CCSD line. The small magnitude of the UCC3 transition is motivated by the fact that for UCC3 this is a purely two-electron transition, which is not true for CCSD, where the mixing introduces also a partial one-electron transition contribution.

For the Si^{2+} dication, the excited states with at least a partial doubly-excited character cannot be very accurately described by UCC3 and CCSD, as it had already been observed for the CH^+ cation in sec. 5.1.3. This is due to the consideration of just singly- and doubly-excited determinants in the definition of the cluster operator. In the framework of this approximation, Si^{2+} offers a example of a case in which CC theory cannot be applied to the calculation of transition dipole moments. It is important to emphasize that these results could not be foreseen by just analysing the energies of the excited states, which are here real for both UCC3 and CCSD. Under these circumstances, the Hermiticity of UCC represents a valid alternative to standard CC theory, in order to obtain physically interpretable results.

5.2.6 Methylidyne ion

In this section, another example of a system for which CC response theory obtains negative transition probabilities is analysed, the CH^+ cation. Its energies in a strong magnetic field have already been studied in sec. 5.1.3. The discussion focuses here on the comparison between the dipole moments and transition dipole moments obtained via the CCSD and the UCC3 method, respectively. investigating the importance of a response-theory approach with respect to the EOM one.

Electronic dipole moments

The understanding of the behaviour of the CH^+ cation in a magnetic field oriented at an angle of $\alpha = \pi/6$ with respect to its bond axis, gained in sec. 5.1.3, is a prerequisite for the analysis of ground- and excited-state properties. It has been shown in sec. 5.1.3 that, depending on α, various avoided crossing occur between the ground and excited states.

In fig. 5.16, the dipole moments (calculated with respect to the center of mass) corresponding to the states analysed in chapter 5.1.3 are displayed (the same colours are maintained for the sake of clarity). In fig. 5.16a the dipole moments of the ground state 1^1A (purple line in the plot) and the lowest excited state 2^1A (red line in the plot) are shown. In fig. 5.2 it was observed that the CCSD, UCC2, and UCC3 energy results for these two states did not show significant discrepancies. However, when looking at the dipole moments, the results differ also from a qualitative point of view. For the ground state 1^1A (purple line in the plot), CCSD and UCC2 predict rather similar dipole moments. However, the curve describing the UCC3 dipole moment has quite a different shape, with differences up to $0.04\, e^2 a_0^2$. As for the excited state 2^1A (red line in the plot), the CCSD and UCC3 results show the same trend of decreasing dipole moment, while the UCC2 results show a qualita-

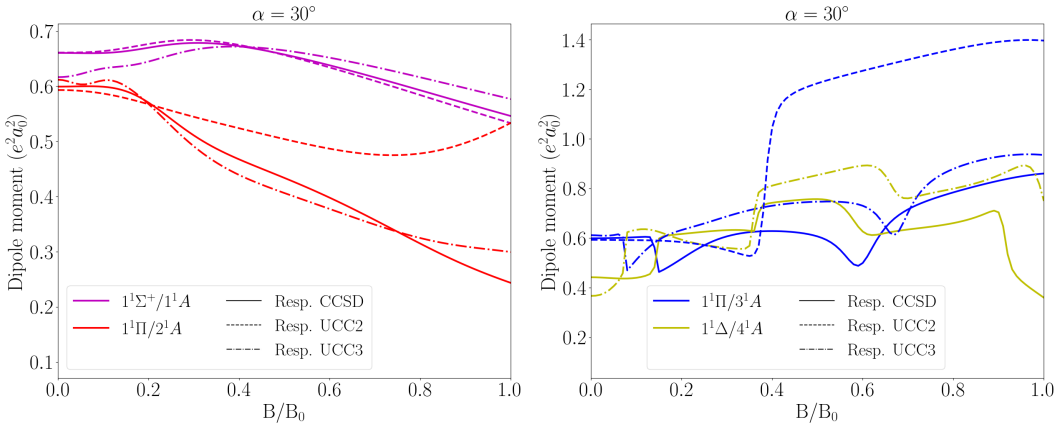

(a) (b)

Figure 5.16: Dipole moments of the CH^+ cation in a magnetic field oriented at $\alpha = \pi/6$ with respect to its bond axis. The first four excited singlet states, those shown in fig. 5.2b, are plotted with the CCSD, UCC2 and UCC3 methods. Results are given in atomic units ($e^2a_0^2$).

tively different trend, with an increase for field strengths larger than 0.8 B_0. Note that the differences for field strengths between 0 B_0 and 0.2 B_0 for the UCC3 dipole moment are a consequence of the slight mixing of the first excited state with the avoided crossing of the states 3^1A and 4^1A, which transfers some doubly-excited character also to the state 2^1A.

In fig. 5.16b, the dipole moments of the states 3^1A and 4^1A are shown. As seen in fig. 5.16a, these states experience two avoided crossings, at about 0.15 B_0 and 0.7 B_0. The effect of the avoided crossings is evident from the inspection of the dipole moments: in correspondence to the avoided crossings, abrupt changes in the magnitude of the dipole moments is observed, around B=0.1 B_0 and around B=0.6 B_0. At the avoided crossings, the states 3^1A and 4^1A exchange their character; also the properties of the two states are exchanged, as shown by the curves, which could be continued one into the other. The dipole moment of state 4^1A also shows a discontinuity around 0.4 B_0. As discussed in sec. 5.1.3, here a mixing with higher-lying states occurs, which explains this discontinuity. For most part of the explored magnetic field range, UCC3 predicts larger dipole moments for these two states than CCSD. As could be expected from the plot in fig. 5.2b, UCC2 fails in the description of the dipole moment of these states, as it can only describe the single-excitation component of the state. UCC2 therefore describes the properties of the mixing states as the envelope of the properties of 3^1A and 4^1A.

Summarising the discussion of single-state dipole moments, it is found out that this property shows the CCSD and UCC3 obtain qualitatively similar results, while UCC2 is not able to describe doubly-excited states, and thus fails in the description of their properties.

Transition dipole moments – response theory vs EOM theory

In fig. 5.17b, the transition dipole moments from the ground state to the first three excited states are shown, calculated for CCSD, UCC2 and UCC3 both using the expectation-value and the response-theory approach, respectively (figs. 5.17a-5.17b). The transition dipole moments for $1^1A \to 2^1A$ (red lines in the plots) are described with similar precision by all three methods, and the inclusion of the response of the wave function to the perturbation does not affect qualitatively the results. The transition dipole moments of $1^1A \to 3^1A$ and

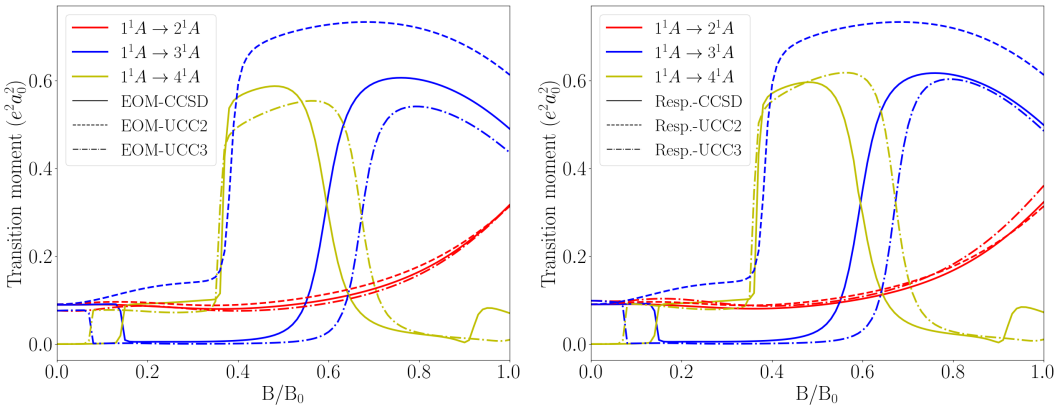

(a) Expectation-value approach (b) Response-theory approach

Figure 5.17: Transition dipole moments between the ground state 1^1A and the first three singlet excited-states of the CH^+ cation, in a magnetic field oriented at $\alpha = \pi/6$ with respect to the bond axis. The magnetic field strength varies between 0 B_0 and 1.0 B_0. The comparison between CCSD, UCC2 and UCC3 is visible for each transition. In fig. 5.17a, transition dipole moments are computed with the expectation-value approach (EOM approach), while in fig. 5.17b the response theory has been exploited.

$1^1A \to 4^1A$ reflect the avoided crossings observed in fig. 5.2b. The discontinuities at about 0.15 B_0 and 0.70 B_0 are explained by the exchange of singly- and doubly-excited characters between the target states. The observed mixing of state 4^1A with the higher-lying states causes the large change in transition dipole moment around 0.4 B_0. The small discontinuity in the right part of the plots, present only in the CCSD case, may be explained by the mixing of state 4^1A with higher-lying states, which was observed in fig. 5.2b. This mixing was not found for the UCC2 and UCC3 methods and therefore no discontinuity is observed for the UCC2 and UCC3 dipole moments. As expected, UCC2 only describes the dipole moment of the single-excitation components of the 3^1A and 4^1A states. In the case of the EOM calculation (fig. 5.17a), CCSD and UCC3 are in good agreement. The shift between the two curves is caused by the different magnetic field strengths at which the avoided crossings occur. In the case of response formulations, discrepancies between CCSD and UCC3 are observed in fig. 5.17b. While the CCSD results are not affected much by the response, the UCC3 transition dipole moments show a larger difference between the EOM and response-theory results. In particular, after the interaction with the higher-lying states at 0.4 B_0 and 0.7 B_0, the UCC3 results match much better the CCSD results, showing a good agreement of the response-theory results.

In fig. 5.18 the transition dipole moments between excited states are displayed. Here the transitions $2^1A \to 3^1A$ (orange line in the plots) and $2^1A \to 4^1A$ (green line in the plots) are analysed. The shape of the transition dipole moments can again be motivated by the presence of avoided crossings characterising states 3^1A and 4^1A at about 0.15 B_0 and 0.7 B_0. The major differences between the expectation-value and the response-theory approach (figs. 5.18a-5.18b) are as follows. In the EOM case, the transition dipole moment for $2^1A \to 4^1A$ gives very small values ($10^{-2}\ e^2a_0^2$) for the unitary approaches, while it starts out at about 0.2 $e^2a_0^2$. for CCSD in the magnetic-field range of 0.0 B_0-0.15 B_0. Furthermore, major differences in the results are found in the higher-field region of the plot. For fig. 5.18b, the major difference in this plot is given by the peak at about 0.2 B_0 for UCC3. This feature is explained by recalling the discussion in sec. 5.1.3. Here it was pointed out that state 2^1A mixes with the higher-lying 3^1A and 4^1A states, which for UCC3 lie at lower energies than

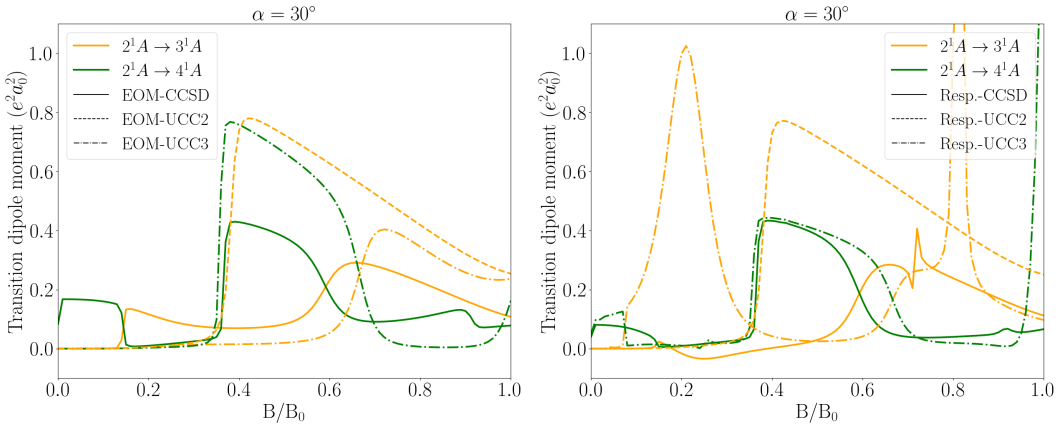

(a) Expectation-value approach (b) Response-theory approach

Figure 5.18: Transition dipole moments between the first excited singlet state 2^1A and the higher-lying states 3^1A and 4^1A of the CH^+ cation, in a magnetic field oriented at $\alpha = \pi/6$ with respect to the bond axis. The magnetic field strength varies between 0 B_0 and 1.0 B_0. The comparison between CCSD, UCC2 and UCC3 is shown for each transition. In fig. 5.18a, transition dipole moments are computed with the expectation-value approach (EOM approach), while in fig. 5.18b the response-theory formulation has been exploited.

for CCSD and hence influences it more strongly. The influence of the doubly-excited state results in this feature for the transition dipole moment calculation. In this range, on the other hand, CCSD yields a negative transition dipole moment.

After the second avoided crossing, at about 0.7 B_0, both CCSD and UCC3 present a singularity point (for UCC3, the shape would be the same as for the CCSD curve, but the plotting of the absolute value squared takes the negative peak of the singularity to positive values). These singularities are explained by the fact that transition dipole moments are calculated from the poles of response functions. In the presence of two excited states with a very similar excitation energy, singularities in the response functions of the amplitudes are expected and present in the literature.[278] Since these methods are approximations of the exact response formulation, singularities are expected to occur also for CCSD and UCC3.

Lastly, in the region around 1 B_0 the description is quite different between CCSD and UCC3, but this is a consequence of the fact that CCSD is already interacting with higher-lying states (as was discussed from fig. 5.2b), while this mixing happens at higher field-strengths for the UCC methods.

Summarising the discussion about transition dipole moments for the CH^+ cation, it is observed that the response of the wave function to the perturbation is of major importance for the transitions between excited states, while for transitions from the ground state the behaviour does not change. Transitions between singly-excited states are faithfully reproduced by all methods, while the discrepancies in the description of doubly-excited states leads to major discrepancies in the properties. Hence, UCC2 cannot be used for the calculation of properties of states which possess a double-excitation character. CCSD suffers from unphysical results, as the quantity $|\mu_{IJ}|^2$ can become negative. This problem cannot occur for the unitary formalism, by construction. However, one has to note that, while for CCSD the cheaper EOM-approach gives a quite accurate description of the properties when compared to the response-theory approach, this is not the case for UCC3, where response theory is essential to obtain good accuracy.

Chapter 6

Magnetic Circular Dichroism

Magnetic circular dichroism (MCD) spectroscopy measures the property of all substances to rotate the plane of circularly polarised light by a certain angle when exposed to an external magnetic field.[121] This spectroscopy can be compared to the more known circular dichroism (CD) spectroscopy, where left and right circularly polarised light interact differently with a chiral molecule. The advantage in MCD is that the molecule is no longer required to be chiral, as the presence of the magnetic field causes the left and right circularly polarised light to interact differently with any molecular system. MCD is largely used to investigate the electronic structure of molecules, both in the ground and in the excited states. It represents a valuable tool complementing other absorption spectroscopies, as it can detect overlapping transitions or transitions having a detectable differential absorption, despite having an absolute absorption too weak to be detected by other spectroscopies. Calculated spectra are therefore interesting to compare to experimental measurements.[117–119] However, it has been observed in the literature that the presence of the solvent results in very broad peaks,[124] complicating the assignment of the measured peaks to the computed ones. Therefore, the agreement of experiment and calculation is often already claimed if the peaks have the same sign, either above or below the x-axis.

The previous chapters have extensively described the development of a finite-field method, by which molecules in a magnetic field can be described. This section shows that the applicability of these methods goes widely beyond the characterisation of magnetic white dwarfs. In fact, it can be exploited also in the case of small magnetic fields, as those used for an MCD measurement, which are typically of the order of $10^{-4}\,\mathrm{B}_0$.

In fig. 6.1, a schematic representation of an MCD experiment is shown.[279] A monochromatic light beam is passed through a so-called Rochon prism linear polariser, which separates the incident radiation into two linear polarised components, perpendicular to each other. The perpendicular beam hits a photomultiplier (PMT), which measures the intensity of the incident radiation. The other component of the linear polarised beam passes through a photoelastic modulator (PEM), oriented in such a way to cause a phase shift alternating between $\frac{1}{4}\lambda$ and $-\frac{1}{4}\lambda$ of one of the two orthogonal components of the linear polarised light. This phase shift gives origin to a circularly polarised light beam, which oscillates between right and left circular polarisation in a periodic manner with frequency ω, as shown in fig. 6.2. The radiation then travels through the sample under inspection, which is inserted into a constant magnetic field, oriented along the direction of propagation of the light beam. The remainig radiation is then recorded by another PMT, recording the intensity of the exiting beam. An amplifier converts this intensity into a two-component voltage. A direct current voltage is obtained from the intensity of the radiation which passed through the

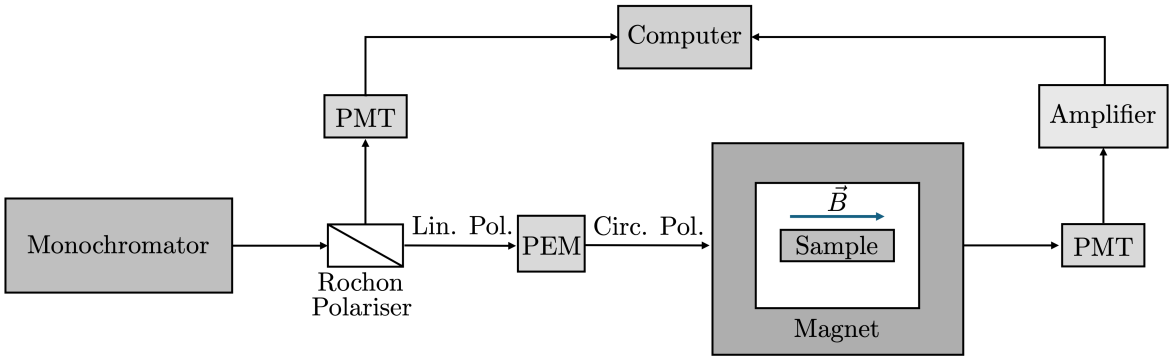

Figure 6.1: Schematic representation of a magnetic circular dichroism (MCD) experiment. Monochromatic light is separated into two linearly polarised components by a Rochon polariser. The perpendicular component is used to measure the initial intensity of the radiation with a photomultiplier (PMT). The other component is transformed into circularly polarised light through a photoelastic modulator (PEM). This radiation is then shone on a sample, inserted into a constant magnetic field oriented along the direction of propagation of the beam. Finally, another PMT records the exiting intensity from the sample, which is converted into a two-component voltage through an amplifier. A direct current voltage is obtained from the intensity of light which passed through the sample. In the case of a difference in absorption between the right and left circularly polarised beam, also an alternating current is recorded, oscillating at the frequency registered by the PEM. From the information on the initial and final light beams, a computer calculates the differential absorption.

sample. If a difference in absorption between the left and right circularly polarised beams is present, an alternating current is measured, with frequency corresponding to ω. A computer can then calculate the differential absorption from the data collected on the initial and the final radiations. The actual experiment is performed with a more sophisticated set up; for further discussion see, for example, the review in ref. 280.

6.1 MCD theory

From a theoretical point of view, the understanding of magnetic circular dichroism derives from the explanation of how a sample absorbs a specific radiation. From the Lambert-Beer law, the absorbance A is proportional to the concentration [c] of the solution in the sample

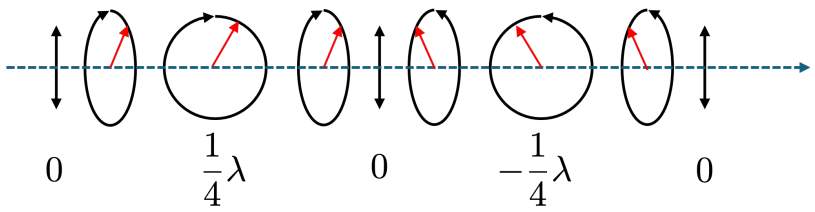

Figure 6.2: Schematic representation of the effect of the photoelastic modulator (PEM) on linear polarised light. The PEM causes an alternating phase of $\frac{1}{4}\lambda$ and $-\frac{1}{4}\lambda$ to one of the two perpendicular components (electric and magnetic fields) of the beam, giving origin to a circularly polarised light beam which oscillates between right and left circular polarisation. The picture shows the path described by the electric-field vector (in red): the radiation starts from being linearly polarised, becomes elliptically polarised, then circularly polarised, *etc.*

and the length of the radiation path l

$$A = \epsilon[\mathrm{c}]l = \log\left(\frac{I_0}{I}\right). \tag{6.1.1}$$

ϵ is the molar extinction coefficient of the medium, I is the intensity of the monochromatic beam, I_0 refers to the intensity measured before the absorption. In order to establish a link between an experimentally measured and a calculated spectrum, the discussion on the calculation of MCD spectra starts from quantum mechanical principles.

6.1.1 The absorption coefficient

Moving to the microscopic frame, the sample is considered to be sufficiently diluted to neglect interactions between molecules and accounting only for the interaction with the magnetic field. The variation in intensity per length of a light beam of given energy can be described as the difference between the number of molecules emitting a photon and those absorbing it

$$-\frac{\mathrm{d}I}{\mathrm{d}l} = h\nu(N_a P_{aj} - N_j P_{ja}), \tag{6.1.2}$$

where N_a labels the number of molecules in state $|a\rangle$ and N_j the number of molecules in state $|j\rangle$; P_{aj} refers to the probability per unit time of the transition $|a\rangle \rightarrow |j\rangle$ and P_{ja} to the probability of the transition $|j\rangle \rightarrow |a\rangle$. Here ν is the frequency of the propagating wave. The differential formulation of the Lambert-Beer law $\frac{\mathrm{d}I}{I} = -\kappa \mathrm{d}l$,[281,282] can be combined with eq. 6.1.2 to give an expression for the absorption coefficient $\kappa(\nu)$ as

$$\kappa(\nu) = \frac{h\nu}{I(\nu)}(N_a - N_j)P_{aj}. \tag{6.1.3}$$

where it has been assumed that the probability P_{aj} equals the probability P_{ja}, implying that the transitions between state $|a\rangle$ and state $|j\rangle$ are equally probable. The conservation of energy is expressed in electrodynamics by means of Poynting's theorem,[283] stating that the intensity of the light beam after the absorption is the time average of the Poynting vector, a quantity defined as $\mathbf{S} = 4\pi\varepsilon_0 \frac{c}{4\pi} \mathrm{Re}\{\mathbf{E}(\nu)\} \times \mathrm{Re}\{\mathbf{B}(\nu)\}$. This relation allows to express the intensity as

$$I(\nu) = 4\pi\varepsilon_0 \left| \frac{c}{4\pi} \{\mathrm{Re}\{\mathbf{E}(\nu)\} \times \mathrm{Re}\{\mathbf{B}(\nu)\}\}_T \right|, \tag{6.1.4}$$

where the T index indicates the time average. The time average is needed to find a time-independent expression for the intensity, in order to eliminate the time-dependence coming from the fields. The fields can both be expressed through the vector potential as $\mathbf{E} = -\frac{1}{c}\frac{\partial \mathbf{A}}{\partial t}$ and $\mathbf{B} = \nabla \times \mathbf{A}$. The vector potential for an electromagnetic wave, propagating at velocity c in vacuum along the positive z axis is

$$\mathbf{A} = \mathrm{Re}\{\mathbf{A}_0\} e^{2\pi i\nu(t - \frac{z}{c})}. \tag{6.1.5}$$

The intensity entering the equation for the determination of κ can be expressed as a function of the field parameters by substituting the expression above in eq. 6.1.4 and performing the time average

$$I(\nu) = 4\pi\varepsilon_0 \frac{A_0^2 \pi \nu^2}{2c}. \tag{6.1.6}$$

The absorption coefficient κ needs to consider that not all molecules are absorbing the radiation at the same time, this effect is accounted for through the probability of transition P_{aj} in eq. 6.1.3. For the evaluation of this probability, the time evolution of the initial and

final states may be analysed. Be $\{|j\rangle\}$ the complete set of time-independent eigenfunctions for which $\hat{H}_0|j\rangle = E_j|j\rangle$. Applying the time-dependent Schrödinger equation

$$\hat{H}_0|j(t)\rangle = i\hbar\frac{\partial|j(t)\rangle}{\partial t}, \tag{6.1.7}$$

the time evolution of these stationary states is found as

$$|j(t)\rangle = |j\rangle e^{-iE_jt/\hbar}. \tag{6.1.8}$$

A stationary state $|a\rangle$ of the molecule can then be expressed in the basis of eigenfunctions of the unperturbed Hamiltonian $\hat{H}_0$

$$|a(t)\rangle = \sum_j c_{aj}(t)|j\rangle. \tag{6.1.9}$$

In the magnetic field, the states are subjected to a perturbation $\hat{H}'$, which is given by the coupling of the fields to the momentum of each electron k, i.e. $\hat{H}' = \sum_k \frac{q_k}{m_kc}\mathrm{Re}\{\mathbf{A}_0\cdot\mathbf{p}_k\}$, where m_k is the mass of the electron k and q_k is its charge. The state $|a(t)\rangle$ must satisfy the Schrödinger equation

$$(\hat{H}_0+\hat{H}')|a(t)\rangle = i\hbar\frac{\partial|a(t)\rangle}{\partial t}. \tag{6.1.10}$$

The time evolution of the wave function may be expressed via the time evolution of the expansion coefficients $c_{aj}(t)$. Inserting the time evolution of the wave function from eq. 6.1.9 and projecting on $\langle j|$, a differential equation for $c_{aj}(t)$ is obtained

$$\frac{\mathrm{d}c_{aj}(t)}{\mathrm{d}t} = -\frac{i}{\hbar}\sum_k c_{ak}(t)\langle j|\hat{H}'|k\rangle e^{i(E_j-E_k)t/\hbar}. \tag{6.1.11}$$

A solution for the expansion coefficient is obtained by integrating eq. 6.1.11, from $t=0$ to $t=t'$

$$\begin{aligned} c_{aj}(t)' = \frac{\pi}{h}\Bigg[&\langle j|\sum_k\frac{q_k}{m_kc}\mathrm{Re}\{\mathbf{A}_0\cdot\mathbf{p}_k\}e^{-2\pi i\nu z_k/c}|a\rangle\left(\frac{1-e^{2\pi i(\nu_{aj}+\nu)t'}}{2\pi(\nu_{aj}+\nu)}\right)\\ &+\langle j|\sum_k\frac{q_k}{m_kc}\mathrm{Re}\{\mathbf{A}_0^*\cdot\mathbf{p}_k\}e^{2\pi i\nu z_k/c}|a\rangle\left(\frac{1-e^{2\pi i(\nu_{aj}-\nu)t'}}{2\pi(\nu_{aj}-\nu)}\right)\Bigg], \end{aligned} \tag{6.1.12}$$

where $\nu_{aj} = (E_j - E_a)/h$. P_{aj} indicates the probability per unit time that a transition from state $|a\rangle$ to state $|j\rangle$ occurs and is expressed as $P_{aj} = \frac{|c_{aj}(t')|^2}{t'}$.
This derivation assumes a perfectly monochromatic radiation of frequency ν_{aj}; however, this condition is never satisfied in the experimental setting. More realistically, the frequencies are distributed over a range around ν_{aj}. To account for this experimental reality, eq. 6.1.12 is modified by introducing a band-shape function $\rho_{aj}(\nu)$, describing the distribution of the frequencies. The probability P_{aj} becomes

$$P_{aj} = \frac{\pi^2}{h^2}\left|\langle j|\sum_k\frac{q_k}{m_kc}\mathbf{A}_0^*\cdot\mathbf{p}_ke^{2\pi i\nu z_k/c}|a\rangle\right|^2\rho_{aj}(\nu). \tag{6.1.13}$$

Writing the vector potential as $\mathbf{A}_0 = A_0\boldsymbol{\pi}$, where $\boldsymbol{\pi}$ is the vector of unit norm directed as $\mathbf{A}_0$, the transition probability is

$$P_{aj} = \frac{4\pi^4A_0^2\nu^2}{h^2c^2}|\langle j|\mathbf{m}\cdot\boldsymbol{\pi}^*|a\rangle|^2\rho_{aj}(\nu), \tag{6.1.14}$$

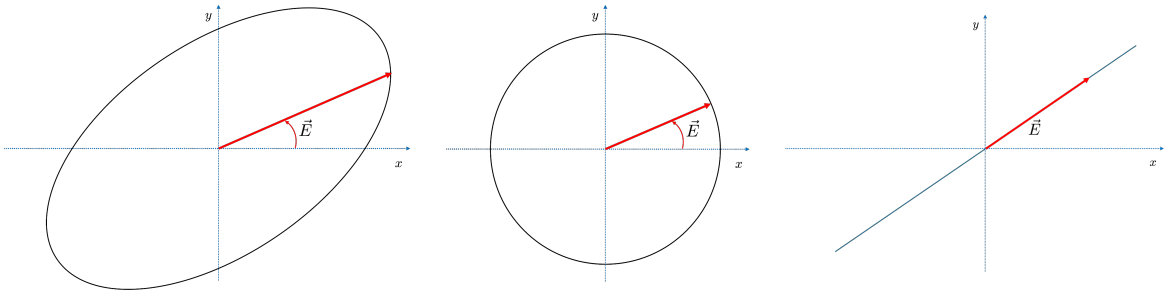

Elliptical polarisation Circular polarisation Linear polarisation

Figure 6.3: Representation of the different polarisations of the electromagnetic wave. The most general case is described by the left picture, where the electric field **E** traces an elliptical path; in this case, the wave is elliptically polarised. In the case the ellipse transforms to a perfect circle, the second picture is obtained, where a circularly polarised beam is shown. Squeezing the ellipse along the major axis, a linear polarised wave is obtained, shown in the right picture. In this case, the electric field oscillates along the line.

with $\mathbf{m} = \sum_k q_k \mathbf{r}_k$ as the electric dipole of the system. Through this expression, the probability of transition depends on the transition dipole moment between state j and state a. Once all the quantities contributing to the determination of the absorption coefficient κ have been defined, a closed expression is gained substituting eqs. 6.1.4 and 6.1.14 into eq. 6.1.3

$$\kappa(\nu) = \frac{1}{4\pi\varepsilon_0}\frac{8\pi^3\nu}{hc}(N_a - N_j)|\langle j|\,\mathbf{m}\cdot\boldsymbol{\pi}^*\,|a\rangle|^2\rho_{aj}(\nu). \tag{6.1.15}$$

The absorption of a system is directly proportional to the squared norm of the transition dipole moment, as well as to the energy of the radiation and to the number of absorbing molecules. These quantities are all defined in the presence of the magnetic field. Notice that the dependence on the field amplitude A_0 cancels out, which is intuitively understood, as the absorption of a radiation only depends on its frequency.

The displayed equations describe an ideal situation of molecules interacting in vacuum with the fields. In a real system, the molecules also experience interactions with the solvent molecules, leading to a modification of the macroscopic fields determined by the radiation. The fields acting on each molecule are referred to as microscopic fields and are described as $\mathbf{E}_{\text{micro}} = \alpha\mathbf{E}_{\text{macro}}$ and $\mathbf{B}_{\text{micro}} = \alpha\mathbf{B}_{\text{macro}}$. Furthermore, the velocity of propagation of the radiation in the solvent is c/n, with n the refractive index of the medium. The whole derivation can be performed again with the scaled velocity and the screening constant α, leading to a more accurate determination of the coefficient $\kappa(\nu)$

$$\kappa(\nu) = \frac{1}{4\pi\varepsilon_0}\frac{8\pi^3\nu\alpha^2}{hcn}(N_a - N_j)|\langle j|\,\mathbf{m}\cdot\boldsymbol{\pi}^*\,|a\rangle|^2\rho_{aj}(\nu). \tag{6.1.16}$$

6.1.2 The ellipticity

In this section, an expression for the rotation of the plane of polarisation of a circularly polarised electromagnetic wave, after crossing a medium of thickness l, on a path parallel to an applied magnetic field **B**, is derived. The right $(+)$ and left $(-)$ circularly polarised components of the electric field are

$$\mathbf{E}_\pm = \text{Re}\{\frac{1}{\sqrt{2}}(\mathbf{e}_\text{x} \pm \mathbf{e}_\text{y})E_0 e^{2\pi i\nu(t-\frac{zn_\pm}{c})}\}, \tag{6.1.17}$$

where z is the distance travelled inside the sample and $\mathbf{e}_x, \mathbf{e}_y, \mathbf{e}_z$ are the unit vectors of a right-handed Cartesian coordinate system. The magnetic field is assumed to be aligned to $\mathbf{e}_z$. The electric field $\mathbf{E}$ is given by the sum of the right and left circularly polarised components, allowing to separate the electric-field components along $\mathbf{e}_x$ and $\mathbf{e}_y$

$$\begin{aligned}\mathbf{E} &= \frac{1}{\sqrt{2}}(\mathbf{E}_+ + \mathbf{E}_-) = \\ &= E_0\left[\mathbf{e}_x \cos\left(\frac{\pi\nu z\Delta n}{c}\right)\cos\left(2\pi\nu(t-\frac{zn}{c})\right) - \mathbf{e}_y \sin\left(\frac{\pi\nu z\Delta n}{c}\right)\cos\left(2\pi\nu(t-\frac{zn}{c})\right)\right].\end{aligned} \tag{6.1.18}$$

Here $\Delta n = n_- - n_+$ accounts for the difference in refraction between the two polarisations and $n = (n_- + n_+)/2$. The resulting field $\mathbf{E}$ can have different polarisations, depending on the parameters in eq. 6.1.18, illustrated in fig. 6.3. In the first picture, the most general case is shown, where the radiation is elliptically polarised, i.e. the tip of the electric field vector traces an ellipse. In the second picture, the elliptical path is assumed to have the same major and minor axes, resulting in a circularly polarised radiation. In the third picture of fig. 6.3, the other limiting case is shown, where the ellipse is squeezed to the point to become a line. In this case, a linear polarised radiation is obtained, where the electric field is oscillating along the direction of polarisation.
If left and right circularly polarised waves are combined with equal amplitudes but arbitrary relative phase, linear polarised light is obtained for $\Delta n = 0$

$$\mathbf{E} = \frac{1}{\sqrt{2}}(\mathbf{E}_+ + \mathbf{E}_-) = E_0\mathbf{e}_x \cos\left(2\pi\nu(t-\frac{zn}{c})\right). \tag{6.1.19}$$

In the case of $\Delta n \neq 0$, but a real number, eq. 6.1.18 still gives a linear polarised wave, as the amplitudes are the same for the x and y components, but the polarisation plane rotates as the wave progresses in the z direction. After having travelled for a distance l, the corresponding rotation angle ϕ is calculated from the ratio between the y and x components of the electric field vector

$$\phi = \arctan\left(-\frac{E_y}{E_x}\right) = \frac{\pi\nu l\Delta n}{c}. \tag{6.1.20}$$

In the case of naturally active systems, an intrinsic chirality causes the refraction indices to differ ($n_+ \neq n_-$). The presence of a longitudinal magnetic field, however, induces different refractive indices in all substances, with $n_+ \neq n_-$. Though both effects manifest a rotation of the plane of polarisation, it is clear that natural optical activity describes asymmetries that are intrinsic to the molecular system, while magnetically induced optical activity is a consequence of the Zeeman interactions. In the most general case, the refraction index is a complex quantity, allowing for absorption inside the medium: $\tilde{n}_\pm = n_\pm - ik_\pm$. It can be proven[284] that the absorption parameter κ in eq. 6.1.3 is related to k through the equation $\kappa = 4\pi k\nu/c$. Assuming n to be the complex refractive index $\tilde{n}$ in eq. 6.1.18, the x and y field components no longer share the same amplitude, resulting in an elliptically polarised wave. The rotation of the plane of polarisation defined as the ratio $\frac{E_y}{E_x}$ also becomes complex

$$\tilde{\phi} = \phi - i\theta = \frac{\pi\nu l}{c}(\tilde{n}_- - \tilde{n}_+). \tag{6.1.21}$$

Fig. 6.4 shows the ellipse traced by the electric field vector if projected on the xy-plane, over one cycle of oscillation. A polarisation state is fully characterised through the geometrical parameters of the ellipse and the specification of its *handedness*, i.e. clockwise or counter-clockwise rotation. The first geometrical parameter is provided by the angle ϕ, defined as the angle between the major axes of the ellipse and the x-axis. Furthermore, the ellipticity

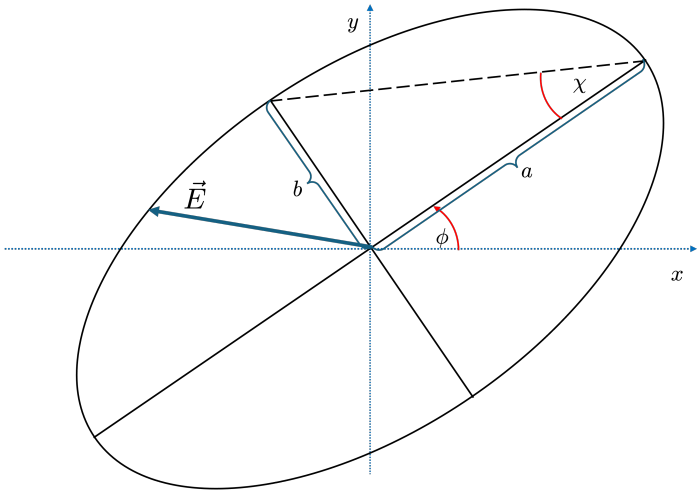

Figure 6.4: Elliptical path traced by the tip of the electric-field vector during one cycle of oscillation, projected on the fixed xy plane, perpendicular to the direction of propagation. The angle ϕ measures the rotation of the polarisation plane as the wave progresses along the z-axis. The ellipticity angle χ is calculated as $\tan\chi = \frac{b}{a}$ and indicates the "squeezing" of the ellipse. Note that for $b = a$, circularly polarised light is obtained, while for $b = 0$, linearly polarised light is obtained.

angle χ is highlighted in the figure, accounting for the ratio between the minor and the major axes of the ellipse, giving $\tan\chi = \frac{b}{a}$. Exploiting trigonometric relations, this ratio can be linked to the imaginary part of the angle $\tilde{\phi}$, as

$$\tan\chi = \tanh\frac{\pi\nu l\Delta k}{c} \approx \frac{\pi\nu l\Delta k}{c}, \tag{6.1.22}$$

where Δk is assumed to be small. In MCD theory, $\tan\chi$ is identified with the angle θ, called *ellipticity*, and measures the squeezing of the ellipse traced by the fields. For a non-absorbing medium, for which $k = 0$, or when $k_+ = k_-$, the angle χ is zero and the fields are linearly polarised. The more the anisotropy induced by the magnetic field leads to differences in absorbance, the less the ellipse will be squeezed.

Usually, the molar ellipticity is adopted, as it does not depend on the experimental parameters of the concentration and length of the probe. It is defined as

$$[\theta]_{\mathrm{M}} = \frac{18N_0\theta}{\pi NlB} = \frac{4500}{\pi\log e}\cdot\frac{\Delta A}{[c]lB}. \tag{6.1.23}$$

Therefore, the molar ellipticity $[\theta]_{\mathrm{M}}$ is related to the difference of absorption ΔA. Exploiting the Lambert-Beer law

$$\Delta A = \epsilon[c]l = \Delta\kappa l\log e, \tag{6.1.24}$$

the difference in absorption is expressed through the difference $\Delta\kappa$

$$\Delta\kappa = \kappa_- - \kappa_+ = \frac{1}{4\pi\varepsilon_0}\frac{8\pi^3\nu\alpha^2}{hcn}\sum_{aj}(N_a - N_j)[|\langle a|\,\hat{m}_-\,|j\rangle|^2 - |\langle a|\,\hat{m}_+\,|j\rangle|^2]\rho_{aj}(\nu), \tag{6.1.25}$$

where $\hat{m}_\pm = \frac{1}{\sqrt{2}}(\hat{m}_{\mathrm{x}} \pm i\hat{m}_{\mathrm{y}})$. Before obtaining the final form for ΔA, the factor describing the ratio of absorbing molecules can be simplified introducing the Avogadro constant N_0

$$\frac{N_a - N_j}{[c]} = \frac{N_a - N_j}{N}\cdot\frac{N}{[c]} = \frac{N_a - N_j}{N}\cdot N_0\cdot 10^{-3}, \tag{6.1.26}$$

where N is the total number of molecules per cm^3. The difference in absorption is calculated per photon energy ($\mathscr{E} = h\nu$) and corresponds to

$$\frac{\Delta A}{\mathscr{E}} = \frac{\epsilon_- - \epsilon_+}{\mathscr{E}}[c]l = \Gamma \sum_{aj} \frac{N_a - N_j}{N} \frac{1}{4\pi\varepsilon_0}[|\langle a|\,\hat{m}_-\,|j\rangle|^2 - |\langle a|\,\hat{m}_+\,|j\rangle|^2]\rho_{aj}(\nu), \tag{6.1.27}$$

where the collection of physical constants is grouped to give the factor

$$\Gamma = \frac{N_0\pi^2\alpha^2[c]l\log_{10}e}{250\hbar cn}. \tag{6.1.28}$$

The concentration is given in mol/L, the path length l in cm. Usually the electronic transitions considered are characterised by $E_j - E_a > 1000\text{cm}^{-1}$, therefore leading to $N_j \approx 0$.

The molar ellipticity is found substituting eq. 6.1.27 in eq. 6.1.23

$$[\theta]_\text{M} = \frac{36\pi^2 N_0\alpha^2}{hcn} \cdot h\nu \sum_{aj} \frac{1}{4\pi\varepsilon_0} \frac{[|\langle a|\,\hat{m}_-\,|j\rangle|^2 - |\langle a|\,\hat{m}_+\,|j\rangle|^2]}{B}\rho_{aj}(\nu). \tag{6.1.29}$$

In the literature,[107,126,284] $h\nu$ and $\sum_{aj} \frac{1}{4\pi\varepsilon_0\mu_\text{B}}[|\langle a|\,\hat{m}_-\,|j\rangle|^2 - |\langle a|\,\hat{m}_+\,|j\rangle|^2]\rho_{aj}(\nu)$ are expressed in atomic units (μ_B being the Bohr magneton), and have an overall dimension of [$length^3$]. Because of this dimensionality, the conversion from SI units to atomic units implies a multiplication by a_0^3, where a_0 is the Bohr radius. The molar ellipticity $[\theta]_\text{M}$ is measured in deg L mol^{-1} m^{-1} G^{-1} and is expressed as

$$[\theta]_\text{M} = \frac{36\pi^2 N_0\alpha^2 a_0^3\mu_\text{B}}{hcn} \cdot \nu \sum_{aj} \frac{1}{4\pi\varepsilon_0\mu_\text{B}} \frac{[|\langle a|\,\hat{m}_-\,|j\rangle|^2 - |\langle a|\,\hat{m}_+\,|j\rangle|^2]}{B}\rho_{aj}(\nu). \tag{6.1.30}$$

The product of physical constants in eq. 6.1.30 is expressed via the factor $\tilde{\Gamma} = \frac{36\pi^2 N_0\alpha^2 a_0^3\mu_\text{B}}{hcn} = 0.0014803$. From now on, the expressions will be written as function of $\omega = 2\pi\nu$, as this is the usual form of the equations found in the literature. Furthermore, in the systems under consideration, all molecules are assumed to be in the ground state, i.e. $|a\rangle = |0\rangle$.
To this point, the transition dipole moments have been calculated for a specific direction of the magnetic field. However, in an MCD experiment the molecules are rotating in space and are not aligned to a single direction. An isotropic average over the orientations introduces a sum over the orientations γ, and a factor 1/3,

$$\begin{aligned}[\theta]_\text{M} &= \tilde{\Gamma}\omega \sum_j \frac{1}{3\mu_\text{B}} \sum_\gamma \frac{1}{4\pi\varepsilon_0} \frac{[|\langle 0|\,\hat{m}_-\,|j\rangle^\gamma|^2 - |\langle 0|\,\hat{m}_+\,|j\rangle^\gamma|^2]}{B} f(\omega,\omega_j) = \\ &= \tilde{\Gamma}\omega \sum_j \frac{1}{3\mu_\text{B}} \frac{1}{4\pi\varepsilon_0} \sum_{\alpha\beta\gamma} \varepsilon_{\alpha\beta\gamma} \frac{(\langle 0|\,\hat{m}_\alpha\,|j\rangle^\gamma \langle j|\,\hat{m}_\beta\,|0\rangle^\gamma)}{B} f(\omega,\omega_j).\end{aligned} \tag{6.1.31}$$

where the definition $m_\pm = \frac{1}{\sqrt{2}}(m_\alpha \pm m_\beta)$ has been exploited to introduce the Levi-Civita tensor $\varepsilon_{\alpha\beta\gamma}$, with $\{\alpha,\beta,\gamma\} = \{x,y,z\}$, $\{y,z,x\}$, $\{z,x,y\}$. The band-shape function ρ_{0j} has been replaced by a model broadening function $f(\omega,\omega_J)$, chosen to be either Gaussian or Lorentzian. The index γ indicates that the transition dipole moments are computed in a magnetic field in the γ direction.

Defining the so-called spectroscopic term $\mathscr{R}_J$ as

$$\mathscr{R}_J = \frac{1}{4\pi\epsilon_0} \frac{i}{3\mu_\text{B}} \sum_{\alpha\beta\gamma} \varepsilon_{\alpha\beta\gamma} \frac{(\langle 0|\,\hat{m}_\alpha\,|J\rangle^\gamma \langle J|\,\hat{m}_\beta\,|0\rangle^\gamma)}{B} \tag{6.1.32}$$

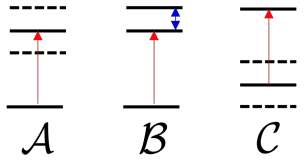

Figure 6.5: Schematic depiction of the spectroscopic terms $\mathcal{A},\mathcal{B},\mathcal{C}$.

the molar ellipticity is given as

$$[\theta]_{\mathrm{M}} = \tilde{\Gamma}\omega \sum_J \mathcal{R}_J f(\omega - \omega_J). \tag{6.1.33}$$

The calculation of the MCD spectra can be performed directly computing the transition dipole moments and the excitation energies within an external magnetic field. However, not all computational codes can perform such a calculation; a different approach is therefore often exploited, obtained using perturbation theory to express the molar ellipticity. The next section is concerned with this perturbative treatment of eq. 6.1.33.

6.1.3 Perturbative approach

In the case of a small magnetic field, the molar ellipticity in eq. 6.1.31 can be expanded in Taylor series around $B = 0$ as

$$[\theta]_{\mathrm{M}} = ([\theta]_{\mathrm{M}})_0 + \left(\frac{\partial [\theta]_{\mathrm{M}}}{\partial B}\right)_0 B + \mathcal{O}(B^2). \tag{6.1.34}$$

At $B = 0$, the molar ellipticity $([\theta]_{\mathrm{M}})_0$ vanishes, as the difference in absorption between left and right circularly polarised light for non-chiral molecules is zero in the field-free case. Therefore, the molar ellipticity is approximated at first order as

$$[\theta]_{\mathrm{M}} \approx \left(\frac{\partial [\theta]_{\mathrm{M}}}{\partial B}\right)_0 B = \tilde{\Gamma}\omega \frac{1}{4\pi\varepsilon_0} \frac{i}{3\mu_{\mathrm{B}}} \sum_J \sum_{\alpha\beta\gamma} \varepsilon_{\alpha\beta\gamma} \Bigg(\frac{\partial (\langle 0|\hat{m}_\alpha|J\rangle \langle J|\hat{m}_\beta|0\rangle)}{\partial B_\gamma} f(\omega - \omega_J) + (\langle 0|\hat{m}_\alpha|J\rangle \langle J|\hat{m}_\beta|0\rangle) \frac{\partial f(\omega - \omega_J)}{\partial B_\gamma} \Bigg). \tag{6.1.35}$$

Note that eq. 6.1.31 depends on the field both through the transition dipole moments and through the broadening function, accounting for the two terms in eq. 6.1.35. This form can be related to the perturbative formulation found in the literature[123]

$$[\theta]_{\mathrm{M}} = \tilde{\Gamma}\omega \sum_J \left\{ -\frac{\partial f(\omega, \omega_J)}{\partial \omega} \mathcal{A}_J + f(\omega, \omega_J) \left(\mathcal{B}_J + \frac{\mathcal{C}_J}{kT} \right) \right\}. \tag{6.1.36}$$

$\mathcal{A},\mathcal{B},\mathcal{C}$ are the spectroscopic terms (*Faraday terms*) depicted in fig. 6.5 and they characterise the structure of the MCD spectrum. $\mathcal{B}_J$ describes the energy shift which state J undergoes in a magnetic field. When J is a degenerate excited state, $\mathcal{A}_J$ describes the effect of the orbital-Zeeman splitting and is multiplied by a derivative band shape. Finally, $\mathcal{C}_J$ needs to be considered in the case in which J corresponds to a degenerate ground state. The $\mathcal{C}_J$ term is temperature dependent and weighted by the Boltzmann factor determining the occupation of the near-degenerate ground states. This last term does not contribute for the systems analysed in this work, as they have non-degenerate ground states.

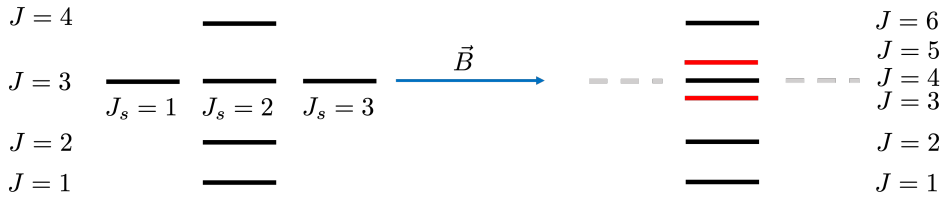

Figure 6.6: Graphical scheme of the labelling of excited states: the index J refers to a given n-fold degenerate state. In the case of a degenerate state, the index J_s refers to the single components of state J. In a magnetic field $\mathbf{B}$, the degenerate states undergo orbital-Zeeman splitting (right side of the figure). In this case, only the index J is needed, as there are no degenerate states anymore.

The $\mathscr{B}_J$ term can be recognised in the first term of eq. 6.1.35, where the differentiation is performed on the linear contributions in the magnetic field to $(\langle 0|\hat{m}_\alpha|J\rangle\langle J|\hat{m}_\beta|0\rangle)$.[126] In order to obtain linear terms in $\mathbf{B}$, the states $|J\rangle$ and $|0\rangle$ can be expanded in perturbation orders. Therefore, a perturbative treatment of the Hamiltonian needs to be formulated.

In an MCD experiment, the magnetic field is very small, of the order of 10^{-4} B_0. In the magnetic field Hamiltonian

$$\hat{H} = \hat{H}_0 + \frac{1}{2}\mathbf{B}\cdot\mathbf{L} + \mathbf{B}\cdot\mathbf{S} + \frac{1}{8}\sum_i^N (B^2 r_{iO}^2 - (\mathbf{B}\cdot\mathbf{r}_{iO})^2), \tag{6.1.37}$$

the diamagnetic term, of second order in the magnetic field, can be neglected. Furthermore, for simplicity the focus is here on singlet states; the spin-Zeeman term $\mathbf{B}\cdot\mathbf{S}$ does therefore not contribute. Therefore, the perturbation is given by the paramagnetic term $\hat{H}' = \mu_B \mathbf{B}\cdot\mathbf{L} = \frac{1}{2}\mathbf{B}\cdot\mathbf{L}$, where the second equality is expressed in atomic units, in which $\mu_B = \frac{1}{2}$.

The first-order correction to the energy of a state $|J\rangle$ is given by $E^{(1)} = \langle J|\hat{H}'|J\rangle = \mu_B B\langle J|\hat{L}_z|J\rangle$, where the z axis is aligned to the direction of the applied magnetic field, coincident with the direction of light propagation in the experimental setting. The first-order wave function is given by

$$\left|J^{(1)}\right\rangle = \sum_{K\notin\mathscr{D}_J} \frac{\langle K|\hat{H}'|J\rangle}{E_J - E_K}|K\rangle = \mu_B B \sum_{K\notin\mathscr{D}_J} \frac{\langle K|\hat{L}_z|J\rangle}{E_J - E_K}|K\rangle, \tag{6.1.38}$$

where $\{K\}$ denotes the set of unperturbed eigenfunctions of $\hat{H}_0$. The sum excludes the states in the space $\mathscr{D}_J$, made of states degenerate to $|J\rangle$ in the field-free case. For a visual description, see fig. 6.6.

The $\mathscr{B}_J$ term is obtained from the first term in eq. 6.1.35, where the terms of first order in $\mathscr{B}$ are differentiated

$$\begin{aligned}\mathscr{B}_J = \frac{1}{4\pi\varepsilon_0}\frac{i}{3\mu_B}\sum_{\alpha\beta\gamma}\varepsilon_{\alpha\beta\gamma}\Bigg(&\frac{\partial\langle 0|\hat{m}_\alpha\left|J^{(1)}\right\rangle\langle J|\hat{m}_\beta|0\rangle}{\partial B_\gamma} + \frac{\partial\langle 0|\hat{m}_\alpha|J\rangle\langle J|\hat{m}_\beta\left|0^{(1)}\right\rangle}{\partial B_\gamma} \\ &+ \frac{\partial\left\langle 0^{(1)}\right|\hat{m}_\alpha|J\rangle\langle J|\hat{m}_\beta|0\rangle}{\partial B_\gamma} + \frac{\partial\langle 0|\hat{m}_\alpha|J\rangle\left\langle J^{(1)}\right|\hat{m}_\beta|0\rangle}{\partial B_\gamma}\Bigg).\end{aligned} \tag{6.1.39}$$

Substituting the first-order perturbed eigenfunction from eq. 6.1.38 into eq. 6.1.39, the ex-

pression for the $\mathscr{B}_J$ term is obtained*

$$\mathscr{B}_J = -\frac{1}{4\pi\varepsilon_0}\frac{2i}{3}\sum_{\alpha\beta\gamma}\varepsilon_{\alpha\beta\gamma}\Big[\sum_{K\neq 0}\frac{\langle K|\,\hat{L}^\gamma\,|0\rangle}{E_K-E_0}\langle 0|\,\hat{m}_\alpha\,|J\rangle\langle J|\,\hat{m}_\beta\,|K\rangle + \sum_{K\notin\mathscr{D}_J}\frac{\langle J|\,\hat{L}^\gamma\,|K\rangle}{E_K-E_J}\langle 0|\,\hat{m}_\alpha\,|J\rangle\langle K|\,\hat{m}_\beta\,|0\rangle\Big]. \tag{6.1.40}$$

The $\mathscr{A}_J$ term arises from the second term in eq. 6.1.35; the differentiation of the band-shape function can be performed through the chain rule

$$\frac{\partial f(\omega-\omega_J)}{\partial B} = \frac{\partial f(\omega-\omega_J)}{\partial \omega_J}\frac{\partial \omega_J}{\partial B} = -\frac{\partial f(\omega-\omega_J)}{\partial \omega}\frac{\partial \omega_J}{\partial B}, \tag{6.1.41}$$

with

$$\frac{\partial \omega_J}{\partial B} = \mu_{\mathrm{B}}(\langle J|\,\hat{L}^\gamma\,|J\rangle - \langle 0|\,\hat{L}^\gamma\,|0\rangle)\,. \tag{6.1.42}$$

Note that eq. 6.1.42 vanishes for non-degenerate states (for further theoretical insight, the time-reversal symmetry may be checked in ref. 284).

The $\mathscr{A}_J$-term is defined as the sum of all contributions given by all the components of the degenerate state $|J\rangle$; here the basis of the degenerate space $\mathscr{D}_J$ is chosen to be the one diagonalising $\hat{L}^\gamma$ and is labelled as $|J_s\rangle$ (see fig. 6.6)

$$\mathscr{A}_J = \frac{1}{4\pi\varepsilon_0}\frac{i}{3}\sum_{\alpha\beta\gamma}\varepsilon_{\alpha\beta\gamma}\sum_{J_s\in\mathscr{D}_J}\langle 0|\,\hat{m}_\alpha\,|J_s\rangle\langle J_s|\,\hat{m}_\beta\,|0\rangle\,(\langle J_s|\,\hat{L}^\gamma\,|J_s\rangle - \langle 0|\,\hat{L}^\gamma\,|0\rangle). \tag{6.1.43}$$

Comparing the finite-field method to the perturbative one described here, it may be noted that the sum of both Faraday terms $\mathscr{A}_J$ and $\mathscr{B}_J$ correspond to the first order of the $\mathscr{R}_J$ term. In fact, the exact expression of $\mathscr{R}_J$ describes both the splitting of degenerate states in a magnetic field (given by $\mathscr{A}_J$ in the perturbative approach) and the shift in energy of non-degenerate states (given by the $\mathscr{B}_J$ contributions). Therefore, the finite-field theory accounts for the effects of an external magnetic field to infinite order, and not just to first order.

For experimental spectra, the field strength is small enough (of the order of 10^{-4} B_0) to allow both a comparison with spectra obtained through the perturbation-theory approach and through the finite-field approach. However, the applicability of the finite-field approach includes in principle any arbitrary magnetic field, even outside the limit of small B, while the perturbative approach fails by construction when the influence of the magnetic field can no longer be considered a small perturbation. MCD spectra in a non-perturbative limit can therefore be explored only through the finite-field methods.

6.1.4 Gauge-origin dependence

From the previous section, it is clear that $[\theta]_{\mathrm{M}}$ is defined in presence of a magnetic field. For approximated wave functions, it may happen that the results for the physical observables are gauge-origin dependent. It has been described in sec. 2.4.1 that the use of Gauge Including Atomic Orbitals (GIAOs)[184] allows to find gauge-origin independent results. The results obtained in the GIAO basis set are no longer dependent on the gauge origin, and can be exploited to predict MCD spectra.

*Note that the spectroscopic $\mathscr{B}_J$ term in eq. 6.1.40 is calculated through a sum-over-states expression, which is dependent on the number of states considered. Faber *et al.*, in ref. 124, exploit the so-called *derivative formulation*, exploiting the CC response formulation,[57,219] which avoids the sum-over-states method.

Even when performing a calculation in the field-free setting, which is gauge-origin independent, the gauge dependence is present in the perturbative terms, which describe the effect of the magnetic field. The unwanted gauge dependence in the perturbative approach has been addressed in ref. 285, exploiting GIAOs in the field-free calculations. However, in the perturbative framework the dependence of the GIAO basis set on the magnetic field complicates the calculation of the Faraday terms, as these terms are defined through differentiations with respect to **B**. Therefore, the achievement of gauge-origin independence in the perturbative approach is rather involved, requiring the formulation of additional terms coming from the differentiation of the GIAOs. Thus, perturbative calculations often neglect the magnetic-field dependence of the Faraday terms, obtaining gauge-origin dependent results.[124] These can also lead to qualitative wrong descriptions of MCD spectra, as it will be shown in the results section (sec. 6.3).

In the case of the finite-field approach, ensurance of gauge-origin independence is straightforward. Due to the presence of the magnetic field, the calculations are already performed with the GIAO basis set, leading to gauge-origin independent transition dipole moments and transition frequencies. Unlike for the perturbative approach, the equations do not need to be modified when using the GIAO basis set and the $\mathscr{R}_J$ term is computed following eq. 6.1.32.

Concluding the theoretical description of MCD theory, it may be observed that the computation of MCD spectra through a finite-field approach possesses numerous advantages over the usually exploited perturbative approach. In fact, a finite-field computation needs only first-order response theory, for the computation of the transition dipole moments, while the perturbative treatment exploits second-order response theory, with respect to both the electric and the magnetic fields. Furthermore, gauge-origin invariant results are more easily obtained with a finite-field computation. Lastly, the exact inclusion of magnetic effects allows to explore also field strengths, for which the perturbative approximation cannot be applied. All these advantages are discussed in the next sections, on the basis of some test molecules.

6.2 MCD protocol

The magnetic circular dichroism spectra are obtained from the transition dipole moments calculated in QCUMBRE. An MCD spectrum is composed of the isotropic average of the different orientations the magnetic field can assume in space with respect to the molecular system. As described in eq. 6.1.32, three calculations need to be performed, with either $\mathbf{B} \parallel \hat{x}$, $\mathbf{B} \parallel \hat{y}$ or $\mathbf{B} \parallel \hat{z}$. These can be started manually or the script `MCDGlobal.sh` may be used, which is part of the QCUMBRE package. Each calculation has its own CFOUR and QCUMBRE input files, for the different orientations of the field. In particular, in the latter the keyword `mcd=I`, with `I=x,y,z`, signals to QCUMBRE that the calculation of transition properties is performed for an MCD spectrum and specifies which orientation of the field is chosen.

As seen in eq. 6.1.32, only transition moments from the ground state are needed; for an MCD calculation, only these transitions are computed, while those between different excited states are not considered. The transition dipole moments are written on an external file, `MCD_tramo_I`, while the transition energies are written on `MCD_ee_I`. These are the outputs needed for the computation of an MCD spectrum.

The actual spectrum is assembled through an external Python script, `MCD.py` (which is part of the QCUMBRE package). This Python script computes $\mathscr{R}_J$ through the expression in eq. 6.1.32. The input file `inputMCD` contains the necessary input parameters:

- `concentration`: concentration of the solute in the experimental setting in mol/L (default: 1);

- `length`: length of the probe in cm (default: 1);
- `refractiveIndex`: refractive index of the solution (default: 1);
- `sigma`: broadening parameter of the broadening function (default: 0.005);
- `bfield`: magnetic field strength in B_0 (default: 10^{-5});
- `spectrumMode`: output option of the molar ellipticity in atomic units (0) or experimental units (1) (default: 0);
- `energyMode`: output option, determining the x axis to be either in eV (0) or in nm (1) (default: 1);
- `bandshapeFunction`: choice of the broadening function (default: 0):
  - Gaussian function (0): $f(\omega-\omega_J)=\frac{1}{\sqrt{\pi}\vartheta}e^{-(\frac{\omega-\omega_J}{\vartheta})^2}$;[107]
  - Lorentzian function (1) $f(\omega-\omega_J)=\frac{\vartheta}{\pi}\frac{1}{(\omega-\omega_J)^2+\vartheta^2}$;[124]
- `ucc`: CC transition moments (0) or UCC transition moments (1) (default: 0).

Providing the input files `MCD_tramo_I` and `MCD_ee_I` to the Python script, the MCD spectrum is given as an output.

This script has been debugged by ensuring that the multiplied quantities are treated correctly (with particular attention to the complex algebra necessary); the obtained results have been compared to the spectra in ref. 124 (this comparison is described in more detail in the results section hereafter).

6.3 MCD spectroscopy

The theoretical framework developed in sec. 6.1 needs to be validated by applying it to some test molecules, in order to verify that the perturbative and the finite-field methods give agreeing results at low magnetic-field strengths. Therefore, the developed methodology is tested against perturbative calculations reported in the literature. The importance of gauge-origin invariance is then assessed through the comparison of spectra calculated both with and without GIAOs. Once the finite-field approach has been validated, the method can be exploited in connection to UCC transition dipole moments, discussing the differences between a CCSD and a UCC3 calculation of the MCD spectrum. In the last part, a *Gedankenexperiment* is performed, calculating an MCD spectrum in a magnetic field typical for magnetic white dwarf stars.

6.3.1 Perturbative vs finite-field approach

This work wants to prove the equivalence of the two explained approaches by performing calculations on the same systems as in ref. 124, urea and cyclopropane, with geometries and basis sets (aug-cc-pVDZ[266–271]) there adopted. The Lorentzian broadening function of sec. 6.2 was chosen in order to best compare to the mentioned reference, with $\vartheta = 2000\text{cm}^{-1} = 0.0045563$ a.u. The comparison of the finite-field approach with the results from perturbation theory is performed by setting the magnetic field to a strength of 10^{-4} B_0.

In figures 6.7a and 6.7b, the comparison between the perturbative method (blue lines in the plots) and the finite-field calculation (red lines) is visualised for urea and cyclopropane. The blue lines were adopted from ref. 124, where the CCSD calculations are not using

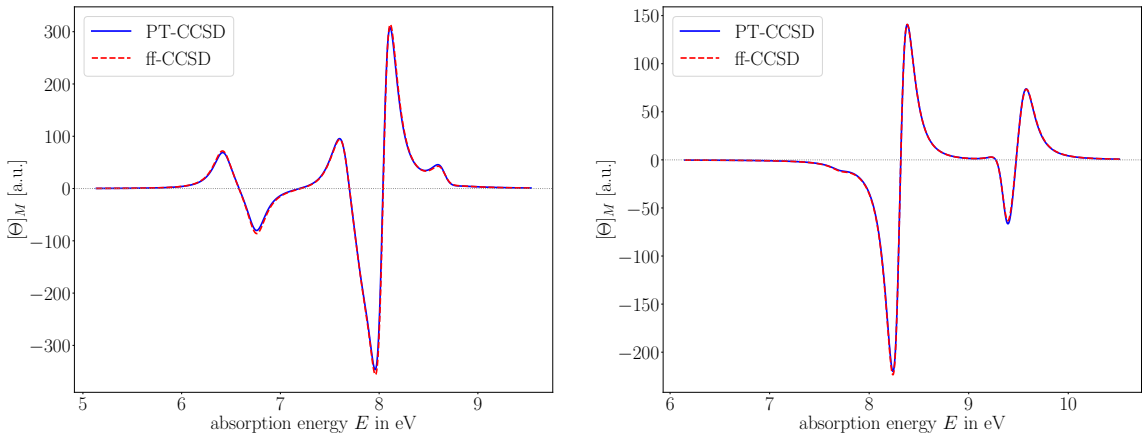

(a) MCD spectrum computed for urea.

(b) MCD spectrum computed for cyclopropane.

Figure 6.7: MCD spectra for urea (fig. 6.7a) and cyclopropane (fig. 6.7b): in blue, the reference from ref. 124 (no GIAOs, perturbation theory), in red the curves computed with the non-perturbative approach, with direct calculation in a magnetic field of 10^{-4} B_0, without GIAOs as well. When calculating without GIAOs, the gauge origin was chosen in the centre of mass of the system.

GIAOs. In order to obtain a comparison, also the finite-field calculations were performed without GIAOs, thus giving origin-dependent results. The perturbative method, in blue, and the finite-field (ff) calculation in red, are exploited at the CCSD level of theory.

In fig. 6.7a, the first 10 excited states of urea are considered, as these lie in the typical range of an MCD spectrum. As there are no degenerate states for this molecule in the field-free case, only the $\mathscr{B}_J$ term determines the MCD spectrum obtained with the perturbative approach. For this system, the comparison between the description given by the $\mathscr{B}_J$ term for the perturbative approach and the description given by the $\mathscr{R}_J$ term for the finite-field approach can be discussed. On the other hand, in fig. 6.7b the first 7 excited states of cyclopropane are calculated. Cyclopropane has multiple degenerate states in the zero-field case, as a consequence of its molecular symmetry. This molecule is therefore suitable to test the equivalence of the $\mathscr{R}_J$ term to the simultaneous contribution of both $\mathscr{A}_J$ and $\mathscr{B}_J$. It is observed that for both systems the two spectra are practically indistinguishable, reproducing the same intensity and position of the peaks (the same broadening function has been adopted). As was suggested in ref. 124, the MCD spectrum of cyclopropane can be compared to the experimental data in ref. 120. A good qualitative agreement with the experiment is achieved by the theoretical treatment.

6.3.2 Gauge-origin independent calculations

In order to obtain gauge-origin independent results, the calculations ought to be performed in the GIAO basis. Figure 6.8 shows the effects given by the inclusion of GIAOs for the test systems urea (fig. 6.8a) and cyclopropane (fig. 6.8b). The intensity of the peaks is affected by the use of GIAOs and qualitative differences are observed. Especially for cyclopropane the spectrum is not qualitatively well reproduced without GIAOs, as the relative intensities of the positive peaks changes. Therefore the effect of gauge-origin independence is not negligible and all calculations should be performed in the GIAO basis for physically consistent results.

Fig. 6.8a also pictures the effect of the formalism used for the calculation of CCSD properties. Transition dipole moments were computed both in the response-theory framework

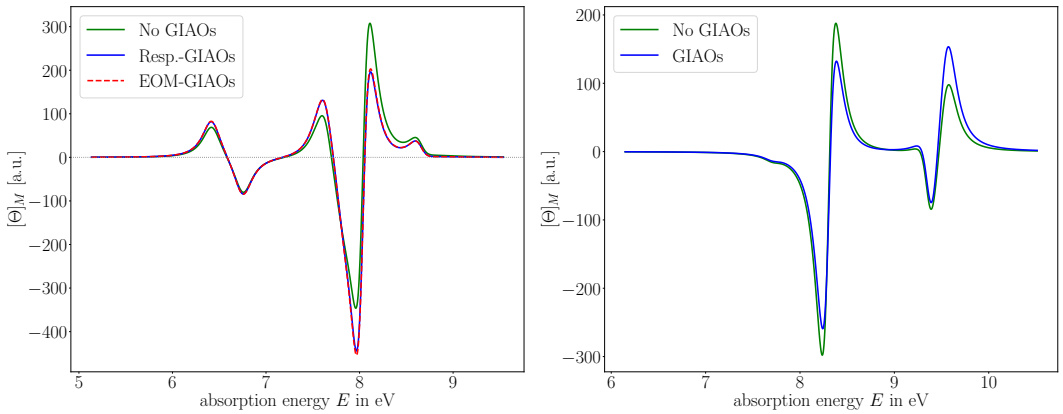

(a) Urea (b) Cyclopropane

Figure 6.8: Comparison of MCD spectra analysing the effect of GIAOs: in green, the reference[124] (no GIAOs, perturbation theory), in blue the curves computed using GIAOs. When calculating without GIAOs, the gauge origin was chosen in the centre of mass of the system. In fig. 6.8a the comparison between MCD spectra computed with CCSD response-theory properties (blue line) and EOM-CCSD properties (red line) is reported.

(blue lines in the plot) and in the EOM one (red line in the plot). No noticeable differences are observed in the MCD spectrum, confirming the small effect given by the perturbed amplitudes on CCSD properties,[115] as it was observed in the previous section 5.2.

Summarising, the two approaches for the prediction of MCD spectra, perturbation theory and finite field, have been shown to be equivalent in the perturbative limit of small magnetic fields. The inclusion of GIAOs is necessary to obtain qualitative correct spectra, which however is not as straightforward in the perturbative framework. For CCSD, the calculation of properties can be approximated with the EOM framework, without loss in accuracy in the MCD spectrum.

6.3.3 UCC spectra

In the previous sections, the validity of the implemented finite-field method for MCD spectra has been tested. The method can be used in combination with different wave-function ansätze; in this work, CCSD and UCC3 are compared. In fig. 6.9 this comparison is shown for the two test systems urea (fig. 6.9a) and cyclopropane (fig. 6.9b). For both methods, the EOM definition of the transition moments has been used, as it has been shown in sec. 5.2 that the transition dipole moments from the ground state are not drastically changing when adding the response of the amplitudes. The qualitative reproduction of the spectrum is very similar between the two methods, with a slight shift to higher energies for UCC3. The only major difference is visible in fig. 6.7a around 8 eV, where CCSD shows a unique negative peak, while UCC3 shows a double peak. Through inspection of the excitation energies, it is seen that the CCSD peak is given by the overlap between two smaller peaks, while the corresponding UCC3 peaks are more clearly distinguished. The difference in the shape of the spectrum is therefore motivated by the shift between the excitation energies computed with the two methods. The relative intensities are the same for the two methods, with slightly more intense peaks for UCC3.

For both systems under inspection, the MCD spectra are agreeing from a qualitative point of view, with UCC3 shifted to higher energies than CCSD. However, it has to be noted that this may not be a general result, as systems (sec. 5.2.6) have been found in the

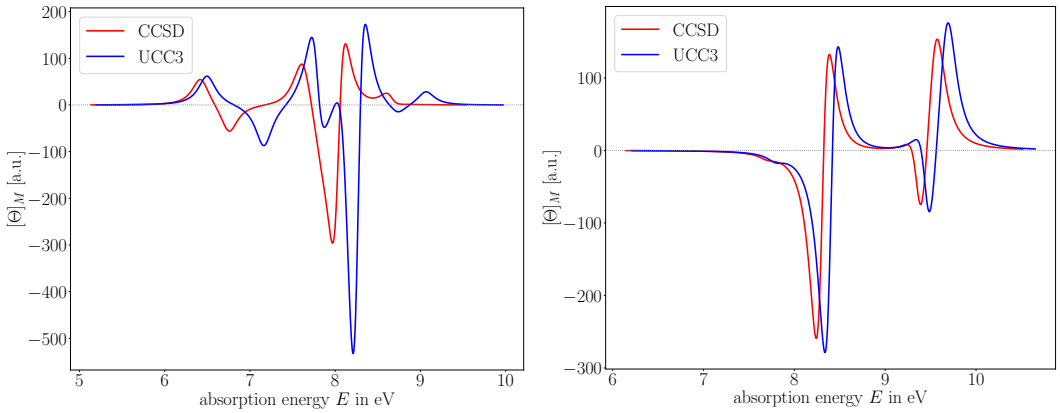

(a) Urea. (b) Cyclopropane.

Figure 6.9: MCD spectrum computed for cyclopropane in a magnetic field of 10^{-4} B_0, using GIAOs. The red lines correspond to results obtained with the CCSD method and the blue ones to results obtained with the UCC3.

framework of this thesis where the UCC3 excitation energies are smaller than the CCSD ones. As these differences between the two methods do not translate in a constant shift, the spectra may appear qualitatively different when two peaks overlap in the same energy region for only one of the two methods.

In all these cases, the comparison with the experiment (ref. 124) does not provide information on the accuracy of the calculated spectra. In fact, experiments present very broad peaks, making the identification of their position not accurate enough to be compared to the calculations. The MCD spectra are experimentally measured in a solvent, while all calculations are performed without a solvent. Inclusion of solvent effects may be achieved through embedding methods, such as the polarizable continuum model (PCM),[286–294] or other methods combining quantum mechanical and molecular mechanical (QM/MM) approaches.[295–297]

6.3.4 MCD spectra in a strong magnetic fields

In sec. 6.1 the differences and advantages of using the exact formulation for the calculation of the MCD ellipticity with respect to the perturbative approach have been discussed. The finite-field formalism in principle applies also to strong magnetic fields, for which the perturbative limit does not apply.

Therefore, a *Gedankenexperiment* of placing an MCD spectrometer on a magnetic white dwarf star can be performed, predicting the spectrum for cyclopropane. In fig. 6.10a, the MCD spectrum of cyclopropane in strong magnetic fields ranging from 0.010 B_0 to 0.030 B_0 is displayed, showing the evolution of spectral lines in relation to the field strength. The interpretation of the behaviour of these spectra is not trivial and it is of some advantage to unravel the spectrum into the single contributions, given by each orientation of the magnetic field. In a strong magnetic field the molecules are not expected to be isotropically distributed in space, as the confinement of the magnetic field hinders the free rotational movement. In this study, however, the approximation of an isotropic distribution is adopted, assuming the validity of eq. 6.1.33.

For cyclopropane it is sufficient to analyse the orientations where the magnetic field is aligned along the C_3 axis (fig. 6.10c) and the C_2 axis (fig. 6.10b).

In order to understand the evolution of the peaks, the states contributing to the MCD spectrum need to be considered. Starting from fig. 6.10b, the excited states and their corre-

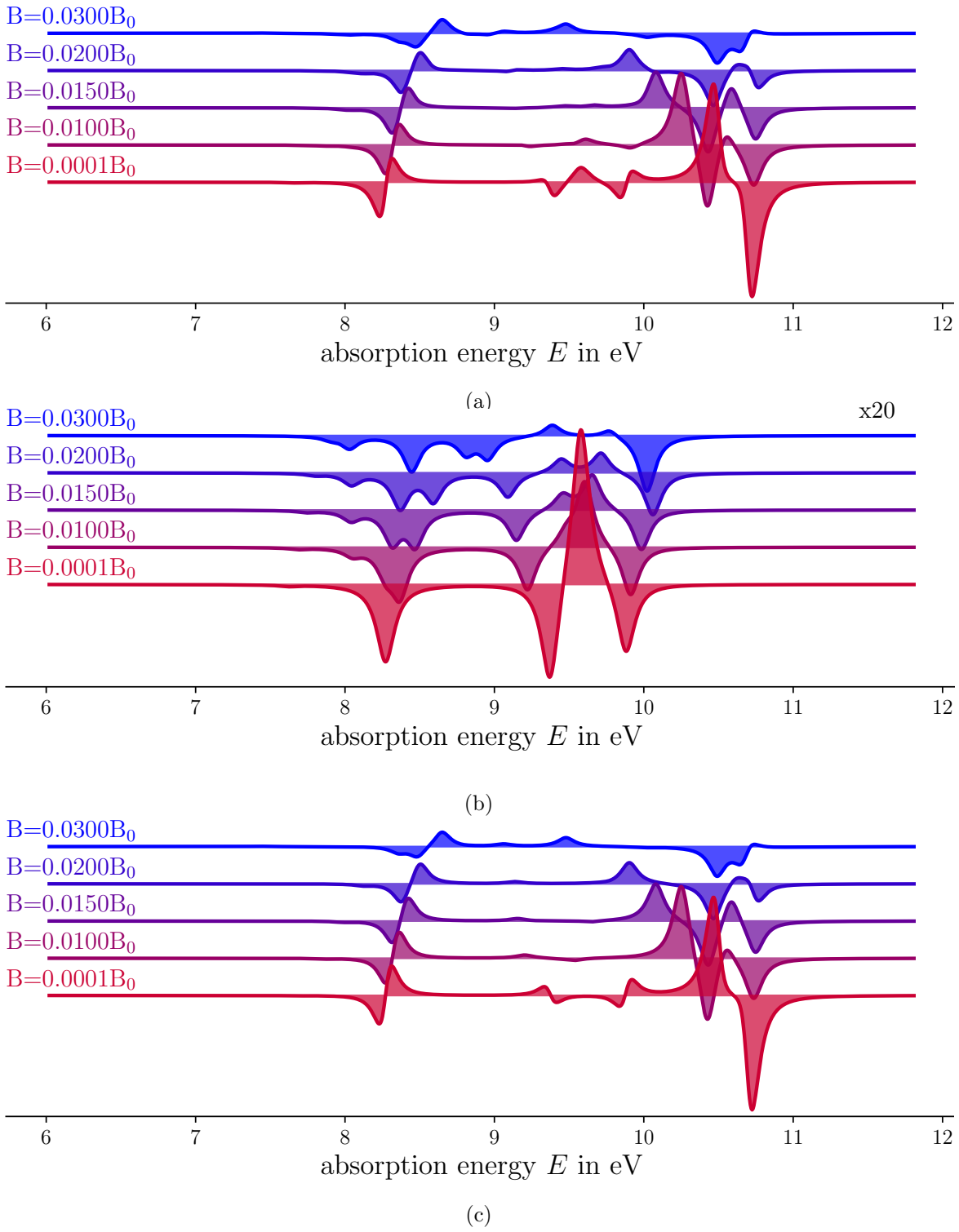

Figure 6.10: MCD spectra computed for cyclopropane in a strong magnetic field of various strength (fig. 6.10a). Contribution of the $B \parallel C_2$ component (fig. 6.10b) contribution of the $B \parallel C_3$ component to the MCD spectrum (fig. 6.10c). The intensity of the latter spectrum is scaled by a factor of 20.

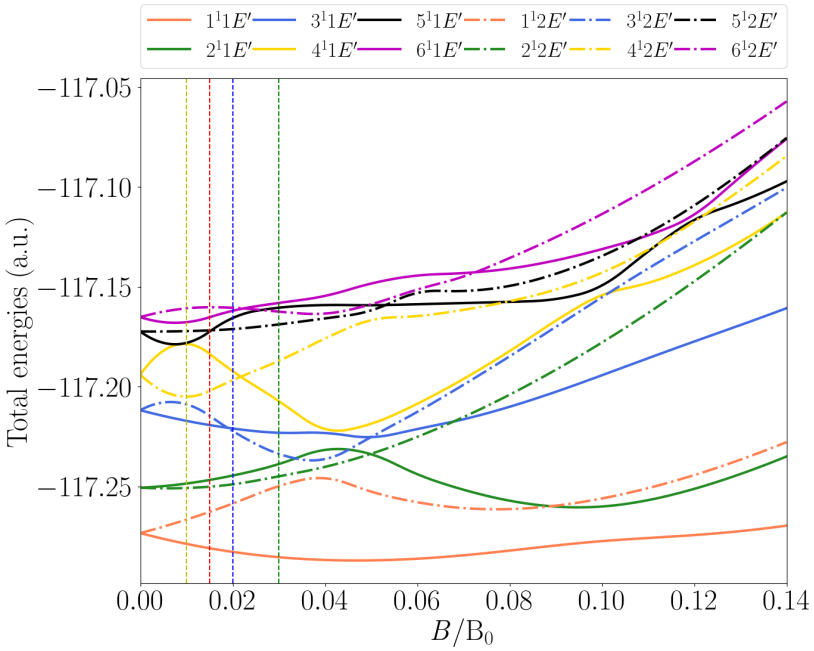

(a) $B \parallel C_3$. The vertical lines mark the magnetic field strength of the correspondingly colored spectra of fig. 6.10c.

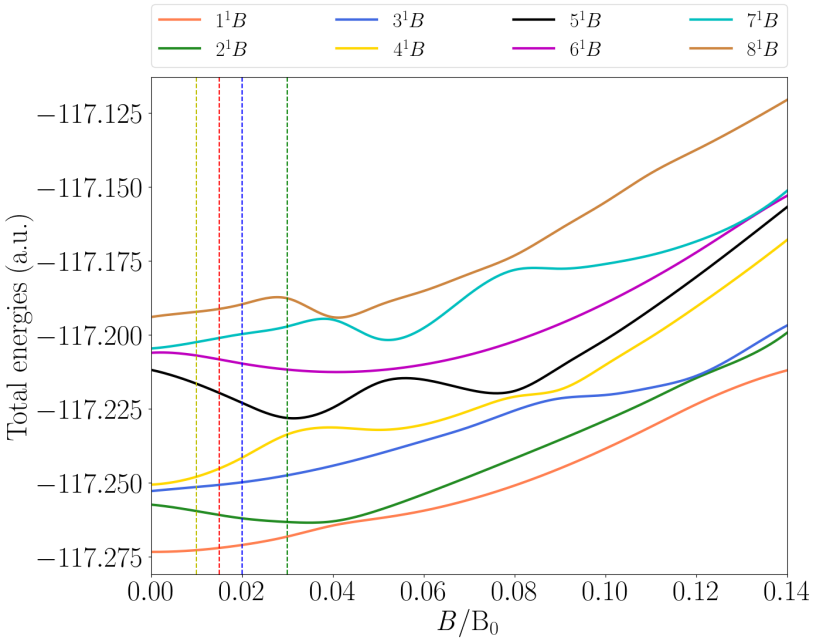

(b) $B \parallel C_2$. The vertical lines mark the magnetic field strength of the correspondingly colored spectra of fig. 6.10b.

Figure 6.11: Total energies of the excited states of cyclopropane contributing to the MCD spectrum, in an interval up to $B = 0.14$ B_0. The denomination of the states refers to the point group C_2 and only the states contributing to the MCD spectrum are shown.

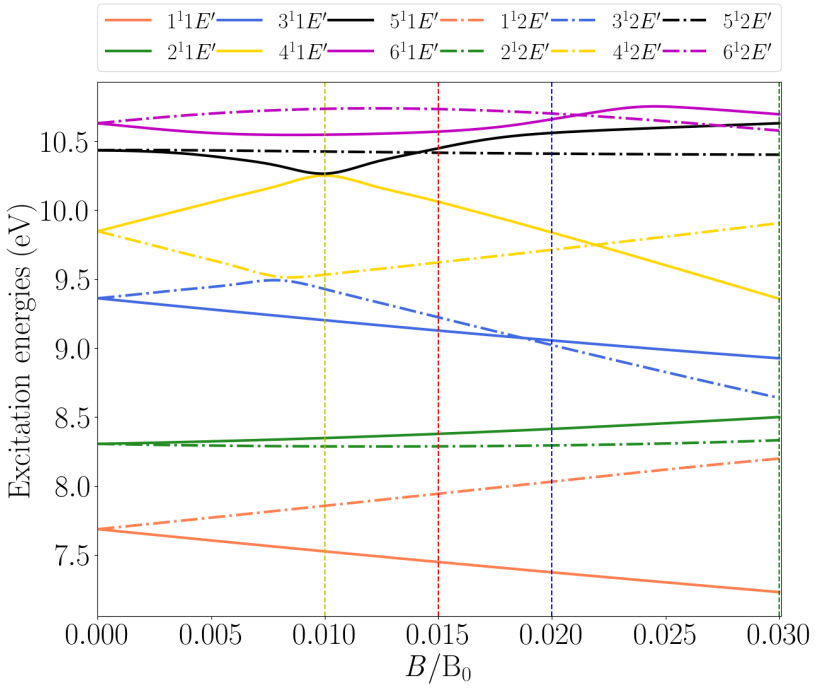

(a) $B \parallel C_3$. The vertical lines mark the magnetic field strength of the correspondingly colored spectra of fig. 6.10c.

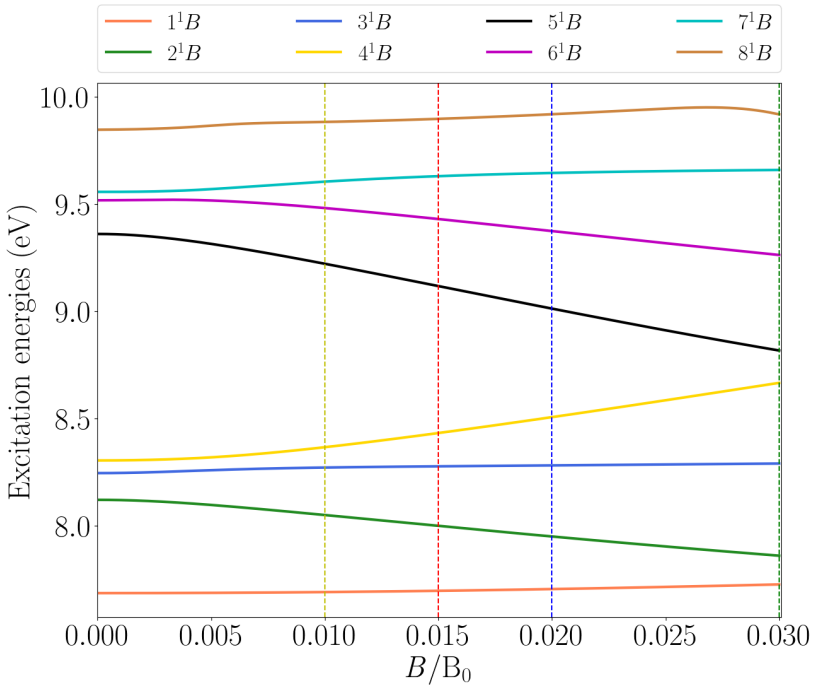

(b) $B \parallel C_2$. The vertical lines mark the magnetic field strength of the correspondingly colored spectra of fig. 6.10b.

Figure 6.12: Excitation energies of the excited states of cyclopropane contributing to the MCD spectrum, in an interval up to $B = 0.03$ B_0. Only the states contributing to the MCD spectrum are shown.

sponding excitation energies (fig. 6.12b and fig. 6.11b) need to be examined. The evolution of the peaks in an increasing magnetic field may be understood by analysing the behaviour of the corresponding excited states at the same field strengths. The states are evolving by gaining or lowering their excitation energy, causing a shift in the position of the peaks in the MCD spectrum. The different evolution of distinct states may therefore result in a split of previously superimposed features or, on the contrary, the superposition of peaks which were distinct before. The first meaningful feature at ≈ 8.25 eV corresponds to the overlap of the excitations to 3^1B and 4^1B. Increasing the field strength, the 3^1B excitation energy remains relatively constant, while the 4^1B transition is shifted to higher values. The previously overlapping peaks are therefore evolving into two distinct peaks of smaller intensity than the original one (whose intensity was the sum of the two peaks). The second feature analysed here is situated at ≈ 9.3 eV (5^1B). This peak is shifted to lower energies as the magnetic field strength increases, until the 5^1B and 4^1B states start to mix at higher magnetic field strengths. Finally, the $\mathscr{A}$ feature at ≈ 9.5 eV is obtained from the states 6^1B and 7^1B, which are nearly degenerate in the field-free case. The last peak, at ≈ 9.85 eV comes from the transition dipole moment of the excitation to state 8^1B, the last considered in this study. In principle, also higher-lying states could be considered, but this study has been restricted to the usual range of energies of an MCD spectrum, up to about 10 eV.

The spectrum of fig. 6.10c is more involved, but offers a good example to understand the effect of avoided crossings and mixing of states on the MCD spectrum. The behaviour of these states in an increasing field is analysed in figs. 6.11a-6.12a. The first $\mathscr{A}$ feature at $\approx$ 8.3 eV originates from the previously degenerate $2^11E'$ and $2^12E'$ states, which are split by the magnetic field. The higher-lying states experience avoided crossings, where the character of the states is mixing. As seen before, in the perturbative limit of a small magnetic field, three $\mathscr{A}$-like shapes are observed. The first and smallest feature at ≈ 9.36 eV is due to states $3^11E'$ and $3^12E'$, the second one at ≈ 9.85 eV to states $4^11E'$ and $4^12E'$. The third and largest feature at ≈ 10.43 eV-10.63 eV is caused by two overlapping peaks, originating from states $5^11E'$ and $5^12E'$ on one side, and $6^11E'$ and $6^12E'$ on the other side. From fig. 6.11a it is clear that these two couples of states lie close to each other. The avoided crossings between $3^12E'$ and $4^12E'$ and of $4^11E'$ and $5^11E'$ cause a complexity in the peak structure not predictable from the field-free spectrum. The mixing of the excited states brings in the contribution of states which in the field-free case had a vanishing transition dipole moment. Therefore, increasing the magnetic field strength, the MCD spectrum is undergoing major changes. These changes are only explained by looking at the evolution of the excited states and cannot be understood by simply referring to the field free case, as avoided crossings and splitting of degeneracies have a large influence on the peak structure.

6.3.5 MCD spectra of pyrazine and pyrimidine

The discussion on MCD spectroscopy may be concluded by showing the application of the developed finite-field approach to the calculation of the MCD spectra for two larger molecules, pyrazine (fig. 6.13a) and pyrimidine (fig. 6.13b). For both molecules a field-free geometry optimisation on B3LYP/6-31G* level was performed using Qchem.[298] The corresponding computation was performed by Simon Blaschke, using Cholesky decomposition of two-electron integrals.[103,299]

For both molecules, a comparison with experimental data is possible. The calculated spectra are very similar to the experimental ones in both cases. The reference spectra show that both molecules have a very similar MCD spectra. The highest peak of the pyrimidine spectrum is shifted of about $4 \cdot 10^3$ cm^{-1} with respect to the highest peak in the pyrazine spectrum. The accuracy of the finite-field method therefore is good enough to allow to

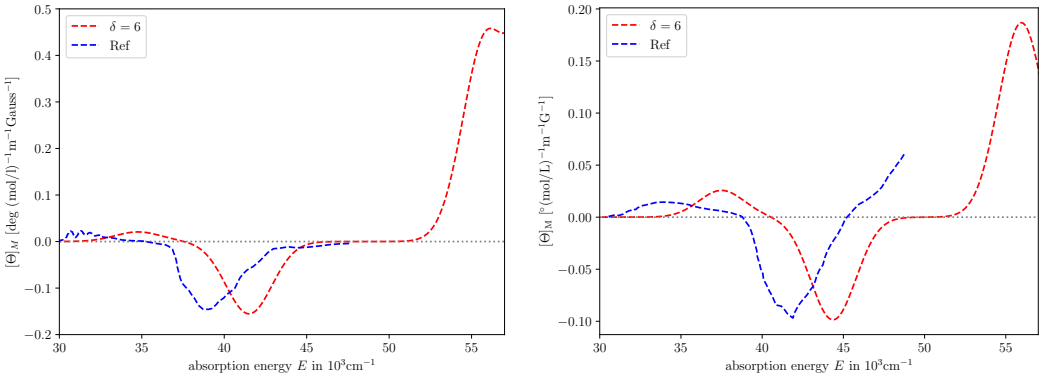

(a) (b)

Figure 6.13: Simulated MCD spectrum of pyrazine (fig. 6.13a) and pyrimidine (fig. 6.13b) in comparison to experimental spectrum (n-heptane) from ref. 117 (blue). The spectrum was calculated in a magnetic field of 10^{-4} B_0 on ff-CCSD/aug-cc-pVTZ level of theory. (Gaussian bandshape, $\sigma = 0.009$, Cholesky threshold $\delta = 6$).

distinguish between the spectra of the two molecules. The shape of the spectra computed with the finite-field approach shows a good agreement with the shape of the measured spectra. The relative position of the peaks is well-reproduced. The shift of the computed spectra with respect to the experiment is probably due to the lack of embedding effects in the computation, as the experiment was conducted in n-heptane.

Chapter 7

Quantum electrodynamics (QED): cavity chemistry

This thesis focuses on the description of molecules interacting with a finite magnetic field, in the regime of weak coupling between matter and light. However, a confinement in space of the electromagnetic fields results in a much more intense light-matter interaction, reaching the *strong-coupling regime*. Hybrid light-matter states are called *polaritons*;[143,300] because of the entanglement between light and matter, they cannot be explained through the features of the uncoupled states.[301] From a physical point of view, polaritonic states are used to fine-tune the photonic part of the system, modulating matter properties in a non-invasive way.[151,302]

Strong light-matter coupling is achieved inside optical cavities, which consist of highly reflective mirrors, with the role of confining the electromagnetic field in a restricted volume.[130] In the last years major advances have been made from an experimental point of view, reducing the cavity length to the order of nanometers,[303,304] therefore allowing to study regimes with a strong light-matter interaction. The mirrors constituting the cavity influence the characteristics of this coupling, and studies on absorption spectra, photochemical reaction rates and conductivity have been carried out from an experimental point of view.[143–147] Major results are documented from the Ebbesen group, where it was demonstrated that strong light-matter coupling can influence the reaction rate, slowing down or catalysing a reaction, and even inducing selectivity in the product formation.[148–150]

In order to predict and explain experimental results, a consistent theory has been developed in the literature for the description of polaritonic states.[131–133] As photons behave as bosons, a formalism in second quantisation consistent with the principle of quantum electrodynamics (QED) has been adopted. In general, the theories describing the chemistry inside optical cavities are seen as generalisations of the quantum-chemical methods in use: quantum electrodynamics density functional theory (QEDFT),[140,141,152] quantum electrodynamics Hartree-Fock (QED-HF),[136,137] quantum electrodynamics coupled cluster (QED-CC),[136,153–155] quantum electrodynamics FCI (QED-FCI)[137] and others.[156–159] In this thesis, the main aspects of field quantisation and QED Hamiltonians are discussed, necessary for the description of QED-HF and QED-CC. QED-UCC has been explored in the framework of quantum computing.[155] In this thesis, the first development of a QED-UCC2 approach is discussed, considered to be the first step towards higher-order QED-UCCn approximations.

7.1 Quantum Electrodynamic theory

7.1.1 Quantisation of fields

The experimental set up of an electromagnetic cavity is given by highly-reflective mirrors, in the simplest case, two parallel flat mirrors placed at a fixed distance (*Fabry-Pèrot* cavity).[305–307] The description of electrodynamics seen in sec. 2.2 is here continued to treat electromagnetic cavities.[130] The confinement of the electromagnetic field inside the volume of the cavity determines specific boundary conditions. In order to investigate the allowed modes, the vector potential $\mathbf{A}$ can be expanded in a Fourier series

$$\mathbf{A}(\mathbf{r},t) = \sum_{\mathbf{k}} \left[\mathbf{a}_{\mathbf{k}}(t) e^{i\mathbf{k}\cdot\mathbf{r}} + \mathbf{a}_{\mathbf{k}}{}^{*}(t) e^{-i\mathbf{k}\cdot\mathbf{r}} \right]. \tag{7.1.1}$$

Only modes whose half wavelength is a multiple of the cavity length are stable; a modulation of the mirror distance allows to control the allowed modes. In this chapter, the mirrors are assumed to be perfect reflectors, without any losses, which in fact is an ideal setup. For a cavity of volume V, the permitted wave vectors $\mathbf{k}$ have components

$$k_x = \frac{2\pi}{\sqrt[3]{V}} n_x, \qquad k_y = \frac{2\pi}{\sqrt[3]{V}} n_y, \qquad k_z = \frac{2\pi}{\sqrt[3]{V}} n_z, \tag{7.1.2}$$

where n_x, n_y, n_z are integer numbers. The frequency associated to a cavity is given by $\omega_k = kc$. From the literature,[130] it is known that the Hamiltonian for the fields in free space is

$$H = \frac{1}{8\pi} \int [(\frac{\partial \mathbf{A}}{\partial t})^2 + c^2 |\nabla \times \mathbf{A}|^2] \mathrm{d}^3\mathbf{r}. \tag{7.1.3}$$

Inserting the Fourier transform of the vector potential, the Hamiltonian becomes

$$H = \frac{V}{4\pi} \sum_{\mathbf{k}} (\dot{\mathbf{a}}_{\mathbf{k}}^{*}(t) \dot{\mathbf{a}}_{\mathbf{k}}(t) + c^2 k^2 \mathbf{a}_{\mathbf{k}}^{*}(t) \mathbf{a}_{\mathbf{k}}(t)) = \frac{1}{2} \sum_{\mathbf{k}} (\mathbf{p}_{\mathbf{k}}^{*} \cdot \mathbf{p}_{\mathbf{k}} + c^2 k^2 \mathbf{q}_{\mathbf{k}}^{*}(t) \mathbf{q}_{\mathbf{k}}(t)), \tag{7.1.4}$$

where $\mathbf{p}_{\mathbf{k}} = \dot{\mathbf{a}}_{\mathbf{k}} \sqrt{\frac{V}{2\pi}}$ and $\mathbf{q}_{\mathbf{k}} = \mathbf{a}_{\mathbf{k}} \sqrt{\frac{V}{2\pi}}$ have been defined.

Referring to the theory in free space in sec. 2.2, eq. 2.2.14 reduces to a standard wave equation when the current vector vanishes, i.e., $\mathbf{J} = 0$:

$$\frac{\partial^2 \mathbf{a}_{\mathbf{k}}(t)}{\partial t^2} + c^2 \mathbf{a}_{\mathbf{k}}(t) = 0. \tag{7.1.5}$$

The Fourier components $\mathbf{a}_{\mathbf{k}}(t)$ depend on t as $\mathbf{a}_{\mathbf{k}}(t) \sim e^{-i\omega t}$, with $\omega = ck$. The vector potential therefore corresponds to a wave propagating in the direction $\hat{\mathbf{k}}$ at the speed of light. In this thesis, the Coulomb gauge is chosen (eq. 2.2.11), which for the quantised vector potential yields

$$\nabla \cdot \sum_{\mathbf{k}} \left[\mathbf{a}_{\mathbf{k}}(t) e^{i\mathbf{k}\cdot\mathbf{r}} + \mathbf{a}_{\mathbf{k}}^{*}(t) e^{-i\mathbf{k}\cdot\mathbf{r}} \right] = i \sum_{\mathbf{k}} \left[\mathbf{k} \cdot \mathbf{a}_{\mathbf{k}}(t) e^{i\mathbf{k}\cdot\mathbf{r}} - \mathbf{k} \cdot \mathbf{a}_{\mathbf{k}}^{*}(t) e^{-i\mathbf{k}\cdot\mathbf{r}} \right] = 0, \tag{7.1.6}$$

therefore implying the mode amplitudes to be orthogonal to the propagation direction ($\mathbf{k} \cdot \mathbf{a}_{\mathbf{k}}(t) = 0$). The vector potential is orthogonal to $\mathbf{k}$ and defined in the space spanned by two basis vectors, $\boldsymbol{\varepsilon}_{\mathbf{k},\nu}$, with $\nu = 1, 2$

$$\mathbf{a}_{\mathbf{k}} = \sum_{\nu} \boldsymbol{\varepsilon}_{\mathbf{k},\nu} a_{\mathbf{k},\nu}. \tag{7.1.7}$$

Substitution yields an expression of the vector potential expressed through the basis vectors $a_{\mathbf{k},\nu}$

$$\mathbf{A}(\mathbf{r}) = \sum_{\mathbf{k},\nu} \left[\boldsymbol{\varepsilon}_{\mathbf{k},\nu} a_{\mathbf{k},\nu} e^{i\mathbf{k}\cdot\mathbf{r}} + \boldsymbol{\varepsilon}^*_{\mathbf{k},\nu} a^*_{\mathbf{k},\nu} e^{-i\mathbf{k}\cdot\mathbf{r}} \right]. \tag{7.1.8}$$

From Maxwell's equations, the quantised electric and magnetic fields are obtained

$$\mathbf{E}(\mathbf{r}) = ic \sum_{\mathbf{k},\nu} \mathbf{k} \left(\boldsymbol{\varepsilon}_{\mathbf{k},\nu} a_{\mathbf{k},\nu} e^{i\mathbf{k}\cdot\mathbf{r}} - \boldsymbol{\varepsilon}^*_{\mathbf{k},\nu} a^*_{\mathbf{k},\nu} e^{-i\mathbf{k}\cdot\mathbf{r}} \right), \tag{7.1.9}$$

$$\mathbf{B}(\mathbf{r}) = i \sum_{\mathbf{k},\nu} \left[\left(\mathbf{k} \times \boldsymbol{\varepsilon}_{\mathbf{k},\nu} \right) a_{\mathbf{k},\nu} e^{i\mathbf{k}\cdot\mathbf{r}} - \left(\mathbf{k} \times \boldsymbol{\varepsilon}^*_{\mathbf{k},\nu} \right) a^*_{\mathbf{k},\nu} e^{-i\mathbf{k}\cdot\mathbf{r}} \right]. \tag{7.1.10}$$

7.1.2 Hamiltonian in free space

From eq. 7.1.4, it appears that the Hamiltonian in free space can be seen as a sum of decoupled oscillators. Shifting from classical mechanics to quantum mechanics, the classical quantities of position and momentum become operators, yielding

$$\hat{H} = \frac{1}{2} \sum_{\mathbf{k},\nu} \left(\hat{p}_{\mathbf{k},\nu} \right)^2 + \omega^2_{\mathbf{k}} \left(\hat{q}_{\mathbf{k},\nu} \right)^2. \tag{7.1.11}$$

Defining suitable creation and annihilation operators

$$\hat{b}_{\mathbf{k},\nu} = \sqrt{\frac{1}{2\omega_{\mathbf{k}}}} \left(\omega_{\mathbf{k}} \hat{q}_{\mathbf{k},\nu} + i \hat{p}_{\mathbf{k},\nu} \right), \qquad \hat{b}^\dagger_{\mathbf{k},\nu} = \sqrt{\frac{1}{2\omega_{\mathbf{k}}}} \left(\omega_{\mathbf{k}} \hat{q}_{\mathbf{k},\nu} - i \hat{p}_{\mathbf{k},\nu} \right), \tag{7.1.12}$$

the Hamiltonian is reformulated to give

$$\hat{H} = \sum_{\mathbf{k}\nu} \left(\hat{b}^\dagger_{\mathbf{k},\nu} \hat{b}_{\mathbf{k},\nu} + \frac{1}{2} \right) \omega_k. \tag{7.1.13}$$

Electromagnetic fields are described by photons, which behave as bosons. Therefore, they have to fulfill the commutation relations

$$[\hat{b}^\dagger_{\mathbf{k},\nu}, \hat{b}^\dagger_{\mathbf{k}',\nu'}] = 0, \qquad [\hat{b}_{\mathbf{k},\nu}, \hat{b}_{\mathbf{k}',\nu'}] = 0, \qquad [\hat{b}^\dagger_{\mathbf{k},\nu}, \hat{b}^\dagger_{\mathbf{k}',\nu'}] = \delta_{\mathbf{k}\mathbf{k}'} \delta_{\nu\nu'}. \tag{7.1.14}$$

Analogously to the occupation number vectors exploited by the second quantisation for electrons, occupation number vectors are used for bosons. These have no restriction on the occupations, which can be arbitrarily high

$$|n_{\mathbf{k},\nu}\rangle = \prod_{\mathbf{k},\nu} \frac{\left(\hat{b}^\dagger_{\mathbf{k},\nu} \right)^{n_{\mathbf{k},\nu}}}{(n_{\mathbf{k},\nu})!} |0\rangle. \tag{7.1.15}$$

The associated energies are the eigenvalues of eq. 7.1.13

$$E_n = \omega_{\mathbf{k}} \left(n + \frac{1}{2} \right). \tag{7.1.16}$$

In terms of $\hat{b}_{\mathbf{k},\nu}$ and $\hat{b}^\dagger_{\mathbf{k},\nu}$, the vector potential and the electric and magnetic fields are rewritten as

$$\mathbf{A}(\mathbf{r}) = \sum_{\mathbf{k},\nu} \sqrt{\frac{2\pi}{ckV}} \left[\boldsymbol{\varepsilon}_{\mathbf{k},\nu} \hat{b}_{\mathbf{k},\nu} e^{i\mathbf{k}\cdot\mathbf{r}} + \boldsymbol{\varepsilon}^*_{\mathbf{k},\nu} \hat{b}^\dagger_{\mathbf{k},\nu} e^{-i\mathbf{k}\cdot\mathbf{r}} \right], \tag{7.1.17}$$

$$\mathbf{E}(\mathbf{r}) = i \sum_{\mathbf{k},\nu} \sqrt{\frac{2\pi ck}{V}} \left(\boldsymbol{\varepsilon}_{\mathbf{k},\nu} \hat{b}_{\mathbf{k},\nu} e^{i\mathbf{k}\cdot\mathbf{r}} - \boldsymbol{\varepsilon}^*_{\mathbf{k},\nu} \hat{b}^\dagger_{\mathbf{k},\nu} e^{-i\mathbf{k}\cdot\mathbf{r}} \right), \tag{7.1.18}$$

$$\mathbf{B}(\mathbf{r}) = i \sum_{\mathbf{k},\nu} \sqrt{\frac{2\pi}{ckV}} \left[\left(\mathbf{k} \times \boldsymbol{\varepsilon}_{\mathbf{k},\nu} \right) \hat{b}_{\mathbf{k},\nu} e^{i\mathbf{k}\cdot\mathbf{r}} - \left(\mathbf{k} \times \boldsymbol{\varepsilon}^*_{\mathbf{k},\nu} \right) \hat{b}^\dagger_{\mathbf{k},\nu} e^{-i\mathbf{k}\cdot\mathbf{r}} \right]. \tag{7.1.19}$$

7.1.3 Hamiltonian for light-matter interaction

In optical cavities, the system is exposed to a strong light-matter coupling. The Hamiltonian describing this situation is known as *minimal-coupling* Hamiltonian[140,159,308]

$$\hat{H} = \frac{1}{2}\sum_i (\hat{p}_i + \mathbf{A}(\mathbf{r}_i))^2 + \frac{1}{8\pi}\int [(\frac{\partial \mathbf{A}}{\partial t})^2 + c^2 |\nabla \times \mathbf{A}|^2] \mathrm{d}^3\mathbf{r} + \hat{V}_{\mathrm{ee}} + \hat{V}_{\mathrm{NN}} + \hat{V}_{\mathrm{eN}}. \tag{7.1.20}$$

The light-matter coupling is given by the paramagnetic ($\sum_i \hat{p}_i \cdot \mathbf{A}(\mathbf{r}_i)$) and the diamagnetic terms ($\frac{1}{2}\sum_i \mathbf{A}(\mathbf{r}_i)^2$). Substituting the quantised vector potential into eq. 7.1.20, the minimal-coupling Hamiltonian becomes

$$\begin{aligned}\hat{H} = \hat{H}_{\mathrm{el}} + \sum_{\mathbf{k},\nu} \omega_k \hat{b}^\dagger_{\mathbf{k},\nu} \hat{b}_{\mathbf{k},\nu} + \sum_i \sum_{\mathbf{k},\nu} \frac{\lambda}{\sqrt{2\omega_k}} (\hat{p}_i \cdot \boldsymbol{\varepsilon}_{\mathbf{k},\nu})(\hat{b}_{\mathbf{k},\nu} e^{i\mathbf{k}\cdot\mathbf{r}_i} + \hat{b}^\dagger_{\mathbf{k},\nu} e^{-i\mathbf{k}\cdot\mathbf{r}_i}) + \\ + \sum_i \sum_{\mathbf{k},\mathbf{k}',\nu} \frac{\lambda^2}{4\sqrt{\omega_k \omega_{k'}}} (\hat{b}_{\mathbf{k},\nu} e^{i\mathbf{k}\cdot\mathbf{r}_i} + \hat{b}^\dagger_{\mathbf{k},\nu} e^{-i\mathbf{k}\cdot\mathbf{r}_i})(\hat{b}_{\mathbf{k}',\nu} e^{i\mathbf{k}'\cdot\mathbf{r}_i} + \hat{b}^\dagger_{\mathbf{k}',\nu} e^{-i\mathbf{k}'\cdot\mathbf{r}_i}),\end{aligned} \tag{7.1.21}$$

where $\lambda = \sqrt{\frac{4\pi}{V}}$ is the light-matter coupling strength. From this formulation, it is apparent that smaller cavities achieve higher coupling strengths, and therefore the light-matter interaction has a larger effect.[303,309,310] In eq. 7.1.21 the sum over the wave numbers is in principle infinite; here the discussion is restricted to one single mode, which is in most cases enough to obtain a qualitatively accurate description of the field effects.

Furthermore, in most experimental settings the field wave length is significantly larger than the molecular size. Thus, $e^{i\mathbf{k}'\cdot\mathbf{r}_i}$ can be approximated with 1 (*dipole approximation*).[136,159,308,311] This approximation is valid in most cases for linearly polarised cavities, in which the wavelength of the field is much larger than the size of the cavity. The Hamiltonian simplifies to

$$\hat{H} = \hat{H}_{\mathrm{el}} + \omega \hat{b}^\dagger \hat{b} + \sum_i \frac{\lambda}{\sqrt{2\omega}} (\hat{p}_i \cdot \boldsymbol{\varepsilon})(\hat{b} + \hat{b}^\dagger) + \sum_i \frac{\lambda^2}{4\omega} (\hat{b} + \hat{b}^\dagger)^2. \tag{7.1.22}$$

The third term is describing the light-matter interaction, through the momentum operator. Since it is known that $\hat{p}$ makes the convergence quite slow with respect to the basis set size, in literature the light-matter interaction is usually described by a unitarily transformed version of eq. 7.1.22, known as *Pauli-Zienau-Woolley* (PZW) form,[312–316]

$$\hat{U} = e^{i(\hat{d}\cdot\boldsymbol{\varepsilon})(\hat{b}+\hat{b}^\dagger)}, \tag{7.1.23}$$

passing from the so-called *length gauge* to the *velocity gauge*. Here $\hat{d}$ represents the molecular dipole operator, defined as the sum of the electronic and the nuclear dipole $\hat{d} = \hat{d}_{\mathrm{nuc}} + \hat{d}_{\mathrm{el}}$. The PZW Hamiltonian in dipole approximation yields

$$\hat{H} = \hat{H}_{\mathrm{el}} + \omega \hat{b}^\dagger \hat{b} - \lambda \sqrt{\frac{\omega}{2}} (\hat{d}\cdot\boldsymbol{\varepsilon})(\hat{b} + \hat{b}^\dagger) + \frac{\lambda^2}{2} (\hat{d}\cdot\boldsymbol{\varepsilon})^2. \tag{7.1.24}$$

Light-matter interaction is mediated by the molecular dipole operator. The last term is the dipole self-interaction term, whose presence has been debated in the literature, which proves that it is necessary to ensure a Hamiltonian bound from below.[141,317]

In order to construct a framework for UCC inside a cavity, the HF reference has to be constructed and analysed. In this thesis, the work by Haugland *et al.* in ref. 136 is followed.

7.1.4 QED-HF

In this section, the Hartree-Fock method is expanded to the QED framework, in order to provide a starting point for the targeted post-HF methods. The wave function for non-interacting electrons and photons can be factorised into a pure electronic and a pure photonic part

$$|\Psi\rangle = |\Psi_{\text{el}}\rangle\,|\Psi_{\text{ph}}\rangle\,, \tag{7.1.25}$$

where the photonic part is an occupation number vector as seen in eq. 7.1.15. Due to the factorisation of the wave function, also the Schrödinger equation can be split into the solution of the electronic and of the photonic part

$$\hat{H}_{\text{QED}}\,|\Psi\rangle = E\,|\Psi\rangle \implies \begin{cases} \langle\Psi_{\text{el}}|\,\hat{H}_{\text{QED}}\,|\Psi_{\text{el}}\rangle\,|\Psi_{\text{ph}}\rangle = E\,\langle\Psi_{\text{el}}|\Psi_{\text{el}}\rangle\,|\Psi_{\text{ph}}\rangle \\ \langle\Psi_{\text{ph}}|\,\hat{H}_{\text{QED}}\,|\Psi_{\text{ph}}\rangle\,|\Psi_{\text{el}}\rangle = E\,\langle\Psi_{\text{ph}}|\Psi_{\text{ph}}\rangle\,|\Psi_{\text{el}}\rangle\,. \end{cases} \tag{7.1.26}$$

The two equations have to be solved simultaneously. For a chosen HF state, the electronic expectation value $\langle\Psi_{\text{el}}|\,\hat{H}_{\text{QED}}\,|\Psi_{\text{el}}\rangle$ may be minimised with respect to the photonic coefficient

$$\langle\Psi_{\text{el}}|\,\hat{H}_{\text{QED}}\,|\Psi_{\text{el}}\rangle = E_{\text{el}} + \omega\hat{b}^\dagger\hat{b} - \lambda\sqrt{\frac{\omega}{2}}(\langle\Psi_{\text{el}}|\,\hat{d}\,|\Psi_{\text{el}}\rangle\cdot\boldsymbol{\varepsilon})(\hat{b}+\hat{b}^\dagger) + \frac{\lambda^2}{2}\,\langle\Psi_{\text{el}}|\,(\hat{d}\cdot\boldsymbol{\varepsilon})^2\,|\Psi_{\text{el}}\rangle\,. \tag{7.1.27}$$

This purely photonic Hamiltonian can be diagonalised through a *coherent-state* transformation, performed through the unitary operator

$$\hat{U} = e^{z\hat{b}^\dagger - z^*\hat{b}} \qquad \text{with} \qquad z = -\frac{\lambda\boldsymbol{\varepsilon}\cdot\langle\Psi_{\text{el}}|\,\hat{d}\,|\Psi_{\text{el}}\rangle}{\sqrt{2\omega}}. \tag{7.1.28}$$

In the coherent-state basis, the transformed Hamiltonian simplifies to

$$\langle\Psi_{\text{el}}|\,\hat{\tilde{H}}_{\text{QED}}\,|\Psi_{\text{el}}\rangle = E_{\text{el}} + \omega\hat{b}^\dagger\hat{b} + \frac{\lambda^2}{2}\,\langle\Psi_{\text{el}}|\,(\boldsymbol{\varepsilon}\cdot\hat{d})^2\,|\Psi_{\text{el}}\rangle\,. \tag{7.1.29}$$

where no terms linear in the creation or annihilation operators appear. The eigenstates of this transformed Hamiltonian are the photon number states $|n\rangle$, which in the untransformed basis are expressed as

$$|n\rangle \longrightarrow e^{z\hat{b}^\dagger - z^*\hat{b}}\frac{\hat{b}^{\dagger n}}{\sqrt{n!}}\,|0\rangle\,. \tag{7.1.30}$$

Applying the coherent-state basis to the PZW Hamiltonian in eq. 7.1.24 leads to the final form which will be used for the construction of QED-UCC

$$\hat{\tilde{H}}_{\text{QED}} = \hat{H}_{\text{el}} + \omega\hat{b}^\dagger\hat{b} + \frac{\lambda^2}{2}(\boldsymbol{\varepsilon}\cdot(\hat{d}-\langle d\rangle))^2 - \sqrt{\frac{\omega}{2}}\lambda(\boldsymbol{\varepsilon}\cdot(\hat{d}-\langle d\rangle))(\hat{b}^\dagger+\hat{b}). \tag{7.1.31}$$

This expression is manifestly origin independent.

7.1.5 QED-CC

Following the notation in ref. 136, the Coupled Cluster method used to describe the wave function inside an optical cavity. The excitation operator $\hat{T}$ has here to account for purely electronic, purely photonic and mixed electronic and photonic excitations

$$|\Psi_{\text{QED-CC}}\rangle = e^{\hat{Z}}\,|0,0\rangle = e^{\hat{T}+\hat{S}+\hat{\Gamma}}\,|0,0\rangle\,, \tag{7.1.32}$$

where the excitation operators are defined as follows

$$\begin{cases} \hat{T} = \hat{T}_1 + \hat{T}_2 + \cdots = \sum_{ia} t_i^a \hat{a}_a^\dagger \hat{a}_i + \frac{1}{4}\sum_{ijab} t_{ij}^{ab} \hat{a}_a^\dagger \hat{a}_b^\dagger \hat{a}_j \hat{a}_i + \dots \\ \hat{S} = \hat{S}_1^1 + \hat{S}_2^1 + \cdots + \hat{S}_1^2 + \hat{S}_2^2 + \cdots = \sum_{ia}\sum_\alpha s_{ia}^\alpha \hat{a}_a^\dagger \hat{a}_i \hat{b}_\alpha^\dagger + \frac{1}{4}\sum_{ijab}\sum_\alpha s_{ijab}^\alpha \hat{a}_a^\dagger \hat{a}_b^\dagger \hat{a}_j \hat{a}_i \hat{b}_\alpha^\dagger + \dots \\ \qquad + \frac{1}{2}\sum_{ia}\sum_{\alpha\beta} s_{ia}^{\alpha\beta} \hat{a}_a^\dagger \hat{a}_i \hat{b}_\alpha^\dagger \hat{b}_\beta^\dagger + \frac{1}{8}\sum_{ijab}\sum_{\alpha\beta} s_{ijab}^{\alpha\beta} \hat{a}_a^\dagger \hat{a}_b^\dagger \hat{a}_j \hat{a}_i \hat{b}_\alpha^\dagger \hat{b}_\beta^\dagger + \dots \\ \qquad + \frac{1}{2}\sum_{ia}\sum_{\alpha} s_{ia}^{\alpha\alpha} \hat{a}_a^\dagger \hat{a}_i \hat{b}_\alpha^\dagger \hat{b}_\alpha^\dagger + \frac{1}{8}\sum_{ijab}\sum_{\alpha} s_{ijab}^{\alpha\alpha} \hat{a}_a^\dagger \hat{a}_b^\dagger \hat{a}_j \hat{a}_i \hat{b}_\alpha^\dagger \hat{b}_\alpha^\dagger + \dots \\ \hat{\Gamma} = \hat{\Gamma}_1 + \hat{\Gamma}_2 + \cdots = \sum_\alpha \gamma_\alpha \hat{b}_\alpha^\dagger + \frac{1}{2}\sum_{\alpha\beta} \gamma_{\alpha\beta} \hat{b}_\alpha^\dagger \hat{b}_\beta^\dagger + \frac{1}{2}\sum_\alpha \gamma_{\alpha\alpha} \hat{b}_\alpha^\dagger \hat{b}_\alpha^\dagger + \dots \end{cases} \tag{7.1.33}$$

As in ref. 136, only operators with at most one photon operator are considered, leading to the simplification of the photonic and mixed excitation operators to $\hat{S} = \hat{S}_1^1 + \hat{S}_2^1 + \dots$ and $\hat{\Gamma} = \hat{\Gamma}_1$. In the QED frame, the expansion basis is given by $\{|0,0\rangle, |\mu,0\rangle, |0,1\rangle, |\mu,1\rangle\}$, where the first position is reserved to the electronic excitations and the second position to the photonic ones ($|0,0\rangle$ is the ground state). The QED-CC energy is expressed as

$$E_{\mathrm{QED-CC}} = \langle 0,0| e^{-(\hat{T}+\hat{S}+\hat{\Gamma})} \hat{H} e^{\hat{T}+\hat{S}+\hat{\Gamma}} |0,0\rangle = \langle 0,0| e^{-\hat{Z}} \hat{H} e^{\hat{Z}} |0,0\rangle . \tag{7.1.34}$$

The similarity transformed Hamiltonian is treated with the Baker-Campbell-Hausdorff expansion. The series truncates after the fourth commutator, as the QED-Hamiltonian is still a two particle operator.

In analogy to the electronic CC theory, the amplitudes are found through projection on the basis $\langle \mu, k|$, where μ labels the electronic excitations and k the number of photons (here k=0,1),

$$\langle \mu,0| e^{-(\hat{T}+\hat{S}+\hat{\Gamma})} \hat{H} e^{\hat{T}+\hat{S}+\hat{\Gamma}} |0,0\rangle = 0 \qquad \text{ampl. eq. for } t_\mu, \tag{7.1.35}$$

$$\langle \mu,1| e^{-(\hat{T}+\hat{S}+\hat{\Gamma})} \hat{H} e^{\hat{T}+\hat{S}+\hat{\Gamma}} |0,0\rangle = 0 \qquad \text{ampl. eq. for } s_\mu^1, \tag{7.1.36}$$

$$\langle 0,1| e^{-(\hat{T}+\hat{S}+\hat{\Gamma})} \hat{H} e^{\hat{T}+\hat{S}+\hat{\Gamma}} |0,0\rangle = 0 \qquad \text{ampl. eq. for } \gamma_1. \tag{7.1.37}$$

7.1.6 QED-UCC

The unitary parameterisation can be adapted to the optical cavity to obtain a Hermitian theory

$$|\Psi_{\mathrm{QED-UCC}}\rangle = e^{\hat{Z}-\hat{Z}^\dagger} |0,0\rangle = e^{\hat{\sigma}-\hat{\sigma}^\dagger+\hat{S}-\hat{S}^\dagger+\hat{\Gamma}-\hat{\Gamma}^\dagger} |0,0\rangle , \tag{7.1.38}$$

where the operators are defined as in eq. 7.1.33. Like in the previous sections, only single photonic excitations are considered here. The expansion basis consists of $\{|0,0\rangle, |\mu,0\rangle, |0,1\rangle, |\mu,1\rangle\}$. Furthermore, electronic excitations are restricted to singles and doubles excitations. The energy and amplitude equations are

$$\begin{aligned} &\langle 0,0| e^{-(\hat{Z}-\hat{Z}^\dagger)} \hat{H} e^{\hat{Z}-\hat{Z}^\dagger} |0,0\rangle = E_{\mathrm{QED-UCC}}, \\ &\langle \mu,0| e^{-(\hat{Z}-\hat{Z}^\dagger)} \hat{H} e^{\hat{Z}-\hat{Z}^\dagger} |0,0\rangle = 0 \qquad \text{ampl. eq. for } \sigma_\mu, \\ &\langle \mu,1| e^{-(\hat{Z}-\hat{Z}^\dagger)} \hat{H} e^{\hat{Z}-\hat{Z}^\dagger} |0,0\rangle = 0 \qquad \text{ampl. eq. for } s_\mu^1, \\ &\langle 0,1| e^{-(\hat{Z}-\hat{Z}^\dagger)} \hat{H} e^{\hat{Z}-\hat{Z}^\dagger} |0,0\rangle = 0 \qquad \text{ampl. eq. for } \gamma_1. \end{aligned} \tag{7.1.39}$$

The expansion of the unitarily transformed Hamiltonian $e^{-(\hat{Z}-\hat{Z}^\dagger)} \hat{H} e^{\hat{Z}-\hat{Z}^\dagger}$ has the same issues as discussed in sec. 3; the Bernoulli expansion will be exploited once again.[160]

Adopting the same truncation scheme as for UCCn, the amplitude equations are truncated at nth order. Here the zeroth order Hamiltonian is

$$\hat{H}_0 = \hat{F}^{\mathrm{QED-HF}} + \omega \hat{b}^\dagger \hat{b} \tag{7.1.40}$$

where the QED-Fock operator is

$$F_{pq}^{\mathrm{QED-HF}} = \hat{F}_{\mathrm{el}} + \frac{\lambda^2}{2}\sum_a (\hat{\tilde{d}}\cdot\varepsilon)_{pa}(\hat{\tilde{d}}\cdot\varepsilon)_{aq} - \frac{\lambda^2}{2}\sum_i (\hat{\tilde{d}}\cdot\varepsilon)_{pi}(\hat{\tilde{d}}\cdot\varepsilon)_{iq}, \tag{7.1.41}$$

as in ref. 318; the notation $\hat{\tilde{d}} = \hat{d} - \langle d\rangle$ has been adopted. The perturbation is composed as follows:

$$\hat{H}' = \hat{H}_{\mathrm{el}} - \hat{F}^{\mathrm{QED-HF}} - \lambda\sqrt{\frac{\omega}{2}}(\hat{\tilde{d}}\cdot\boldsymbol{\varepsilon})(\hat{b}+\hat{b}^\dagger), \tag{7.1.42}$$

consisting of a pure electronic term and a coupling term of light and matter. The perturbative order of the mixed operators $\hat{S}_1^1$ and $\hat{S}_2^1$ is derived from the first order correction to the wave function in MP theory. As $\hat{H}'$ only has one-electron one-photon operators, only $\hat{S}_1^1$ contributes to the first order correction to the wave function. $\hat{S}_2^1$ is needed only from the second order correction. The $\hat{\Gamma}_1$ amplitudes cannot contribute to the first order wave function, as

$$\langle 0,1|\,(\hat{\tilde{d}}\cdot\boldsymbol{\varepsilon})(\hat{b}+\hat{b}^\dagger)\,|0,0\rangle = \langle d\rangle - \langle d\rangle = 0. \tag{7.1.43}$$

However, this result is bound to the choice of the HF method. The coherent-state HF wave function is not the only possible choice. Therefore, for other choices of the HF reference determinant, the operator $\hat{\Gamma}_1$ also has contributions at first order in perturbation theory.

The perturbation orders are here recapitulated:

- $\hat{\sigma}_1$ second order and $\hat{\sigma}_2$ first order;
- $\hat{S}_1^1$ first order and $\hat{S}_2^1$ second order;
- $\hat{\Gamma}_1$ second order.

The UCC amplitude equations can therefore be truncated according to perturbation theory. In this thesis, only the QED-UCC2 method is developed, as QED-UCC3 needs further inspection.

7.2 QED-UCC2 implementation

In this thesis, QED-UCC theory war explicitly developed at second order in perturbation theory. Not only amplitude equations for the electronic amplitudes need to be solved, but also equations for the purely photonic amplitudes γ and the mixed amplitudes s have to be derived. The σ-amplitudes have to account for the coupling to the cavity and are altered by it. Therefore, the σ-amplitude equations are not the same as outside the cavity, as some terms depending on the mixed electronic-photonic amplitudes arise

$$\begin{aligned} \bar{H}_{ai} &= \bar{H}_{ai}^{\mathrm{el}} + \tilde{d}_{ab}^{\alpha} s_{bi}^{\alpha} - \tilde{d}_{ji}^{\alpha} s_{aj}^{\alpha} = 0, \\ \bar{H}_{abij} &= \bar{H}_{abij}^{\mathrm{el}} + P(ab)P(ij)\tilde{d}_{ai}^{\alpha} s_{bj}^{\alpha} = 0, \end{aligned} \tag{7.2.1}$$

where it has to be underlined that the wave function is constructed on top of the coherent-state HF determinant (sec. 3.2.1), for which $\hat{\tilde{d}}_{pq} = \hat{d}_{pq} - \langle\hat{d}\rangle\delta_{pq}$. The terms $\bar{H}_{ai}^{\mathrm{el}}$ and $\bar{H}_{abij}^{\mathrm{el}}$ represent the electronic amplitude equations in free space, the same as in section 4.3. In order to be consistent with the perturbation order, no contributions exceeding second order are considered. It can be recalled here that for the mixed amplitudes, $\hat{S}_1^1$ is first order and $\hat{S}_2^1$ second order in perturbation theory, while the photonic amplitude Γ_1 is second order.

The amplitude equations for the mixed operators $\hat{S}_1^1$ and $\hat{S}_2^1$ are derived

$$\begin{aligned}\bar{H}_{ai}^{\alpha} =& \tilde{d}_{ai}^{\alpha} + \omega s_{ai}^{\alpha} + \tilde{d}_{jb}^{\alpha}\sigma_{ij}^{ab} - f_{ji}s_{aj}^{\alpha} + f_{ab}s_{bi}^{\alpha} + f_{jb}s_{abij}^{\alpha} + s_{ai}^{\alpha}\tilde{d}_{jj}^{\alpha} + \langle aj||ib\rangle\, s_{bj}^{\alpha} = 0 \\ \bar{H}_{abij}^{\alpha} =& \omega s_{abij}^{\alpha} - P(ij)f_{ki}s_{abkj}^{\alpha} + P(ab)f_{ac}s_{cbij}^{\alpha} - P(ij)\tilde{d}_{ki}^{\alpha}\sigma_{kj}^{ab} + P(ab)\tilde{d}_{ac}^{\alpha}\sigma_{ij}^{cb} \\ &+ \langle ab||cj\rangle\, s_{ci}^{\alpha} - \langle kb||ij\rangle\, s_{ak}^{\alpha} = 0.\end{aligned} \tag{7.2.2}$$

The purely photonic amplitude γ_α is derived from the equation

$$\bar{H}^{\alpha} = \tilde{d}_{ii}^{\alpha} + f_{jb}s_{bj}^{\alpha} + \omega\gamma_\alpha = 0. \tag{7.2.3}$$

In the coherent-state HF framework, $\tilde{d}_{jj}^{\alpha} = 0$. Each of these amplitude equations are solved iteratively, by isolating the diagonal part of the equations on the right hand side of the equations. In particular, for the mixed amplitudes it can be observed that the frequency associated to the cavity is shifting the pole of the iterative equation

$$\begin{aligned}s_{ai}^{\alpha(n+1)} &= \frac{\bar{H}_{ai}^{\alpha(n)} - (\varepsilon_a - \varepsilon_i - \omega)s_{ai}^{\alpha(n)}}{\varepsilon_a - \varepsilon_i - \omega}, \\ s_{abij}^{\alpha(n+1)} &= \frac{\bar{H}_{abij}^{\alpha(n)} - (\varepsilon_a + \varepsilon_b - \varepsilon_i - \varepsilon_j - \omega)s_{ai}^{\alpha(n)}}{\varepsilon_a + \varepsilon_b - \varepsilon_i - \varepsilon_j - \omega}.\end{aligned} \tag{7.2.4}$$

For the purely photonic amplitude, no iteration is needed

$$\gamma_\alpha = -\frac{\tilde{d}_{ii}^{\alpha} + f_{jb}s_{bj}^{\alpha}}{\omega}. \tag{7.2.5}$$

It may be observed that the photonic amplitude equation is decoupled from eqs. 7.2.1-7.2.2. Furthermore, in the canonical orbital basis, f_{jb} vanishes, as well as the second term in eq. 7.2.3, due to the coherent-state HF reference, leaving $\gamma_\alpha = 0$. This result is not surprising, as the coherent-state transformation in eq. 7.1.28 has the form of a unitary photonic exponential ansatz.

With the converged amplitudes, the energy can be computed. Also in this case, some additional terms have to be accounted for, alongside those which had already been considered outside the cavity

$$E_{\mathrm{QED-UCC2}} = E_{\mathrm{UCC2,el}} + \frac{1}{2}\tilde{d}_{ai}^{\alpha}s_{ai}^{\alpha} + \frac{1}{2}\tilde{d}_{ia}^{\alpha}s_{ai}^{\alpha *} + \gamma^{\alpha}\tilde{d}_{ii}^{\alpha} + \gamma^{\alpha *}\tilde{d}_{ii}^{\alpha *}. \tag{7.2.6}$$

The last two terms vanish for the coherent-state HF ansatz. In fact, this result is not surprising, as these two terms are already accounted for in the HF energy expression, when performing the coherent-state transformation.

It is also possible to develop a QED unitary theory built on top of a different ansatz for the HF determinant. In that case, the dipole operator is not referred to its mean value and the integrals d_{ii}^{α} do not vanish. In particular, in that case the Γ_1 operator also counts contributions at first order.

Note that the prefactors in eq. 7.2.6 have been obtained following the diagrammatic rules of the Bernoulli expansion, where the photonic part of the potential operator has been considered to be part of V_{ND} (eq. 3.1.26).

The implementation has been performed by Laurenz Monzel.

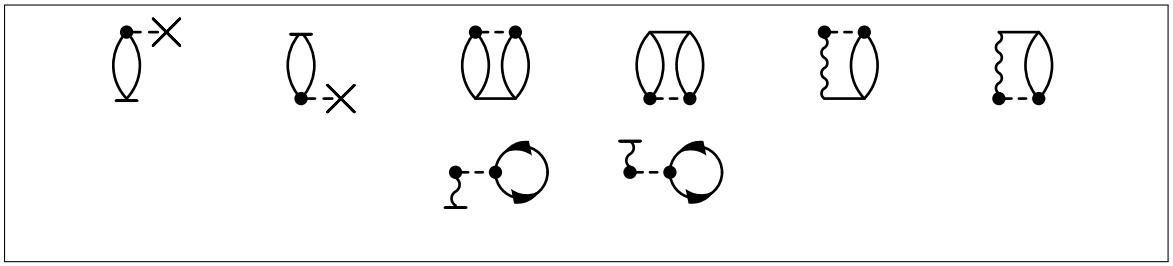

Diagrams 17: QED-UCC2 energy in the dipole approximation. As before, the cross depicts the Fock operator, the dashes the two-electron Hamiltonian operator and the plain lines the σ-amplitudes. The waved lines symbolize the photons.

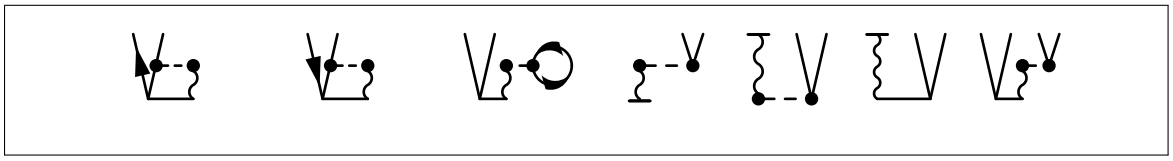

Diagrams 18: Additional diagrams for σ_1 and σ_2-amplitude equation, which need to be added to those already presented for the general case, outside the cavity. The same conventions as before are used for the representation of the operators.

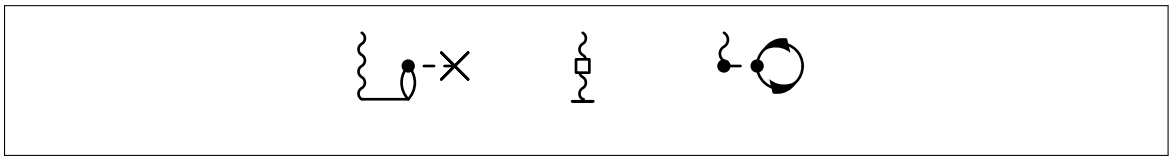

Diagrams 19: Diagrams to determine the Γ_1-amplitudes. The square represents the purely photonic part of the Hamiltonian, $\hat{H}_{\mathrm{ph}}$.

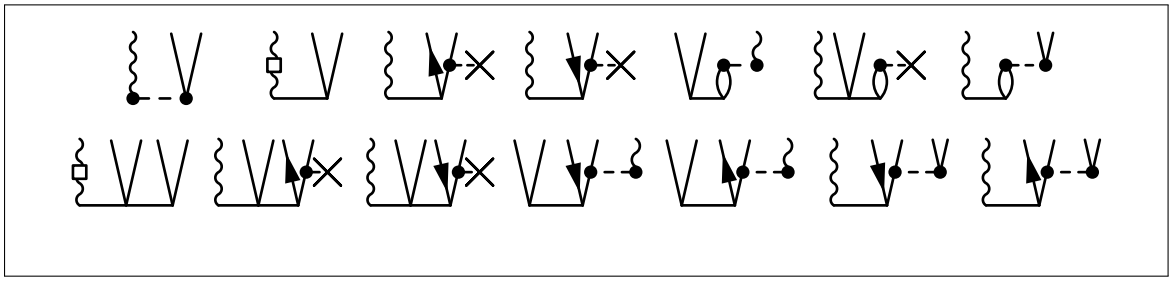

Diagrams 20: Diagrams to determine the S_1^1 amplitude (first row) and the S_2^1 amplitudes (second row). The same diagrammatic notation illustrated for the previous diagrams has been adopted.

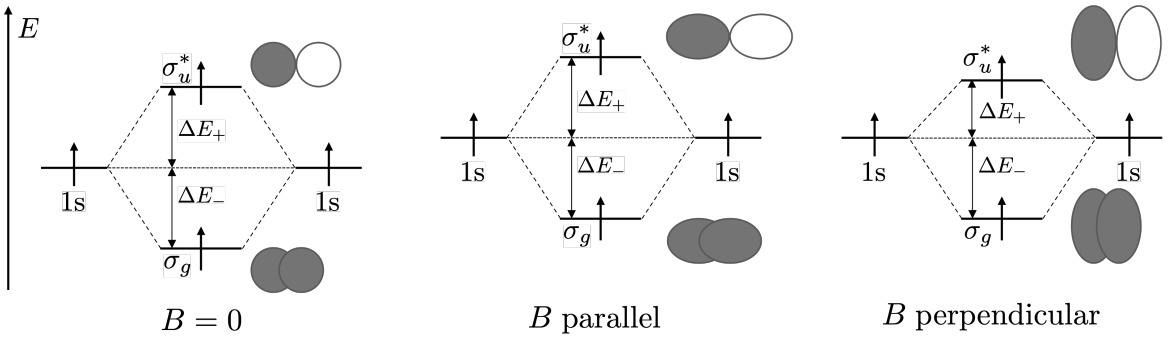

Figure 7.1: Paramagnetic bonding for the H_2 molecule.

7.3 Paramagnetic bonding in a cavity

Strong magnetic fields are known to influence the formation of bonds of molecular systems, giving the possibility to have bound molecules from systems which are not bound in the field-free case. The phenomenon of *paramagnetic bonding* is documented in the literature[66,162] for various diatomic systems in a perpendicular magnetic field. The simplest example is given by the triplet state $^3\Sigma_u^+$ of H_2, which in a general molecular-orbital picture is not bound, as can be seen from the MO diagram in fig. 7.1. When subjected to a strong magnetic field, the diamagnetic term in the Hamiltonian gives a positive shift to higher energies for both MOs, leaving the energy difference more or less unchanged. As in the triplet state both electrons have the same s_z value, the spin-Zeeman term in eq. 2.3.12 also leaves the energy difference unaffected. In the case of a magnetic field parallel to the bond axis, $\langle \hat{L}_z \rangle = \sum_i m_{l,i} = 0$, where m_l is the eigenvalue of the $\hat{L}_z$ operator associated to the orbitals. In this specific case, the energy difference between the orbitals is not changed (see fig. 7.1). For all other orientations, the secondary quantum number m_l is no longer a good quantum number due to the lowering of point group symmetry induced by the magnetic field. Therefore, in general the orbital-Zeeman term affects the energies of the orbitals, inducing an inhomogeneous shift.

For the H_2 molecule, this difference in shift is motivated by the different $\langle \hat{L}_z \rangle$ values for the σ_g and σ_u^* orbitals. In a perpendicular magnetic field, the system has C_{2h} symmetry. The σ_g orbital transforms as A_g and is given by a linear combination of s-type orbitals, giving an overall value $\langle \hat{L}_z \rangle = 0$. The σ_u^* orbital, on the other hand, transforms as B_u and may be expressed through the $p_\pm$ orbitals, also transforming as $p_\pm$. The σ_u^* orbital is stabilised by the orbital-Zeeman term, which results in a lower energy. Despite the bond order being formally zero, the magnetic field induces a bond which is strongest in the perpendicular orientation.

The hydrogen molecule is the simplest example to treat for the understanding of this phenomenon, but it may also be applied to other diatomic molecules.[66,162] Here the focus is on the $^1\Sigma_g^+$ state of the helium dimer He_2, which in zero field is not bound. It is known[162] that a perpendicular strong magnetic field induces a bonding situation, which can be described in analogy to the hydrogen molecule (the MO diagram is analogous to fig. 7.1, with double occupation of all orbitals).

It has already been mentioned that placing chemical systems inside an electromagnetic cavity may alter the chemistry considerably. The present discussion is therefore concerned about the effect of a cavity on the paramagnetic bonding, comparing results obtained at the QED-UCC2 level to those obtained with the QED-CCSD level of theory, with the unc-aug-cc-pVQZ basis set.[266–270,319] In fig. 7.3, the energy curves for the He_2 dimer are shown for various coupling and magnetic field strengths. The frequency associated to the cavity

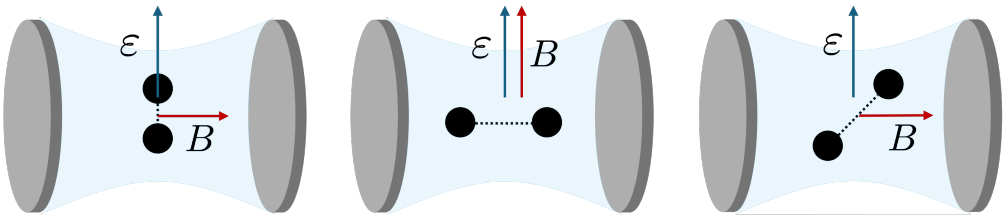

(a) $B \parallel y, \varepsilon \parallel x$ (b) $B \parallel y, \varepsilon \parallel y$ (c) $B \parallel y, \varepsilon \parallel z$

Figure 7.2: Orientations of the helium dimer in an electromagnetic cavity, with respect to the magnetic field vector B (red) and the polarisation vector of the cavity ε (blue).

is satisfying the resonance condition of the system ($\omega = 0.466$). The different orientations of the system are pictured in fig. 7.2. For all calculations, the dimer was chosen to be parallel to the x axis and the magnetic field perpendicular to it, along the y axis, without loss of generality. In order to evaluate the effects due to the coupling with the cavity, the reference is given by the calculation outside the cavity (blue lines in the plots in fig. 7.3). The polarisation vector of the cavity can either be oriented parallel to the dimer (fig. 7.2a), parallel to the magnetic field (fig. 7.2b), or perpendicular to both dimer and field (fig. 7.2c).

It is observed that both the magnetic field strength and the coupling with the cavity have a stabilising effect on the dimer, as the minimum of the energy curves is lowered both when increasing B (from fig. 7.3b to fig. 7.3c) and λ (from fig. 7.3a to fig. 7.3b). For all coupling and field strengths, when the cavity is oriented parallel to the molecule (red lines), the paramagnetic bonding is less pronounced, resulting in a higher minimum. In the case of the polarisation vector perpendicular to the dimer, the curves are very similar and do not show large discrepancies. For these orientations, the coupling to the cavity enhances the paramagnetic bonding, giving lower minima.

These observations can be explained considering the physical setting of the system. As was discussed in sec. 7.1.3, $\hat{H}_{\text{QED}}$ in the dipole approximation contains the scalar product $\hat{d} \cdot \varepsilon$, which does only contribute when the molecular dipole and the polarisation vector are parallel, as in fig. 7.2a. From a physical point of view, the fields are always perpendicular to the polarisation vector. Therefore, photons can be exchanged between the two helium atoms only when these are perpendicular to ε. The orientations in figs. 7.2b-7.2c satisfy this condition and are stabilised by the cavity.

For a quantitative discussion, in table 7.1 the positions of the minima and their values for QED-CCSD and QED-UCC2 are listed. The equilibrium geometry only slightly shifts between the different orientations of the cavity. An increase in the magnetic field strength causes the paramagnetic bonding to happen at smaller distances. On the other side, the change in the coupling does not affect the equilibrium geometry much, but causes the discrepancy with the cavity-free case to become more pronounced. The differences between QED-CCSD and QED-UCC2 increases when increasing the magnetic field and the coupling to the cavity, but is always of the order of $10^{-4}\, E_{\text{h}}$. For the orientation $\varepsilon \parallel x$, QED-UCC2 overestimated the energy, giving a higher minimum, while in the more stabilised orientations, QED-UCC2 predicts a slightly lower minimum. The differences are not very pronounced and QED-UCC2 can be taken as a cheaper method to predict the effects of paramagnetic bonding in an electromagnetic cavity.

Summarising, it has been shown that an electromagnetic cavity can enhance the paramagnetic bonding effect, when the polarisation vector is perpendicular to the molecular bond axis. Increasing the coupling parameter, i.e., decreasing the size of the cavity, leads to a larger stabilisation. The comparison of the results obtained with QED-UCC2 to the

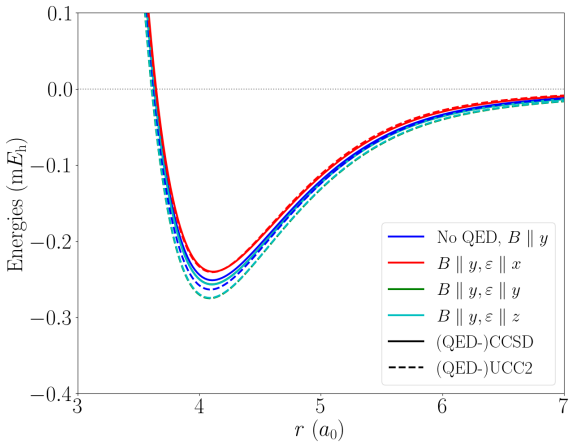

(a) B=0.5 B_0, $\lambda = 0.05$.

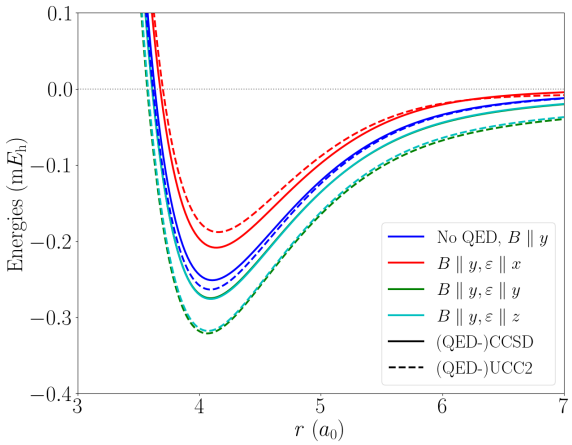

(b) B=0.5 B_0, $\lambda = 0.1$.

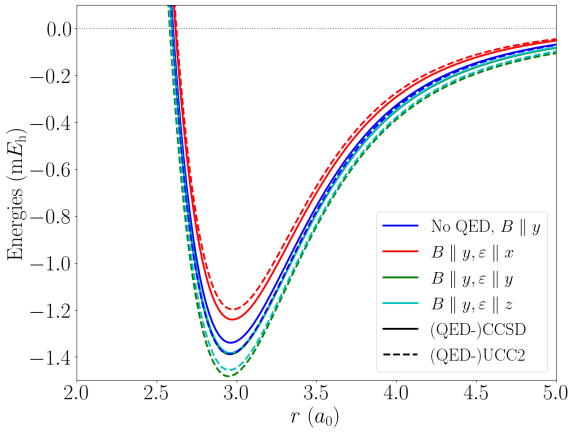

(c) B=1 B_0, $\lambda = 0.1$.

Figure 7.3: Energy curves for the dissociation of the He_2 dimer, plotted as $E_{He_2} - 2E_{He}$, for different orientations of the cavity. Results are obtained in the single-photon approximation for QED-CCSD and QED-UCC2 ($\omega = 0.466$). For all calculations, the dimer is parallel to the x axis, without loss of generality.

B=$0.5B_0, \lambda = 0.05$	$r_{\mathrm{min,CCSD}}$	$r_{\mathrm{min,UCC2}}$	$E_{\mathrm{min,CCSD}}$	$E_{\mathrm{min,UCC2}}$	$\Delta E_{\mathrm{CCSD-UCC2}}$
$\varepsilon = 0$	4.10	4.08	-0.2512	-0.2634	0.0122
$\varepsilon \parallel x$	4.10	4.10	-0.2399	-0.2406	0.0006
$\varepsilon \parallel y$	4.10	4.08	-0.2566	-0.2749	0.0183
$\varepsilon \parallel z$	4.10	4.08	-0.2569	-0.2744	0.0175
B=$0.5B_0, \lambda = 0.1$					
$\varepsilon = 0$	4.10	4.08	-0.2512	-0.2634	0.0122
$\varepsilon \parallel x$	4.14	4.14	-0.2084	-0.1879	-0.0205
$\varepsilon \parallel y$	4.08	4.06	-0.2748	-0.3211	0.0463
$\varepsilon \parallel z$	4.08	4.06	-0.2758	-0.3177	0.0419
B=$1.0B_0, \lambda = 0.1$					
$\varepsilon = 0$	2.96	2.94	-1.3398	-1.3881	0.0483
$\varepsilon \parallel x$	2.96	2.96	-1.2411	-1.1976	-0.0435
$\varepsilon \parallel y$	2.94	2.94	-1.3889	-1.4831	0.0942
$\varepsilon \parallel z$	2.96	2.96	-1.3834	-1.4564	0.0730

Table 7.1: Equilibrium geometry (in a_0) and energies (in mE_h), calculated as $E_{\mathrm{He_2}} - 2E_{\mathrm{He}}$, for the helium dimer obtained at the unc-aug-cc-pVQZ/QED-CCSD and unc-aug-cc-pVQZ/QED-UCC2 levels of theory.

QED-CCSD ones shows that the cheaper QED-UCC2 method already gives a qualitatively correct description of the physical phenomenon, while the quantitative values do not differ much from the more accurate QED-CCSD ones. A more accurate calculation in the unitary framework would be provided by QED-UCC3.

Chapter 8

Conclusions and Perspectives

This thesis represents a contribution to the field of electronic-structure theory, discussing a unitary formulation of coupled-cluster theory. The development of the unitary coupled-cluster approach was motivated by the limitations of coupled-cluster theory originating from the non-Hermiticity of its energy formulation. These limitations are well-documented in the literature: complex energy eigenvalues are obtained in a magnetic field[35] and for excited states in the proximity of conical intersections.[34,320] Furthermore, another shortcoming of CC theory is observed in the calculation of oscillator strengths, which in the CC framework are not guaranteed to be positive.[36,37]

The UCC ansatz maintains the advantages of an exponential parameterisation of the wave function, and the additional constraint given by the unitary transformation solves the issues which have been outlined as problematic for CC theory. It was shown in chapter 5 that UCC theory can be used instead of CC theory for the calculation of molecular energies and properties.

The UCC formalism has been applied to different fields of quantum chemistry.

- Following the formalism first proposed by Liu *et al.*,[160] the method has been adapted to the finite magnetic-field case, implying the use of complex algebra. Through this adaptation, both ground- and excited states could be targeted, maintaining a structure of the equations as similar as possible to CC theory. This work focuses on two flavours of unitary coupled-cluster theory, determined by a perturbative truncation of the amplitude equations to second order (UCC2) and to third order (UCC3). Both methods have been implemented in the QCUMBRE program package[161] and their accuracy has been tested in comparison to FCI, CCSD, and CC3 as this method possesses the same scaling as UCC3. The CH^+ cation in a magnetic field of various orientations was discussed, showing how the different UCC truncations deal with states with a double-excitation character. This system was chosen because of its low-lying doubly-excited state, which for some orientations possesses avoided crossings with singly-excited ones. This system allowed to observe the comparable accuracy of the CCSD and UCC3 results, and the inability of UCC2 to treat states with a double-excitation character.

- The issue of complex eigenvalues obtained in the CC framework was analysed for two cases. The case of complex energy values in a finite magnetic field was discussed first on the example of the water molecule in a strong magnetic field with varying orientation. It was shown that by exploiting the developed UCC theory the problem of complex energies is solved in a mathematically rigorous way (as shown in the results chapter 5), therefore obtaining real energies. The qualitative description of the ground- and

excited-state energies was found to agree for CCSD and UCC3, but in particular for the excited states, imaginary contributions to the energy values were found not to be negligible. The presence of complex energy values, however, could not be used as a diagnostics for the behaviour of the real energy part of CCSD results.
While for the water molecule the temptation may exist of considering only the real part of the results, neglecting the imaginary one, the example of boric acid was shown to present a case in which a real-valued quantum-chemical code cannot describe the excited states of the irreducible representations E' and E''. Due to its symmetry, complex algebra is needed for the CC calculation of these states already in the field-free case. Alternatively, the calculation in the field-free case only needs real algebra when using UCC theory and is therefore preferable. This molecule has then been analysed also in the magnetic field, where UCC represents a solution to the non-negligible imaginary parts in the excited-state energies. From the analysis of water and boric acid, it was clear that from the magnitude of the imaginary part no conclusion on the behaviour of the real part can be obtained. In fact, major discrepancies between the UCC3 and CCSD results were not observed in correspondence to the largest values of the imaginary part of the energy results. This important consideration underlines the need to turn to UCC in the case of complex energy values in order to ensure physically acceptable results. The real part of CC energies is often a good approximation, however it is uncertain to which extent it may be trusted.

- A further major part of this thesis is the development of UCC response theory for the calculation of molecular properties. The focus of the theoretical development has been on the formulation of a description common to CC and UCC theory. In sec. 3.2.1, the differences to the expectation-value based approach found in the literature[59] were discussed. A deeper insight into the CC description of molecular properties showed that the expectation-value approach leads to non size-extensive properties. The response-theory formalism is shown to solve this issue, including the response of the wave function to the perturbation. The importance of including the effect of the perturbed wave function in the calculation of properties had already been discussed in ref. 57. Furthermore, response theory allows to find a description of those properties for which the Hellmann-Feynman theorem does not hold. These motivations strongly suggested the adaptation of response theory to the UCC method. This thesis presents a consistent formulation for the evaluation of both single-state and transition properties in the response UCC framework.

- With the developed UCC response theory, the issue of negative oscillator strengths was discussed for the silicon dication and the cation CH^+. A specific transition of the silicon dication, observed to be present on white dwarf stars, was analysed both in the field-free case and in a magnetic field of varying strength. Negative oscillator strengths for the inspected transition in the field-free case are obtained by means of the CCSD method. UCC3 could be exploited to obtain physically meaningful results. The example of the cation CH^+ in a varying magnetic field has been discussed next. This system, though having real CCSD energies, has negative CCSD transition probabilities, which do not have any physical interpretation. For these cases, UCC theory offers a valid method for the computation of transition dipole moments.
Further investigations were done on the sodium, water, and lithium hydride, showing that the UCC3 results are in good agreement to CCSD when exploiting the developed response theory. The inclusion of effects describing the response of the wave function to the perturbation was observed to have a larger impact on the UCC3 results than on

the CCSD results, making the use of response theory in the UCC3 framework essential to get accurate results.

- In chapter 6, the developed UCC finite-field theory was used for the computation of magnetic circular dichroism spectra. MCD represents a valuable tool for the analysis of the electronic structure of both the ground and the excited states, as it detects overlapping transitions and weak transitions which are not visible with other spectroscopies. Transition dipole moments, computed with the developed finite-field methods, are used in this work for the computation of MCD spectra, differently from the approach described in the literature, where the calculation of MCD spectra is performed through a perturbative treatment of the magnetic field.[121–128] An alternative approach has been developed, inspired by a formalism existing for TDDFT,[107,129] and an adaptation for CC and UCC theory has been developed. The finite-field approach was shown to correspond to the perturbative one described in literature in the limit of small magnetic-field strengths. However, the finite-field approach includes effects of the magnetic field to infinite order. Only first-order properties are needed for the finite-field approach, while the perturbative approach needs second-order response theory. Furthermore, gauge-origin independence is easily included through the use of GIAOs.[183,321–323] The importance of the gauge-origin independence has been investigated for the examples of urea and cyclopropane, observing that without GIAOs the experimental spectra could possess differences in the relative intensities. GIAOs should therefore be used to have a correct qualitative reproduction of the spectra. Comparing the spectra obtained with UCC3 and CCSD for the test molecules urea and cyclopropane, it has been observed that both give a qualitatively correct reproduction of the spectrum, with the UCC3 spectrum shifted to slightly higher energies.
  The main differences to the already formulated perturbative treatment of MCD spectroscopy may be discussed in the presence of a strong magnetic field. Such a calculation is, in fact, only possible using the finite-field formulation. As a *Gedankenexperiment* the investigation on the evolution of the MCD spectrum of cyclopropane in an increasing magnetic field has been discussed. As observed already for other molecules, the strong magnetic field causes the excited states to dramatically change and interact with each other, resulting in a completely changed spectrum with respect to the weak-field limit. An explanation to the evolution of the spectrum in the field was given by means of the analysis of the behaviour of the excited states involved in the relevant transitions for the calculation of the spectrum. The discussion is based on the assumption that the distribution of the molecular orientations is isotropic. However, this may not be realistic for strong magnetic fields, as alignment effects could gain importance. For practical comparison to experiments this does not play a decisive role, as MCD spectra are (at the moment) measurable only in magnetic fields belonging to the perturbative limit.
  Finally, the MCD spectra computed for pyrazine and pyrimidine were shown to agree quite well with the experimental spectra. A shift of the calculated spectra with respect to the experiment was motivated by the fact that the computations are performed without a solvent, neglecting the solvent effects present in the experiment.

- The growing interest in recent years in light-matter interactions inside an electromagnetic cavity[131–142] motivated the curiosity to inspect the performance of the UCC methods in a cavity with an external magnetic field (chapter 7). A first step in this direction has been made with the development of the QED-UCC2 theory. This approximation has been conceived in analogy to the QED-CCSD method.[136] Further considerations

on the perturbative orders of the photonic and mixed photonic-electronic amplitudes have been discussed for a consistent truncation of the Bernoulli-expanded QED-UCC Hamiltonian. Through this formalism, the phenomenon of paramagnetic bonding has been investigated in an electromagnetic cavity. In the literature it has been documented that, in the presence of a magnetic field directed perpendicular to the bond axis of small diatomic molecules (H_2, He_2, LiH), bond formation is induced despite a formally zero bond order.[66,162] The effect of the coupling to an electromagnetic cavity on the bond formation of the dimer He_2 has been investigated. The performed calculations showed that the relative orientation of the propagation vector with respect to the dimer axis may lead to a stronger or weaker bonding character. The tuning of the coupling parameter through the volume of the cavity can therefore be exploited to enhance the perpendicular paramagnetic bonding. These first calculations showed that the QED-UCC2 results are in good agreement with the more accurate QED-CCSD results, providing a cheaper alternative for a first inspection of the phenomenon. Of course, QED-UCC2 would not be suitable for the characterisation of doubly-excited states. For this purpose, as well as for major accuracy, QED-UCC3 may be developed in future.

Outlook

The present work represents a contribution to the investigation of the fields of applicability of unitary coupled-cluster theory. Many interesting developments are opened by the insights gained so far in various directions. For example, some of these directions may be the following.

- The UCC method allows for various truncation schemes and different UCC formalisms may be explored. Most UCC methods are based on a perturbative truncation of the expansion. However, recent studies have analysed truncation schemes based on expansions up to a certain rank of commutators.[324–328] These methods seem to be more accurate than the ones based on perturbation theory for molecules for which the Møller-Plesset series does not show smooth convergence at low orders. For example, the qUCCSD approach is argued to bring some improvement to the UCC3 method for molecules with strong orbital relaxation and electron correlation.[324,325]

- The theory for molecular properties discussed in sec. 3.2.1 can be exploited to calculate the properties originating from an electromagnetic perturbation, but does not include the relaxation of the Hartree-Fock orbitals. A future development of UCC response theory should include this effect. Furthermore, the calculation of molecular gradients has not been discussed here and surely represents an interesting future challenge.

- In the field of MCD spectroscopy, new perspectives could be obtained considering a more accurate description of the experimental medium in which the measurement of an MCD spectra is performed. A desirable development consists in performing the calculations of transition dipole moments in the magnetic field taking into account solvent effects. Environmental effects are accounted for by various embedding models, of which the polarisation continuum model[286–294] is one of the best known. Otherwise, a more refined estimate is provided by the whole class of QM/MM methods,[295–297] where a part of the system is described through quantum chemistry and the remaining part through classical mechanics. These methods also offer the possibility to describe the directionality of the interactions,[329–332] which is not possible with a homogeneous continuum model.

In the limiting case of strong magnetic field, one possible development consists in the correct evaluation of orientational effects of the molecules in the magnetic field. As already pointed out, the equations for the calculation of MCD spectra via the finite-field approach discussed in chapter 6 are based on the assumption of an isotropic distribution of the molecular orientations in space. This may not be the case in the presence of a strong magnetic field, where the molecular spin tends to align to the external magnetic field. To account for this effect, a weighting strategy of the contributions of each orientation may be developed.

- The field of quantum electrodynamics opens various challenges for the next steps of investigation. The QED-UCC2 is a quite rough approximation and different truncations of the exponential operators may be explored. Based on the results outside the cavity, the single-mode QED-UCC3 method probably offers a better agreement with QED-CCSD also inside the cavity. Thus QED-UCC3 would provide an alternative method for the calculation of systems proven to be problematic for CCSD. Throughout the discussion, the single-photon mode is adopted. The double- and higher-photon regimes may be explored, although the theory becomes more involved than for the single-photon case. Therefore, the perturbative truncation of the Bernoulli-expanded Hamiltonian and of the amplitude equation has to be carefully evaluated. Additionally, the present theory can only describe the ground-state energy in a cavity, but it is surely desirable to obtain a characterisation of excited states as well.[155,333]

- The focus has been placed on Hamilton operator for which the occurrence of complex energy values is motivated by the presence of an external magnetic field. In ref. 35, conditions determining a complex part in the Hamiltonian have been extensively analysed. Among these, the vicinity to conical intersections is documented in the literature to cause the CCSD results to become complex.[320] The Hermitian formulation of the UCC energy evidently solves the problem of unphysical results also in this setting. An alternative approach to this problem has been presented in the literature with the similarity-transformed CCSD method (SCCSD).[320] Therefore, a comparison of the results obtained with the SCCSD method with those obtained with the UCC method could be of interest. Some preliminary studies in this direction were pursued by the author of this thesis, in collaboration with the authors of the aforementioned work. For instance, the molecule HOF is one of the systems for which complex eigenvalues are found with CCSD in vicinity of the intersection seam. The results obtained from a pilot investigation showed that both SCCSD and UCC3 are able to solve the problem of dimensionality in the intersection seam, but the position of the conical intersection itself is slightly different for the two methods. It would be interesting to test the two methods also for other systems, in order to gain a more complete understanding on the advantages and disadvantages characterising them.

The outlined perspectives are only part of the potential applications unitary coupled cluster could find in quantum chemistry. Future investigations using UCC theory may open other fields for which this method is preferable to standard CC methods.

Appendix A

Application of UCC diagrammatic rules

In fig. A.1, a few examples of UCC diagrams are discussed, in order to explain the diagrammatic rules listed in sec. 4.2.

- I: a part of the $\hat{V}_{\mathrm{R}}$ operator is involved, as it is not a pure excitation nor a pure de-excitation operator. This term arises from the single commutator, and belongs to both $\frac{1}{2}[\hat{V}_{\mathrm{R}}, \hat{\sigma}]$ and $\frac{1}{2}[\hat{V}, \hat{\sigma}]$. These two contributions add, and the term has a prefactor $\frac{1}{2} + \frac{1}{2}$ in front of the commutator. The same global prefactor is found for the single commutator in the BCH expansion, where there is $[\hat{V}, \hat{\sigma}]$. The term has the formulation $\frac{1}{2} \langle ab||cd \rangle \sigma_{ij}^{cd}$, where the factor $\frac{1}{2}$ comes from the pair of equivalent lines.

- II: as for term I, here a part of the $\hat{V}_{\mathrm{R}}$ operator is involved. As the global prefactor of the single commutators in the Bernoulli expansion sums to unity, the same rules as for the diagrammatic formalism of CC apply. The term is evaluated as $P(ij)P(ab) \langle ak||ic \rangle \sigma_{jk}^{bc}$.

- III: the potential operator here is part of $\hat{V}_{\mathrm{ND}}$, as it only involves de-excitations. Furthermore, the contraction with the $\hat{\sigma}$ operator results in a term belonging to $[\hat{V}, \hat{\sigma}]_{\mathrm{R}}$. This term is therefore part of the double commutators $\frac{1}{12}[[\hat{V}_{\mathrm{ND}}, \hat{\sigma}], \hat{\sigma}]$ and $\frac{1}{4}[[\hat{V}, \hat{\sigma}]_{\mathrm{R}}, \hat{\sigma}]$. The global prefactor to this double commutator for this diagram is $\frac{1}{12} + \frac{1}{4} = \frac{1}{3}$. This prefactor differs from the prefactor of the BCH expansion, where $\frac{1}{2}[[\hat{V}, \hat{\sigma}], \hat{\sigma}]$ is found. From the CC diagrammatic rules, a factor $\frac{1}{2}$ arises from the connection of the potential operator with two equivalent operators. This factor here needs to be scaled, in order

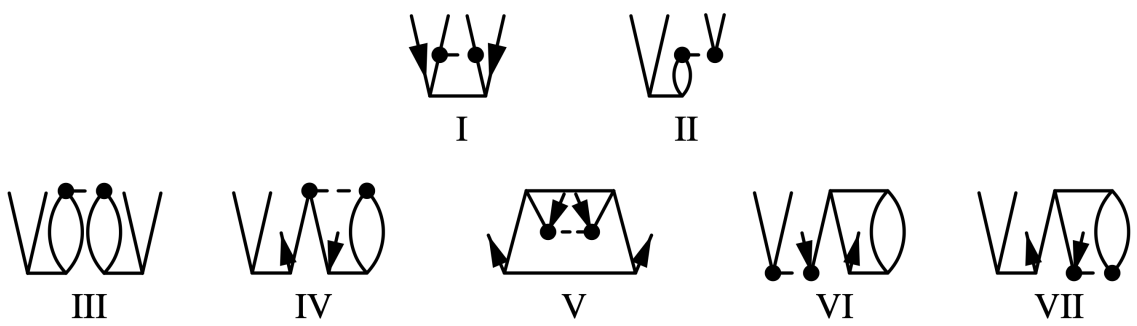

Figure A.1

to account for the different prefactor in the expansion, obtaining $(\frac{1}{2} \cdot \frac{1}{3})/\frac{1}{2} = \frac{1}{3}$. The term therefore is $P(ij)P(ab)\,\langle kl||cd\rangle\,\sigma_{ik}^{ac}\sigma_{jl}^{bd}$.

- IV: as for term III, the potential operator is part of $\hat{V}_{\mathrm{ND}}$. As before, the global prefactor from the double commutators adds to $\frac{1}{3}$.
  From the CC diagrammatic rules, a factor $\frac{1}{2}$ needs to be considered, arising from one pair of equivalent lines, connecting $\hat{\sigma}$ and $\hat{V}_{\mathrm{ND}}$ with particle lines. Accounting for the different prefactors of the Bernoulli and the BCH expansion, a resulting prefactor of $\frac{1}{3}$ is found. Term IV is $P(ij)\frac{1}{3}\,\langle kl||cd\rangle\,\sigma_{il}^{ab}\sigma_{jk}^{dc}$.

- V: once more, the potential operator is part of $\hat{V}_{\mathrm{ND}}$ and the term acquires a global prefactor of $\frac{1}{3}$. From the CC rules, here a prefactor $\frac{1}{4}$ is predicted, because of two pairs of equivalent lines in the diagrams. Scaling this factor in order to account for the difference of the Bernoulli and the BCH expansion, giving $(\frac{1}{4} \cdot \frac{1}{3})/\frac{1}{2} = \frac{1}{6}$. The last rule of sec. 4.2 applies here, as the potential operator is connected only to one of the amplitudes. A further factor of $\frac{1}{2}$ is therefore multiplied here, giving the expression $\frac{1}{12}\,\langle cd||ij\rangle\,\sigma_{kl}^{cd*}\sigma_{kl}^{ab}$ for this term.

- VI and VII: both terms involve a pure-excitation part of $\hat{V}$, therefore contributing to $\frac{1}{12}[[\hat{V}_{\mathrm{ND}},\hat{\sigma}],\hat{\sigma}]$ and $\frac{1}{4}[[\hat{V},\hat{\sigma}]_{\mathrm{R}},\hat{\sigma}]$. Both have one pair of equivalent lines, and the scaling of the prefactor leads to $\frac{1}{3}$. In both cases, the potential operator is connected to only one of the amplitudes, thus requiring an additional factor $\frac{1}{2}$. These terms are VI: $-P(ab)\frac{1}{6}\,\langle ad||ij\rangle\,\sigma_{kl}^{cd*}\sigma_{kl}^{cb}$ and VII: $-P(ij)\frac{1}{6}\,\langle cd||kj\rangle\,\sigma_{il}^{ab}\sigma_{kl}^{cd*}$.

List of Acronyms

- FCI: Full Configuration Interaction
- HF: Hartree-Fock
- MP: Møller-Plesset
- CC: Coupled-Cluster
- UCC: Unitary Coupled-Cluster
- EOM: Equation-Of-Motion
- ADC: Adiabatic Diagrammatic Construction
- MCD: Magnetic Circular Dichroism
- SD: Slater Determinant
- LCAO:Linear Combination of Atomic Orbitals
- SCF: Self-Consistent Field
- unc: uncontracted (basis set)
- ff: finite field
- PT: Perturbation Theory
- GIAO: Gauge-Including Atomic Orbital

- AO: Atomic Orbital
- BO: Born-Oppenheimer
- BCH: Baker-Campbell-Hausdorff
- QED: Quantum ElectroDynamics
- DIIS: direct inversion of the iterative subspace

References

[1]W. Heisenberg, "Über quantentheoretische Umdeutung kinematischer und mechanischer Beziehungen", Z. Phys. **33**, 879–893 (1925).

[2]E. Schrödinger, "Die Erfüllbarkeit der Relativitätsforderung in der klassischen Mechanik", Ann. Phys. **382**, 325–336 (1925).

[3]M. Planck, "Über das Gesetz der Energieverteilung in Normalspectrum", Ann. Phys. **4**, 533–563 (1901).

[4]A. Einstein, "Über einen die Erzeugung und Verwandlung des Lichtes betreffenden heuristischen Gesichtspunkt ", Ann. Phys. **17**, 132–148 (1905).

[5]W. Heitler and F. London, "Wechselwirkung neutraler Atome und homöpolare Bindung nach der Quantenmechanik", Z. Phys. **44**, 455–472 (1927).

[6]J. Čížek and J. Paldus, "Coupled cluster approach", Phys. Scr. **21**, 251 (1980).

[7]J. Čížek, "Origins of coupled cluster technique for atoms and molecules", Theor. chim. acta **80**, 91–94 (1991).

[8]R. J. Bartlett and M. Musiał, "Coupled-cluster theory in quantum chemistry", Rev. Mod. Phys. **79**, 291 (2007).

[9]P. Piecuch, S. Zarrabian, J. Paldus, and J. Čížek, "Coupled-cluster approaches with an approximate account of triexcitations and the optimized-inner-projection technique. II. Coupled-cluster results for cyclic-polyene model systems", Phys. Rev. B **42**, 3351–3379 (1990).

[10]P. Piecuch and R. J. Bartlett, "EOMXCC: a new coupled-cluster method for electronic excited states", in *Adv. quantum chem.* (Elsevier, 1999), pp. 295–380.

[11]P. Piecuch, K. Kowalski, I. S. O. Pimienta, and M. J. Mcguire, "Recent advances in electronic structure theory: method of moments of coupled-cluster equations and renormalized coupled-cluster approaches", Int. Rev. Phys. Chem. **21**, 527–655 (2002).

[12]P. Piecuch, "Active-space coupled-cluster methods", Mol. Phys. **108**, 2987–3015 (2010).

[13]K. Kowalski and P. Piecuch, "The active-space equation-of-motion coupled-cluster methods for excited electronic states: full EOMCCSDt", J. Chem. Phys. **115**, 643–651 (2001).

[14]K. Kowalski and P. Piecuch, "Extensive generalization of renormalized coupled-cluster methods", J. Chem. Phys. **122**, 074107 (2005).

[15]M. Nooijen and R. J. Bartlett, "Equation of motion coupled cluster method for electron attachment", J. Chem. Phys. **102**, 3629–3647 (1995).

[16]M. Nooijen and R. J. Bartlett, "A new method for excited states: similarity transformed equation-of-motion coupled-cluster theory", J. Chem. Phys. **106**, 6441–6448 (1997).

[17]O. Christiansen, "Coupled cluster theory with emphasis on selected new developments", Theor. Chem. Acc. **116**, 106–123 (2005).

[18]A. Köhn, M. Hanauer, L. A. Mück, T.-C. Jagau, and J. Gauss, "State-specific multireference coupled-cluster theory", Wiley Interdiscip. Rev. Comput. Mol. Sci. **3**, 176–197 (2012).

[19]N. Oliphant and L. Adamowicz, "Multireference coupled cluster method for electronic structure of molecules", Int. Rev. Phys. Chem. **12**, 339–362 (1993).

[20]J. Shen and P. Piecuch, "Biorthogonal moment expansions in coupled-cluster theory: review of key concepts and merging the renormalized and active-space coupled-cluster methods", Chem. Phys. **401**, 180–202 (2012).

[21]J. Liu and L. Cheng, "Relativistic coupled-cluster and equation-of-motion coupled-cluster methods", Wiley Interdiscip. Rev. Comput. Mol. Sci. **11**, e1536 (2021).

[22]J. F. Stanton and R. J. Bartlett, "The equation of motion coupled-cluster method. A systematic biorthogonal approach to molecular excitation energies, transition probabilities, and excited state properties", J. Chem. Phys. **98**, 7029–7039 (1993).

[23]D. C. Comeau and R. J. Bartlett, "The equation-of-motion coupled-cluster method. Applications to open- and closed-shell reference states", Chem. Phys. Lett. **207**, 414–423 (1993).

[24]S. Hirata, "Higher-order equation-of-motion coupled-cluster methods", J. Chem. Phys. **121**, 51–59 (2004).

[25]G. D. Purvis and R. J. Bartlett, "A full coupled-cluster singles and doubles model: the inclusion of disconnected triples", J. Chem. Phys. **76**, 1910–1918 (1982).

[26]J. Noga and R. J. Bartlett, "Erratum: The full CCSDT model for molecular electronic structure [J. Chem. Phys. 8 6, 7041 (1987)]", J. Chem. Phys. **89**, 3401–3401 (1988).

[27]G. E. Scuseria and H. F. Schaefer III, "A new implementation of the full CCSDT model for molecular electronic structure", Chem. Phys. Lett. **152**, 382–386 (1988).

[28]S. A. Kucharski and R. J. Bartlett, "The coupled-cluster single, double, triple, and quadruple excitation method", J. Chem. Phys. **97**, 4282–4288 (1992).

[29]O. Christiansen, H. Koch, and P. Jørgensen, "The second-order approximate coupled cluster singles and doubles model CC2", Chem. Phys. Lett. **243**, 409–418 (1995).

[30]H. Koch and P. Jørgensen, "Coupled cluster response functions", J. Chem. Phys. **93**, 3333 (1990).

[31]K. Raghavachari, G. W. Trucks, J. A. Pople, and M. Head-Gordon, "A fifth-order perturbation comparison of electron correlation theories", Chem. Phys. Lett. **157**, 479–483 (1989).

[32]K. Emrich, "An extension of the coupled cluster formalism to excited states (I)", Nucl. Phys. A **351**, 379–396 (1981).

[33]K. Emrich, "An extension of the coupled cluster formalism to excited states (II)", Nucl. Phys. A **351**, 397–438 (1981).

[34]A. Köhn and A. Tajti, "Can coupled-cluster theory treat conical intersections?", J. Chem. Phys. **127**, 044105 (2007).

[35]S. Thomas, F. Hampe, S. Stopkowicz, and J. Gauss, "Complex ground-state and excitation energies in coupled-cluster theory", Mol. Phys. **119**, e1968056 (2021).

[36]A. M. Tucholska, M. Lesiuk, and R. Moszynski, "Transition moments between excited electronic states from the Hermitian formulation of the coupled cluster quadratic response function", J. Chem. Phys. **146**, 034108 (2017).

[37]O. Christiansen, H. Koch, and P. Jørgensen, "Response functions in the CC3 iterative triple excitation model", J. Chem. Phys. **103**, 7429–7441 (1995).

[38]Y. Cao, J. Romero, J. P. Olson, M. Degroote, P. D. Johnson, M. Kieferová, I. D. Kivlichan, T. Menke, B. Peropadre, N. P. D. Sawaya, S. Sim, L. Veis, and A. Aspuru-Guzik, "Quantum chemistry in the age of quantum computing", Chem. Rev. **119**, 10856–10915 (2019).

[39]S. McArdle, S. Endo, A. Aspuru-Guzik, S. C. Benjamin, and X. Yuan, "Quantum computational chemistry", Rev. Mod. Phys. **92**, 015003 (2020).

[40]A. Peruzzo, J. McClean, P. Shadbolt, M.-H. Yung, X.-Q. Zhou, P. J. Love, A. Aspuru-Guzik, and J. L. O'Brien, "A variational eigenvalue solver on a photonic quantum processor", Nat. Commun. **5**, 4213 (2014).

[41]J. R. McClean, J. Romero, R. Babbush, and A. Aspuru-Guzik, "The theory of variational hybrid quantum-classical algorithms", New J. Phys. **18**, 023023 (2016).

[42]M.-H. Yung, J. Casanova, A. Mezzacapo, J. McClean, L. Lamata, A. Aspuru-Guzik, and E. Solano, "From transistor to trapped-ion computers for quantum chemistry", Sci. Rep. **4**, 3589 (2014).

[43]R. P. Feynman, "Simulating physics with computers", Int. J. Theor. Phys. **21**, 467–488 (1982).

[44]D. S. Abrams and S. Lloyd, "Simulation of many-body Fermi systems on a universal quantum computer", Phys. Rev. Lett. **79**, 2586–2589 (1997).

[45]J. Romero, R. Babbush, J. R. McClean, C. Hempel, P. J. Love, and A. Aspuru-Guzik, "Strategies for quantum computing molecular energies using the unitary coupled cluster ansatz", Quantum Sci. Technol. **4**, 014008 (2018).

[46]A. Anand, P. Schleich, S. Alperin-Lea, P. W. K. Jensen, S. Sim, M. Díaz-Tinoco, J. S. Kottmann, M. Degroote, A. F. Izmaylov, and A. Aspuru-Guzik, "A quantum computing view on unitary coupled cluster theory", Chem. Soc. Rev. **51**, 1659–1684 (2022).

[47]T. Helgaker, P. Jørgensen, and J. Olsen, *Molecular electronic-structure theory* (John Wiley & Sons, Chichester, 2013).

[48]W. Kutzelnigg, "Pair correlation theories", in *Methods of electronic structure theory*, edited by H. F. Schaefer III (Springer, Boston, MA, 1977), pp. 129–188.

[49]R. J. Bartlett, S. A. Kucharski, and J. Noga, "Alternative coupled-cluster ansätze II. The unitary coupled-cluster method", Chem. Phys. Lett. **155**, 133–140 (1989).

[50]R. Gilmore, "Baker-Campbell-Hausdorff formulas", J. Math. Phys. **15**, 2090–2092 (1974).

[51]A. G. Taube and R. J. Bartlett, "New perspectives on unitary coupled-cluster theory", Int. J. Quantum Chem. **106**, 3393–3401 (2006).

[52]J. Lee, W. J. Huggins, M. Head-Gordon, and K. B. Whaley, "Generalized unitary coupled cluster wave functions for quantum computation", J. Chem. Theory Comput. **15**, 311–324 (2018).

[53]F. A. Evangelista, G. K.-L. Chan, and G. E. Scuseria, "Exact parameterization of fermionic wave functions via unitary coupled cluster theory", J. Chem. Phys. **151**, 244112 (2019).

[54]T. B. Pedersen and H. Koch, "Coupled cluster response functions revisited", J. Chem. Phys. **106**, 8059–8072 (1997).

[55]T. B. Pedersen, H. Koch, and C. Hättig, "Gauge invariant coupled cluster response theory", J. Chem. Phys. **110**, 8318–8327 (1999).

[56]P. Norman, K. Ruud, and T. Saue, *Principles and practices of molecular properties: theory, modeling, and simulations* (John Wiley & Sons, Hoboken, 2018).

[57]O. Christiansen, P. Jørgensen, and C. Hättig, "Response functions from Fourier component variational perturbation theory applied to a time-averaged quasienergy", Int. J. Quantum Chem. **68**, 1–52 (1998).

[58]T. Helgaker, S. Coriani, P. Jørgensen, K. Kristensen, J. Olsen, and K. Ruud, "Recent advances in wave function-based methods of molecular-property calculations", Chem. Rev. **112**, 543–631 (2012).

[59]M. Hodecker and A. Dreuw, "Unitary coupled cluster ground- and excited-state molecular properties", J. Chem. Phys. **153**, 084112 (2020).

[60]J. Noga and M. Urban, "On expectation value calculations of one-electron properties using the coupled cluster wave functions", Theor. Chim. Acta **73**, 291–306 (1988).

[61]R. J. Bartlett and J. Noga, "The expectation value coupled-cluster method and analytical energy derivatives", Chem. Phys. Lett. **150**, 29–36 (1988).

[62]L. Z. Stolarczyk and H. J. Monkhorst, "Coupled-cluster method in Fock space. IV. Calculation of expectation values and transition moments", Phys. Rev. A **37**, 1926–1933 (1988).

[63]T. Korona and B. Jeziorski, "One-electron properties and electrostatic interaction energies from the expectation value expression and wave function of singles and doubles coupled cluster theory", J. Chem. Phys. **125**, 184109 (2006).

[64]H. Sekino and R. J. Bartlett, "A linear response, coupled-cluster theory for excitation energy", Int. J. Quantum Chem. **26**, 255–265 (1984).

[65]S. Stopkowicz, J. Gauss, K. K. Lange, E. I. Tellgren, and T. Helgaker, "Coupled-cluster theory for atoms and molecules in strong magnetic fields", J. Chem. Phys. **143**, 074110 (2015).

[66]S. Stopkowicz, "Perspective: Coupled cluster theory for atoms and molecules in strong magnetic fields", Int. J. Quantum Chem. **118**, e25391 (2018).

[67]E. I. Tellgren, A. Soncini, and T. Helgaker, "Nonperturbative ab initio calculations in strong magnetic fields using London orbitals", J. Chem. Phys. **129**, 154114 (2008).

[68]M. J. Pemberton, T. J. P. Irons, T. Helgaker, and A. M. Teale, "Revealing the exotic structure of molecules in strong magnetic fields", J. Chem. Phys. **156**, 204113 (2022).

[69]A. Pausch, C. Holzer, and W. Klopper, "Efficient calculation of magnetic circular dichroism spectra using spin-noncollinear linear-response time-dependent density functional theory in finite magnetic fields", J. Chem. Theory Comput. **18**, 3747–3758 (2022).

[70]D. Nakamura, A. Ikeda, H. Sawabe, Y. H. Matsuda, and S. Takeyama, "Record indoor magnetic field of 1200 T generated by electromagnetic flux-compression", Rev. Sci. Instrum. **89**, 095106 (2018).

[71]B. Franzon and S. Schramm, "Effects of strong magnetic fields and rotation on white dwarf structure", Phys. Rev. D **92**, 083006 (2015).

[72]B. Franzon and S. Schramm, "Effects of magnetic fields in white dwarfs", J. Phys. Conf. Ser. **861**, 012015 (2017).

[73]P. Bera and D. Bhattacharya, "Mass–radius relation of strongly magnetized white dwarfs: nearly independent of Landau quantization", Mon. Not. R. Astron. Soc. **445**, 3951–3958 (2014).

[74]K. Boshkayev, J. A. Rueda, R. Ruffini, and I. Siutsou, "General relativistic white dwarfs and their astrophysical implications", J. Korean Chem. Soc. **65**, 855–860 (2014).

[75]Y. Terada, T. Hayashi, M. Ishida, K. Mukai, T. Dotani, S. Okada, R. Nakamura, S. Naik, A. Bamba, and K. Makishima, "Suzaku discovery of hard X-ray pulsations from a rotating magnetized white dwarf, AEAquarii", Publ. Astron. Soc. Jpn. **60**, 387–397 (2008).

[76]D. Koester and G. Chanmugam, "Physics of white dwarf stars", Reports Prog. Phys. **53**, 837–915 (1990).

[77]R. H. Garstang, "Atoms in high magnetic fields (white dwarfs)", Reports Prog. Phys. **40**, 105–154 (1977).

[78]S. Jordan, P. Schmelcher, W. Becken, and W. Schweizer, "Evidence for helium in the magnetic white dwarf GD 229", Astron. Astrophys. **336**, L33–L36 (1998).

[79]D. T. Wickramasinghe and L. Ferrario, "Magnetism in isolated and binary white dwarfs", Publ. Astron. Soc. Pacific **112**, 873–924 (2000).

[80]B. Zuckerman, D. Koester, I. N. Reid, and M. Hunsch, "Metal lines in DA white dwarfs", Astrophys. J. **596**, 477–495 (2003).

[81]B. Zuckerman, C. Melis, B. Klein, D. Koester, and M. Jura, "Ancient planetary systems are orbiting a large fraction of white dwarf stars", Astrophys. J. **722**, 725–736 (2010).

[82]E. L. Degl'Innocenti and M. Landolfi, *Polarization in Spectral Lines* (Springer Netherlands, Dordrecht, 2004).

[83]P. Dufour, J. Liebert, G. Fontaine, and N. Behara, "White dwarf stars with carbon atmospheres", Nature **450**, 522–524 (2007).

[84]S. Jordan, "Magnetic fields in white dwarfs and their direct progenitors", Proc. Int. Astron. Union **4**, 369–378 (2008).

[85]S. Xu, M. Jura, D. Koester, B. Klein, and B. Zuckerman, "Discovery of molecular hydrogen in white dwarf atmospheres", Astrophys. J. **766**, L18 (2013).

[86]L. Ferrario, D. de Martino, and B. T. Gänsicke, "Magnetic white dwarfs", Space Sci. Rev. **191**, 111–169 (2015).

[87]W. Rosner, G. Wunner, H. Herold, and H. Ruder, "Hydrogen atoms in arbitrary magnetic fields. I. Energy levels and wavefunctions", J. Phys. B At. Mol. Phys. **17**, 29–52 (1984).

[88]A. Kawka, S. Vennes, L. Ferrario, and E. Paunzen, "Evidence of enhanced magnetism in cool, polluted white dwarfs", Mon. Not. R. Astron. Soc. **482**, 5201–5210 (2019).

[89]J. L. Greenstein, "The identification of hydrogen in GRW +70 deg 8247", Astrophys. J. **281**, L47–L50 (1984).

[90]J. L. Greenstein, R. J. W. Henry, and R. F. Oconnell, "Futher identifications of hydrogen in GRW +708247", Astrophys. J. **289**, L25–L29 (1985).

[91]R. J. W. Henry and R. F. Oconnell, "On the magnetic field in the white dwarf GRW + 70.8247 deg", Astrophys. J. **282**, L97–L98 (1984).

[92]R. J. W. Henry and R. F. Oconnell, "Hydrogen spectrum in magnetic white dwarfs - H-alpha, H-beta and H-gamma transitions", Publ. Astron. Soc. Pacific **97**, 333 (1985).

[93]G. D. Schmidt, R. G. Allen, P. S. Smith, and J. Liebert, "Combined ultraviolet-optical spectropolarimetry of the magnetic white dwarf GD 229", Astrophys. J. **463**, 320 (1996).

[94]H. Forster, W. Strupat, W. Rosner, G. Wunner, H. Ruder, and H. Herold, "Hydrogen atoms in arbitrary magnetic fields. II. Bound-bound transitions", J. Phys. B At. Mol. Phys. **17**, 1301–1319 (1984).

[95]S. V. Berdyugina, A. V. Berdyugin, and V. Piirola, "Molecular magnetic dichroism in spectra of white dwarfs", Phys. Rev. Lett. **99**, 091101 (2007).

[96]J. D. Landstreet, S. Bagnulo, G. G. Valyavin, L. Fossati, S. Jordan, D. Monin, and G. A. Wade, "On the incidence of weak magnetic fields in DA white dwarfs", Astron. Astrophys. **545**, A30 (2012).

[97]S. Bagnulo and J. D. Landstreet, "Discovery of six new strongly magnetic white dwarfs in the 20 pc local population", Astron. Astrophys. **643**, A134 (2020).

[98]M. A. Hollands, S. Stopkowicz, M.-P. Kitsaras, F. Hampe, S. Blaschke, and J. Hermes, "A DZ white dwarf with a 30 MG magnetic field", Mon. Not. R. Astron. Soc. **520**, 3560–3575 (2023).

[99]P. Schmelcher, L. S. Cederbaum, and H. D. Meyer, "Electronic and nuclear motion and their couplings in the presence of a magnetic field", Phys. Rev. A **38**, 6066–6079 (1988).

[100]P. Schmelcher, L. S. Cederbaum, and H. D. Meyer, "On the validity of the Born-Oppenheimer approximation in magnetic fields", J. Phys. B At. Mol. Opt. Phys. **21**, L445–L450 (1988).

[101]P. Schmelcher and L. S. Cederbaum, "Molecules in strong magnetic fields: Properties of atomic orbitals", Phys. Rev. A **37**, 672–681 (1988).

[102]P. Schmelcher and L. S. Cederbaum, "On molecules and ions in strong magnetic fields", Int. J. Quantum Chem. **40**, 371–385 (1991).

[103]S. Blaschke and S. Stopkowicz, "Cholesky decomposition of complex two-electron integrals over GIAOs: efficient MP2 computations for large molecules in strong magnetic fields", J. Chem. Phys. **156**, 044115 (2022).

[104]A. Soncini and P. Fowler, "Non-linear ring currents: effect of strong magnetic fields on π-electron circulation", Chem. Phys. Lett. **400**, 213–220 (2004).

[105]E. I. Tellgren, A. M. Teale, J. W. Furness, K. K. Lange, U. Ekström, and T. Helgaker, "Non-perturbative calculation of molecular magnetic properties within current-density functional theory", J. Chem. Phys. **140**, 034101 (2014).

[106]S. Sen, K. K. Lange, and E. I. Tellgren, "Excited states of molecules in strong uniform and nonuniform magnetic fields", J. Chem. Theory Comput. **15**, 3974–3990 (2019).

[107]S. Sun, D. Williams-Young, and X. Li, "An ab initio linear response method for computing magnetic circular dichroism spectra with nonperturbative treatment of magnetic field", J. Chem. Theory Comput. **15**, 3162–3169 (2019).

[108]F. Hampe and S. Stopkowicz, "Equation-of-motion coupled-cluster methods for atoms and molecules in strong magnetic fields", J. Chem. Phys. **146**, 154105 (2017).

[109]J. W. Furness, J. Verbeke, E. I. Tellgren, S. Stopkowicz, U. Ekström, T. Helgaker, and A. M. Teale, "Current density functional theory using meta-generalized gradient exchange-correlation functionals", J. Chem. Theory Comput. **11**, 4169–4181 (2015).

[110]S. Reimann, A. Borgoo, J. Austad, E. I. Tellgren, A. M. Teale, T. Helgaker, and S. Stopkowicz, "Kohn–Sham energy decomposition for molecules in a magnetic field", Mol. Phys. **117**, 97–109 (2019).

[111]A. Pausch and W. Klopper, "Efficient evaluation of three-centre two-electron integrals over London orbitals", Mol. Phys. **118**, e1736675 (2020).

[112]C. Holzer, A. Pausch, and W. Klopper, "The GW/BSE Method in Magnetic Fields", Front. Chem. **9**, 746162 (2021).

[113]L. Monzel, A. Pausch, L. D. M. Peters, E. I. Tellgren, T. Helgaker, and W. Klopper, "Molecular dynamics of linear molecules in strong magnetic fields", J. Chem. Phys. **157**, 054106 (2022).

[114]F. Hampe, N. Gross, and S. Stopkowicz, "Full triples contribution in coupled-cluster and equation-of-motion coupled-cluster methods for atoms and molecules in strong magnetic fields", Phys. Chem. Chem. Phys. **22**, 23522–23529 (2020).

[115]F. Hampe and S. Stopkowicz, "Transition-dipole moments for electronic excitations in strong magnetic fields using equation-of-motion and linear response coupled-cluster theory", J. Chem. Theory Comput. **15**, 4036–4043 (2019).

[116]C. Holzer, A. M. Teale, F. Hampe, S. Stopkowicz, T. Helgaker, and W. Klopper, "GW quasiparticle energies of atoms in strong magnetic fields", J. Chem. Phys. **150**, 214112 (2019).

[117]A. Kaito, M. Hatano, and A. Tajiri, "CNDO treatment for Faraday B terms of some azaheterocycles", J. Am. Chem. Soc. **99**, 5241–5246 (1977).

[118]A. A. Meier and G. H. Wagnière, "The long-wavelength MCD of some quinones and its interpretation by semi-empirical MO methods", Chem. Phys. **113**, 287–307 (1987).

[119]A. Gedanken and M. D. Rowe, "Magnetic circular dichroism spectra of the methyl halides. Resolution of the $n \to \sigma^*$ continuum", Chem. Phys. Lett. **34**, 39–43 (1975).

[120]A. Gedanken and O. Schnepp, "The excited states of cycloporane. MCD spectrum, and CD spectrum of an optically active derivative", Chem. Phys. **12**, 341–348 (1976).

[121]A. Buckingham and P. Stephens, "Magnetic optical activity", Annu. Rev. Phys. Chem. **17**, 399–432 (1966).

[122]P. Stephens, "Magnetic circular dichroism", Annu. Rev. Phys. Chem. **25**, 201–232 (1974).

[123]T. Kjærgaard, K. Kristensen, J. Kauczor, P. Jørgensen, S. Coriani, and A. J. Thorvaldsen, "Comparison of standard and damped response formulations of magnetic circular dichroism", J. Chem. Phys. **135**, 024112 (2011).

[124]R. Faber, S. Ghidinelli, C. Hättig, and S. Coriani, "Magnetic circular dichroism spectra from resonant and damped coupled cluster response theory", J. Chem. Phys. **153**, 114105 (2020).

[125]M. Seth and T. Ziegler, "Formulation of magnetically perturbed time-dependent density functional theory", J. Chem. Phys. **127**, 134108 (2007).

[126]M. Seth, M. Krykunov, T. Ziegler, J. Autschbach, and A. Banerjee, "Application of magnetically perturbed time-dependent density functional theory to magnetic circular dichroism: calculation of B terms", J. Chem. Phys. **128**, 144105 (2008).

[127]M. Seth, M. Krykunov, T. Ziegler, and J. Autschbach, "Application of magnetically perturbed time-dependent density functional theory to magnetic circular dichroism. II. Calculation of A terms", J. Chem. Phys. **128**, 234102 (2008).

[128]M. Seth, T. Ziegler, and J. Autschbach, "Application of magnetically perturbed time-dependent density functional theory to magnetic circular dichroism. III. Temperature-dependent magnetic circular dichroism induced by spin-orbit coupling", J. Chem. Phys. **129**, 104105 (2008).

[129]S. Sun and X. Li, "Relativistic effects in magnetic circular dichroism: restricted magnetic balance and temperature dependence", J. Chem. Theory Comput. **16**, 4533–4542 (2020).

[130]D. P. Craig and T. Thirunamachandran, *Molecular quantum electrodynamics: an introduction to radiation-molecule interactions*, Dover Books on Chemistry (Dover Publications, London, 2012).

[131]M. V. Imperatore, J. B. Asbury, and N. C. Giebink, "Reproducibility of cavity-enhanced chemical reaction rates in the vibrational strong coupling regime", J. Chem. Phys. **154**, 191103 (2021).

[132]G. D. Wiesehan and W. Xiong, "Negligible rate enhancement from reported cooperative vibrational strong coupling catalysis", J. Chem. Phys. **155**, 241103 (2021).

[133]A. P. Fidler, L. Chen, A. M. McKillop, and M. L. Weichman, "Ultrafast dynamics of CN radical reactions with chloroform solvent under vibrational strong coupling", J. Chem. Phys. **159**, 164302 (2023).

[134]R. R. Riso, T. S. Haugland, E. Ronca, and H. Koch, "Molecular orbital theory in cavity qed environments", Nat. Commun. **13**, 1368 (2022).

[135]R. R. Riso, L. Grazioli, E. Ronca, T. Giovannini, and H. Koch, "Strong coupling in chiral cavities: nonperturbative framework for enantiomer discrimination", Phys. Rev. X **13**, 031002 (2023).

[136]T. S. Haugland, E. Ronca, E. F. Kjønstad, A. Rubio, and H. Koch, "Coupled cluster theory for molecular polaritons: changing ground and excited states", Phys. Rev. X **10**, 041043 (2020).

[137]T. S. Haugland, C. Schäfer, E. Ronca, A. Rubio, and H. Koch, "Intermolecular interactions in optical cavities: an ab initio QED study", J. Chem. Phys. **154**, 094113 (2021).

[138]J. Flick, M. Ruggenthaler, H. Appel, and A. Rubio, "Atoms and molecules in cavities, from weak to strong coupling in quantum-electrodynamics (QED) chemistry", Proc. Natl. Acad. Sci. **114**, 3026–3034 (2017).

[139]J. Flick, N. Rivera, and P. Narang, "Strong light-matter coupling in quantum chemistry and quantum photonics", Nanophotonics **7**, 1479–1501 (2018).

[140]M. Ruggenthaler, J. Flick, C. Pellegrini, H. Appel, I. V. Tokatly, and A. Rubio, "Quantum-electrodynamical density-functional theory: bridging quantum optics and electronic-structure theory", Phys. Rev. A **90**, 012508 (2014).

[141]M. Ruggenthaler, N. Tancogne-Dejean, J. Flick, H. Appel, and A. Rubio, "From a quantum-electrodynamical light–matter description to novel spectroscopies", Nat. Rev. Chem. **2**, 0118 (2018).

[142]M. Ruggenthaler, D. Sidler, and A. Rubio, "Understanding polaritonic chemistry from ab initio quantum electrodynamics", Chem. Rev. **123**, 11191–11229 (2023).

[143]C. A. DelPo, S.-U.-Z. Khan, K. H. Park, B. Kudisch, B. P. Rand, and G. D. Scholes, "Polariton decay in donor–acceptor cavity systems", J. Phys. Chem. Lett. **12**, 9774–9782 (2021).

[144]J. Fregoni, G. Granucci, E. Coccia, M. Persico, and S. Corni, "Manipulating azobenzene photoisomerization through strong light–molecule coupling", Nat. Commun. **9**, 4688 (2018).

[145]J. Fregoni, G. Granucci, M. Persico, and S. Corni, "Strong coupling with light enhances the photoisomerization quantum yield of azobenzene", Chem **6**, 250–265 (2020).

[146]F. Herrera, "Photochemistry with quantum optics from a non-adiabatic quantum trajectory perspective", Chem **6**, 7–9 (2020).

[147]M. A. Sentef, M. Ruggenthaler, and A. Rubio, "Cavity quantum-electrodynamical polaritonically enhanced electron-phonon coupling and its influence on superconductivity", Science Advances **4**, eaau6969 (2018).

[148]A. Thomas, L. Lethuillier-Karl, K. Nagarajan, R. M. A. Vergauwe, J. George, T. Chervy, A. Shalabney, E. Devaux, C. Genet, J. Moran, and T. W. Ebbesen, "Tilting a ground-state reactivity landscape by vibrational strong coupling", Science **363**, 615–619 (2019).

[149]J. Lather, P. Bhatt, A. Thomas, T. W. Ebbesen, and J. George, "Cavity catalysis by cooperative vibrational strong coupling of reactant and solvent molecules", Angew. Chem., Int. Ed. **58**, 10635–10638 (2019).

[150]K. Hirai, J. A. Hutchison, and H. Uji-i, "Recent progress in vibropolaritonic chemistry", ChemPlusChem **85**, 1981–1988 (2020).

[151]F. J. Garcia-Vidal, C. Ciuti, and T. W. Ebbesen, "Manipulating matter by strong coupling to vacuum fields", Science **373**, eabd0336 (2021).

[152]C. Schäfer, M. Ruggenthaler, H. Appel, and A. Rubio, "Modification of excitation and charge transfer in cavity quantum-electrodynamical chemistry", Proc. Natl. Acad. Sci. **116**, 4883–4892 (2019).

[153]M. D. Liebenthal, N. Vu, and A. E. DePrince III, "Equation-of-motion cavity quantum electrodynamics coupled-cluster theory for electron attachment", J. Chem. Phys. **156**, 054105 (2022).

[154]A. E. DePrince III, "Cavity-modulated ionization potentials and electron affinities from quantum electrodynamics coupled-cluster theory", J. Chem. Phys. **154**, 094112 (2021).

[155]F. Pavošević and J. Flick, "Polaritonic unitary coupled cluster for quantum computations", J. Phys. Chem. Lett. **12**, 9100–9107 (2021).

[156]A. Mandal, S. Montillo Vega, and P. Huo, "Polarized Fock states and the dynamical Casimir effect in molecular cavity quantum electrodynamics", J. Phys. Chem. Lett. **11**, 9215–9223 (2020).

[157]C. Schäfer, F. Buchholz, M. Penz, M. Ruggenthaler, and A. Rubio, "Making ab initio QED functional(s): nonperturbative and photon-free effective frameworks for strong light–matter coupling", Proc. Natl. Acad. Sci. **118**, e2110464118 (2021).

[158]J. McTague and J. J. Foley, "Non-Hermitian cavity quantum electrodynamics–configuration interaction singles approach for polaritonic structure with ab initio molecular Hamiltonians", J. Chem. Phys. **156**, 154103 (2022).

[159]Y. Ashida, A. İmamoğlu, and E. Demler, "Cavity quantum electrodynamics at arbitrary light-matter coupling strengths", Phys. Rev. Lett. **126**, 153603 (2021).

[160]J. Liu, A. Asthana, L. Cheng, and D. Mukherjee, "Unitary coupled-cluster based self-consistent polarization propagator theory: A third-order formulation and pilot applications", J. Chem. Phys. **148**, 244110 (2018).

[161]F. Hampe, S. Stopkowicz, N. Groß, M.-P. Kitsaras, L. Grazioli, S. Blaschke, L. Monzel, and Ü. P. Yergün, *QCUMBRE, quantum chemical utility enabling magnetic-field dependent investigations benefitting from rigorous electron-correlation treatment*, qcumbre.org.

[162]K. K. Lange, E. I. Tellgren, M. R. Hoffmann, and T. Helgaker, "A paramagnetic bonding mechanism for diatomics in strong magnetic fields", Science **337**, 327–331 (2012).

[163]P. Bunker, "On the breakdown of the Born-Oppenheimer approximation for a diatomic molecule", J. Mol. Spectrosc. **42**, 478–494 (1972).

[164]P. Bunker and R. Moss, "The breakdown of the Born-Oppenheimer approximation: the effective vibration-rotation Hamiltonian for a diatomic molecule", Mol. Phys. **33**, 417–424 (1977).

[165]S. Pisana, M. Lazzeri, C. Casiraghi, K. S. Novoselov, A. K. Geim, A. C. Ferrari, and F. Mauri, "Breakdown of the adiabatic Born–Oppenheimer approximation in graphene", Nat. Mater. **6**, 198–201 (2007).

[166]I. Rahinov, R. Cooper, D. Matsiev, C. Bartels, D. J. Auerbach, and A. M. Wodtke, "Quantifying the breakdown of the Born–Oppenheimer approximation in surface chemistry", Phys. Chem. Chem. Phys. **13**, 12680 (2011).

[167]G. Stockes, "On the dynamical theory of diffraction", Cambridge Philosophical Transactions **9**, 1–62 (1849).

[168]H. v. Helmholtz, "Über Integrale der hydrodynamischen Gleichungen, welche den Wirbelbewegungen entsprechen.", J. für Reine Angew. Math. **55**, 25–55 (1858).

[169]W. Pauli, "Zur Quantenmechanik des magnetischen Elektrons", Z. Phys. **43**, 601–623 (1927).

[170]D. R. Hartree, "The wave mechanics of an atom with a non-Coulomb central field. Part I. Theory and methods", Math. Proc. Camb. Philos. Soc. **24**, 89–110 (1928).

[171]D. R. Hartree and W. Hartree, "Self-consistent field, with exchange, for beryllium", Proc. Math. Phys. Eng. Sci. **150**, 9–33 (1935).

[172]V. Fock, "Näherungsmethode zur Lösung des quantenmechanischen Mehrkörperproblems", Z. Phys. **61**, 126–148 (1930).

[173]J. C. Slater, "The Self Consistent Field and the structure of atoms", Phys. Rev. **32**, 339–348 (1928).

[174]C. C. J. Roothaan, "New developments in molecular orbital theory", Rev. Mod. Phys. **23**, 69–89 (1951).

[175]C. C. J. Roothaan, "Self-consistent field theory for open shells of electronic systems", Rev. Mod. Phys. **32**, 179–185 (1960).

[176]J. A. Pople and R. K. Nesbet, "Self-consistent orbitals for radicals", J. Chem. Phys. **22**, 571–572 (1954).

[177]A. Cohen and N. Handy, "Dynamic correlation", Mol. Phys. **99**, 607–615 (2001).

[178]W. T. Borden and E. R. Davidson, "The importance of including dynamic electron correlation in ab initio calculations", Acc. Chem. Res. **29**, 67–75 (1996).

[179]J. W. Hollett and P. M. W. Gill, "The two faces of static correlation", J. Chem. Phys. **134** (2011).

[180]I. W. Bulik, T. M. Henderson, and G. E. Scuseria, "Can single-reference coupled cluster theory describe static correlation?", J. Chem. Theory Comput. **11**, 3171–3179 (2015).

[181]D. L. Crittenden, "A hierarchy of static correlation models", J. Phys. Chem. A **117**, 3852–3860 (2013).

[182]T. Helgaker and P. Jørgensen, "An electronic Hamiltonian for origin independent calculations of magnetic properties", J. Chem. Phys. **95**, 2595–2601 (1991).

[183]F. London, "Théorie quantique des courants interatomiques dans les combinaisons aromatiques", J. Phys. Radium **8**, 397–409 (1937).

[184]J. Gauss, "Calculation of NMR chemical shifts at second-order many-body perturbation theory using gauge-including atomic orbitals", Chem. Phys. Lett. **191**, 614–620 (1992).

[185]P. Pulay, J. Hinton, and K. Wolinski, "Efficient implementation of the GIAO method for magnetic properties: theory and application", in *Nuclear magnetic shieldings and molecular structure*, edited by J. A. Tossell (Springer, 1993), pp. 243–262.

[186]G. C. Wick, "The evaluation of the collision matrix", Phys. Rev. **80**, 268–272 (1950).

[187]B. O. Roos, P. R. Taylor, and P. E. Siegbahn, "A complete active space SCF method (CASSCF) using a density matrix formulated super-CI approach", Chem. Phys. **48**, 157–173 (1980).

[188]J. Olsen, B. O. Roos, P. Jørgensen, and H. J. Aa. Jensen, "Determinant based configuration interaction algorithms for complete and restricted configuration interaction spaces", J. Chem. Phys. **89**, 2185–2192 (1988).

[189]J. Olsen, P. Jørgensen, and J. Simons, "Passing the one-billion limit in full configuration-interaction (FCI) calculations", Chem. Phys. Lett. **169**, 463–472 (1990).

[190]P. Knowles and N. Handy, "A new determinant-based full configuration interaction method", Chem. Phys. Lett. **111**, 315–321 (1984).

[191]F. Coester and H. Kümmel, "Short-range correlations in nuclear wave functions", Nucl. Phys. **17**, 477–485 (1960).

[192]J. Čížek, "On the correlation problem in atomic and molecular systems. Calculation of wavefunction components in Ursell-type expansion using quantum-field theoretical methods", J. Chem. Phys. **45**, 4256–4266 (1966).

[193]J. Paldus, "Correlation problems in atomic and molecular systems. V. Spin-adapted coupled cluster many-electron theory", J. Chem. Phys. **67**, 303–318 (1977).

[194]J. Paldus, J. Čížek, M. Saute, and A. Laforgue, "Correlation problems in atomic and molecular systems. VI. Coupled-cluster approach to open-shell systems", Phys. Rev. A **17**, 805–815 (1978).

[195]D. Cremer, "From configuration interaction to coupled cluster theory: the quadratic configuration interaction approach", Wiley Interdiscip. Rev. Comput. Mol. Sci. **3**, 482–503 (2013).

[196]R. J. Bartlett, "Coupled-cluster theory and its equation-of-motion extensions", Wiley Interdiscip. Rev. Comput. Mol. Sci. **2**, 126–138 (2011).

[197]C. Hättig, "Structure optimizations for excited states with correlated second-order methods: CC2 and ADC(2)", in *Adv. quantum chem.* (Elsevier, 2005), pp. 37–60.

[198]E. F. Kjønstad, R. H. Myhre, T. J. Martínez, and H. Koch, "Crossing conditions in coupled cluster theory", J. Chem. Phys. **147**, 164105 (2017).

[199]D. R. Yarkony, "Diabolical conical intersections", Rev. Mod. Phys. **68**, 985–1013 (1996).

[200]S. Matsika and D. R. Yarkony, "On the effects of spin-orbit coupling on conical intersection seams in molecules with an odd number of electrons. I. Locating the seam", J. Chem. Phys. **115**, 2038–2050 (2001).

[201]D. G. Truhlar and C. A. Mead, "Relative likelihood of encountering conical intersections and avoided intersections on the potential energy surfaces of polyatomic molecules", Phys. Rev. A **68**, 032501 (2003).

[202]X. Zhu and D. R. Yarkony, "Non-adiabaticity: the importance of conical intersections", Mol. Phys. **114**, 1983–2013 (2016).

[203]L. Visscher, T. J. Lee, and K. G. Dyall, "Formulation and implementation of a relativistic unrestricted coupled-cluster method including noniterative connected triples", J. Chem. Phys. **105**, 8769–8776 (1996).

[204]A. Shee, T. Saue, L. Visscher, and A. Severo Pereira Gomes, "Equation-of-motion coupled-cluster theory based on the 4-component Dirac–Coulomb(–Gaunt) Hamiltonian. Energies for single electron detachment, attachment, and electronically excited states", J. Chem. Phys. **149**, 174113 (2018).

[205]F. Wang, J. Gauss, and C. van Wüllen, "Closed-shell coupled-cluster theory with spin-orbit coupling", J. Chem. Phys. **129**, 064113 (2008).

[206]J. Liu, Y. Shen, A. Asthana, and L. Cheng, "Two-component relativistic coupled-cluster methods using mean-field spin-orbit integrals", J. Chem. Phys. **148**, 034106 (2018).

[207]M.-P. Kitsaras, "Finite magnetic-field coupled-cluster methods: efficiency and utilities", PhD thesis (Johannes-Gutenberg Universität Mainz, July 2023).

[208]K. B. Bravaya, D. Zuev, E. Epifanovsky, and A. I. Krylov, "Complex-scaled equation-of-motion coupled-cluster method with single and double substitutions for autoionizing excited states: theory, implementation, and examples", J. Chem. Phys. **138**, 124106 (2013).

[209]T.-C. Jagau, D. Zuev, K. B. Bravaya, E. Epifanovsky, and A. I. Krylov, "Correction to "A fresh look at resonances and complex absorbing potentials: density matrix-based approach"", J. Phys. Chem. Lett. **6**, 3866–3866 (2015).

[210]T.-C. Jagau, K. B. Bravaya, and A. I. Krylov, "Extending quantum chemistry of bound states to electronic resonances", Annu. Rev. Phys. Chem. **68**, 525–553 (2017).

[211]Z. Benda and T.-C. Jagau, "Locating exceptional points on multidimensional complex-valued potential energy surfaces", J. Phys. Chem. Lett. **9**, 6978–6984 (2018).

[212]L. Grazioli, S. Stopkowicz, A. Krylov, and J. Gauss, "Coupled-cluster and unitary coupled-cluster transition dipole moments through response theory", in preparation (2024).

[213]L. Grazioli, S. Stopkowicz, and J. Gauss, "Unitary coupled-cluster one-electron density matrices for the calculation of dipole moments in strong magnetic fields", in preparation (2024).

[214]H. Sekino and R. J. Bartlett, "On the extensivity problem in coupled-cluster property evaluation", in *Adv. quant. chem.* (Elsevier, 1999), pp. 149–173.

[215]J. F. Stanton, "Separability properties of reduced and effective density matrices in the equation-of-motion coupled cluster method", J. Chem. Phys. **101**, 8928–8937 (1994).

[216]J. Linderberg and Y. Öhrn, *Propagators in quantum chemistry* (John Wiley & Sons, Hoboken, 2004).

[217]J. Olsen and P. Jørgensen, "Linear response calculations for large scale multiconfiguration self–consistent field wave functions", J. Chem. Phys **82**, 3235–3264 (1985).

[218]H. Hellmann, *Einführung in die Quantenchemie* (Franz Deuticke, Leipzig, 1937), pp. 1–350.

[219]C. Hättig, O. Christiansen, and P. Jørgensen, "Multiphoton transition moments and absorption cross sections in coupled cluster response theory employing variational transition moment functionals", J. Chem. Phys. **108**, 8331–8354 (1998).

[220]H. J. Monkhorst, "Calculation of properties with the coupled-cluster method", Int. J. Quantum Chem. **12**, 421–432 (1977).

[221]H. Koch, H. J. Aa. Jensen, P. Jørgensen, and T. Helgaker, "Excitation energies from the coupled cluster singles and doubles linear response function (CCSDLR). Applications to Be, CH^+, CO, and H_2O", J. Chem. Phys. **93**, 3345–3350 (1990).

[222]S. Ghosh, D. Mukherjee, and S. Bhattacharyya, "Application of linear response theory in a coupled cluster framework for the calculation of ionization potentials", Mol. Phys. **43**, 173–179 (1981).

[223]T. D. Crawford, A. Kumar, A. P. Bazanté, and R. Di Remigio, "Reduced-scaling coupled cluster response theory: challenges and opportunities", Wiley Interdiscip. Rev. Comput. Mol. Sci. **9**, e1406 (2019).

[224]J. F. Stanton, "Many-body methods for excited state potential energy surfaces. I. General theory of energy gradients for the equation-of-motion coupled-cluster method", J. Chem. Phys. **99**, 8840–8847 (1993).

[225]T. Helgaker and P. Jørgensen, "Configuration-interaction energy derivatives in a fully variational formulation", Theor. Chim. Acta **75**, 111–127 (1989).

[226]A. Dalgarno and A. L. Stewart, "A perturbation calculation of properties of the helium iso-electronic sequence", Proc. R. Soc. A **247**, 245–259 (1958).

[227]N. C. Handy and H. F. Schaefer III, "On the evaluation of analytic energy derivatives for correlated wave functions", J. Chem. Phys. **81**, 5031–5033 (1984).

[228]S. N. Afriat, "Theory of maxima and the method of Lagrange", J. Appl. Math. **20**, 343–357 (1971).

[229]G. Floquet, "Sur les équations différentielles linéaires à coefficients périodiques", Annales scientifiques de l'École normale supérieure **12**, 47–88 (1883).

[230]K. Sasagane, F. Aiga, and R. Itoh, "Higher-order response theory based on the quasienergy derivatives: the derivation of the frequency-dependent polarizabilities and hyperpolarizabilities", J. Chem. Phys. **99**, 3738–3778 (1993).

[231]H. Sambe, "Steady states and quasienergies of a quantum-mechanical system in an oscillating field", Phys. Rev. A **7**, 2203–2213 (1973).

[232]P. W. Langhoff, S. T. Epstein, and M. Karplus, "Aspects of time-dependent perturbation theory", Rev. Mod. Phys. **44**, 602–644 (1972).

[233]W. Kutzelnigg, "Error analysis and improvements of coupled-cluster theory", Theor. Chim. Acta **80**, 349–386 (1991).

[234]W. Kutzelnigg, "Quantum chemistry in Fock space. I. The universal wave and energy operators", J. Chem. Phys. **77**, 3081–3097 (1982).

[235]W. Kutzelnigg and S. Koch, "Quantum chemistry in Fock space. II. Effective Hamiltonians in Fock space", J. Chem. Phys. **79**, 4315–4335 (1983).

[236]P. G. Todorov, "On the theory of the Bernoulli polynomials and numbers", J. Math. Anal. Appl. **104**, 309–350 (1984).

[237]A. Asthana, A. Kumar, V. Abraham, H. Grimsley, Y. Zhang, L. Cincio, S. Tretiak, P. A. Dub, S. E. Economou, E. Barnes, et al., "Quantum self-consistent equation-of-motion method for computing molecular excitation energies, ionization potentials, and electron affinities on a quantum computer", Chem. Sci. **14**, 2405–2418 (2023).

[238]Y. Kim and A. I. Krylov, "Two algorithms for excited-state quantum solvers: theory and application to EOM-UCCSD", J. Phys. Chem. A **127**, 6552–6566 (2023).

[239]F. A. Evangelista, "Alternative single-reference coupled cluster approaches for multireference problems: the simpler, the better", J. Chem. Phys. **134**, 224102 (2011).

[240]W. von Niessen, J. Schirmer, and L. Cederbaum, "Computational methods for the one-particle Green's function", Comput. Phys. Rep **1**, 57–125 (1984).

[241]L. S. Cederbaum, "On Green's functions and their applications", Int. J. Quantum Chem. **38**, 393–404 (1990).

[242]C. Møller and M. S. Plesset, "Note on an approximation treatment for many-electron systems", Phys. Rev. **46**, 618–622 (1934).

[243]J. Schirmer, "Beyond the random-phase approximation: a new approximation scheme for the polarization propagator", Phys. Rev. A **26**, 2395–2416 (1982).

[244]J. Schirmer, "Closed-form intermediate representations of many-body propagators and resolvent matrices", Phys. Rev. A **43**, 4647–4659 (1991).

[245]F. Mertins and J. Schirmer, "Algebraic propagator approaches and intermediate-state representations. I. The biorthogonal and unitary coupled-cluster methods", Phys. Rev. A **53**, 2140–2152 (1996).

[246]F. Mertins, J. Schirmer, and A. Tarantelli, "Algebraic propagator approaches and intermediate-state representations. II. The equation-of-motion methods for N, N±1, and N±2 electrons", Phys. Rev. A **53**, 2153–2168 (1996).

[247]A. B. Trofimov and J. Schirmer, "Molecular ionization energies and ground- and ionic-state properties using a non-Dyson electron propagator approach", J. Chem. Phys. **123** (2005).

[248]M. Hodecker, S. M. Thielen, J. Liu, D. R. Rehn, and A. Dreuw, "Third-order Unitary Coupled Cluster (UCC3) for excited electronic states: efficient implementation and benchmarking", J. Chem. Theory Comput. **16**, 3654–3663 (2020).

[249]M. Hodecker, A. L. Dempwolff, J. Schirmer, and A. Dreuw, "Theoretical analysis and comparison of unitary coupled-cluster and algebraic-diagrammatic construction methods for ionization", J. Chem. Phys. **156**, 074104 (2022).

[250]A. Dreuw, A. Papapostolou, and A. L. Dempwolff, "Algebraic Diagrammatic Construction schemes employing the intermediate state formalism: theory, capabilities, and interpretation", J. Phys. Chem. A **127**, 6635–6646 (2023).

[251]J. F. Stanton, J. Gauss, L. Cheng, M. E. Harding, D. A. Matthews, and P. G. Szalay, *CFOUR, Coupled-Cluster techniques for Computational Chemistry, a quantum-chemical program package*, With contributions from A. Asthana, A.A. Auer, R.J. Bartlett, U. Benedikt, C. Berger, D.E. Bernholdt, S. Blaschke, Y. J. Bomble, S. Burger, O. Christiansen, D. Datta, F. Engel, R. Faber, J. Greiner, M. Heckert, O. Heun, M. Hilgenberg, C. Huber, T.-C. Jagau, D. Jonsson, J. Jusélius, T. Kirsch, M.-P. Kitsaras, K. Klein, G.M. Kopper, W.J. Lauderdale, F. Lipparini, J. Liu, T. Metzroth, L.A. Mück, D.P. O'Neill, T. Nottoli, J. Oswald, D.R. Price, E. Prochnow, C. Puzzarini, K. Ruud, F. Schiffmann, W. Schwalbach, C. Simmons, S. Stopkowicz, A. Tajti, T. Uhlířová, J. Vázquez, F. Wang, J.D. Watts, P. Yergün, C. Zhang, X. Zheng, and the integral packages MOLECULE (J. Almlöf and P.R. Taylor), PROPS (P.R. Taylor), ABACUS (T. Helgaker, H.J.Aa. Jensen, P. Jørgensen, and J. Olsen), and ECP routines by A. V. Mitin and C. van Wüllen. For the current version, see http://www.cfour.de.

[252]D. A. Matthews, L. Cheng, M. E. Harding, F. Lipparini, S. Stopkowicz, T.-C. Jagau, P. G. Szalay, J. Gauss, and J. F. Stanton, "Coupled-cluster techniques for computational chemistry: the CFOUR program package", J. Chem. Phys. **152**, 214108 (2020).

[253]J. J. Barton and L. R. Nackman, *Scientific and engineering C++ an introduction with advanced techniques and examples* (Addison-Wesley Longman Publishing Co., Inc., 1994).

[254]E. Tellgren, T. Helgaker, A. Soncini, K. K. Lange, A. M. Teale, U. Ekström, S. Stopkowicz, J. H. Austad, and S. Sen, *LONDON, a quantum-chemistry program for plane-wave/GTO hybrid basis sets and finite magnetic field calculations*, londonprogram.org.

[255]*BAGEL, Brilliantly Advanced General Electronic-structure Library. http://www.nubakery.org under the GNU General Public License.*

[256]D. B. Williams-Young, A. Petrone, S. Sun, T. F. Stetina, P. Lestrange, C. E. Hoyer, D. R. Nascimento, L. Koulias, A. Wildman, J. Kasper, J. J. Goings, F. Ding, A. E. DePrince III, E. F. Valeev, and X. Li, "The Chronus Quantum software package", WIREs Comput. Mol. Sci. **10** (2020).

[257]*QUEST, A rapid development platform for QUantum Electronic Structure Techniques, 2017; quest.codes.*

[258]S. G. Balasubramani, G. P. Chen, S. Coriani, M. Diedenhofen, M. S. Frank, Y. J. Franzke, F. Furche, R. Grotjahn, M. E. Harding, C. Hättig, A. Hellweg, B. Helmich-Paris, C. Holzer, U. Huniar, M. Kaupp, A. Marefat Khah, S. Karbalaei Khani, T. Müller, F. Mack, B. D. Nguyen, S. M. Parker, E. Perlt, D. Rappoport, K. Reiter, S. Roy, M. Rückert, G. Schmitz, M. Sierka, E. Tapavicza, D. P. Tew, C. van Wüllen, V. K. Voora, F. Weigend, A. Wodyński, and J. M. Yu, "TURBOMOLE: Modular program suite for ab initio quantum-chemical and condensed-matter simulations", J. Chem. Phys. **152**, 184107 (2020).

[259]I. Shavitt and R. J. Bartlett, *Many-body methods in chemistry and physics: mbpt and coupled-cluster theory* (Cambridge University Press, Cambridge, 2009).

[260]P. Pulay, "Convergence acceleration of iterative sequences. The case of SCF iteration", Chem. Phys. Lett. **73**, 393–398 (1980).

[261]E. R. Davidson, "Use of double cosets in constructing integrals over symmetry orbitals", J. Chem. Phys. **62**, 400–403 (1975).

[262]K. Hirao and H. Nakatsuji, "A generalization of the Davidson's method to large nonsymmetric eigenvalue problems", J. Comput. Phys. **45**, 246–254 (1982).

[263]M. Crouzeix, B. Philippe, and M. Sadkane, "The Davidson method", J. Sci. Stat. Comput. **15**, 62–76 (1994).

[264]R. B. Morgan and D. S. Scott, "Generalizations of Davidson's method for computing eigenvalues of sparse symmetric matrices", J. Sci. Stat. Comput. **7**, 817–825 (1986).

[265]M. Hodecker, A. L. Dempwolff, D. R. Rehn, and A. Dreuw, "Algebraic-diagrammatic construction scheme for the polarization propagator including ground-state coupled-cluster amplitudes. I. Excitation energies", J. Chem. Phys. **150**, 174104 (2019).

[266]B. P. Pritchard, D. Altarawy, B. Didier, T. D. Gibsom, and T. L. Windus, "A new basis set exchange: an open, up-to-date resource for the molecular sciences community", J. Chem. Inf. Model. **59**, 4814–4820 (2019).

[267]D. Feller, "The role of databases in support of computational chemistry calculations", J. Comput. Chem. **17**, 1571–1586 (1996).

[268]K. L. Schuchardt, B. T. Didier, T. Elsethagen, L. Sun, V. Gurumoorthi, J. Chase, J. Li, and T. L. Windus, "Basis set exchange: a community database for computational sciences", J. Chem. Inf. Model. **47**, 1045–1052 (2007).

[269]T. H. Dunning, "Gaussian basis sets for use in correlated molecular calculations. I. The atoms boron through neon and hydrogen", J. Chem. Phys. **90**, 1007–1023 (1989).

[270]R. A. Kendall, T. H. Dunning, and R. J. Harrison, "Electron affinities of the first-row atoms revisited. Systematic basis sets and wave functions", J. Chem. Phys. **96**, 6796–6806 (1992).

[271]B. P. Prascher, D. E. Woon, K. A. Peterson, T. H. Dunning, and A. K. Wilson, "Gaussian basis sets for use in correlated molecular calculations. VII. Valence, core-valence, and scalar relativistic basis sets for Li, Be, Na, and Mg", Theor. Chem. Acc. **128**, 69–82 (2011).

[272]S. Lehtola, M. Dimitrova, and D. Sundholm, "Fully numerical electronic structure calculations on diatomic molecules in weak to strong magnetic fields", Mol. Phys. **118**, e1597989 (2019).

[273]T. Helgaker, T. A. Ruden, P. Jørgensen, J. Olsen, and W. Klopper, "A priori calculation of molecular properties to chemical accuracy", J. Phys. Org. Chem. **17**, 913–933 (2004).

[274]M.-P. Kitsaras, L. Grazioli, and S. Stopkowicz, "The approximate coupled-cluster methods CC2 and CC3 in a finite magnetic field", J. Chem. Phys. **160**, 094112 (2024).

[275]L. Grazioli and S. Stopkowicz, "Unitary coupled-cluster theory for the treatment of molecules in strong magnetic fields", in preparation (2024).

[276]F. C. Bruhweiler and Y. Kondo, "The interstellar medium and the highly ionized species observed in the spectrum of the nearby white dwarf G191-B2B", Astrophys. J. **248**, L123–L127 (1981).

[277]A. Kramida and Y. Ralchenko, *NIST Atomic Spectra Database, NIST Standard Reference Database 78*, 1999.

[278]E. Dalgaard and H. J. Monkhorst, "Some aspects of the time-dependent coupled-cluster approach to dynamic response functions", Phys. Rev. A **28**, 1217–1222 (1983).

[279]K. Ando, H. Saito, M. C. Debnath, V. Zayets, and A. K. Bhattacharjee, "Zeeman splittings near the L-point of the Brillouin zone in zinc-blende semiconductors", Phys. Rev. B **77**, 125123 (2008).

[280]G. A. Osborne, J. C. Cheng, and P. J. Stephens, "A near-infrared circular dichroism and magnetic circular dichroism instrument", Rev. Sci. Instrum. **44**, 10–15 (1973).

[281]J.-H. Lambert, *Photometria sive de mensura et gradibus luminis, colorum et umbrae* (Sumptibus viduae Eberhardi Klett, typis Christophori Petri Detleffsen, 1760).

[282]A. Beer, "Bestimmung der Absorption des rothen Lichts in farbigen Flüssigkeiten", Ann. Phys. **162**, 78–88 (1852).

[283]J. H. Poynting, "On the transfer of energy in the electromagnetic field", Phil. Trans. R. Soc. **175**, 343–361 (1884).

[284]S. B. Piepho and P. N. Schatz, *Group theory in spectroscopy: with applications to magnetic circular dichroism* (John Wiley & Sons, New York, 1983).

[285]S. Coriani, C. Hättig, P. Jørgensen, and T. Helgaker, "Gauge-origin independent magneto-optical activity within coupled cluster response theory", J. Chem. Phys. **113**, 3561–3572 (2000).

[286]B. Mennucci and R. Cammi, *Continuum solvation models in chem. phys.: from theory to applications* (John Wiley & Sons, 2008).

[287]B. Mennucci, E. Cancès, and J. Tomasi, "Evaluation of solvent effects in isotropic and anisotropic dielectrics and in ionic solutions with a unified integral equation method: theoretical bases, computational implementation, and numerical applications", J. Phys. Chem. B **101**, 10506–10517 (1997).

[288]B. Mennucci, "Polarizable continuum model", Wiley Interdiscip. Rev.-Comput. Mol. Sci. **2**, 386–404 (2012).

[289]J. Tomasi and M. Persico, "Molecular interactions in solution: an overview of methods based on continuous distributions of the solvent", Chem. Rev. **94**, 2027–2094 (1994).

[290]J. Tomasi, B. Mennucci, and R. Cammi, "Quantum mechanical continuum solvation models", Chem. Rev. **105**, 2999–3094 (2005).

[291]E. Cancès, B. Mennucci, and J. Tomasi, "A new integral equation formalism for the polarizable continuum model: theoretical background and applications to isotropic and anisotropic dielectrics", J. Chem. Phys. **107**, 3032–3041 (1997).

[292]E. Cancès and B. Mennucci, "New applications of integral equations methods for solvation continuum models: ionic solutions and liquid crystals", J. Math. Chem. **23**, 309–326 (1998).

[293]S. Miertuš, E. Scrocco, and J. Tomasi, "Electrostatic interaction of a solute with a continuum. A direct utilizaion of ab initio molecular potentials for the prevision of solvent effects", Chem. Phys. **55**, 117–129 (1981).

[294]C. J. Cramer, D. G. Truhlar, et al., "Implicit solvation models: equilibria, structure, spectra, and dynamics", Chem. Rev. **99**, 2161–2200 (1999).

[295]C. E. Tzeliou, M. A. Mermigki, and D. Tzeli, "Review on the QM/MM methodologies and their application to metalloproteins", Molecules **27**, 2660 (2022).

[296]T. Kirsch, J. M. H. Olsen, V. Bolnykh, S. Meloni, E. Ippoliti, U. Rothlisberger, M. Cascella, and J. Gauss, "Wavefunction-based electrostatic-embedding QM/MM using CFOUR through MiMiC", J. Chem. Theory Comput. **18**, 13–24 (2021).

[297]H. Lin and D. G. Truhlar, "QM/MM: what have we learned, where are we, and where do we go from here?", Theor. Chem. Acc. **117**, 185–199 (2006).

[298]Y. Shao et al., "Advances in molecular quantum chemistry contained in the Q-Chem 4 program package", Mol. Phys. **113**, 184–215 (2014).

[299]J. Gauss, S. Blaschke, S. Burger, T. Nottoli, F. Lipparini, and S. Stopkowicz, "Cholesky decomposition of two-electron integrals in quantum-chemical calculations with perturbative or finite magnetic fields using gauge-including atomic orbitals", Mol. Phys. **121**, e2101562 (2022).

[300]W. Wu, A. E. Sifain, C. A. Delpo, and G. D. Scholes, "Polariton enhanced free charge carrier generation in donor–acceptor cavity systems by a second-hybridization mechanism", J. Chem. Phys. **157**, 161102 (2022).

[301]Y. Wu, J. Duan, W. Ma, Q. Ou, P. Li, P. Alonso-González, J. D. Caldwell, and Q. Bao, "Manipulating polaritons at the extreme scale in van der Waals materials", Nat. Rev. Phys. **4**, 578–594 (2022).

[302]C. Schäfer, J. Flick, E. Ronca, P. Narang, and A. Rubio, "Shining light on the microscopic resonant mechanism responsible for cavity-mediated chemical reactivity", Nat. Commun. **13**, 7817 (2022).

[303]R. Chikkaraddy, B. de Nijs, F. Benz, S. J. Barrow, O. A. Scherman, E. Rosta, A. Demetriadou, P. Fox, O. Hess, and J. J. Baumberg, "Single-molecule strong coupling at room temperature in plasmonic nanocavities", Nature **535**, 127–130 (2016).

[304]J. J. Baumberg, "Picocavities: a primer", Nano Lett. **22**, 5859–5865 (2022).

[305]T. Steinmetz, Y. Colombe, D. Hunger, T. W. Hänsch, A. Balocchi, R. J. Warburton, and J. Reichel, "Stable fiber-based Fabry-Pérot cavity", App. Phys. Lett. **89**, 111110 (2006).

[306]H. Pfeifer, L. Ratschbacher, J. Gallego, C. Saavedra, A. Faßbender, A. von Haaren, W. Alt, S. Hofferberth, M. Köhl, S. Linden, and D. Meschede, "Achievements and perspectives of optical fiber Fabry–Perot cavities", App. Phys. B **128**, 29 (2022).

[307]A. Muller, E. B. Flagg, J. R. Lawall, and G. S. Solomon, "Ultrahigh-finesse, low-mode-volume Fabry–Perot microcavity", Opt. Lett. **35**, 2293 (2010).

[308]C. Schäfer, M. Ruggenthaler, and A. Rubio, "Ab initio non-relativistic quantum electrodynamics: bridging quantum chemistry and quantum optics from weak to strong coupling", Phys. Rev. A **98**, 043801 (2018).

[309]O. Bitton and G. Haran, "Plasmonic cavities and individual quantum emitters in the strong coupling limit", Acc. Chem. Res. **55**, 1659–1668 (2022).

[310]K. Santhosh, O. Bitton, L. Chuntonov, and G. Haran, "Vacuum Rabi splitting in a plasmonic cavity at the single quantum emitter limit", Nat. Commun. **7**, ncomms11823 (2016).

[311]A. Frisk Kockum, A. Miranowicz, S. De Liberato, S. Savasta, and F. Nori, "Ultrastrong coupling between light and matter", Nat. Rev. Phys. **1**, 19–40 (2019).

[312]M. A. D. Taylor, A. Mandal, W. Zhou, and P. Huo, "Resolution of gauge ambiguities in molecular cavity quantum electrodynamics", Phys. Rev. Lett. **125**, 123602 (2020).

[313]O. Di Stefano, A. Settineri, V. Macrì, L. Garziano, R. Stassi, S. Savasta, and F. Nori, "Resolution of gauge ambiguities in ultrastrong-coupling cavity quantum electrodynamics", Nat. Phys. **15**, 803–808 (2019).

[314]D. L. Andrews, G. A. Jones, A. Salam, and R. G. Woolley, "Perspective: quantum Hamiltonians for optical interactions", J. Chem. Phys. **148**, 040901 (2018).

[315]M. Babiker, E. A. Power, and T. Thirunamachandran, "On a generalization of the Power – Zienau – Woolley transformation in quantum electrodynamics and atomic field equations", Proc. R. Soc. A: Math. Phys. Eng. **338**, 235–249 (1974).

[316]R. G. Woolley, "Power-Zienau-Woolley representations of nonrelativistic QED for atoms and molecules", Phys. Rev. Res. **2**, 013206 (2020).

[317]V. Rokaj, D. M. Welakuh, M. Ruggenthaler, and A. Rubio, "Light–matter interaction in the long-wavelength limit: no ground-state without dipole self-energy", J. Phys. B At. Mol. Opt. Phys. **51**, 034005 (2018).

[318]M. Bauer and A. Dreuw, "Perturbation theoretical approaches to strong light–matter coupling in ground and excited electronic states for the description of molecular polaritons", J. Chem. Phys. **158**, 124128 (2023).

[319]D. E. Woon and T. H. Dunning, "Gaussian basis sets for use in correlated molecular calculations. IV. Calculation of static electrical response properties", J. Chem. Phys. **100**, 2975–2988 (1994).

[320]E. F. Kjønstad and H. Koch, "An orbital invariant similarity constrained coupled cluster model", J. Chem. Theory Comput. **15**, 5386–5397 (2019).

[321]H. F. Hameka, "On the nuclear magnetic shielding in the hydrogen molecule", Mol. Phys. **1**, 203–215 (1958).

[322]R. Ditchfield, "Molecular orbital theory of magnetic shielding and magnetic susceptibility", J. Chem. Phys. **56**, 5688–5691 (1972).

[323]K. Wolinski, J. F. Hinton, and P. Pulay, "Efficient implementation of the gauge-independent atomic orbital method for NMR chemical shift calculations", J. Am. Chem. Soc. **112**, 8251–8260 (1990).

[324]J. Liu and L. Cheng, "Unitary coupled-cluster based self-consistent polarization propagator theory: A quadratic unitary coupled-cluster singles and doubles scheme", J. Chem. Phys. **155**, 174102 (2021).

[325]J. Liu, D. A. Matthews, and L. Cheng, "Quadratic unitary coupled-cluster singles and doubles scheme: efficient implementation, benchmark study, and formulation of an extended version", J. Chem. Theory Comput. **18**, 2281–2291 (2022).

[326]N. P. Bauman and K. Kowalski, "Coupled cluster downfolding methods: the effect of double commutator terms on the accuracy of ground-state energies", J. Chem. Phys. **156** (2022).

[327]M. R. Hoffmann and J. Simons, "A unitary multiconfigurational coupled-cluster method: theory and applications", J. Chem. Phys. **88**, 993–1002 (1988).

[328]E. Neuscamman, T. Yanai, and G. K.-L. Chan, "Quadratic canonical transformation theory and higher order density matrices", J. Chem. Phys. **130**, 124102 (2009).

[329]T. Giovannini, M. Olszòwka, and C. Cappelli, "Effective fully polarizable QM/MM approach to model vibrational circular dichroism spectra of systems in aqueous solution", J. Chem. Theory Comput. **12**, 5483–5492 (2016).

[330]T. Giovannini, A. Puglisi, M. Ambrosetti, and C. Cappelli, "Polarizable QM/MM approach with fluctuating charges and fluctuating dipoles: the QM/FQFμ model", J. Chem. Theory Comput. **15**, 2233–2245 (2019).

[331]T. Giovannini, R. R. Riso, M. Ambrosetti, A. Puglisi, and C. Cappelli, "Electronic transitions for a fully polarizable QM/MM approach based on fluctuating charges and fluctuating dipoles: linear and corrected linear response regimes", J. Chem. Phys. **151**, 174104 (2019).

[332]T. Giovannini, L. Grazioli, M. Ambrosetti, and C. Cappelli, "Calculation of IR spectra with a fully polarizable QM/MM approach based on fluctuating charges and fluctuating dipoles", J. Chem. Theory Comput. **15**, 5495–5507 (2019).

[333]M. D. Liebenthal, N. Vu, and A. E. DePrince III, "Assessing the effects of orbital relaxation and the coherent-state transformation in quantum electrodynamics density functional and coupled-cluster theories", J. Phys. Chem. A **127**, 5264–5275 (2023).